

# Dissertation

*submitted to the*

Combined Faculties of the Natural Sciences and Mathematics  
*of the* Ruperto-Carola University of Heidelberg, Germany

*for the degree of*

Doctor of Natural Sciences

*Put forward by*

Manuel Reichert

*born in:* Stuttgart, Germany

Oral examination: Mai 2nd, 2018



# **Towards a UV-complete Standard Model: From baryogenesis to asymptotic safety**

Referees: Prof. Dr. Jan M. Pawłowski  
Prof. Dr. Joerg Jaeckel

# **UV-Vervollständigung des Standardmodells: Von Baryogenese zu asymptotischer Sicherheit**

In dieser Dissertation untersuchen wir Aspekte der UV-Vervollständigung des Standardmodells der Teilchenphysik. Wir konzentrieren uns auf zwei Beispiele, die unausweichlich neue Freiheitsgrade benötigen: Baryonenasymmetrie und Quantengravitation.

Baryogenese kann am elektroschwachen Phasenübergang stattfinden, falls neue Physik den Phasenübergang zu einem der ersten Ordnung macht. Wir betrachten allgemeine Klassen von Physik jenseits des Standardmodells und zeigen, dass diese zu einer stark erhöhten Higgs-Selbstkopplung führen, wenn wir elektroschwache Baryogenese fordern. Die Higgs-Selbstkopplung wird beim Lauf des LHC mit erhöhter Luminosität genau genug gemessen werden.

Die Quantengravitation wird mit dem asymptotisch sicheren Szenario untersucht, welches die Existenz eines UV Fixpunkts des Renormierungsgruppenflusses mutmaßt. Dieser würde eine nichtperturbative Renormierung der Quantengravitation erlauben. Wir entwickeln den Zugang hin zu quantitativer Präzision durch die systematische Berechnung der Flüsse der höheren Korrelationsfunktionen. Wir beginnen von einem minimalen Setup, das eine echte, dynamische Newton-Kopplung beinhaltet. Das ist das Setup mit der Graviton-Zwei- und Dreipunktfunktion. In einer ersten Erweiterung nehmen wir die Graviton-Vierpunktfunction hinzu, was die Untersuchung von Konvergenzeigenschaften und von der Wiederherstellung von Diffeomorphismussymmetrie im IR erlaubt. In einer zweiten Erweiterung werten wir die Korrelationsfunktionen auf einem konstant gekrümmten Hintergrund aus. Davon ausgehend stellen wir die Bewegungsgleichungen auf und finden eine Lösung bei negativer Hintergrundkrümmung. Insgesamt liefern diese Resultate weitere signifikante Hinweise für die Existenz des UV Fixpunkts.

Diesem Setup der Quantengravitation fügen wir den Materieinhalt des Standardmodells hinzu. Wir beginnen mit minimal gekoppelten Skalaren und Fermionen und koppeln anschließend auch Yang-Mills-Theorie zur Quantengravitation. Wir legen ein formales Argument vor, das aussagt, dass solche Systeme mit asymptotischer Sicherheit vereinbar sein müssen, unabhängig von der Anzahl der Eich- oder Materiefelder. Weiterhin zeigen wir eine effektive Universalität zwischen verschiedenen Avataren der Newton-Kopplung, was bedeutet, dass ihre Flüsse im Skalierungsbereich des UV Fixpunktes quantitativ übereinstimmen. Diese Ergebnisse sind die Grundlage für zukünftige Untersuchungen des Standardmodells vollständig gekoppelt mit Quantengravitation.

## **Towards a UV-complete Standard Model: From baryogenesis to asymptotic safety**

In this dissertation we investigate aspects of the UV completion of the Standard Model of particle physics. We focus on two examples that inevitably require new degrees of freedom: baryon asymmetry and quantum gravity.

Baryogenesis can occur at the electroweak phase transition if new physics triggers the phase transition to be of strong first order. We consider generic classes of beyond the Standard Model physics and show that all of them give rise to a strongly enhanced Higgs self-coupling if we demand electroweak baryogenesis. The Higgs self-coupling will be measured precisely enough in the high-luminosity run of the LHC.

Quantum gravity is investigated with the asymptotic safety approach, which conjectures the existence of a UV fixed point of the renormalisation group flow. The latter allows for a non-perturbative renormalisation of quantum gravity. We develop the approach towards quantitative precision by systematically computing flows of higher-order correlation functions. We start from a minimal setup that includes a genuine Newton's coupling, which is the setup with the graviton two- and three-point function. In a first extension we include the graviton four-point function, which allows to investigate convergence properties and the restoration of diffeomorphism symmetry in the IR. In a second extension we evaluate the correlation functions on a constantly-curved background. From this we set up the equations of motion and find a solution at negative background curvature. Overall, these results add further significant evidence for the existence of the UV fixed point.

We include Standard Model matter content into the quantum gravity setup. We start with minimally coupled scalars and fermions and subsequently also couple Yang-Mills theory to quantum gravity. We provide a formal argument that such systems must be compatible with asymptotic safety independent of the number of gauge or matter fields. Furthermore we show an effective universality between different avatars of Newton's coupling, which means that their flows are in quantitative agreement in the scaling region of the UV fixed point. These results are the basis for future investigations of the Standard Model fully coupled to quantum gravity.

# Contents

<b>1. Introduction</b>	<b>11</b>
1.1. Publications . . . . .	15
1.2. Outline . . . . .	16
<b>2. Electroweak baryogenesis</b>	<b>19</b>
2.1. Introduction . . . . .	19
2.1.1. Electroweak phase transition . . . . .	20
2.1.2. Higgs self-coupling measurement . . . . .	21
2.2. Modified Higgs potentials . . . . .	23
2.3. Phase transition . . . . .	26
2.3.1. First-order phase transition . . . . .	27
2.3.2. Scale of new physics . . . . .	29
2.3.3. Baryogenesis vs Higgs self-coupling . . . . .	30
2.4. Summary . . . . .	32
<b>3. Quantum gravity introduction</b>	<b>35</b>
3.1. Introduction . . . . .	35
3.2. Diffeomorphism invariance . . . . .	37
3.2.1. Approaches to fluctuation and background correlation functions . . . . .	38
3.3. Functional renormalisation group . . . . .	39
3.3.1. Flow equation . . . . .	40
3.3.2. Vertex expansion . . . . .	40
3.4. Flows of correlation functions . . . . .	41
3.4.1. Covariant tensors and uniformity . . . . .	42
3.4.2. Projection onto $n$ -point functions . . . . .	44
3.4.3. Flow equations for the couplings . . . . .	45
3.5. Results . . . . .	46
3.5.1. Locality . . . . .	46
3.5.2. UV fixed point . . . . .	48
3.5.3. Phase diagram and flow equations . . . . .	49
3.6. Summary . . . . .	50
<b>4. Towards apparent convergence</b>	<b>51</b>
4.1. Introduction . . . . .	51
4.2. Flows of correlation functions . . . . .	52
4.2.1. Recap . . . . .	52
4.2.2. Momentum dependence of the graviton $n$ -point functions . . . . .	52
4.2.3. Higher-order vertices and the background effective action . . . . .	54
4.2.4. Flow equations for the couplings . . . . .	55
4.2.5. Disentangling $R$ and $R^2$ tensor structures . . . . .	55

4.2.6. Computational details . . . . .	57
4.3. Asymptotic safety . . . . .	57
4.3.1. UV fixed point . . . . .	57
4.3.2. Stability . . . . .	58
4.3.3. Importance of the $R^2$ tensor structure . . . . .	59
4.4. IR behaviour . . . . .	61
4.5. Towards apparent convergence . . . . .	63
4.6. Summary . . . . .	64
<b>5. Curvature dependence</b>	<b>67</b>
5.1. Introduction . . . . .	67
5.2. General framework . . . . .	68
5.2.1. Quantum and background equation of motion . . . . .	68
5.2.2. Background independence in non-perturbative expansion schemes . .	70
5.3. Vertices in curved backgrounds . . . . .	72
5.3.1. Spectral decomposition . . . . .	72
5.3.2. Vertex construction . . . . .	73
5.3.3. Flow equations and trace evaluation . . . . .	74
5.4. Results . . . . .	76
5.4.1. Fixed point solutions . . . . .	76
5.4.2. Background potential . . . . .	77
5.4.3. Quantum equation of motion . . . . .	81
5.5. Summary . . . . .	82
<b>6. Scalars &amp; fermions with gravity</b>	<b>85</b>
6.1. Introduction . . . . .	85
6.2. Functional renormalisation group . . . . .	86
6.3. Flows of correlation functions . . . . .	88
6.3.1. Matter contributions to gravity flows . . . . .	89
6.3.2. Gravity contributions to matter flows . . . . .	90
6.3.3. Anomalous dimensions . . . . .	91
6.3.4. Anomalous dimensions and bounds for the generic class of regulators	91
6.4. Results . . . . .	93
6.4.1. Pure gravity . . . . .	93
6.4.2. Scalars . . . . .	94
6.4.3. Fermions . . . . .	96
6.4.4. Mixed scalar-fermion systems . . . . .	98
6.4.5. Independence on the approximation in the gravity sector . . . . .	99
6.5. Background couplings . . . . .	99
6.5.1. Background fixed points in the full system . . . . .	101
6.5.2. Comparison to background fixed points in the literature . . . . .	102
6.6. Summary . . . . .	104
<b>7. UV dominance of gravity</b>	<b>105</b>
7.1. Introduction . . . . .	105
7.2. Asymptotic freedom & safety . . . . .	106
7.2.1. Yang-Mills coupled to gravity: the setup . . . . .	106
7.2.2. Asymptotic freedom in Yang-Mills with gravity . . . . .	107

7.2.3. Asymptotic safety in gravity with Yang-Mills . . . . .	110
7.3. Renormalisation group with YM . . . . .	111
7.4. Graviton contributions to YM . . . . .	113
7.4.1. Background observables . . . . .	114
7.4.2. Gravity supports asymptotic freedom . . . . .	115
7.5. YM contributions to gravity . . . . .	118
7.5.1. General structure . . . . .	118
7.5.2. Contributions to the graviton propagator . . . . .	118
7.5.3. Contributions to the three-point function . . . . .	119
7.5.4. Mixed graviton-gluon coupling . . . . .	120
7.5.5. Momentum locality . . . . .	121
7.6. Asymptotic safety . . . . .	121
7.6.1. Finite $N_c$ . . . . .	121
7.6.2. Large $N_c$ scaling . . . . .	122
7.6.3. Decoupling of gravity-induced gluon self-interactions . . . . .	124
7.7. UV dominance of gravity . . . . .	125
7.7.1. Dynamical scale fixing . . . . .	125
7.7.2. Results in the extended approximation . . . . .	128
7.7.3. Resumé: Signatures of asymptotic safety of Yang-Mills-gravity systems . . . . .	129
7.8. Summary . . . . .	130
<b>8. Effective universality</b>	<b>133</b>
8.1. Introduction . . . . .	133
8.2. Avatars of couplings . . . . .	134
8.2.1. Avatars of couplings in matter-gravity systems . . . . .	134
8.2.2. Effective universality . . . . .	135
8.3. RG for scalar-gravity systems . . . . .	136
8.4. Dynamical couplings . . . . .	137
8.4.1. Effective universality at the fixed point . . . . .	138
8.4.2. Quenched quantum gravity . . . . .	138
8.4.3. Unquenching quantum gravity . . . . .	141
8.4.4. Effective universality beyond the fixed point . . . . .	144
8.5. Background-fluctuation system . . . . .	146
8.5.1. Effective universality for the background Newton's coupling . . . . .	146
8.5.2. The fate of effective universality in commonly used approximations .	147
8.5.3. Effective gravitational coupling . . . . .	149
8.6. Level-one improvement . . . . .	150
8.6.1. Nielsen or split Ward identity and its applications . . . . .	150
8.6.2. Fixed-point results for level-one couplings . . . . .	153
8.7. Summary . . . . .	155
<b>9. Summary and outlook</b>	<b>157</b>
<b>A. Electroweak baryogenesis</b>	<b>163</b>
A.1. Flow equations . . . . .	163
A.2. Grid approach and benchmarking . . . . .	167
A.3. Mean-field approximation . . . . .	170

<b>B. Towards apparent convergence</b>	<b>172</b>
B.1. Approximations of the stability matrix . . . . .	172
B.2. Background couplings . . . . .	173
B.3. Identification scheme . . . . .	174
B.4. Local momentum projection . . . . .	175
B.5. Derivation of flow equations . . . . .	176
B.6. Analytic flow equations . . . . .	179
<b>C. Curvature dependence</b>	<b>181</b>
C.1. Propagator . . . . .	181
C.2. Flow equations . . . . .	182
C.3. Check of approximations . . . . .	183
C.4. Insensitivity on initial conditions . . . . .	184
<b>D. Scalars &amp; fermions with gravity</b>	<b>186</b>
D.1. Analytic flow equations . . . . .	186
D.2. Background quantities . . . . .	186
<b>E. UV dominance of gravity</b>	<b>187</b>
E.1. Regulators . . . . .	187
E.2. Regulator dependence of the gluon contribution to the graviton mass parameter . . . . .	187
E.3. Scaling equations . . . . .	188
E.4. Flow equations . . . . .	190
E.5. Coefficients in the scaling equations . . . . .	192
<b>F. Effective universality</b>	<b>193</b>
F.1. Background flow equations . . . . .	193
F.2. Level-1 flow equations . . . . .	193
F.3. Evaluation of traces . . . . .	194
<b>Acknowledgements</b>	<b>198</b>
<b>Bibliography</b>	<b>200</b>



# 1. Introduction

The Standard Model of particle physics is a great success story for physics. It is based on Abelian and non-Abelian gauge theories [8, 9]. The underlying gauge group is  $U(1) \otimes SU(2) \otimes SU(3)$  [10–13]. The last missing piece was found at the Large Hadron Collider (LHC) [14] in 2012: the discovery of the predicted Higgs boson [15–18]. The Standard Model successfully predicts cross sections that are measured at the LHC within the error bars. This is for instance impressively seen at the precisely measured and with theory predictions agreeing Higgs production and decay rates [19]. This demonstrates the remarkable understanding of fundamental physics at the TeV scale, but also leaves scientists without hints for new physics. Importantly, new physics is not optional since there is a rich phenomenology that is so far not explained by the Standard Model. This phenomenology includes for instance dark matter, dark energy, the matter-antimatter asymmetry, neutrino masses and even gravity. We further know that the Standard Model is not a fundamental theory: it cannot be valid on all energy scales since some of its couplings run into a Landau pole [20]. In this dissertation we work towards the ultraviolet (UV) completion of the Standard Model and focus on the matter-antimatter asymmetry as well as the inclusion of quantum gravity.

This dissertation can be seen as a journey from the energy scales of the LHC where we probe electroweak baryogenesis up to energy scales beyond the Planck scale where we combine the Standard Model with quantum gravity. For this introduction we let us guide by the perturbative running of the marginal Standard Model couplings to higher energy scales [21–23], also displayed in Fig. 1.1. This point of view allows to start from the well known physics at the LHC and to go further into the realm of potential new physics. We gain an upper bound on the energy scale where the Standard Model is certainly not predictive anymore.

The first topic of this dissertation, the observed matter-antimatter asymmetry in the universe [24], is investigated at the smallest energy scales considered in this dissertation, at the electroweak phase transition. Already in 1963, three necessary conditions for baryogenesis were formulated by Sakharov [25]. The first condition is the existence of baryon number violating processes. In the Standard Model this can happen via non-perturbative sphaleron processes associated to the degenerate minima of the electroweak sector [26–29]. The second condition is charge (C) and charge-parity (CP) violation. The Cabibbo–Kobayashi–Maskawa (CKM) matrix [30, 31] contains a small CP violation, which however appears too small to account for the observed baryon asymmetry [32]. Higher dimensional operators can induce another source of CP violation [33, 34]. The last condition is the departure from thermal equilibrium. Consequently the electroweak phase transition seemed predestined for baryogenesis: if the electroweak phase transition is of strong first order then all conditions are fulfilled [35]. The sphaleron processes can generate the asymmetry in the bubble walls of the expanding regions with broken electroweak symmetry [36, 37]. Lattice and perturbative computations showed that this scenario is very sensitive to the value of the Higgs mass [38–42]. Only with a Higgs mass well below the measured 125 GeV the electroweak phase transition is first order and thus this simple

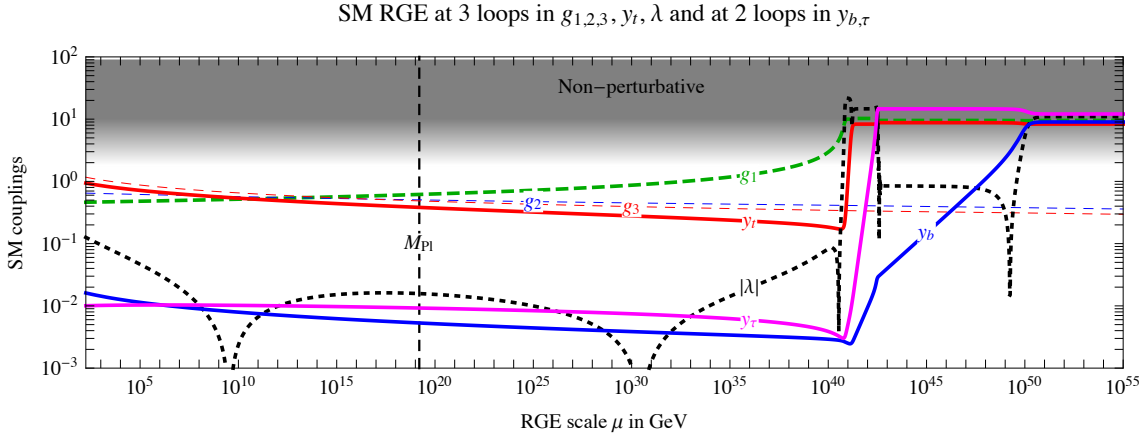


Figure 1.1.: Perturbative running of the marginal Standard Model couplings at two/three-loop order. Displayed are the gauge couplings  $g_1$ ,  $g_2$  and  $g_3$  corresponding to the gauge groups  $U(1)$ ,  $SU(2)$  and  $SU(3)$ , respectively, the top quark, bottom quark and tau lepton Yukawa couplings,  $y_t$ ,  $y_b$  and  $y_\tau$ , as well as the absolute value of the quartic Higgs coupling  $|\lambda|$ . Certain three-loop contributions were artificially removed from the beta functions in order to continue the running beyond  $10^{40}$  GeV. The figure is taken from [23].

scenario was soon excluded. Consequently other alternatives were explored as for example baryogenesis via leptogenesis [43–48]. This scenario introduces new degrees of freedom, usually heavy neutrinos that are the seesaw partners of the light neutrinos. However, there is no measurable impact at low energy scales in most leptogenesis scenarios.

In this dissertation electroweak baryogenesis is investigated with respect to measurable consequences. In the Standard Model electroweak baryogenesis is not possible, but with the appropriate beyond Standard Model physics the phase transition becomes first order [49–51]. This can cause measurable consequences for example in the Higgs self-couplings [52–54]. It is of great interest to map out large classes of beyond the Standard Model physics on their measurable impact at the LHC if electroweak baryogenesis is demanded. This is precisely where this dissertation contributes.

We now increase the energy scales and follow the Standard Model couplings in Fig. 1.1. Interestingly the quartic Higgs coupling  $\lambda$  turns negative at roughly  $10^{10}$  GeV. While a naive point of view associates this with an instability in the Higgs potential, a more elaborate Coleman-Weinberg resummation [55] shows that the electroweak minimum of the Higgs potential is only metastable [56–60]. The true vacuum of the theory lies beyond the Planck scale and the tunnelling time to this minimum is much larger than the age of the universe [61]. These statements are very sensitive to the precise mass of the top quark [62]. The latter is extracted from the LHC data via Monte-Carlo event generators and the relation of this Monte-Carlo mass to the pole mass causes a significant uncertainty [63–65]. A precise measurement of the top pole mass would be provided by an electron-positron collider at sufficiently large energies, such as the planned International Linear Collider [66]. In such colliders the relation between experimental observables and the mass schemes is well understood [67–69]. Thus, the electroweak minimum might be stable within the error bars of the top pole mass. But even assuming metastability, the metastable vacuum seems to survive all tests: for instance after inflation the Higgs field appears to settle in

the electroweak minimum [70–73]. Due to these findings, it is widely believed that the Standard Model can be extended up to the Planck Scale. Indeed recent approaches added new physics at the Planck scale and investigate observable effects in the infrared (IR) [74–76]. In this dissertation we also pursue this attitude and continue with modifications at the Planck scale.

The Planck scale is of great importance as it is the scale where quantum gravity effects set in. The fundamental force of gravity has so far not been incorporated into the Standard Model. The reason is the seemingly different nature of gravity compared to the other fundamental forces. Quantum gravity based on the Einstein-Hilbert action is perturbatively non-renormalisable: the first hint is the negative canonical mass dimension of Newton's coupling. Actual computations of the one-loop [77] and two-loop [78–80] divergences reveal that at the two-loop level the infamous Goroff-Sagnotti counter term cannot be reabsorbed into terms of the Einstein-Hilbert action. This is interpreted as the onset of an infinite number of counter terms that necessarily need to be introduced and hence the theory is not predictive. On the other hand, quantum gravity based on higher-derivative gravity is either perturbatively non-unitary and perturbatively renormalisable or still perturbatively non-renormalisable [81–83]. There are further conceptual issues, for example that quantum field theories usually are constructed on flat spacetime, while it is not possible to define a unique ground state on generically curved backgrounds. But of course a generically curved background is inherently necessary for a correct description of gravity. All these problems have led in the past to many different approaches to quantum gravity: string theory [84–89], loop quantum gravity and spin foams [90–97], asymptotic safety [98–101], causal and euclidean dynamical triangulations [102–106], Hořava-Lifshitz gravity [107–110], causal sets [111–113], and many more. Some of them are continuum approaches and others are lattice approaches. All of them are facing different conceptual and technical issues, and even worse, a lack of quantum gravity measurements. The latter asks for clear guidelines for the construction of a theory of quantum gravity. Indeed many different guidelines can be found in the above named approaches: starting from Occham's razor, over the resolution of black hole or cosmological singularities [114, 115] or the black hole information paradox [116–118], to postdictions of the Standard Model parameters [119, 120]. Even the requirement to fully reproduce all Standard Model measurements is not as trivial as it might appear. For example graviton fluctuations could induce chiral symmetry breaking and thus enforce that all fermions have a mass of the order of the Planck mass [121, 122].

In this dissertation we work with asymptotically safe quantum gravity. Compared to the other approaches above it is based on a rather small set of assumptions. It is based on non-perturbative continuum quantum field theory methods. The metric carries the fundamental degrees of freedom and diffeomorphism invariance is the underlying symmetry. Importantly, asymptotic safety conjectures the existence of a non-trivial UV fixed point of the renormalisation group flow. The idea was brought up by Weinberg in 1976 [98] and soon investigated afterwards in  $d < 4$  spacetime dimensions [123–125]. The first work in  $d = 4$  spacetime dimensions was the pioneering work of Reuter [99]. The concept of asymptotic safety can be viewed as a generalisation of asymptotic freedom [126–130]. The investigation of this scenario requires non-perturbative continuum computations that are provided by functional methods. These methods are based on the renormalisation group idea [131–134] and implemented via Dyson-Schwinger equations [135–137], the Wegner-Houghton equation [138],  $n$ -PI approaches [139], the Polchinski equation [140], or the

Wetterich equation [141]. Due to its fundamental one-loop structure and many different systematic approximation schemes the Wetterich equation in particular is predestined for computations in asymptotically safe quantum gravity. In fact almost all computations up today utilise this equation, also called the functional renormalisation group. Asymptotically safe quantum gravity must in the end account for non-perturbative renormalisability, predictivity and unitarity. Non-perturbative renormalisability corresponds precisely to the existence of the conjectured UV fixed point and predictivity to a finite number of relevant directions at this fixed point. The question of non-perturbative unitarity has to be clarified most likely on the level of the resulting spectral functions. This dissertation contributes to this approach by providing further evidence for the existence of the non-trivial UV fixed point and corroborating that there is only a finite number of relevant directions. A more detailed introduction to asymptotically safe quantum gravity can be found in [Chapter 3](#).

If we leave quantum gravity aside, we can still increase the energy scales and follow the perturbative running of the marginal Standard Model couplings, as depicted in [Fig. 1.1](#). At roughly  $10^{30}$  GeV the quartic Higgs coupling becomes positive again, which ensures that the electroweak vacuum is metastable. At even higher energy scales we find the certain end of predictivity of the Standard Model: at around  $10^{40}$  GeV the  $U(1)$  hypercharge coupling  $g_1$  reaches its Landau pole [20]. In [Fig. 1.1](#) the authors artificially removed the bottom and tau Yukawa contributions to the three-loop coefficients in order to avoid an explicit singularity. Nonetheless the running of the couplings is certainly untrustworthy beyond  $10^{40}$  GeV. In a subsystem of the Standard Model without the  $U(1)$  hypercharge coupling also the quartic Higgs coupling reaches a Landau pole. The existence of these Landau poles has also been confirmed with non-perturbative methods [142–144]. If one insists to make these theories fundamental, the trivial theory is the only solution [145]. These Landau poles have to be resolved in order to make extensions of the Standard Model a fundamental theory. This can be accomplished for example with asymptotically safe extensions of the Standard Model. A large number of new degrees of freedom guarantee a perturbative non-Gaussian UV fixed point. These theories are constructed such that they could be valid on all energy scales and are thus UV complete [146–150]. Considering the combined quantum gravity and Standard Model theory one has to check whether gravity removes these Landau poles and renders the UV behaviour finite. First positive indications in this direction have been gathered [151, 152]. This dissertation contributes to this topic by setting up a quantum gravity system with Standard Model matter content that is orientated towards quantitative precision by computing higher-order correlation functions. This is the basis for future investigations of the fully coupled Standard-Model–gravity system, which can clarify the existence or absence of Landau poles in the theory.

In summary, the Standard Model definitely has a maximum range of validity. Where the validity ends can of course only be determined by measurements. From a theoretical view point it is however a formidable task to determine the necessary and possible extensions in order to make the Standard Model a fundamental theory, which is valid on all energy scales. This is the overarching goal of this dissertation. With baryogenesis and gravity we focus on two examples that inevitably require new degrees of freedom. In case of quantum gravity the challenge is to get quantitative control over the Standard-Model–gravity system and thus the quantum gravity projects in this dissertation work towards higher-order computations of asymptotically safe quantum gravity. The individual projects are motivated in the respective chapters.

## 1.1. Publications

The compilation of this dissertation was solely performed by the author. The presented results were obtained with various collaborators, which is highly appreciated by the author. Most of the results are already published. They are available as preprint and partly as journal published version. The publications are:

[1] **Local Quantum Gravity**

Nicolai Christiansen, Benjamin Knorr, Jan Meibohm, Jan M. Pawłowski, Manuel Reichert

Published in Phys.Rev. D92 (2015) no.12, 121501

E-Print: arXiv:1506.07016 [hep-th]

Comment: Parts of [Chapter 3](#) are based on this publication.

[2] **Asymptotic safety of gravity-matter systems**

Jan Meibohm, Jan M. Pawłowski, Manuel Reichert

Published in Phys.Rev. D93 (2016) no.8, 084035

E-Print: arXiv:1510.07018 [hep-th]

Comment: [Chapter 6](#) and App. [D](#) are based on this publication.

[3] **Towards apparent convergence in asymptotically safe quantum gravity**

Tobias Denz, Jan M. Pawłowski, Manuel Reichert

E-Print: arXiv:1612.07315 [hep-th]

Comment: [Chapter 4](#), parts of [Chapter 3](#) and App. [B](#) are based on this publication.

[4] **One force to rule them all: asymptotic safety of gravity with matter**

Nicolai Christiansen, Daniel F. Litim, Jan M. Pawłowski, Manuel Reichert

E-Print: arXiv:1710.04669 [hep-th]

Comment: [Chapter 7](#) and App. [E](#) are based on this publication.

[5] **Probing Baryogenesis through the Higgs Self-Coupling**

Manuel Reichert, Astrid Eichhorn, Holger Gies, Jan M. Pawłowski, Tilman Plehn, Michael M. Scherer

Accepted for publication in Phys.Rev. D

E-Print: arXiv:1711.00019 [hep-ph]

Comment: [Chapter 2](#) and parts of App. [A](#) are based on this publication.

[6] **Curvature dependence of quantum gravity**

Nicolai Christiansen, Kevin Falls, Jan M. Pawłowski, Manuel Reichert

Published in Phys.Rev. D97 (2018) no.4, 046007

E-Print: arXiv:1711.09259 [hep-ph]

Comment: [Chapter 5](#), parts of [Chapter 3](#) and App. [C](#) are based on this publication.

[7] **Effective universality in quantum gravity**

Astrid Eichhorn, Peter Labus, Jan M. Pawłowski, Manuel Reichert

In preparation

Comment: [Chapter 8](#) and App. [F](#) are based on this publication in preparation.

## 1.2. Outline

In this dissertation [Chapter 2](#) concerns itself with electroweak baryogenesis, while [Chapter 3](#), [4](#) and [5](#) deal with pure quantum gravity, and finally in [Chapter 6](#), [7](#) and [8](#) quantum gravity is coupled to Standard Model matter content. Consequently [Chapter 3](#) and [Chapter 6](#) contain longer introductions to asymptotically safe quantum gravity and quantum gravity with matter, respectively. The introductions in [Chapter 4](#), [5](#), [7](#) and [8](#) are kept slightly shorter. In more details, this dissertation is structured in the following way:

[Chapter 2](#) is dedicated to electroweak baryogenesis and its measurable consequences at the LHC. We give a detailed introduction on the topics baryogenesis, electroweak phase transition and the measurement of Higgs self-couplings. The beyond Standard Model physics, which triggers the first-order phase transition, is parameterised via modifications of the Higgs potential. The focus is put on polynomial and non-polynomial modifications, where the latter cannot be Taylor expanded around a vanishing field value. We show that all of these modifications can lead to a first-order phase transition and the scale where these systems become strongly coupled is of the order of 10 TeV. Most importantly, all modifications lead to strongly enhanced Higgs self-couplings measurable at the high-luminosity run of the LHC. This chapter focuses on phenomenology and thus does not contain many technical details, for instance the functional renormalisation group is used but not introduced.

In [Chapter 3](#) we introduce asymptotically safe quantum gravity. We present the functional renormalisation group and the systematic vertex expansion scheme that we use throughout the quantum gravity part of this dissertation. There will be a focus on the arising non-trivial Nielsen identities as well as their relation to background independence and diffeomorphism invariance. We set up the minimal quantum gravity truncation that contains a genuine dynamical Newton's coupling. It includes the graviton two- and three-point function. We show that the Wilsonian RG is well defined in such a system as the flows of all correlation functions are momentum local. As a main result we find a UV fixed point with two relevant directions in this truncation. In the subsequent chapters we build upon this minimal setup.

In [Chapter 4](#) we extend the truncation to the graviton four-point function. This is not only a significant, technical challenging improvement of the truncation, but also allows to disentangle contributions from  $R^2$  and  $R_{\mu\nu}^2$  tensor structures. It turns out that the  $R_{\mu\nu}^2$  tensor structures are non-trivially suppressed while the  $R^2$  tensor structures are dynamically generated. We find a UV fixed point in this truncation with three relevant directions due to the overlap with  $R^2$ . We will present extensive studies of the apparent convergence properties as well as results towards the restoration of diffeomorphism symmetry in the IR. Indeed the UV fixed point and its critical exponents become less sensitive with respect to closure of the flow equations compared to the previous truncation.

In [Chapter 5](#) we investigate the background curvature dependence of quantum gravity. To that end we construct an approximate momentum space on constantly curved backgrounds that allows to use the previously developed techniques on a flat background. We obtain fixed point functions that depend on the background curvature and this allows for the first time to disentangle the quantum and background equation of motion. We argue that the quantum equation of motion is the relevant one at the UV fixed point. and we indeed find a solution with the presented fixed point functions at negative background curvature. We check the stability of this solution with respect to changes of the truncation.

In [Chapter 6](#) we add  $N_s$  minimally coupled scalars and  $N_f$  minimally coupled fermions to the setup of asymptotically safe quantum gravity. We further introduce a reliability bound on generic classes of regulators commonly used in the literature. We analyse the UV fixed point from [Chapter 3](#) as a function of  $N_s$  and  $N_f$ . We find that fermions are generically stabilising the system and all  $N_f$  are compatible with asymptotic safety. For scalars we encounter the above mentioned reliability bound at  $N_s \approx 21$ . This prevents us to go to large numbers of  $N_s$  and draw final conclusions. Generally we find qualitative differences to results in the background field approximation, which cast doubts on the use of this approximation.

In [Chapter 7](#) we couple a  $SU(N_c)$ -Yang-Mills theory to gravity. We manifest results from the literature that the gravity contribution to Yang-Mills preserves asymptotic freedom in the gauge sector. This allows us to make a formal argument for all gravitationally coupled matter-gauge-gravity systems. By first integrating out the matter or gauge fields and then subsequently the gravity system we find that the system must remain asymptotically safe independent on numbers of matter or gauge fields. This argument includes the scalar-fermion-gravity system from [Chapter 6](#) and these results are reassessed. We support the formal argument with explicit computations. We indeed find that the system is compatible with asymptotic safety for all  $N_c$  and we provide explicit results for  $N_c \rightarrow \infty$ . The underlying physics can manifest itself in different ways depending on the choice of regulators and we show that although we find a strong scheme dependence that the physics remains the same.

In [Chapter 8](#) we introduce and investigate the concept of effective universality in a scalar-gravity system. The concept is similar to two-loop universality in gauge theories. We show that gravity couplings originating from different vertices, in our case the three-graviton- and the graviton-scalar-vertex, agree on a semi-quantitative level, if they are evaluated in the scaling region of the UV fixed point. This highly non-trivial result lays the basis for future truncations that allow the identifications of different avatars of Newton's coupling. We further try to devise simple truncations that contain this effective universality and are based on heat-kernel techniques. We upgrade background couplings to level-one couplings with the use of Nielsen identities. These level-one couplings do however not fully imitate the running of the fluctuation system, which highlights again that at least a level-two computation is necessary.

Finally, in [Chapter 9](#) we give a general summary and outlook. In the subsequent appendices many technical details as well as analytic flow equations are presented.



## 2. Probing electroweak baryogenesis at the LHC

### 2.1. Introduction

The existence of a scalar Higgs potential is the most fundamental insight from the LHC to date. It is based on the observation of a likely fundamental Higgs scalar in combination with measurements of the massive electroweak bosons, fixing the infrared theory and its model parameters after electroweak symmetry breaking to high precision. The one remaining parameter is the Higgs self-coupling and its relation to the Higgs mass, defining a standard benchmark measurement for current and future colliders. This in itself very interesting measurement may also be related to more fundamental physics questions. A prime candidate for such a question is electroweak baryogenesis, specifically the nature of the electroweak phase transition.

For the single Higgs boson of the renormalizable Standard Model we can test the electroweak phase transition through the Higgs mass. Here, electroweak baryogenesis [25, 32, 35, 153–160] requires a Higgs mass well below the observed value of 125 GeV [33, 38–42, 161, 162]. Only then will the electroweak phase transition be strongly first-order. If we consider the Standard Model an effective field theory (EFT), a sizeable dimension-6 contribution to the Higgs potential,  $(\phi^\dagger \phi)^3/\Lambda^2$ , is known to circumvent this bound [52, 54, 163–173]. In principle, this scenario can be tested through a measurement of the Higgs self-coupling at colliders [52, 54, 165–175]. The problem with this link is that the new-physics scale required by a first-order phase transition is typically not large,  $\Lambda \gtrsim v = 246$  GeV. If LHC data should indeed point to a dimension-6 Lagrangian with a low new-physics scale, we will see this in many other channels long before we will actually measure the Higgs self-coupling [176]. As a matter of fact, a global analysis of the effective Higgs Lagrangian including  $(\phi^\dagger \phi)^3/\Lambda^2$  might never probe the required values of the Higgs self-coupling once we take into account all operators and all uncertainties, so it hardly serves as a motivation to measure a Standard Model like Higgs self-coupling.

In this dissertation we take a slightly different approach. First, we assume that the new physics responsible for the strong first-order electroweak phase transition only appears in the Higgs sector. In the EFT framework we would consider, for example, the operator  $(\phi^\dagger \phi)^3/\Lambda^2$  [52, 54, 165–173]. While this approach systematically includes higher-dimensional operators in a power-counting expansion, it is not at all guaranteed that such an expansion is appropriate for the underlying new physics. Furthermore, a description of first-order phase transitions requires to extract global information about the effective potential. Again, a simple polynomial expansion around a vanishing Higgs field might not be sufficient to resolve the fluctuation-driven competition between different minima of the effective potential that induce a first-order phase transition.

A simple global approximation to the effective potential is provided by mean-field theory, which works remarkably well for Standard Model parameters [75, 177–183] because of the dominance of the top quark. Depending, however, on the strength of the bosonic and

order-parameter fluctuations in the new physics model, mean-field approaches may become unreliable. We demonstrate this explicitly using a simple example case. This situation calls for non-perturbative methods. Recently, lattice simulations have been used to study the possibility of first-order phase transition in the presence of the operator  $(\phi^\dagger \phi)^3/\Lambda^2$ , both in a Higgs-Yukawa model [184, 185] and in a gauged-Higgs system [186]. Here we use the functional renormalization group (FRG) [141] as a non-perturbative tool, for reviews see, e.g. [187–190]. It is able to provide global information about the Higgs potential, bridge a wide range of scales, include fluctuations of bosonic and fermionic matter fields as well as gauge bosons and deal with extended classes of Higgs potentials. The two questions which will guide us are:

1. Do extended Higgs potentials help with electroweak baryogenesis?
2. Can they be systematically tested by measuring the Higgs self-coupling?

We study the influence of operators or functions of operators in the Higgs sector on the electroweak phase transition using several representative examples. We determine the consequences for the Higgs self-coupling for suitable extended Higgs potentials supporting electroweak baryogenesis and being compatible with the standard-model mass spectrum.

The global properties of the Higgs potential are also intimately related to the questions of vacuum stability and Higgs mass bounds [21, 58, 191]. In fact, higher-dimensional operators can also increase the stability regime of the vacuum [74, 180–182, 184, 185, 192–199]. The example Higgs potentials studied in this dissertation suggest new-physics scales well below a possible instability scale of  $10^{10\cdots 12}$  GeV of the Standard Model. While vacuum instability is therefore not an issue for our study, extended potentials generally do have the potential to both support electroweak baryogenesis and stabilize the Higgs vacuum. A measurement of the Higgs self-coupling can therefore be indicative for both aspects.

### 2.1.1. Electroweak phase transition

The asymmetry between the matter and anti-matter contents in the Universe is one of the great mysteries in cosmology and particle physics. Experimentally, the effective absence of anti-matter in the Universe has been proven in many different ways [24]. A quantitative measurement is given by the baryon-to-photon ratio  $n_B/n_\gamma \approx 6 \cdot 10^{-10}$ , which is many orders of magnitude larger than what we would expect from the thermal history in the presence of anti-matter. It can be explained by a small initial asymmetry in the number of baryons and anti-baryons that leads to a finite density of baryons after essentially all anti-baryons have annihilated away.

Theoretically, the mechanisms behind the baryon asymmetry are well understood. Most notably, it can be shown that the presence of an asymmetry is equivalent to the three Sakharov conditions for our fundamental theory [25, 32, 35, 154]: baryon number violation, C as well as CP violation, and departure from thermal equilibrium. The first two conditions can be probed by precision measurements of the Lagrangian of the Standard Model and its extensions. The third condition can in principle be achieved at the time of the electroweak phase transition, where it then requires a strong first-order phase transition. The nature of the electroweak phase transition can be read off from the scalar potential in or beyond the Standard Model.

The strength of the phase transition that occurs at the critical temperature  $T_c$  is measured by the ratio  $\phi_c/T_c$ , where  $\phi_c = \langle \phi \rangle_{T_c}$  is the expectation value of the Higgs at the

critical temperature. The critical temperature describes the transition where for small temperatures  $T < T_c$  the potential exhibits a single, non-trivial minimum for some value of the scalar field  $\phi$ . The field value at the minimum is temperature dependent, approaching  $v = 246$  GeV for  $T \rightarrow 0$ . With increasing temperature, a second minimum at zero field value and with an unbroken electroweak symmetry appears in a first-order scenario. At the critical temperature  $T_c$ , the two minima of the potential, i.e. the one at finite field value and the one at vanishing field value are degenerate, and the system undergoes a phase transition from the symmetry-broken regime with a finite Higgs expectation value to the symmetric regime.

The field value at the minimum constitutes an order parameter. For  $\phi_c \neq 0$  the transition is of first order, i.e. the vacuum does not evolve continuously through the phase transition. For electroweak baryogenesis, the transition has to be a strong first-order one,

$$\frac{\phi_c}{T_c} \gtrsim 1, \quad (2.1)$$

otherwise the baryon asymmetry is washed out [42].

### 2.1.2. Higgs self-coupling measurement

At energy scales relevant for the LHC, the self-interaction of the Higgs boson is described by the infrared (IR) Higgs potential in the broken phase. In the renormalizable Standard Model, and ignoring Goldstone modes, it reads at tree level

$$V = \frac{\mu^2}{2} (v + H)^2 + \frac{\lambda_4}{4} (v + H)^4, \quad (2.2)$$

where  $H$  is the physical Higgs field. The two parameters describing the Standard Model Higgs potential in the IR,  $\mu$  and  $\lambda_4$ , can be traded for the vacuum expectation value  $v$  and the Higgs mass  $m_H$  (we use the conventions of [200])

$$v = \sqrt{\frac{\mu^2}{2\lambda_4}} = 246 \text{ GeV}, \quad m_H = \sqrt{2\lambda_4} v = 125 \text{ GeV}. \quad (2.3)$$

The interaction between three and four physical Higgs bosons in the Standard Model is then given by

$$\lambda_{H^3,0} = \frac{3m_H^2}{v}, \quad \lambda_{H^4,0} = \frac{3m_H^2}{v^2}. \quad (2.4)$$

In the limit of heavy top quarks,  $2m_t > m_H$ , an effective Higgs–gluon Lagrangian [201–203]

$$\mathcal{L}_{ggH} = \frac{\alpha_s}{12\pi} G^{\mu\nu} G_{\mu\nu} \log\left(1 + \frac{H}{v}\right) = \frac{\alpha_s}{12\pi} G^{\mu\nu} G_{\mu\nu} \frac{1}{v} \left(H - \frac{H^2}{2v} + \dots\right), \quad (2.5)$$

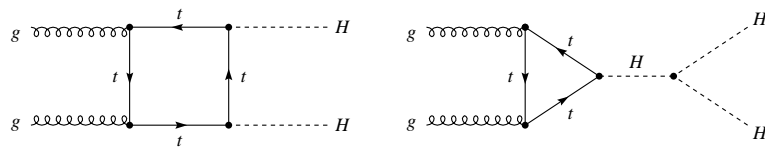


Figure 2.1.: Feynman diagrams contributing to Higgs pair production at the LHC. Figure from Ref. [174, 175].

with the gluon field strength tensor  $G_{\mu\nu}$  and the strong coupling  $\alpha_s$ , can be used to describe many relevant LHC observables.

When we include new physics contributions in the Higgs potential, the relations in (2.3) change. It is instructive to follow the simple example of the modified Higgs potential (again, with exception of a different normalization of  $\lambda_6$  we use the conventions of [200])

$$V = \frac{\mu^2}{2} (v + H)^2 + \frac{\lambda_4}{4} (v + H)^4 + \frac{\lambda_6}{\Lambda^2} (v + H)^6. \quad (2.6)$$

The modified relations between the observables become

$$\begin{aligned} m_H &= \sqrt{2\lambda_4} v \left( 1 + 12 \frac{\lambda_6 v^2}{\lambda_4 \Lambda^2} \right), \\ \lambda_{H^3} &= \frac{3m_H^2}{v} \left( 1 + \frac{16\lambda_6 v^4}{m_H^2 \Lambda^2} \right) \equiv \lambda_{H^{3,0}} \left( 1 + \frac{16\lambda_6 v^4}{m_H^2 \Lambda^2} \right), \\ \lambda_{H^4} &= \frac{3m_H^2}{v^2} \left( 1 + \frac{96\lambda_6 v^4}{m_H^2 \Lambda^2} \right) \equiv \lambda_{H^{4,0}} \left( 1 + \frac{96\lambda_6 v^4}{m_H^2 \Lambda^2} \right). \end{aligned} \quad (2.7)$$

Because  $m_H$  and  $v$  have to keep their measured values, we need to adjust  $\lambda_4$  to compensate for the effect of  $\lambda_6$  on the Higgs mass. This shift has to be accounted for in the expressions for the Higgs self-couplings as a function of  $m_H$  and  $v$ . The reference couplings  $\lambda_{H^n,0}$  keep their Standard Model values in terms of the unchanged parameters  $m_H$  and  $v$ , but the physical Higgs couplings  $\lambda_{H^n}$  change.

The standard channel to measure  $\lambda_{H^3}$  at the LHC is Higgs pair production in gluon fusion, as illustrated in Fig. 2.1, [174, 175, 204–212]. Its production rate is known including NLO [213–215] and NNLO [216–219]. One of the problems with such a measurement is that the link between the total di-Higgs production rate and the Higgs self-coupling requires us to know the top Yukawa coupling. An appropriate framework is the global Higgs analysis [176, 220–225], which is expected to give at best a 10% measurement of the top Yukawa coupling. A model-independent precision measurement of the top Yukawa coupling at the per-cent level will only be possible at a 100 TeV collider [226, 227].

The experimental situation improves once we include kinematic information in the di-Higgs production process. Two kinematic regimes are well known to carry information on the Higgs self-coupling, both exploiting the (largely) destructive interference between the two graphs shown in Fig. 2.1. While the continuum contribution dominates over most of the phase space, the two diagrams become comparable close to threshold [174, 175, 207–209]. The low-energy theory of (2.5) gives us for the combined di-Higgs amplitude

$$\mathcal{A} \propto \frac{\alpha_s}{12\pi v} \left( \frac{\lambda_{H^3}}{s - m_H^2} - \frac{1}{v} \right) \xrightarrow{\lambda_{H^3} = \lambda_{H^{3,0}}} \frac{\alpha_s}{12\pi v^2} \left( \frac{3m_H^2}{3m_H^2 - 1} \right) = 0 \quad \text{for } m_{HH} \rightarrow 2m_H, \quad (2.8)$$

where  $m_{HH}$  is the invariant di-Higgs mass. An exact cancellation occurs in the Standard Model. Whereas the heavy-top approximation is known for giving completely wrong kinematic distributions for Higgs pair production [174, 175], it does correctly predict this threshold behaviour. Note that the momenta of the outgoing particles in such processes are typically small compared to the Higgs mass and the low-energy regime of the theory is probed. In the analysis in Sec. 2.3, we thus read off the Higgs self-couplings from the low-energy effective potential.

The second relevant kinematic regime is boosted Higgs pair production [228, 229], because of top threshold contributions to the triangle diagram around  $m_{HH} = 2m_t$ . In terms of the transverse momentum this happens around  $p_{T,H} \approx 100$  GeV, where the combined amplitude develops a minimum for large Higgs self-couplings.

At the LHC, we define di-Higgs signatures simply based on Higgs decay combinations. The most promising channel is the  $b\bar{b}\gamma\gamma$  final state [211, 230–234], where we can easily reconstruct one of the two Higgs bosons and measure the continuum background in the side bands. We can also use the  $b\bar{b}\tau\tau$  final state [210, 228, 229], assuming very efficient tau-tagging. The combination  $b\bar{b}WW$  [235] requires an efficient suppression of the  $t\bar{t}$  background, while the  $4b$  [210, 236–238] and  $4W$  [174, 175, 239] signatures are unlikely to work for Standard Model like Higgs bosons. Finally, the  $b\bar{b}\mu\mu$  is in many ways similar for the  $b\bar{b}\gamma\gamma$  channel [211], but with a much lower rate in the Standard Model.

To get an idea of what to expect, we quote the optimal reach of the high-luminosity LHC run with  $3 \text{ ab}^{-1}$ , based on the Neyman-Pearson theorem applied to the  $b\bar{b}\gamma\gamma$  channel for self-couplings relatively close to the Standard Model [230],

$$\frac{\lambda_{H^3}}{\lambda_{H^3,0}} = 0.4 \dots 1.7 \quad \text{at 68\% CL,} \quad (2.9)$$

so any value for  $\lambda_{H^3}/\lambda_{H^3,0}$  outside the range given above will not be compatible with the vanishing di-Higgs amplitude in (2.8). This reach will be improved when we combine several Higgs decay channels, but will also suffer from systematic uncertainties. In addition, it assumes a perfect knowledge of the top Yukawa coupling. This implies that models that predict a change in the Higgs self-coupling by less than 50% will not be testable at the LHC.

## 2.2. Modified Higgs potentials

Similar to the EFT approach we assume that beyond a ultraviolet (UV) scale or cutoff scale  $\Lambda$  new physics exists and modifies the form of the Higgs potential. As the additional degrees of freedom are heavy, their effects below  $\Lambda$  can be parametrized by additional terms in the Higgs potential, without modifying the propagating degrees of freedom. The details of the new physics are encoded in the initial condition for the RG flow of the Standard Model at  $k = \Lambda$ . Exploring different higher-order terms thus provides access to large classes of high-scale physics scenarios, for which we do not have to investigate the detailed matching of the additional terms in the Higgs potential and the underlying high-scale degrees of freedom at  $k = \Lambda$ .

Our system features three relevant energy scales. First, the RG scale  $k$  ranges between  $k = 0$ , where all quantum fluctuations are taken into account, and  $k = \Lambda$ , where we initialise the flow. Second, the temperature  $T$  defines the external physics scale with which we probe our system. Third, the field value  $\phi$  defines an additional, internal energy scale of our system. As is usual in EFT analyses, it is important to clearly disentangle these three scales, even though  $\phi$  and  $T$  can in principle act similarly to the RG scale  $k$  in that they suppress IR quantum fluctuations [74]. We employ a method that can straightforwardly account for the RG flow in the presence of these different scales, namely the functional renormalization group. In this setting, quantum fluctuations in the presence of further internal and external scales are taken into account by a functional differential equation that is structurally one-loop, without being restricted to a weak-coupling regime.

This provides access to classes of non-perturbative microscopic models with a manageable computational effort. Most importantly, the FRG approach enables us to keep track of the separate dependence of the potential on the RG scale  $k$ , the temperature and the field value even in cases with non-perturbative UV potentials, where for instance a mean-field approach breaks down.

For our study, we concentrate on that part of the Standard Model that is relevant for the RG flow of the Higgs potential using the framework developed in [74]. Here, we follow that framework by implementing the effects of weak gauge bosons through a fiducial coupling, and upgrade our treatment by including a thermal mass generated by the corresponding fluctuations as their leading contribution instead of implementing a fully-fledged dynamical treatment of that sector, see App. A.1 for details. Similarly, would-be Goldstone modes do not need to be considered explicitly, such that it suffices to concentrate on a real scalar field  $\phi$ , that can be described in terms of the physical Higgs field  $H$  as  $\phi = H + v$  after electroweak symmetry breaking. At the UV scale  $k = \Lambda$ , the Higgs-potential is parametrized as

$$V_{k=\Lambda} = \frac{\mu^2}{2} \phi^2 + \frac{\lambda_4}{4} \phi^4 + \Delta V, \quad (2.10)$$

where  $\Delta V$  contains the contribution of some higher dimensional operator. In principle, higher-order modifications of the Yukawa sector could also be included, cf. [198, 240–242]. We investigate three classes of modifications to the Standard Model Higgs potential:

1. additional  $\phi^6$  or  $\phi^8$  terms, which cover the leading-order terms in an effective-field theory approach and have been extensively studied in the literature [52, 54, 163–173];
2. a logarithmic dependence on the Higgs-field, inspired by Coleman-Weinberg potentials. It does not allow for a Taylor expansion around  $\phi = 0$ . Logarithmic modifications are naturally generated by functional determinants, i.e. by integrating out heavy scalars or fermions.
3. a simple example of non-perturbative contributions of the form  $\exp(-1/\phi^2)$ , i.e. an exponential dependence on the inverse field, consequently not admitting a Taylor expansion in the field around  $\phi = 0$ . This is inspired by semiclassical contributions to the path integral with  $\phi$  reminiscent to a moduli parameter of an underlying model.

We denote these modifications of the potential by

$$\begin{aligned} \Delta V_6 &= \lambda_6 \frac{\phi^6}{\Lambda^2}, & \Delta V_8 &= \lambda_6 \frac{\phi^6}{\Lambda^2} + \lambda_8 \frac{\phi^8}{\Lambda^4}, \\ \Delta V_{\ln,2} &= -\lambda_{\ln,2} \frac{\phi^2 \Lambda^2}{100} \ln \frac{\phi^2}{2\Lambda^2}, & \Delta V_{\ln,4} &= \lambda_{\ln,4} \frac{\phi^4}{10} \ln \frac{\phi^2}{2\Lambda^2}, \\ \Delta V_{\exp,4} &= \lambda_{\exp,4} \phi^4 \exp \left( -\frac{2\Lambda^2}{\phi^2} \right), & \Delta V_{\exp,6} &= \lambda_{\exp,6} \frac{\phi^6}{\Lambda^2} \exp \left( -\frac{2\Lambda^2}{\phi^2} \right). \end{aligned} \quad (2.11)$$

In all these potentials  $\Lambda$  describes a new physics scale, which absorbs the mass dimension of the Higgs field. The case of  $\phi^6/\Lambda^2$  has been explored in the literature [52, 54, 165–173] and serves as a test of our method, as discussed in App. A.2. Neither the logarithmic nor the exponential potentials can be expanded around  $\phi = 0$ , so they cannot be treated in

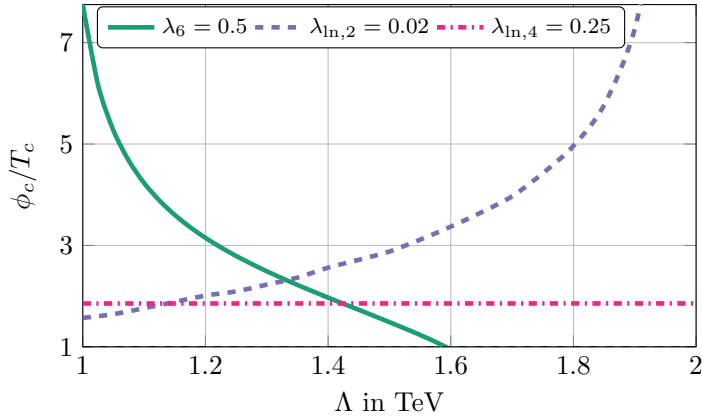


Figure 2.2.: Mean-field results for  $\phi_c/T_c$  as a function of the cutoff for different modifications of the Higgs potential. Second-order and weak first-order phase transitions are excluded from the plot. The results of the  $\phi^6$  modification are reasonable, while the results for the  $\phi^2 \ln \phi^2$  and the  $\phi^4 \ln \phi^2$  modifications are clearly unphysical, see explanation in the text. More elaborate methods than mean-field are needed.

an EFT framework. Similar bare potentials have been suggested in [75] in the context of Higgs mass bounds and vacuum stability. Instead, all potentials that can be expanded around  $\phi = 0$  can be approximated by the power-ordered, first kind of potentials. As expected by canonical power counting, terms of higher order in  $\phi$  can only play a role for very low values of  $\Lambda/v$ , unless their prefactors are non-perturbatively large. From a more general viewpoint, the set of power law, logarithmic and exponential potential functions does not only reflect the physics structures arising from local vertex expansions, one-loop determinants or semiclassical approximations. It also includes the set of functions to be expected on mathematical grounds if the effective potential permits a potentially resurgent transseries expansion [243].

To investigate the different classes of modifications, a variety of tools appears to be at our disposal, a priori ranging from mean-field techniques to non-perturbative lattice tools and functional methods. It turns out that the former are only applicable to a restricted class of potentials, not allowing us to adequately explore the full range of possible UV potentials corresponding to diverse underlying microscopic models. This is displayed in Fig. 2.2 where the  $\phi^6$ -modification of the Higgs potentials shows the expected physical behaviour as the strength of the first-order phase transition is decreasing with an increasing cutoff. The logarithmic modifications on the other hand show a rather unphysical behaviour as the strength of the first-order phase transition remains constant or even increases with the UV scale. This indicates that scalar order-parameter fluctuations are important, which are ignored in simple mean-field theory. Therefore we make use of powerful functional techniques, which treat bosonic and fermionic fluctuations on the same footing.

When allowing for modifications of the Higgs potential, we need to ensure that at  $T = 0$  the IR-values for  $\mu$ ,  $\lambda_4$ , and the top-Yukawa-coupling  $y_t$  are such that the measured observables do not change. We adjust the corresponding masses to

$$v = 246 \text{ GeV}, \quad m_H = 125 \text{ GeV}, \quad m_t = 173 \text{ GeV}. \quad (2.12)$$

Within our numerical analysis, we require  $v$  and  $m_t$  to be reproduced to an accuracy

of  $\pm 0.5$  GeV. The Higgs mass is adjusted within a somewhat larger numerical band of  $\pm 1.5$  GeV. Since it is related to the second derivative (curvature) of the potential at the minimum, a higher precision is numerically more expensive, see App. A.2 for details. Moreover, it is expected that the curvature mass used here shows small deviations from the pole mass  $m_H$  of the Higgs, see [244], and the above band also contains an estimate of this systematic error. In the symmetry broken regime, the potential given in (2.10) can be expanded in powers of  $(\phi^2 - v^2)$ . In the decoupling region in the deep IR, we use the parametrization

$$\begin{aligned} V_{k \ll v} &= \frac{\lambda_{4,\text{IR}}}{4} (\phi^2 - v^2)^2 + \frac{\lambda_{6,\text{IR}}}{8v^2} (\phi^2 - v^2)^3 + \frac{\lambda_{8,\text{IR}}}{16v^4} (\phi^2 - v^2)^4 + \dots \\ &= \lambda_{4,\text{IR}} v^2 H^2 + (\lambda_{4,\text{IR}} + \lambda_{6,\text{IR}}) v H^3 + \frac{1}{4} (\lambda_{4,\text{IR}} + 6\lambda_{6,\text{IR}} + 4\lambda_{8,\text{IR}}) H^4 + \dots \end{aligned} \quad (2.13)$$

Note that this is the full effective potential in the IR, differing from the tree-level potential in (2.6). In particular, higher-order terms, encoded in  $\lambda_{6,\text{IR}}$  are generated by quantum fluctuations even if the tree-level potential is quartic. At tree level, the Higgs potential is described by two parameters, i.e.  $\lambda_{6,\text{IR}} = \lambda_{8,\text{IR}} = \dots = 0$ . If we allow higher-order terms, all measurable parameters are affected, in close analogy to (2.7). As described in Sec. 2.1.2 the vacuum expectation value  $v$  and the Higgs mass  $m_H^2/(2v^2) \equiv \lambda_4$  are known very precisely from collider measurements and thus we have to keep them fixed. The physical Higgs self-couplings change from the values given in (2.4) to the more general form

$$\begin{aligned} \lambda_{H^3} &= \frac{\delta^3}{\delta H^3} V_{k=0} = 6v(\lambda_{4,\text{IR}} + \lambda_{6,\text{IR}}), \\ \lambda_{H^4} &= \frac{\delta^4}{\delta H^4} V_{k=0} = 6(\lambda_{4,\text{IR}} + 6\lambda_{6,\text{IR}} + 4\lambda_{8,\text{IR}}). \end{aligned} \quad (2.14)$$

The first terms are precisely the couplings  $\lambda_{H^3,0} = 6v\lambda_{4,\text{IR}}$  and  $\lambda_{H^4,0} = 6\lambda_{4,\text{IR}}$  familiar from the tree-level structure. With the present setup we can compute the Higgs self-couplings in the pure Standard Model including higher-order terms generated by quantum fluctuations by initialising the flow at some high cutoff scale without any modifications of the Higgs potential. As long as the cutoff is not too close to the electroweak scale the results will be largely independent of the cutoff choice. For our level of numerical precision, a cutoff  $\Lambda = 2$  TeV is sufficient. The Higgs self-couplings are given by

$$\frac{\lambda_{H^3}}{\lambda_{H^3,0}} \approx 0.92, \quad \frac{\lambda_{H^4}}{\lambda_{H^4,0}} \approx 0.68. \quad (2.15)$$

These values are equivalent to computations of the Higgs potential with Coleman-Weinberg corrections. We then go beyond the pure Standard Model by adjusting a combination of the coefficients  $\lambda_j$  and the new physics scale  $\Lambda$  in (2.11). These can now be used to adjust  $\phi_c/T_c$  such that we obtain a strong first-order phase transition.

### 2.3. Phase transition

For the modified Higgs potentials defined in (2.11) we need to explore which values of the UV scale  $\Lambda$  and the coefficients  $\lambda_j$  lead to a sufficiently strong first-order transition. Simultaneously, we monitor whether this leads to a measurable modification of the Higgs self-couplings in the IR.

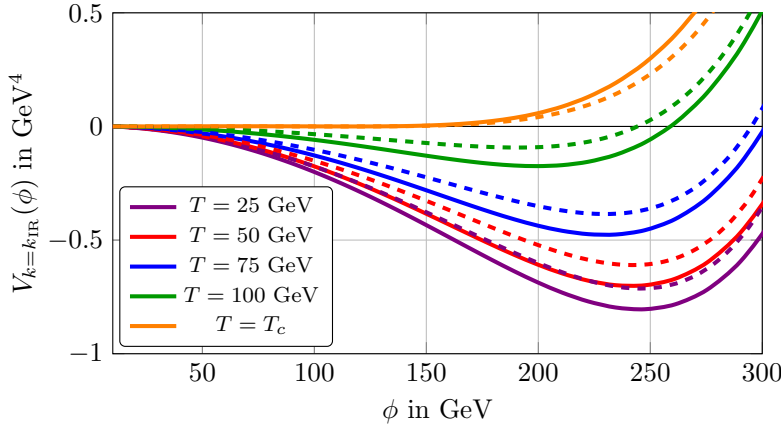


Figure 2.3.: Temperature evolution of the potentials of the type  $\phi^4 \ln \phi^2$  (solid) and  $\phi^4 \exp(-1/\phi^2)$  (dashed) for fixed  $\phi_c/T_c \approx 1$ . We plot the temperatures  $T = 25$  GeV (violet),  $T = 50$  GeV (red),  $T = 75$  GeV (blue),  $T = 100$  GeV (green) and  $T = T_c$  (orange). Note that  $T_c^{\ln,4} = 116.4$  GeV  $> T_c^{\exp,4} = 110.5$  GeV and thus one curve overtakes the other. A magnification of the curves at  $T = T_c$  is displayed in Fig. 2.4

### 2.3.1. First-order phase transition

In Fig. 2.3 we show the evolution of two example potentials from (2.11) from zero temperature to  $T_c$ , where the latter is defined as the temperature at which the two competing minima become degenerate. The latter is not distinctly apparent in Fig. 2.3, but becomes visible in the magnification in the right panel of Fig. 2.4. We also require the second minimum to be at  $\phi_c = T_c$ , to guarantee a sufficiently strong first-order phase transition. This way, the  $\phi$  dependence of the two cases becomes comparable. A key feature already visible in this figure is that the potential with the deeper minimum at small temperature turns into the steeper potential at  $T_c$ . This is achieved by a larger value of  $T_c$  for the potential with the deeper minimum. Note that the potentials in Fig. 2.3 and Fig. 2.4 are read off at the RG scale  $k_{\text{IR}}$ , which is an infrared scale where the Higgs potential and all observables are frozen out. Below this scale only convexity generating processes take place. The freeze out occurs once fluctuations of fields decouple from the RG flow because the RG scale  $k$  crosses their mass-threshold. This decoupling is built into the FRG setup. We choose  $k_{\text{IR}}$  to be smaller than the masses of the model, such that the exact choice of  $k_{\text{IR}}$  does not matter.

In Fig. 2.4 we illustrate the behaviour of all our modified Higgs potentials in the IR at vanishing temperature (left panel) and at the critical temperature (right panel), respectively. Note the different scales on the vertical axes. The UV scale  $\Lambda$  and the respective coefficients  $\lambda_j(\Lambda)$  are chosen such that they result in a strong first-order phase transition,  $\phi_c/T_c = 1$ . The different potentials at zero temperature are similar to that of the Standard Model, as expected from the fact that we fix the Higgs vacuum expectation value and mass to their observed values. In particular, the minima all appear at  $v = 246$  GeV, and the second derivatives have to reproduce the measured Higgs mass. Nevertheless, if we fix  $V_{k=k_{\text{IR}}}(0) = 0$ , an imprint of modified UV physics remains visible.

In the left panel of Fig. 2.4 we see that up to  $\phi \approx 300$  GeV, all modifications we consider lead to a very similar form of the zero-temperature IR potential, if their coefficients are

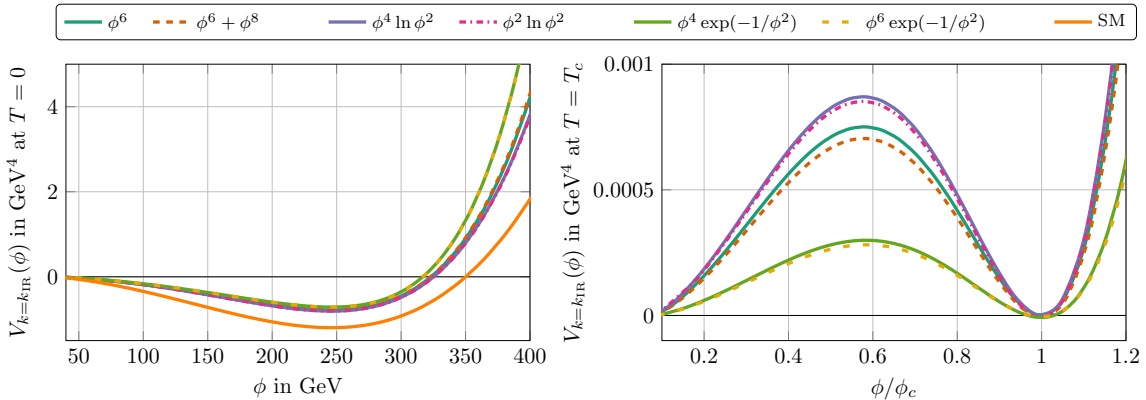


Figure 2.4.: Effective potentials at  $T = 0$  (left) and  $T = T_c$  (right). We show all modified Higgs potentials from (2.11) with  $\Lambda = 2$  TeV. The values of the coefficients at the UV scale  $\Lambda$  are fixed by the requirement  $\phi_c \approx T_c$ , leading to  $\lambda_6 = 1.2$ ,  $\lambda_6 = 1$  with  $\lambda_8 = 1.4$ ,  $\lambda_{\ln,4} = 0.89$ ,  $\lambda_{\ln,2} = 0.27$ ,  $\lambda_{\exp,4} = 23.3$ , and  $\lambda_{\exp,6} = 27.5$ .

fixed such that  $\phi_c/T_c$  is the same for all our potentials. At higher field values the different UV modifications lead to distinct field-dependence of the potential. The sizeable impact of the modified microscopic action on the IR potential is due to the finite UV scale  $\Lambda = 2$  TeV. This is not sufficiently far above the electroweak scale for the contributions  $\Delta V$  to be washed out by the RG flow.

At finite temperature, we see in the right panel of Fig. 2.4 that the potentials show significant deviations and the six different modifications fall into three distinct forms of the IR potential at  $T_c$ . The Standard Model is not displayed, since it exhibits a second-order phase transition with  $\phi_c = 0$ . The other potentials show different sizes of the bump that separates the minima at  $\phi = 0$  and  $\phi = \phi_c$ . The exponential modifications show the smallest bump, while logarithmic modifications show the largest bump. The third class is given by the polynomial UV potentials, which fall in between the two other classes.

It is worth noting that the resulting IR modifications almost coincide *within* each class of UV potentials, i.e. the polynomial, logarithmic, and exponential class. Although there are manifestly different UV modifications within each class, like for instance  $\phi^4 \exp(-1/\phi^2)$  vs  $\phi^6 \exp(-1/\phi^2)$ , the resulting IR behaviour appears to be dominated by the exponential dependence, and accordingly is nearly the same for the two cases – as stressed before, the two exponential cases differ from the two logarithmic cases, which are within a separate class of their own.

Comparing the two panels we observe that zero-temperature potentials with a steeper increase at larger field values turn into more shallow potentials for finite temperature near the broken vacuum. The latter corresponds to a lower barrier between the two minima. The reason for this link is that the phase transition occurs once positive thermal corrections to the mass parameter are large enough to change the extremum at  $\phi = 0$  from a maximum to a minimum, which then becomes degenerate with the minimum at a finite field value. For potentials with a lower zero-temperature depth — and correspondingly a more substantial slope at large  $\phi$  — the corresponding critical temperature  $T_c$  is lower. Therefore, the steepest increase towards large  $\phi$  in the left panel in Fig. 2.4 corresponds to the smallest bump in the right panel of Fig. 2.4. Phrased differently: for potentials with

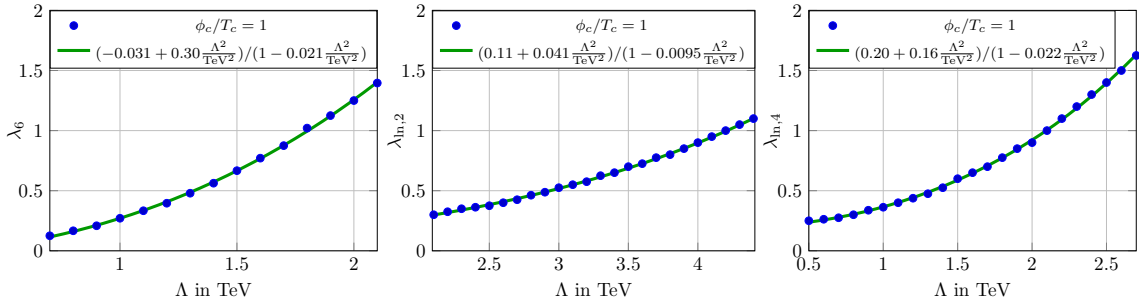


Figure 2.5.: Coefficient  $\lambda_j(\Lambda)$  of the dimension-6 operator  $\phi^6/\Lambda^2$  (left), the modification  $\Lambda^2\phi^2 \ln \phi^2/\Lambda^2$  (centre), and the modification  $\phi^4 \ln \phi^2/\Lambda^2$  (right) as a function of the cutoff, requiring  $\phi_c/T_c = 1 \pm 0.05$ .

a flatter inner region, scalar fluctuations are quantitatively more relevant. At the same time, the phase transition turns first order as soon as the scalar fluctuations dominate over the fermionic ones. This connection will become important when evaluating the prospects of the different cases with regards to detectability at the LHC.

### 2.3.2. Scale of new physics

Given a particular microscopic model containing additional degrees of freedom, the UV scale or cutoff  $\Lambda$  is typically identified with the mass scale of those additional fields, below which their fluctuations are suppressed. From an EFT point of view, one correspondingly associates  $\Lambda$  with the energy scale, above which new physics can appear as on-shell excitations. In turn, below  $\Lambda$  the effect of new physics is only visible indirectly. Such an indirect effect would be a deviation of the Higgs potential from its form in the renormalizable Standard Model. A key aspect of this kind of approach is that an EFT description by definition comes with a region of validity, above which we will be sensitive to the actual UV completion. Hence, before we use our modified Higgs potential to link a strong first-order phase transition to the Higgs self-coupling we need to study the validity range of our description.

Following (2.11) we see that an indirect measurement using an EFT-like approach is only sensitive to a combination of the scale  $\Lambda$  and the (Wilson) coefficients  $\lambda_j$ . In Fig. 2.5 we show the correlation between  $\Lambda$  and the corresponding  $\lambda_j$  evaluated at the UV scale  $\Lambda$  for a set of modified Higgs potentials, assuming a strong first-order phase transition with  $\phi_c/T_c = 1$ . We can interpret these results as lines of constant IR physics: the running coefficient  $\lambda_j(\Lambda)$  then describes a family of effective models defined at different scales  $\Lambda$ , all yielding the same IR observables. Without new physics effects,  $\Delta V = 0$ , this corresponds to fixing  $v$ ,  $m_H$  and  $m_t$  in the IR and simply evolving them toward the UV with their known RG equations. In our extended setup, the additional coefficients measure the strength of the new physics contribution, that we initialise at the UV scale  $\Lambda$ . We then use a corresponding parameter  $\lambda_j$  to fix  $\phi_c/T_c$  to a value of our choice. Doing so for different UV scales  $\Lambda$ , the coefficient  $\lambda_j$  becomes a function of  $\Lambda$ .

Without running effects for the coefficients  $\lambda_j$  the correlation between the coefficient and the UV scale would be simple. For instance, the dimension-6 Wilson coefficient would follow a parabola,  $\lambda_6 \propto \Lambda^2$ . However, the condition on  $\phi_c/T_c$  for the strong first-order phase transition is defined at energies around the Higgs vacuum expectation value, while the shown values of  $\lambda_j$  are defined in the UV. The complete correlation is well-described

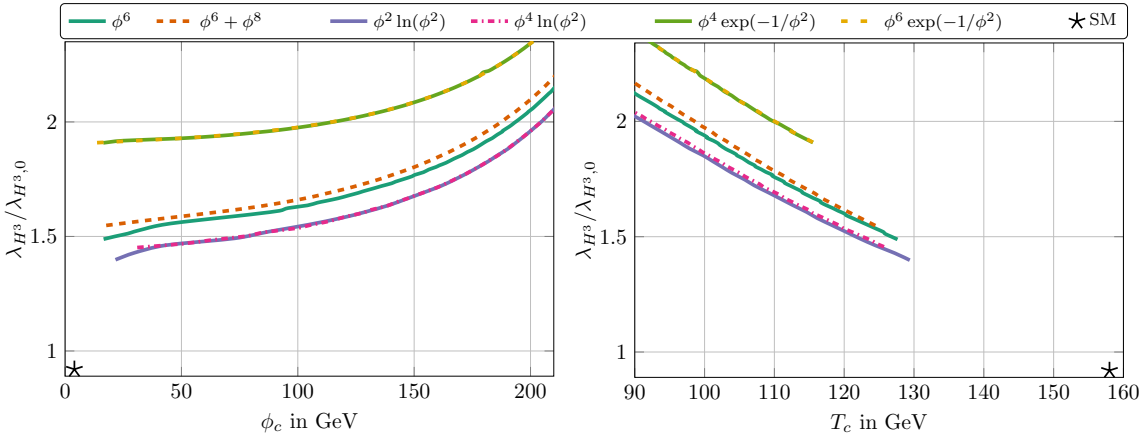


Figure 2.6.: Modification of the self-coupling  $\lambda_{H^3}/\lambda_{H^3,0}$  as a function of  $\phi_c$  (left) and  $1/T_c$  (right) for the UV potentials given in (2.11). The asterisk in both plots represents the Standard Model expectation, including Coleman-Weinberg corrections, cf. (2.15).

by a quadratic polynomial. In the case of  $\lambda_6$ , this reflects the quadratic running due to the canonical dimension. While the normalization of  $\Delta V$  can be adjusted at will and the absolute values of the coefficients  $\lambda_j$  do not carry any physical significance, the growth of these coefficients towards the ultraviolet suggests the possible onset of a strongly coupled regime.

To investigate the onset of this strongly coupled regime we fit the correlation between  $\lambda_j$  and  $\Lambda$  to a broken rational polynomial. A motivation for the particular choice of fit function in Fig. 2.5 is given by an approach to a power-like Landau-pole singularity. Indeed, this ansatz fits our numerical results well for the given range of UV scales. From the broken polynomial we can estimate the critical scales, where the respective models might become strongly coupled,

$$\Lambda_6^{\text{crit}} = 7.0 \text{ TeV}, \quad \Lambda_{\ln,2}^{\text{crit}} = 10 \text{ TeV}, \quad \Lambda_{\ln,4}^{\text{crit}} = 6.8 \text{ TeV}. \quad (2.16)$$

These critical scales should be viewed as conservative estimates of the validity scale up to which our field-theory description using purely Standard-Model degrees of freedom is applicable. These estimates are of the same order of magnitude as maximum values of  $\Lambda$  that lead to a first-order phase transition in studies based on mean-field arguments, see e.g. [52].

### 2.3.3. Baryogenesis vs Higgs self-coupling

After showing how a modified Higgs potential can lead to a strong first-order phase transition in Sec. 2.3.1 and confirming that our approach is consistent in Sec. 2.3.2, we can now explore the link between the strong first-order phase transition and the observable Higgs self-coupling. As laid out in the Introduction, the crucial question is as to whether modifications of the Higgs potential that lead to a sufficiently strong first-order phase transition for electroweak baryogenesis can be tested through the Higgs self-coupling measurement at the LHC.

Following the above discussion, the remaining question is how a value  $\phi_c/T_c \approx 1$  due to the potentials given in (2.11) is reflected in shifted physical Higgs self-couplings  $\lambda_{H^3}$  and

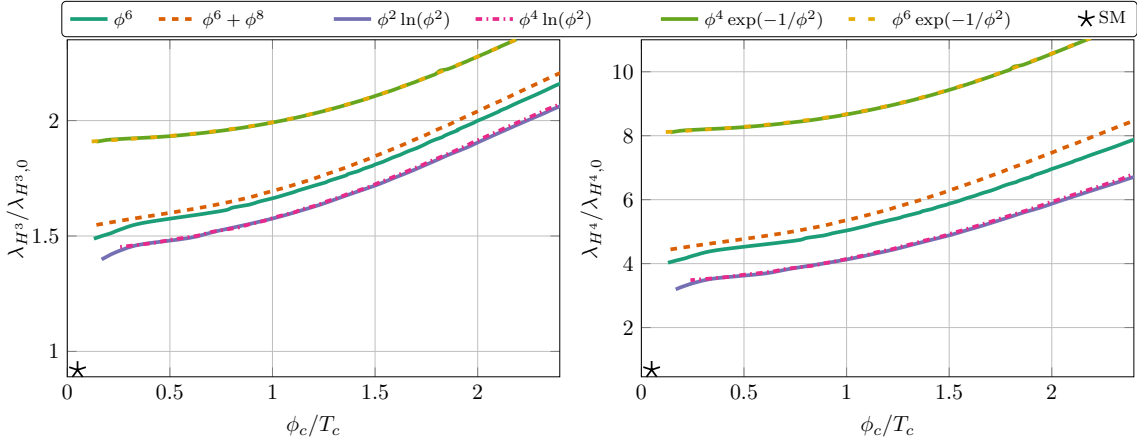


Figure 2.7.: Modification of the self-couplings  $\lambda_{H^3}/\lambda_{H^3,0}$  (left) and  $\lambda_{H^4}/\lambda_{H^4,0}$  (right) as a function of  $\phi_c/T_c$  for the UV potentials given in (2.11). The asterisk in the lower left of both plots represents the Standard Model expectation, including Coleman-Weinberg corrections, cf. (2.15).

$\lambda_{H^4}$ . All new physics models are adjusted to reproduce the low-energy measurements in (2.12). First, we can separate the two parameters  $1/T_c$  and  $\phi_c$  and show their individual effects on the physical Higgs self-couplings. In Fig. 2.6 we first see that the two parameters contribute roughly similar amounts to an increase in the Higgs self-couplings, if we push the model towards a strong first-order phase transition. Second, we see that the individual potentials in the general class of power-series, logarithmic, and exponential potentials give essentially degenerate results. Finally, the effect on the self-couplings is the weakest for the logarithmic potential, slightly stronger for the power-law modification, and the strongest for the exponential modification.

As already observed in Sec. 2.3.1, a steeper zero-temperature potential at large field values can be linked to a decrease in  $T_c$ . On the other hand, a steeper increase at large field values will be tied directly to larger values of the cubic and quartic Higgs self-coupling. This dependence is confirmed by Fig. 2.6, where potentials with smaller  $T_c$  feature larger  $\lambda_{H^3}$ . This feature holds both within each class of potentials where we can decrease  $T_c$  by enhancing  $\Delta V$ , and between different classes of potentials. This trend should be generic in that additions  $\Delta V$  leading to a strong first-order transition at low  $T_c$  will be easier to detect at the LHC.

Given that we do not see any striking effects from the individual dependence on  $1/T_c$  and  $\phi_c$ , we study the dependence of the different Higgs potentials on the physically relevant ratio  $\phi_c/T_c$ . In Fig. 2.7, we show the modifications of both Higgs self-couplings as a function of  $\phi_c/T_c$ . The free model parameter along the shown line is an appropriate combination of new-physics scale  $\Lambda$  and the new-physics coefficient  $\lambda_j$ . For  $\phi_c/T_c \gtrsim 1$  we find a strong first-order phase transition, suitable for electroweak baryogenesis. From the location of the Standard Model point it is clear that there exists a range of modified self-couplings where the electroweak phase transition remains second order. Only for

$$\frac{\lambda_{H^3}}{\lambda_{H^3,0}} \gtrsim 1.5 \quad \text{or} \quad \frac{\lambda_{H^4}}{\lambda_{H^4,0}} \gtrsim 4, \quad (2.17)$$

we have a chance to generate a first-order phase transition. This number should be compared to the LHC reach given in (2.9). We conclude that the prospects of a detectable

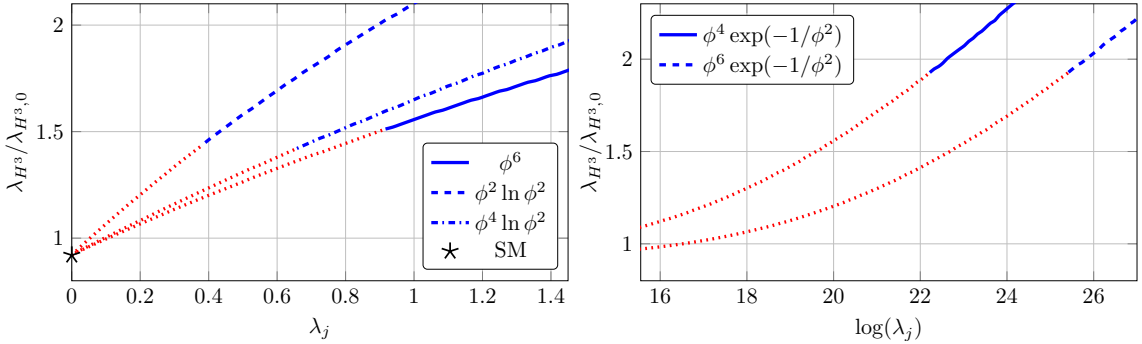


Figure 2.8.: Modification of the self-coupling  $\lambda_{H^3}/\lambda_{H^3,0}$  as a function of the coefficients  $\lambda_j$  from the different UV potentials given in (2.11). Blue lines represent first-order phase transitions and red dotted lines second-order phase transitions. The cutoff is  $\Lambda = 2$  TeV.

imprint appear to be good for all models that we have studied. A strong first-order phase transition corresponding to  $\phi_c/T_c > 1$  can in all scenarios be achieved by further increasing the new physics contributions and thereby increasing the Higgs self-couplings. In particular, we observe that the non-perturbative modifications  $\exp(-1/\phi^2)$  lead to a significantly higher value of the Higgs self couplings at fixed  $\phi_c/T_c$  and are thus easier to detect. Given that for example exponential potentials feature a minimum value of  $\lambda_{H^3}$  significantly larger than the simple  $\phi^6$  extension, the LHC measurement might even allow first clues to the nature of new physics, even if the corresponding scale  $\Lambda$  remains out of direct reach at the LHC.

Because the curves in Fig. 2.7 connect an IR observable with a UV property we can link the two regimes and make two observations. First, we can start in the IR and fix  $\lambda_{H^3}$  for different UV potentials. Here, we find that an increase in  $\phi_c/T_c$  or decrease in  $T_c$  leads to a decrease in  $\lambda_{H^4}$  for constant  $\lambda_{H^3}$ . Alternatively, we can fix  $\phi_c/T_c$  for different UV potentials and find that a decrease in  $\lambda_{H^3}$  corresponds to a decrease also in  $\lambda_{H^4}$  or an increase in  $T_c$ .

Finally, Fig. 2.8 explicitly shows the connection between the strength of the observable effect at LHC scales, measured by  $\lambda_{H^3}/\lambda_{H^3,0}$  and the size of the new physics contribution  $\Delta V$  at the microscopic scale  $\Lambda$ , measured by the value of the dimensionless coefficients  $\lambda_j$ . The nature of the electroweak phase transition is encoded in the colouring of the lines. The onset of the first-order phase transition is at values that can also be read off from Fig. 2.7: for logarithmic modifications we find the lowest value of  $\lambda_{H^3}/\lambda_{H^3,0} \approx 1.4$ , for the  $\phi^6$  modification  $\lambda_{H^3}/\lambda_{H^3,0} \approx 1.5$ , and for exponential modifications  $\lambda_{H^3}/\lambda_{H^3,0} \approx 1.9$ . This size of all modifications can be probed in the high-luminosity run at the LHC. Importantly, the Higgs self-couplings grow continuously as a function of  $\lambda_j$  while  $\phi_c/T_c$  remains zero till the onset of the first-order phase transition and only then starts to grow continuously.

## 2.4. Summary

Higgs pair production or the measurement of the Higgs self-coupling is an extraordinarily interesting LHC analysis. We find that it is well motivated by modified Higgs potentials that allow for a strong first-order electroweak phase transition and hence an explanation of the observed matter-antimatter asymmetry. We have studied a wide range of such

modifications to the Higgs potential, especially potentials that cannot be expanded as an effective field theory. We used the functional renormalization group to describe the dependence on the field value  $\phi$  and on the temperature  $T$ . For all classes of potentials considered here, there exists an appropriate choice of model parameters, for which the phase transition is of first order and sufficiently strong,  $\phi_c/T_c \gtrsim 1$ .

Our numerical analysis indicates that the requirement  $\phi_c/T_c = 1$  corresponds to a critical scale of the order of 10 TeV for all our potentials, where the potentials become strongly coupled. Below this scale we can rely on our assumed potentials to describe LHC signals. We then found that a strong first-order phase transition universally predicts an enhancement of the Higgs self-couplings  $\lambda_{H^3} \gtrsim 1.5\lambda_{H^3,0}$  and  $\lambda_{H^4} \gtrsim 4\lambda_{H^4,0}$ . Extending earlier studies, we systematically established this connection between a first-order transition and a measurable deviation of the Higgs self couplings, employing a method that can describe systems with multiple physical scales in a controlled manner. While it might be possible that a new physics model features a strong first-order transition with all effects on  $\lambda_{H^{3/4}}$  cancelling accidentally [173], none of our examples falls into this class. We conclude that a measurement of the Higgs self-couplings at the LHC indeed serves as an indirect probe of a first-order phase transition and thus of electroweak baryogenesis in generic setups.

On the other hand, we observed that it is possible to obtain large deviations in the Higgs self-interactions for our class of non-perturbative potentials without the condition  $\phi_c/T_c \geq 1$  being fulfilled. For example with an exponential modification of the Higgs potential the physical Higgs self-coupling reaches  $\lambda_{H^3} \approx 1.9\lambda_{H^3,0}$  already significantly below  $\phi_c/T_c = 1$ . On the theoretical side, a quantitative upgrade of our analysis includes, but is not limited to, a full treatment of the weak gauge sector as well as improvements in our treatment of the Yukawa sector, which might result in quantitative changes of the order of 10 %, cf. [242]. An as precise as possible measurement of the triple-Higgs interaction is clearly desirable. For instance a 20% measurement of a relatively small modification of  $\lambda_{H^3}/\lambda_{H^3,0}$  could exclude such exponential potentials as sources of electroweak baryogenesis. Such an actual measurement could therefore provide valuable hints guiding theoretical studies of interesting extended Higgs models.



## 3. Asymptotically safe quantum gravity – Introduction and basic setup

### 3.1. Introduction

Modern theoretical physics is built upon two pillars, namely quantum field theory and general relativity. Theories of quantum gravity aim at the unification of gravity with quantum dynamics. A candidate for a quantum theory of gravity is the asymptotic safety scenario, which goes back to Weinberg’s idea in 1976 [98]. Its construction is based on a non-trivial UV fixed point in the renormalisation group flow. The fixed point of asymptotic safety implies coupling constants that are finite at arbitrarily high energy scales, while they depend only on a finite number of free parameters. Hence, an asymptotically safe quantum field theory does not necessarily have a scale of maximal validity and thus can potentially describe physical interactions at the most fundamental level.

The possibility of an interacting UV fixed point in quantum gravity attracted increasing attention over the last two decades. Beginning with the pioneering work by Reuter [99], good evidence for its existence was found. The work by Reuter and many that followed are based on the Einstein-Hilbert truncation with the diffeomorphism invariant operators  $\sqrt{g}$  and  $\sqrt{g} R$  [100, 101, 245–266]. Different aspects were investigated including for instance gauge and parameterisation dependence, ghost interactions or dependence on the spacetime dimension.

In a perturbative regime the mass dimension of operators gives an ordering principle, which operators are relevant and have to be included in a truncation. At the non-perturbative UV fixed point this ordering principle is weakened: Operators that are canonically irrelevant can become relevant and vice versa. The relevance of an operator can only be determined in truncations by explicit computations. Consequently a lot of effort has been made to investigate higher derivative and  $f(R)$  quantum gravity [267–293]. Fortunately the mass dimension of the operators seems still to be a good ordering principle and operators with a high mass dimension seem to behave near-Gaussian [281, 282]. The question, how many relevant operators there are in pure quantum gravity setting is not fully settled yet. The currently favoured answer is three, which are the Einstein-Hilbert and the canonically marginal  $\sqrt{g} R^2$  operator. The canonically marginal  $\sqrt{g} R_{\mu\nu}^2$  operator becomes irrelevant at the UV fixed point in most truncations [293–295].

It is necessary that the amount of relevant directions at the UV fixed point is finite. This ensures the predictivity of the theory. In the perturbative approach it is the Goroff-Sagnotti two-loop counter term that proclaims the end of predictivity and thus the doom of the theory [78–80]. This term was also investigated in asymptotic safety and found to be asymptotically safe and irrelevant at the UV fixed point [296].

Higher derivative gravity is generally associated with non-unitarity because in the simple perturbative case, negative norm states show up in the theory [81, 82]. This statement is not strict: even in the perturbative setting one can construct higher-derivative theories without negative norm states [297, 298]. Unitarity in asymptotic safe is an incredible

challenging task, as in any non-perturbative quantum field theory. It requires a real-time computation and access to the pole structure of the graviton propagator. A fully conclusive analysis lies far in the future but first attempts towards real time computations and unitarity were made [299–304].

The resulting theory of quantum gravity is only the starting point for phenomenology. One can ask whether the black hole spacetime singularity is resolved by the theory or if cosmic censorship takes place and shields all singularities with an event horizon [114, 305–308]. Also applications to cosmology, for instance how quantum gravity influences the evolution of the universe or whether it resolves the Big Bang singularity, are important [309, 310]. Further applications include the gravitational Unruh effect [311], and the computation of observables via composite operators [312]. For general reviews on asymptotic safety see [313–318].

Urgent key questions concern background independence and the restoration of physical diffeomorphism invariance. All approaches based on metric correlation functions need to introduce a background metric. Consequently the full metric  $g_{\mu\nu}$  is split into background  $\bar{g}_{\mu\nu}$  and fluctuation  $h_{\mu\nu}$ . The gauge fixing and the regularisation scheme introduce separate dependencies of the effective action on background and fluctuation. These dependencies are captured by so called Nielsen or split-Ward identities [319–322] as well as accompanying Slavnov-Taylor identities [323, 324]. In the end observables must be independent of the chosen background and gauge fixing. In order to accomplish this background independence different ways have been pursued. The background and fluctuation field have been disentangle via a vertex expansion [294, 325–329], or an bi-metric approach [330–333]. Also the Nielsen or split-Ward identities have been tried used directly in order to get back to a single metric computation [334–343]. This topic is of uppermost importance to this dissertation and consequently we elaborate on this in much more detail in the following sections and chapters. This dissertation contributes to further progress on these issues within the setup of the systematic vertex expansion.

Most studies on asymptotically safe quantum gravity are based on the functional renormalisation group (FRG) [141, 344, 345]. In its modern form as a flow equation for the effective action of the theory it constitutes a powerful method for non-perturbative calculations in continuum quantum field theory. We use it in most chapters of this dissertation in the context of the systematic vertex expansion scheme around a flat Euclidean background. Importantly such a setup disentangles contributions from the background and the fluctuation field. Indeed it is the fluctuation propagator that drives the flow of the effective action. The flow of the fluctuation propagator in turn depends on the fluctuation four-point function, thus generating an infinite tower of coupled differential equations. This infinite has to be truncated at some order and the parameters of the higher  $n$ -point functions have either be set to zero or identified with lower  $n$ -point functions. Here we use the latter.

In this chapter we present the minimal setup that includes a genuine dynamical Newton's coupling. This setup includes the two-point functions and the graviton three-point function. As a main result we find a UV fixed point with two relevant directions. This UV fixed point will be the basis for extensions to other truncations in the subsequent chapters. We further show that the Wilsonian RG is well defined in this system, meaning that the flow of all correlation functions is momentum local. For perturbatively renormalisable this statement can be shown by simple power counting arguments. In gravity this arises due to highly non-trivial cancellations between different diagrams as we will show later.

## 3.2. Diffeomorphism invariance and background independence

The quantum field theoretical formulation of quantum gravity in terms of metric correlation functions necessitates the introduction of a background metric  $\bar{g}_{\mu\nu}$ , and quantum fluctuations are taken to be fluctuations about this background metric. This begs the question of whether diffeomorphism invariance and background independence of observables are guaranteed in such a framework. While this is an important question, its answer is not directly relevant for the computations presented here. Hence, this section may be skipped in a first reading.

In this dissertation we perform computations in the linear split, where the full metric  $g_{\mu\nu}$  is given by  $g_{\mu\nu} = \bar{g}_{\mu\nu} + h_{\mu\nu}$ . More general splits,  $g_{\mu\nu} = \bar{g}_{\mu\nu} + f(\bar{g}_{\mu\nu}, h_{\mu\nu})$  have been considered for example within the geometrical or Vilkovisky-deWitt approach, e.g. [336, 346–348], or the exponential split, e.g. [259, 262, 349–351]. Observables, on the other hand, are background independent. This property is encoded in the Nielsen (NI) or split-Ward identities (SWI) that relate derivatives of the effective action  $\Gamma[\bar{g}, \phi]$  w.r.t. the background metric  $\bar{g}_{\mu\nu}$  to those w.r.t. the graviton fluctuations  $h_{\mu\nu}$ . Here we have introduced the fluctuation superfield

$$\phi = (h_{\mu\nu}, c_\mu, \bar{c}_\mu). \quad (3.1)$$

The (anti-) ghost fields,  $c$  and  $\bar{c}$ , stem from the Faddeev-Popov gauge fixing procedure, see next section. The effective action generates all one-particle-irreducible correlation functions and as such encodes the symmetries of the theory. Schematically, these identities read [99, 188, 330, 331, 336–341, 347, 352]

$$\frac{\delta\Gamma[\bar{g}, h]}{\delta\bar{g}_{\mu\nu}(x)} = \int_y \mathcal{C}[\bar{g}, h](x, y) \frac{\delta\Gamma[\bar{g}, h]}{\delta h_{\mu\nu}(y)} + \mathcal{N}^{\mu\nu}[\bar{g}, h](x), \quad (3.2)$$

where we have suppressed the ghost fields to improve readability. In the linear split we have  $\mathcal{C}[\bar{g}, h](x, y) \sim \delta(x - y)$  and the second term  $\mathcal{N}[\bar{g}, h]$  carries the information about the non-trivial behaviour under diffeomorphism transformations of the gauge fixing sector and the regularisation. In turn, in the geometrical approach diffeomorphism invariance of the effective action is achieved by a non-linear split with  $f(\bar{g}, h)$  leading to the non-trivial prefactor  $\mathcal{C}[\bar{g}, h]$  in (3.2). The term  $\mathcal{N}[\bar{g}, h]$  then carries the deformation of the Nielsen identity in the presence of a regularisation but does not spoil diffeomorphism invariance.

In both cases the Nielsen identity is a combination of a quantum equation of motion, the Dyson-Schwinger equation, and the Slavnov-Taylor identity (STI) or diffeomorphism constraint. The setup also entails that correlations of the fluctuation fields are necessarily background-dependent. This is easily seen by iterating (3.2). Moreover, in the linear split, diffeomorphism invariance of the observables is encoded in non-trivial STIs for the fluctuation correlation functions, while in the geometrical formulation, the non-trivial STIs are encoded in expectation values of  $f(\bar{g}, h)$  and its derivatives.

Due to (3.2) we have to deal with the peculiarity that background independence and physical diffeomorphism invariance of observables necessitate background-dependence and non-trivial STIs for the correlation functions of the fluctuation fields. This leads to seemingly self-contradictory statements: in particular, for the quantum effective action  $\Gamma[\bar{g}, h]$  it entails that physical diffeomorphism invariance of observables is not achieved by diffeomorphism invariance w.r.t. diffeomorphism transformations of the fluctuation fields. The latter does not do justice to either diffeomorphism invariance or background independence.

This peculiarity can easily be checked in a non-Abelian gauge theory within the background field formulation: in a fluctuation gauge invariant approximation to the effective action, even two-loop universal observables such as the two-loop  $\beta$ -function cannot be computed correctly. Indeed, in this case it is well-known that only the non-trivial STIs for the fluctuation gauge field elevate the auxiliary background gauge invariance to the physical one holding for observables, see e.g. [353, 354].

The above considerations underline the importance of a direct computation of correlation functions of the fluctuation field  $h_{\mu\nu}$ . Indeed, the corresponding set of flow equations for  $\Gamma^{(n)} = \Gamma^{(0,n)}$  is closed in the sense that the flow diagrams only depend on  $\Gamma^{(n)}$  with  $n \geq 2$ . Here,  $\Gamma^{(n,m)}$  stands for the  $n$ -th background field derivative and  $m$ -th fluctuation field derivative of the effective action,

$$\Gamma^{(n,m)}[\bar{g}, \phi] = \frac{\delta^{n+m}\Gamma[\bar{g}, \phi]}{\delta \bar{g}^n \delta \phi^m}. \quad (3.3)$$

In turn, the flows for pure background,  $\Gamma^{(n,0)}$ , or mixed background-fluctuation functions,  $\Gamma^{(n,m)}$  with  $m \neq 0$ , necessitate the fluctuation correlation functions as an input: the background correlation functions can be iteratively computed in powers of the background metric. In other words, the dynamics of the system is solely determined by the pure fluctuation correlation functions. Accordingly, the background field approximation violates the NIs, which leads to the seemingly contradictory situation that it is at odds with background independence even though it only features one metric. In the past decade quite some progress has been made in overcoming the background field approximation, see [188, 294, 325–333, 336–342, 347, 352, 355–357].

### 3.2.1. Approaches to fluctuation and background correlation functions

All these works should be seen in the context of gaining background independence and physical diffeomorphism invariance in asymptotically safe gravity. Here we briefly summarise the state of the art within the different approaches.

(1) One approach utilises the fact that the NIs relate background metric correlations to fluctuation ones. This leaves us with a system of one type of correlations and it is possible to solve the system of flow equations for fluctuation correlation functions either directly or implicitly. This strategy has been set up and pursued in [188, 336–342, 347, 352, 355–360] for generic theories within the background field approach. At present, applications in gravity still utilise the background field approximation beyond either the first order, or the second order in the fluctuation field [336]. Such a closure of the flow equation with the background field approximation is mandatory and all approaches aim at introducing this approximation on a high order of the fluctuation field. Note in this context that it is only the second and higher order  $n$ -point functions of the fluctuation field that drive the flow.

(2a) A second approach utilises the fact that the dynamics of the system is carried by the correlation functions of the fluctuation field. This is also reflected by the fact that the system of flow equations for the fluctuation correlations is closed. Consequently one may solve these flows for a specific background metric that facilitates the computation, e.g. the flat background. Then, background correlations are computed within an expansion or extension about the flat background in order to access the physical background that solves the quantum EoM. This strategy has been set up and pursued in [122, 294, 325–329]

for gravity, also guided by successful applications in non-Abelian gauge theories, see e.g. [361–365].

(2b) A third approach avoids the latter step of extending the results to physical backgrounds by computing instantly the flow equations for the fluctuation correlation functions for general backgrounds. This has been investigated in [330–333]. As in the other approaches, the background field approximation has been used for higher correlation functions. At present, this holds for all correlation functions beyond the one-point function of the fluctuation field.

In the most part of this dissertation we develop an approach in the class (2a). In particular we will use an expansion about a flat Euclidean background. Only in [Chapter 5](#) we use an approach in the class (2b).

### 3.3. Effective action & functional renormalisation group

The set of (covariant) correlation functions of the metric,  $\langle g(x_1) \cdots g(x_n) \rangle$ , defines a given theory of quantum gravity. All observables can be constructed from these basic building blocks. The correlation functions are generated from the single metric effective action,  $\Gamma[g] = \Gamma[g, h = 0]$ , which is the free energy in a given metric background  $g_{\mu\nu} = \bar{g}_{\mu\nu} + h_{\mu\nu}$  at  $h_{\mu\nu} = 0$ . Here we have restricted ourselves to a linear split. The underlying classical action is the gauge-fixed Einstein-Hilbert action,

$$S_{\text{EH}} = \frac{1}{16\pi G_N} \int d^4x \sqrt{g} (2\Lambda - R(g)) + S_{\text{gf}} + S_{\text{gh}}, \quad (3.4)$$

where  $R(g)$  is the Ricci curvature scalar,  $\sqrt{g} = \sqrt{\det g}$ , and  $S_{\text{gf}}[\bar{g}, h]$  and  $S_{\text{gh}}[\bar{g}, \phi]$  describe the gauge-fixing and Faddeev-Popov ghost parts of the action, respectively. The gauge fixing action reads

$$S_{\text{gf}}[\bar{g}, h] = \frac{1}{2\alpha} \int d^4x \sqrt{\bar{g}} \bar{g}^{\mu\nu} F_\mu F_\nu. \quad (3.5)$$

We employ a linear, de-Donder type gauge-fixing,

$$F_\mu = \bar{\nabla}^\nu h_{\mu\nu} - \frac{1+\beta}{4} \bar{\nabla}_\mu h^\nu. \quad (3.6)$$

In particular we use throughout the whole dissertation the harmonic gauge given by  $\beta = 1$  and work in the Landau limit of a vanishing gauge parameter,  $\alpha \rightarrow 0$ . The choice of  $\beta$  simplifies computations considerably due to the fact that the poles of all modes of the classical graviton propagator coincide. Also the Landau-gauge is favourable since it maximally disentangle physical and gauge fluctuation and it further guarantees that the gauge does not change during the flow since  $\alpha = 0$  is a RG fixed point [366]. The ghost part of the action reads

$$S_{\text{gh}}[\bar{g}, \phi] = \int d^4x \sqrt{\bar{g}} \bar{c}^\mu \mathcal{M}_{\mu\nu} c^\nu, \quad (3.7)$$

where  $\bar{c}$  and  $c$  denote the (anti-) ghost field and  $\mathcal{M}$  is the Faddeev-Popov operator deduced from (3.6). For  $\beta = 1$  it is given by

$$\mathcal{M}_{\mu\nu} = \bar{\nabla}^\rho (g_{\mu\nu} \nabla_\rho + g_{\rho\nu} \nabla_\mu) - \bar{\nabla}_\mu \nabla_\nu. \quad (3.8)$$

The gauge fixing and ghost term in (3.5) and (3.7) introduce the separate dependence on  $\bar{g}_{\mu\nu}$  and  $h_{\mu\nu}$  leading to the non-trivial Nielsen identities in (3.2).

### 3.3.1. Flow equation

An efficient way of computing non-perturbative correlation functions is the functional renormalisation group. In its form for the effective action, see [141, 344, 345], it has been applied to quantum gravity [99]. For reviews on the FRG approach to gauge theories and gravity see e.g. [188, 189, 313–316]. The RG flow of the effective action for pure quantum gravity is given by

$$\partial_t \Gamma_k = \frac{1}{2} \text{Tr} [G_k \partial_t R_k]_{hh} - \text{Tr} [G_k \partial_t R_k]_{\bar{c}c} . \quad (3.9)$$

Here,  $\partial_t = k \partial_k$  denotes the scale derivative, where  $k$  is the IR cutoff scale.  $G_k = (\Gamma_k^{(2)} + R_k)^{-1}$  is the fluctuation field propagator, while  $R_k$  is the regulator, which suppresses momenta below  $k$ . The trace sums over internal indices and integrates over space-time.

The introduction of cutoff terms leads to regulator-dependent modifications of STIs and NIs that vanish for  $R_k \rightarrow 0$ . The respective symmetry identities have hence been named modified Slavnov-Taylor identities (mSTIs) and modified Nielsen- or split Ward identities (mNIs/mSWIs). The modification entails the breaking of the physical or quantum diffeomorphism invariance in the presence of a background covariant momentum cutoff. Still, background diffeomorphism invariance is maintained in the presence of the cutoff term.

### 3.3.2. Vertex expansion

The effective action  $\Gamma_k[\bar{g}, \phi]$  depends on the background metric  $\bar{g}_{\mu\nu}$  and the fluctuation superfield  $\phi = (h_{\mu\nu}, c_\mu, \bar{c}_\mu)$ , see (3.1), separately. The functional flow equation (3.9) is accompanied by the functional mSTIs & mNIs for the effective action that monitor the breaking of quantum diffeomorphism invariance, see (3.2) in Sec. 3.2. In order to solve (3.9), we employ a vertex expansion around a given background  $\bar{g}_{\mu\nu}$ , to wit

$$\Gamma_k[\bar{g}, \phi] = \sum_{n=0}^{\infty} \sum_{|n_\phi|=n} \frac{1}{n_\phi!} \Gamma_k^{(\phi_{i_1} \dots \phi_{i_n})} [\bar{g}, 0] \phi_{i_1} \dots \phi_{i_n} , \quad (3.10)$$

Here we have introduced the short-hand notation

$$\Gamma_k^{(\phi_{i_1} \dots \phi_{i_n})} [\bar{g}, 0] = \frac{\delta^n \Gamma_k [\bar{g}, \phi]}{\delta \phi_{i_1} \dots \delta \phi_{i_n}} \bigg|_{\phi=0} , \quad (3.11)$$

which specifies one entry of the general fluctuation  $n$ -point function  $\Gamma_k^{(n)} = \Gamma_k^{(0,n)}$ , see also (3.3). Also we have introduced the tuple  $n_\phi = (n_h, n_c, \dots)$  that contains the number of graviton legs  $n_h$ , ghost legs  $n_c$  in the respective  $n$ -point function. In the later chapters this tuple will also contain the number of matter legs. In (3.10) the super-indices  $i_j$  occurring twice imply a sum over discrete indices and an integral over continuous variables. In this chapter, we include the full flow of the vertex functions up to the graviton three-point function, while in the next chapter we will also include the graviton four-point function.

As discussed in Sec. 3.2, the expansion coefficients  $\Gamma_k^{(n)}$  satisfy mSTIs as well as mNIs with  $\Gamma_k^{(n,m)}$  being defined in (3.3). For the sake of simplicity we now restrict ourselves to the gauge fixing used in this dissertation, (3.6) with  $\alpha = 0$ . Then the fluctuation graviton propagator is transverse: it is annihilated by the gauge fixing condition.

An important feature of the functional RG equations is that for  $\alpha = 0$  the flow equations for the transverse vertices  $\Gamma_{k,T}^{(n)}$  are closed: the external legs of the vertices in the flow are transverse due to the transverse projection of the flow, the internal legs are transverse as they are contracted with the transverse propagator. Schematically this reads

$$\partial_t \Gamma_{k,T}^{(n)} = \text{Flow}_T^{(n)}[\{\Gamma_{k,T}^{(m)}\}]. \quad (3.12)$$

In other words, the system of transverse fluctuation correlation functions is closed and determines the dynamics of the system. On the other hand, the mSTIs are non-trivial relations for the longitudinal parts of vertices in terms of transverse vertices and longitudinal ones. This leads us to the schematic relation

$$\Gamma_{k,L}^{(n)} = \text{mSTI}^{(n)}[\{\Gamma_{k,T}^{(m)}\}, \{\Gamma_{k,L}^{(m)}\}], \quad (3.13)$$

see [367] for non-Abelian gauge theories. In consequence, the mSTIs provide no direct information about the transverse correlation functions without further constraint. In the perturbative regime this additional constraint is given by the uniformity of the vertices, for a detailed discussion in non-Abelian gauge theories see [368].

Accordingly, our task reduces to the evaluation of the coupled set of flow equations for the transverse vertices  $\Gamma_{k,T}^{(n)}$ . Each transverse vertex can be parameterised by a set of diffeomorphism-invariant expressions. Restricting ourselves to local invariants and second order in the curvature we are left with

$$R, \quad R^2, \quad R_{\mu\nu}^2. \quad (3.14)$$

The square of the Weyl tensor  $C^2$  is eliminated via the Gauß-Bonnet term, which is a topological invariant. Higher-derivative terms, such as

$$R^{\mu\nu} f_{\mu\nu\rho\sigma}(\nabla) R^{\rho\sigma} \quad \text{with} \quad f(0) = 0, \quad (3.15)$$

are also taken into account. Without the constraint  $f(0) = 0$ , equation (3.15) also includes  $R^2$  and  $R_{\mu\nu}^2$ , more details on this basis can be found in Sec. 3.4. Note that also non-diffeomorphism-invariant terms are generated by the flow. In the next chapter we will discuss all invariants which are included in the parameterisation of our vertices, see Sec. 4.2.2.

For the background vertices  $\Gamma_k^{(n,0)}$  we use the following: the NIs become trivial in the IR as we approach classical gravity. Moreover, for one of the two IR fixed points this implies that the derivative with respect to a background field is the same as a derivative with respect to a fluctuation field. This allows us to impose the trivial NIs in the IR, and all couplings are related. Then, the couplings at  $k > 0$  follow from the flow equation. However, for the fluctuation couplings this amounts to solving a fine-tuning problem in the UV. This will however only be discussed in the extended four-point truncation in the next chapter, see Sec. 4.4.

### 3.4. Flows of correlation functions

In this section we discuss the technical details of the covariant expansion scheme used in this dissertation, including the approximations used and their legitimisation.

$$\begin{aligned}
\partial_t \Gamma_k &= \frac{1}{2} \text{ (blue loop with } \otimes \text{)} - \text{ (red dotted loop with } \otimes \text{)} \\
\partial_t \Gamma_k^{(h)} &= -\frac{1}{2} \text{ (blue loop with } \otimes \text{)} + \text{ (red dotted loop with } \otimes \text{)} \\
\partial_t \Gamma_k^{(2h)} &= -\frac{1}{2} \text{ (blue loop with } \otimes \text{)} + \text{ (blue loop with } \otimes \text{)} - 2 \text{ (red dotted loop with } \otimes \text{)} \\
\partial_t \Gamma_k^{(c\bar{c})} &= \text{ (red dotted loop with } \otimes \text{)} + \text{ (blue dotted loop with } \otimes \text{)} \\
\partial_t \Gamma_k^{(3h)} &= -\frac{1}{2} \text{ (blue loop with } \otimes \text{)} + 3 \text{ (blue loop with } \otimes \text{)} - 3 \text{ (blue loop with } \otimes \text{)} + 6 \text{ (red dotted loop with } \otimes \text{)} \\
\partial_t \Gamma_k^{(4h)} &= -\frac{1}{2} \text{ (blue loop with } \otimes \text{)} + 3 \text{ (blue loop with } \otimes \text{)} + 4 \text{ (blue loop with } \otimes \text{)} - 6 \text{ (blue loop with } \otimes \text{)} \\
&\quad - 12 \text{ (blue loop with } \otimes \text{)} + 12 \text{ (blue loop with } \otimes \text{)} - 24 \text{ (red dotted loop with } \otimes \text{)}
\end{aligned}$$

Figure 3.1.: Diagrammatic representation of the flow of the vertex functions up to the graviton four-point function. The flow of any  $n$ -point function depends on the  $(n+1)$ - and  $(n+2)$ -point functions. Double and dotted lines represent graviton and ghost propagators, respectively. All vertices are dressed and denoted by filled circles. Crossed circles stand for regulator insertions. Symmetrisation with respect to interchange of external momenta  $p_i$  is understood.

### 3.4.1. Covariant tensors and uniformity

The flows of the  $n$ -point correlation functions are generated from the FRG equation (3.9) by taking  $n$ -th order fluctuation field derivatives in a background  $\bar{g}$ . In Fig. 3.1 we display the all flow equations up the four-point function in a diagrammatic language. In order to solve the flow equation, we employ a vertex ansatz [325, 369] including the flow of all relevant vertices up to the graviton three-point function in this chapter and up to the graviton four-point function in the next chapter. This vertex ansatz disentangles the couplings of background and fluctuation fields by introducing individual couplings  $\Lambda_n$  and  $G_n$  for each  $n$ -point function. These individual couplings are introduced at the level of the  $n$ -point correlators and replace the cosmological constant  $\Lambda$  and Newton's coupling  $G_N$  of the classical Einstein-Hilbert action after performing the respective field derivatives. In summary, for the flat background  $\bar{g}_{\mu\nu} = \delta_{\mu\nu}$  our vertex ansatz reads

$$\Gamma_k^{(\phi_1 \dots \phi_n)}(\mathbf{p}) = \left( \prod_{i=1}^n Z_{\phi_i}^{\frac{1}{2}}(p_i^2) \right) G_n^{\frac{n}{2}-1}(\mathbf{p}) \mathcal{T}^{(\phi_1 \dots \phi_n)}(\mathbf{p}; \Lambda_n), \quad (3.16)$$

where

$$\mathcal{T}^{(\phi_1 \dots \phi_n)}(\mathbf{p}; \Lambda_n) = G_N S_{\text{EH}}^{(\phi_1 \dots \phi_n)}(\mathbf{p}; \Lambda \rightarrow \Lambda_n), \quad (3.17)$$

denote the tensor structures extracted from the classical gauge-fixed Einstein-Hilbert action (3.4). The only flowing parameter in these tensors  $\mathcal{T}^{(\phi_1 \dots \phi_n)}$  is  $\Lambda_n$ , while  $G_n(\mathbf{p})$

carries the global scale- and momentum dependence of the vertex. In the above equations,  $\mathbf{p} = (p_{\phi_1}, \dots, p_{\phi_n})$  denotes the momenta of the external fields  $\phi_i$  of the vertex.

Apart from their flow equations, the  $n$ -point functions in (3.16) also satisfy standard RG-equations, see e.g. [188]. These RG-equations entail the reparameterisation invariance of the theory under a complete rescaling of all scales including  $k$ . With the parameterisation given in (3.16), this RG-running is completely carried by the wave function renormalisations  $Z_{\phi_i}(p_i^2)$  of the fields  $\phi_i$ , see e.g. [327, 369]. Consequently, the  $G_n$  and  $\Lambda_n$  are RG-invariant, and hence are more directly related to observables such as  $S$ -matrix elements. This parameterisation of the vertices also ensures that the wave function renormalisations never appear directly in the flow equations, but only via the anomalous dimensions

$$\eta_{\phi_i}(p_i^2) = -\partial_t \ln Z_{\phi_i}(p_i^2). \quad (3.18)$$

$G_n(\mathbf{p})$  is the gravitational coupling of the  $n$ -point function, while  $\Lambda_n$  denotes the momentum-independent part of the correlation function. In particular,  $\Lambda_2$  is related to the graviton mass parameter  $M^2 = -2\Lambda_2$ . Finally, all the parameters  $Z_{\phi_i}$ ,  $G_n$ , and  $\Lambda_n$  are scale-dependent, but we have dropped the subscript  $k$  in order to improve readability.

In principle, all tensor structures, including non-diffeomorphism-invariant ones, are generated by the flow, but for our vertex functions we choose to concentrate on the classical Einstein-Hilbert tensor structures in the presence of a non-vanishing cosmological constant. Despite the restriction to these tensor structures, the  $n$ -point functions have an overlap with higher curvature invariants via the momentum dependence of the gravitational couplings. For example, the complete set of invariants that span the graviton wave function renormalisation is given by

$$R, \quad R^{\mu\nu} f_{\mu\nu\rho\sigma}^{(2)}(\nabla) R^{\rho\sigma}, \quad (3.19)$$

where the superscript of  $f$  indicates that it is a covariant tensor contributing to the two-point correlation function. Note also that we now drop the restriction on  $f$  present in (3.15). Then, this invariant naturally includes  $R^2$  and  $R_{\mu\nu}^2$  as the lowest order local terms. If we also allow for general momentum-dependencies, the corresponding covariant functions  $f$  are given by given by

$$f_{R^2, \mu\nu\rho\sigma}^{(2)} = \delta_{\mu\nu} \delta_{\rho\sigma} P_{R^2}^{(2)}(-\nabla^2), \quad f_{R_{\mu\nu}^2, \mu\nu\rho\sigma}^{(2)} = \frac{1}{2} (\delta_{\mu\rho} \delta_{\nu\sigma} + \delta_{\mu\sigma} \delta_{\nu\rho}) P_{R_{\mu\nu}^2}^{(2)}(-\nabla^2). \quad (3.20)$$

The lowest order local terms,  $R^2$  and  $R_{\mu\nu}^2$ , are given by  $P_{R^2}^{(2)} = 1$  and  $P_{R_{\mu\nu}^2}^{(2)} = 1$ , respectively. Note that (3.20) also allows for non-local terms in the IR, i.e. anomaly-driven terms with  $P_{R^2}^{(2)} = 1/\nabla^2$ , see e.g. [370]. In turn, higher curvature invariants do not belong to the set of the graviton wave function renormalisation since they are at least cubic in the graviton fluctuation field.

We resort to a uniform graviton propagator in order to limit the already large computer-algebraic effort involved. The uniform wave function renormalisation is then set to be that of the combinatorially dominant tensor structure, the transverse-traceless graviton wave function renormalisation, thereby estimating the wave function renormalisations of the other modes by the transverse-traceless one. Such uniform approximations have been very successfully used in thermal field theory. There, usually the tensor structures transverse to the heat-bath are used as the uniform tensor structure, for a detailed discussion

see e.g. [371] and references therein. This approximation is typically supported by combinatorial dominance of this tensor structure in the flow diagrams. Indeed, as already indicated above, the transverse-traceless mode gives the combinatorially largest contribution to the flow of the vertices computed here. Note that such an approximation would get further support if the  $R$  tensor structures dominate the flows, which indeed happens in the present computation. Within this approximation the  $R^2$  tensor structures drop out on the left-hand side of the graviton flow, since  $R$  is already quadratic in the transverse-traceless graviton fluctuation field: in other words, the tensors defined by  $f_{R^2}^{(2)}$  in (3.20) have no overlap with the transverse-traceless graviton.

The set of invariants that span the gravitational coupling  $G_3(\mathbf{p})$  is given by

$$R, \quad R^{\mu\nu} f_{\mu\nu\rho\sigma}^{(3)}(\nabla) R^{\rho\sigma}, \quad R^{\mu\nu} R^{\rho\sigma} f_{\mu\nu\rho\sigma\omega\zeta}^{(3)}(\nabla) R^{\omega\zeta}. \quad (3.21)$$

Again, the invariants  $R^2$  and  $R^3$  can be excluded from this set due to their order in transverse-traceless graviton fluctuation fields. As we will see in the next chapter,  $G_4(\mathbf{p})$  is first coupling in our expansion scheme that has overlap with  $R^2$  contributions and higher terms in  $f_{R^2}^{(4)}$ . Furthermore, in Sec. 4.2.2 we will show that the by far dominant contribution to  $G_3(\mathbf{p})$  in the momentum range  $0 \leq p^2 \leq k^2$  stems from the invariant  $R$ . We leave however this discussion for the next chapter and for the moment just use this information to justify the approximation of a momentum independent three-point Newton's coupling,  $G_3(\mathbf{p}) = G_3$ , that is used in the remainder of this chapter.

### 3.4.2. Projection onto $n$ -point functions

The flow equations for the couplings  $\Lambda_n$  and  $G_n$  are obtained by the following projection onto the flow of the graviton  $n$ -point functions  $\partial_t \Gamma_k^{(n)}$ . We use the classical Einstein-Hilbert tensor structures  $\mathcal{T}^{(n)}(\mathbf{p}; \Lambda_n)$  (cf. (3.17)) as a basis for our projection operators. Furthermore, we project onto the spin-two transverse-traceless part of the flow, which is numerically dominant. Moreover, classical transverse-traceless graviton propagator is gauge independent and carries the only propagating degrees of freedom. This transverse-traceless projection operator is then applied to all external graviton legs. The flow of the couplings  $\Lambda_n$  is then extracted with the help of the momentum-independent part of said tensor structures, namely  $\Pi_{\Lambda_n} = \mathcal{T}^{(n)}(0; \Lambda_n)/\Lambda_n$ . For the couplings  $G_n$  we use  $\Pi_{G_n} = \mathcal{T}^{(n)}(\mathbf{p}; 0)/p^2$ . Dividing by  $\Lambda_n$  and  $p^2$  ensures that the projection operators are dimensionless and scale-independent.

In principle, the flow of any  $n$ -point function depends on all external momenta  $p_i, i \in \{1, \dots, n\}$ , where e.g.  $p_n$  can be eliminated due to momentum conservation. For the two-point function, the momentum configuration is trivial, and only one momentum squared,  $p^2$ , needs to be taken into account. In contrast, this dependence becomes increasingly complex for the higher  $n$ -point functions: The three-point function depends on three parameters (two momenta squared and one angle), the four-point function already depends on six parameters, and so on. To simplify the computations, we use a maximally symmetric  $(n-1)$ -simplex configuration for all  $n$ -point-functions, thereby reducing the momentum dependence to a single parameter. In the context of Yang-Mills theories, this approximation has been shown to be in good agreement with lattice computations on the level of the flow of the propagator [368]. Notably, in the symmetric momentum configuration all external momenta have the same absolute value  $p$ , and the same angles between each other.

The scalar product of any two momenta in this momentum configuration then reads

$$p_i \cdot p_j = \frac{n\delta_{ij} - 1}{n-1} p^2, \quad (3.22)$$

where  $\delta_{ij}$  denotes the Kronecker delta. Note that such a symmetric momentum configuration only exists up to the  $(d+1)$ -point function, where  $d$  is the dimension of spacetime.

In the following, the expressions  $\text{Flow}^{(n)}$  stand for the dimensionless right-hand sides of the flow equations divided by appropriate powers of the wave function renormalisations. More explicitly, we define

$$\text{Flow}_i^{(n)}(p^2) = \frac{\partial_t \Gamma_i^{(n)}(p^2)}{Z_\phi^{\frac{n}{2}}(p^2) k^{2-n}}, \quad (3.23)$$

where the index  $i$  represents the projection on some tensor structure. We use the transverse-traceless projection operator  $\Pi_{tt}$ , the projection operators  $\Pi_{G_n}$  and  $\Pi_{\Lambda_n}$  mentioned earlier for the graviton  $n$ -point functions, as well as the transverse projection operator  $\Pi_T$  for the ghost propagator. Note that the objects  $\text{Flow}_i^{(n)}$  do not contain any explicit factors of the wave function renormalisations  $Z_\phi$ . Instead, their running appears via the anomalous dimensions  $\eta_\phi$ .

Last but not least, we choose to model the regulator functions  $R^{\phi_i}$  on the corresponding two-point functions at vanishing mass, i.e.

$$R^{\phi_i}(p_i^2) = \Gamma^{(\phi_i \phi_i)}(p_i^2) \Big|_{m_{\phi_i}=0} r_{\phi_i}(p_i^2/k^2). \quad (3.24)$$

Here,  $r_{\phi_i}(p_i^2/k^2)$  denotes the regulator shape function. For all fields we choose the Litim-type flat regulator [372–375], to wit

$$r(x) = (x^{-1} - 1) \Theta(1 - x). \quad (3.25)$$

This choice allows for analytic flow equations for all couplings that are evaluated at vanishing external momenta. Furthermore, we introduce the dimensionless couplings

$$\mu = M^2 k^{-2}, \quad \lambda_n = \Lambda_n k^{-2}, \quad g_n = G_n k^2. \quad (3.26)$$

At the UV and IR fixed points, the flow of these dimensionless couplings vanishes.

### 3.4.3. Flow equations for the couplings

In this section we explain the derivation the flow equations for the couplings from the projected  $n$ -point functions of the last section.

The flow equations for  $\mu$  and  $\eta_h(p^2)$  are extracted from the transverse-traceless part of the flow of the graviton two-point function. We evaluate this two-point function at  $p^2 = 0$  for  $\partial_t \mu$ , and bilocally at  $-\mu k^2$  and  $p^2$  for  $\eta_h(p^2)$ . The algebraic equation for  $\eta_c(p^2)$  can be obtained directly from the transverse part of the flow of the ghost two-point function. The equations for the graviton and ghost anomalous dimensions are Fredholm integral equations, that can be solved for instance with an iteration [327]. For details see also App. B.5.

In the case of the couplings  $\lambda_n$  and  $g_n(p^2)$ , we project onto the flow of the graviton  $n$ -point functions. The flow equations for the couplings  $\lambda_n$  are always obtained at  $p^2 = 0$ ,

since  $\lambda_n$  describes the momentum-independent part of the graviton  $n$ -point functions. For  $\lambda_3$  this leads to

$$\partial_t \lambda_3 = \left( \frac{3}{2} \eta_h(0) - 1 - \frac{\partial_t g_3}{2g_3} \right) \lambda_3 + \frac{\mathcal{N}_\lambda}{\sqrt{g_3}} \text{Flow}_\Lambda^{(3)}(0), \quad (3.27)$$

with a normalisation factor  $\mathcal{N}_\lambda^{-1} := \mathcal{T}^{(3)}(0; 1) \circ \Pi_{tt}^3 \circ \mathcal{T}^{(3)}(0; 1)$ , where  $\circ$  denotes the pairwise contraction of indices. A general form for all  $\lambda_n$  is given in (B.10).

In the case of the couplings  $g_n(p^2)$  it is technically challenging to resolve the full momentum dependence in the flow. Thus, we resort to a further approximation of the momentum-dependence. We have checked that this approximation holds quantitatively. First we note that typically FRG-flows are strongly peaked at  $q \approx k$  due to the factor  $q^3$  from the loop integration and the decay for momenta  $q \gtrsim k$  due to  $\partial_t R_k(q^2)$ . This certainly holds for all the flows considered here. From this we can infer that we extract the leading contribution to the flow diagrams if we feed  $g_n(k^2)$  back into the diagrams. In consequence we compute only the flow equations for  $g_n(k^2)$ , as they form a closed system of equations within the given approximation. Most conveniently this is done with a bilocal projection between  $p = 0$  and  $p = k$ . For  $g_3$  this leads to

$$\begin{aligned} \partial_t g_3 = & (2 + 3\eta_h(k^2))g_3 - \frac{24}{19}(\eta_h(k^2) - \eta_h(0))\lambda_3 g_3 \\ & + 2\mathcal{N}_g \sqrt{g_3} k \left( \text{Flow}_G^{(3)}(k^2) - \text{Flow}_G^{(3)}(0) \right), \end{aligned} \quad (3.28)$$

with  $\mathcal{N}_g^{-1} := \mathcal{T}^{(3)}(k; 0) \circ \Pi_{tt}^3 \circ \mathcal{T}^{(3)}(k; 0)$ . Another possibility is the evaluation with a  $p^2$ -derivative at  $p = 0$ . This procedure is less accurate in approximating the momentum dependence of the flow. On the other hand, it allows for an analytic flow equation for the couplings  $g_n$ . The difference between these momentum projections is discussed in Sec. B.4.

In this chapter we further evaluate the coupling of the one-point function  $\lambda_1/\sqrt{g_1} = \Lambda_1 G_1^{-1/2}/k^3$ , which is at vanishing external momentum. The background couplings  $\bar{g} = \bar{G} k^2$  and  $\bar{\lambda} = \bar{\Lambda}/k^2$  are evaluated with heat-kernel methods and are only discussed in the next chapters.

## 3.5. Results

We now focus on the results obtained from the truncation including all  $n$ -point function up to the graviton three-point function.

### 3.5.1. Locality

The functional renormalisation group is based on the idea of a successive integration of momentum shells, or, more generally, spectral shells of spectral values of the given kinetic operator. Hence, it relies on the distinction of small and large momentum or spectral modes. A functional RG step implements the physics of momentum/spectral modes at a given scale  $k$  and is inherently related to local interactions.

Locality in momentum space implies in particular that the flows of vertices at a given momentum scale  $k$  decay relative to the vertex itself if all momentum transfers (momentum channels)  $t_i$  are taken to infinity. For example, for the four-point vertex we have  $t_1, t_2, t_3$

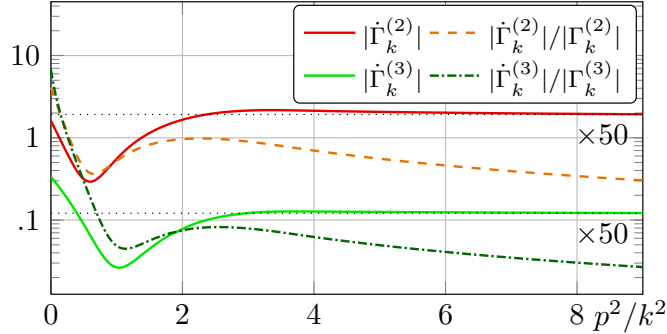


Figure 3.2.: Logarithmic plot of the flows  $|\partial_t \Gamma_k^{(2)}|$  and  $|\partial_t \Gamma_k^{(3)}|$  (solid red and light green curves) and the corresponding ratios  $|\partial_t \Gamma_k^{(2)}|/|\Gamma_k^{(2)}|$  and  $|\partial_t \Gamma_k^{(3)}|/|\Gamma_k^{(3)}|$  (dashed orange and dash-dotted dark green curves) as functions of  $p^2/k^2$ . The norm refers to the tensor projection discussed below (3.23). All quantities are evaluated at  $(g, \mu, \lambda_3) = (1, 0.1, -0.7)$ . The flows are multiplied with 50 for convenience. The ratios decay with  $1/p^2$  for large  $p$  since the associated flows quickly approach constant values, satisfying (3.29).

being the well-known  $s, t, u$ -channels, with e.g.  $s = (p_1 + p_2)^2$ . Hence, locality reads schematically

$$\lim_{t_i/k^2 \rightarrow \infty} \frac{|\partial_t \Gamma_k^{(n)}(\mathbf{p})|}{|\Gamma_k^{(n)}(\mathbf{p})|} = 0, \quad \text{with } \mathbf{p} = (p_1, \dots, p_n), \quad (3.29)$$

where a projection on one of the tensor structure of the vertex is implied. For the limit (3.29) each diagram in the flow of a given vertex has an infinite momentum transfer. Thus, the diagrams are only sensitive to fluctuations far above the cutoff scale.

It is easily proven that (3.29) applies to standard renormalisable quantum field theories in four dimensions including non-Abelian gauge theories that involve momentum-dependent couplings. In these theories, the locality property follows from power-counting arguments. However, for perturbatively non-renormalisable theories in four dimensions power counting suggests non-local flows and (3.29) must be a consequence of non-trivial cancellations. In gravity this has been shown for the graviton propagator [325, 327]. It is also reflected in the symmetry relation between graviton diagrams contributing to the Yang-Mills propagator [376]. Moreover, it is easily verified that a  $\phi^4$ -theory with a momentum-dependent coupling such as  $\int_x \phi^2 \partial^2 \phi^2$  does not satisfy the locality condition (3.29), as no cancellation between tensor structures is possible. This entails that momentum locality in quantum gravity is linked to diffeomorphism invariance, and we conjecture that it is indeed rooted in the latter.

Note that (3.29) does not hold, even for quantum field theories that are perturbatively renormalisable in four dimensions, if some of the channels  $t_i/k^2$  stay finite: the flow always involves diagrams with a finite momentum transfer. However, those diagrams correspond to IR processes such as Bremsstrahlung, which is why they do not reflect the UV behaviour of the theory. In summary the above discussion suggests that the relation (3.29) is a necessary requirement for local quantum field theories.

In this section, we show that (3.29) also applies to the graviton three-point function. Together with the momentum locality of the two-point function shown in [325, 327] this

	Finite difference		Derivative	
	$\eta_{\phi_i}(p^2)$	$\eta_{\phi_i} = 0$	$\eta_{\phi_i}(p^2)$	$\eta_{\phi_i} = 0$
$g^*$	0.66	0.96	0.58	0.57
$\mu^*$	-0.59	-0.35	-0.44	-0.16
$\lambda_3^*$	0.11	-0.024	0.028	-0.16
$\lambda_1^*/\sqrt{g_1}$	0.39	0.19	0.22	0.11
Critical exponents	$1.4 \pm 4.1i$ -14 2.2	$2.1 \pm 2.4i$ -5.8 3	$1.6 \pm 5.5i$ -6.5 2.5	$1.5 \pm 1.8i$ -1.6 3

Table 3.1.: Properties of the UV fixed point for different momentum parametrisations, namely using a finite difference of the flow and a derivative at  $p = 0$ . The values acquired with the latter correspond to the analytic equations given in (3.31). Note, that  $\lambda_1/\sqrt{g_1}$  is a non-dynamical background coupling originating from the graviton one-point function.

provides strong indications for the momentum locality of RG-gravity. Fig. 3.2 depicts the momentum dependence of the flows for the graviton two- and three-point functions,  $|\partial_t \Gamma_k^{(2)}|$  and  $|\partial_t \Gamma_k^{(3)}|$ , respectively as well as the corresponding ratios according to (3.29). Since  $|\partial_t \Gamma_k^{(2)}|$  and  $|\partial_t \Gamma_k^{(3)}|$  quickly approach constants, the ratios decay with  $1/p^2$  for large momenta.

In order to prove (3.29) for the three point function, an arbitrary kinematic configuration is used and parameterised by  $|p_1|$ ,  $|p_2|$  and the angle  $\vartheta_{12}$ . The large momentum limit is then characterised by  $|p_1| = |p_2| = p \rightarrow \infty$ . Simple power counting of the momentum structure of the flow leads to the naive expectation that  $\lim_{p/k \rightarrow \infty} \text{Flow}_G^{(3)} \sim p^2$ . In this case the ratio in (3.29) would tend to a constant. However, an analytic asymptotic expansion around  $p = \infty$  shows that the  $p^2$ -contribution vanishes identically in the large-momentum limit by non-trivial cancellations between all diagrams of the graviton three-point function, see Fig. 3.1. As a consequence,  $\lim_{p/k \rightarrow \infty} \text{Flow}_G^{(3)}$  tends to a constant and the ratio in (3.29) vanishes. This is valid for all values of the angle  $\vartheta_{12}$ , i.e. for all kinematic configurations. For an explicit example see Fig. 3.2 for the symmetric momentum configuration. Fig. 3.2 further displays that (3.29) is also satisfied by the graviton two-point function, see also [325, 327]. We conclude that locality is always satisfied by the flows of two- and three-point functions. We emphasise again that it is indispensable that all external momenta are taken to infinity. Indeed, for configurations with mixed UV-IR limit equation (3.29) does not hold.

### 3.5.2. UV fixed point

Fixed points are defined by vanishing flows of all dimensionless dynamical couplings, that is  $g_3$ ,  $\lambda_3$  and  $\mu$  in the present setup. Most importantly, we find a UV fixed point with one irrelevant direction that is approximately directed along the  $\lambda_3$ -axis.

We identify  $\lambda_3 \equiv \lambda_4 \equiv \lambda_5$  and  $g_3 \equiv g_4 \equiv g_5$  in order to close the flow equations, and use the notation  $g := g_3$ . The UV fixed point described below is obtained with the finite difference procedure, leading to the flow equations (3.28) and (3.27), as well as the one for  $\mu$  already presented in [327]. The anomalous dimensions are evaluated with their full momentum dependence. The fixed point values read

$$(g^*, \mu^*, \lambda_3^*) = (0.66, -0.59, 0.11), \quad (3.30a)$$

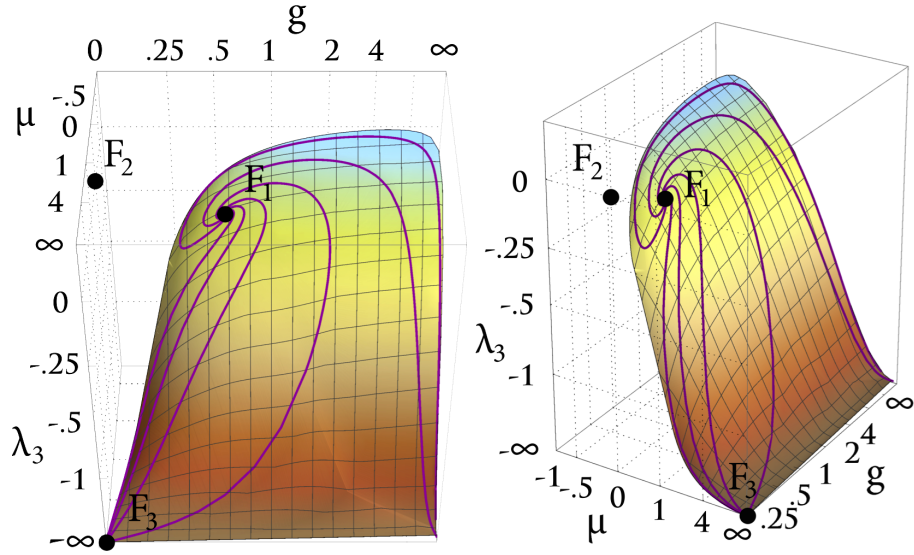


Figure 3.3.: Phase diagram for the couplings  $g$ ,  $\lambda_3$  and  $\mu$  in two different views. The phase diagram was calculated using the analytic equations (3.31). The system exhibits a non-trivial UV fixed point,  $F_1$ , with two attractive and one repulsive direction. The Gaussian fixed point and a non-trivial IR fixed point are denoted as  $F_2$  and  $F_3$ , respectively. The set of trajectories that approach  $F_1$  constitutes two-dimensional UV critical hypersurface represented in gradient colours.

with the critical exponents  $\theta_1$ ,  $\theta_2$  and  $\theta_3$  given by

$$(\theta_{1/2}, \theta_3) = (1.4 \pm 4.1 i, -14). \quad (3.30b)$$

Details on the computation of critical exponents are given in App. B.1. As already mentioned above, the UV fixed point (3.30a) has the interesting property that it is not fully UV attractive: it exhibits two relevant and one irrelevant direction. In (3.30b), this is reflected by two critical exponents with negative real parts,  $\theta_1$  and  $\theta_2$ , and one with positive real part,  $\theta_3$ . The irrelevant direction of the UV fixed point (3.30a) is approximately directed along the  $\lambda_3$  axis. The critical exponents corresponding to the UV relevant directions of the fixed points are complex, which accounts for a spiral behaviour of RG-trajectories in the vicinity of the UV fixed point. Note, that  $\theta_3$  in (3.30b) is one order of magnitude larger than  $\theta_1$  and  $\theta_2$ . This kind of instability of critical exponents was also found in [282] within  $f(R)$ -gravity. There, a convergence of the critical exponents to smaller values was observed after the inclusion of higher order operators, i.e. higher powers  $R^n$ . Similarly, we expect  $\theta_3$  to become smaller, if dynamical couplings  $g_4$  and  $\lambda_4$  are included and we will check that explicitly in the next chapter.

### 3.5.3. Global phase diagram and analytic flow equations

The flow equation (3.28) does not have a closed analytic form. However, for a more accessible presentation, analytic flow equations are favourable. An analytic expression for  $\partial_t g$  is obtained by taking a derivative of  $\text{Flow}_G^{(3)}$  with respect to  $p^2$  at  $p = 0$ . We stress, that this method is considerably less accurate in modelling the momentum dependence of the

flow. Nonetheless, the resulting analytic flow equation for  $g$  shares the main features with (3.28). This even holds for all anomalous dimensions set to zero,  $\eta_{\phi_i} = 0$ . [Tab. 3.1](#) displays the properties of the non-trivial fixed point as obtained from the different methods.

The analytic flow equations for the presented vertex flow of gravity with  $\eta_{\phi_i} = 0$  are given by

$$\begin{aligned} \partial_t g &= 2g + \frac{8g^2}{19\pi} \left( \frac{584\lambda_3^3 - 910\lambda_3^2 + 445\lambda_3 - \frac{299}{4}}{15(\mu+1)^5} - \frac{47}{8(\mu+1)^2} \right. \\ &\quad \left. - \frac{5}{8} + \frac{864\lambda_3^3 + 133\lambda_3^2 - 112\lambda_3 + \frac{49}{4}}{6(\mu+1)^4} - \frac{60\lambda_3^2 - 58\lambda_3 - 15}{6(\mu+1)^3} \right), \\ \partial_t \lambda_3 &= - \left( 1 + \frac{\partial_t g}{2g} \right) \lambda_3 + \frac{g}{\pi} \left( \frac{2\lambda_3^3 - 4\lambda_3^2 + 3\lambda_3 - \frac{11}{20}}{(\mu+1)^4} - 4 \frac{4\lambda_3^2 - \lambda_3}{(\mu+1)^3} + \frac{1 - 3\lambda_3}{(\mu+1)^2} + \frac{6}{5} \right), \\ \partial_t \mu &= -2\mu + \frac{2g}{\pi} \left( \frac{16\lambda_3^2 - 8\lambda_3 + \frac{7}{4}}{3(\mu+1)^3} + \frac{2\lambda_3 - 1}{(\mu+1)^2} - 1 \right), \\ \partial_t \left( \frac{\lambda_1}{\sqrt{g_1}} \right) &= -3 \frac{\lambda_1}{\sqrt{g_1}} + \frac{\sqrt{g}}{2\pi} \left( \frac{1}{(\mu+1)^2} + \frac{4}{3} \right). \end{aligned} \tag{3.31}$$

[Fig. 3.3](#) shows the phase diagram for the couplings  $(g, \mu, \lambda_3)$  as calculated from (3.31). The purple lines are trajectories along the flow that terminate at the non-trivial UV fixed point  $F_1$ . The set of all trajectories constitutes the two-dimensional critical hypersurface represented in gradient colours. In the IR, the trajectories flow towards  $F_3 = (0, \infty, -\infty)$  or, alternatively, towards  $(\infty, \infty, -\infty)$ . The IR fixed point  $F_3$  was also observed in [\[327\]](#). In the vicinity of  $F_3$  all couplings scale classically since for  $\mu \rightarrow \infty$  the loop contributions to the flow tend to zero. Neither the trivial Gaussian fixed point  $F_2$ , nor the third, non-trivial IR fixed point, which was first found in [\[327\]](#) and is located at  $(0, -1, \infty)$ , are reached by any UV-finite trajectory in the presented setup. For the latter, this is expected to change if the vertices are expanded about a non-flat background [\[258\]](#).

## 3.6. Summary

In this chapter we have presented the first computation of a genuine dynamical Newton's coupling based on a vertex flow. The dynamical parameters are the graviton-mass parameter  $\mu$ , Newton's coupling  $g$  derived from the graviton three-point function, and the coupling  $\lambda_3$  of its momentum-independent part. The full momentum-dependence of the propagators is encoded in anomalous dimension,  $\eta_h(p^2)$  and  $\eta_c(p^2)$ . The flows of these quantities constitute a minimally self-consistent truncation of the system of dynamical couplings in quantum gravity. In the UV we found a fixed point with two relevant and one irrelevant direction, the latter being approximately directed along the  $\lambda_3$ -axis. This hints at a finite dimensional critical UV-surface, and supports the asymptotic safety scenario.

We have introduced the property of momentum locality for vertex flows. It is suggestive that this property is a necessary requirement for local quantum field theories. We have shown that it is non-trivially realised for the graviton two- and three-point functions, being linked to diffeomorphism invariance.

## 4. Towards apparent convergence in asymptotically safe quantum gravity

### 4.1. Introduction

In the last chapter the systematic vertex expansion in quantum gravity has been pushed to the graviton three-point function, for the first time including a dynamical graviton-scattering in the asymptotic safety analysis. In this chapter we extend the vertex expansion to the graviton four-point function. Apart from the significant technical challenge such an upgrade of the approximation has posed, we think that this constitutes a necessary and significant progress towards asymptotically safe gravity:

- As such it is an important step towards apparent convergence of the vertex expansion in quantum gravity: apparent convergence aims at the convergence of vertices as well as observables in the order of a given systematic expansion scheme; here we use the vertex expansion scheme. Together with the investigation of the regulator (in-)dependence of observables this provides a systematic error estimate in the present approach, and should be compared with apparent continuum scaling and extrapolation on the lattice.
- The present approximation allows for the identification of diffeomorphism-invariant structures in the vertex expansion, i.e.  $R^2$  and  $R_{\mu\nu}^2$  tensor structures as well as those of higher derivative invariants. This is not only important for getting access to the number of relevant directions at the asymptotically safe UV fixed point in quantum gravity, but can also provide non-trivial support and additional information for computations within the standard background field approximation.
- It is the first approximation in the asymptotic safety approach to gravity where the flow of the pivotal building block, the two-point correlation function or (inverse) propagator, is closed: The flows of all involved vertex functions are computed within given approximations. As the propagator is the core object in the present approach, we consider this an important milestone on the way towards asymptotically safe quantum gravity.

As a main result of this chapter, we find further significant evidence for a non-trivial UV fixed point in quantum gravity. This fixed point has three relevant directions and two repulsive ones. The three relevant directions can be associated with the cosmological constant (graviton mass parameter), Newton's coupling and the  $R^2$ -coupling, see Sec. 4.3. We also investigate the stability of this UV fixed point and observe that the system is significantly less sensitive to the closure of the flow equations than previous truncations. In addition, we observe that the critical exponents also become less sensitive to the details of the approximations. These are two necessary signatures of apparent convergence. Furthermore, we investigate the IR behaviour of the system and find trajectories connecting the UV fixed point with classical general relativity in the IR.

## 4.2. Flows of correlation functions

In this section we recap some details from the previous chapter and specify the some of the details to the present truncation of the graviton four point function

### 4.2.1. Recap

In the last chapter we have introduced the schematic vertex expansion for the functional renormalisation group equation, see [Sec. 3.3.2](#). We have detailed that the momentum dependent coupling  $G_3(\mathbf{p})$  has in principle overlap with

$$R, \quad R^{\mu\nu} f_{\mu\nu\rho\sigma}^{(3)}(\nabla) R^{\rho\sigma}, \quad R^{\mu\nu} R^{\rho\sigma} f_{\mu\nu\rho\sigma\omega\zeta}^{(3)}(\nabla) R^{\omega\zeta}, \quad (4.1)$$

where the invariants  $R^2$  and  $R^3$  can be excluded due to their order in transverse-traceless graviton fluctuation fields, see also [\(3.21\)](#). Consequently we need to include the graviton four-point function and thus the coupling  $G_4(\mathbf{p})$  in order to have an overlap with  $R^2$ . For  $G_4(\mathbf{p})$  we find that the set of invariants is spanned by

$$R, \quad R^{\mu\nu} f_{\mu\nu\rho\sigma}^{(4)}(\nabla) R^{\rho\sigma}, \quad R^{\mu\nu} R^{\rho\sigma} f_{\mu\nu\rho\sigma\omega\zeta}^{(4)}(\nabla) R^{\omega\zeta}, \quad R^{\mu\nu} R^{\rho\sigma} R^{\omega\zeta} f_{\mu\nu\rho\sigma\omega\zeta\xi\eta}^{(4)}(\nabla) R^{\xi\eta}, \quad (4.2)$$

where again the invariants  $R^3$  and  $R^4$  can be excluded.

In the next section we will investigate the momentum dependence of the flow of the graviton  $n$ -point functions. We will show that the by far dominant contribution to  $G_3(\mathbf{p})$  in the momentum range  $0 \leq p^2 \leq k^2$  stems from the invariant  $R$ . All higher momentum dependencies of the graviton three-point function are covered by the momentum dependence of the graviton wave function renormalisation. In terms of [\(3.20\)](#) it implies that the dominant tensor structure for the transverse-traceless mode is given by  $f_R^{(3)}$  with  $P_R^{(3)} = 1$ . The  $R_{\mu\nu}^2$  tensor structure vanishes approximately, see [\(4.4\)](#). This gives support to the approximation of a momentum independent coupling  $G_3$  as used in the last chapter.

In contrast to the situation for the two- and three point function, the  $R^2$  invariant overlaps with our transverse-traceless projection for the graviton four-point function. Indeed, its flow receives significant contributions from the invariant  $R^2$ . It follows that for the graviton four-point function  $R$  is not the only dominant invariant in the momentum range  $0 \leq p^2 \leq k^2$ , as we show in [Sec. 4.2.2](#). In consequence we either have to disentangle contributions from  $R$  and  $R^2$  tensor structures in terms of an additional tensor structure or we resolve the momentum dependence of  $G_4(\mathbf{p})$ . Here we follow the latter procedure, see [Sec. 4.2.4](#) for details.

### 4.2.2. Momentum dependence of the graviton $n$ -point functions

We now investigate the momentum dependence of the flow of the graviton  $n$ -point functions as defined in equation [\(3.23\)](#). We restrict ourselves to the momentum range  $0 \leq p^2 \leq k^2$  as well as to the transverse-traceless part of the graviton  $n$ -point functions.

The first non-trivial result is that the flows of the graviton three- and four-point functions projected on the tensor structure of the gravitational coupling and divided by  $(-\frac{n}{2}\eta_h(p^2) - n + 2)$  are well described by a polynomial in  $p^2$ , provided that the couplings  $\lambda_n$  are small

$$\frac{\text{Flow}_G^{(3)}(p^2)}{-\frac{3}{2}\eta_h(p^2) - 1} \approx a_0 + a_1 p^2, \quad \frac{\text{Flow}_G^{(4)}(p^2)}{-2\eta_h(p^2) - 2} \approx b_0 + b_1 p^2 + b_2 p^4, \quad (4.3)$$

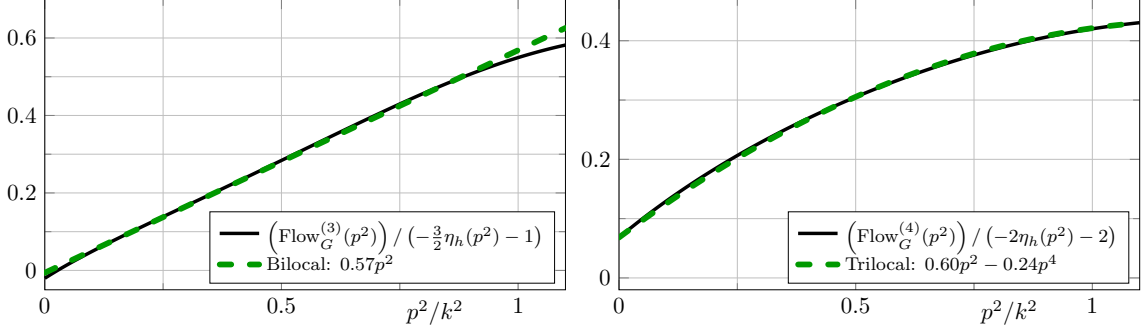


Figure 4.1.: Momentum dependence of the flow of the graviton three-point function (left) and the graviton four-point function (right) divided by  $(-\frac{n}{2}\eta_h(p^2) - n + 2)$  as defined in (4.3). The flows are evaluated at  $(\mu, \lambda_3, \lambda_4, g_3, g_4) = (-0.4, 0.1, -0.1, 0.7, 0.5)$  and  $\lambda_6 = \lambda_5 = \lambda_3$  as well as  $g_6 = g_5 = g_4$ . The flows have such a simple polynomial structure as long as all couplings  $\lambda_n$  remain small, i.e.  $|\lambda_n| \lesssim 1$ . Importantly, the inclusion of a  $p^4$  term in the left panel offers no significant improvement. Note that the constant parts of the functions are irrelevant for the beta functions since they are extracted from a different tensor projection. For  $p^2 > k^2$  the momentum dependence of the flows is not polynomial anymore.

with some constants  $a_i$  and  $b_i$  that depend on the evaluation point in theory space. This momentum dependence is displayed in Fig. 4.1. We emphasise that these equations only hold in the momentum range  $0 \leq p^2 \leq k^2$ , if the flow is generated by Einstein-Hilbert vertices, and if the constant parts of the vertices are small, i.e.  $|\lambda_n| \lesssim 1$ . If the condition of small  $\lambda_n$  is violated, then the flow as in (4.3) is non-polynomial. We did not compute the flow generated by an action including higher curvature terms, however, we suspect that the flow will still be polynomial but possibly of a higher degree.

It is important to note that the graviton three- and four-point functions have a different highest power in  $p^2$ . This is a second non-trivial result for the following reasons: as already mentioned before, the coupling  $g_3(p^2)$  has an overlap with  $R$  and  $R_{\mu\nu}^2$ , and higher derivative terms in  $f_{R_{\mu\nu}^2}^{(3)}$ , but not with any  $R^2$  tensor structures in  $f_{R^2}^{(3)}$ , cf. (3.20). For example, the generation of  $R_{\mu\nu}^2$  with  $P_{R_{\mu\nu}^2}^{(3)} = 1$  would manifest itself in a  $p^4$ -contribution to the flow of the graviton three-point function. Eq.(4.3) and Fig. 4.1 show that such a  $p^4$ -contribution as well as higher ones are approximately vanishing. This demonstrates in particular that the generation of  $R_{\mu\nu}^2$  is non-trivially suppressed. In other words,

$$f_{R_{\mu\nu}^2}^{(3)} \approx 0, \quad (4.4)$$

where the superscript indicates the three-graviton vertex.

On the other hand, the projection on  $g_4(p^2)$  overlaps with  $R$ ,  $R_{\mu\nu}^2$ ,  $R^2$  tensor structures, and the related higher derivatives terms in  $f_{R_{\mu\nu}^2}^{(4)}$  and  $f_{R^2}^{(4)}$ . It also overlaps with curvature invariants to the third power with covariant tensors such as  $f_{R_{\mu\nu}^3}^{(4)}$  and similar ones. Note that it has no overlap with  $f_{R^3}^{(4)}$ .

Similarly to possible  $p^4$ -contributions for the three-graviton vertex,  $p^6$ -contributions and even higher powers in  $p^2$  could be generated but are non-trivially suppressed. The

$p^4$ -contribution to the flow, which is described in (4.3) and displayed in Fig.4.1, could stem from either  $R^2$  or  $R_{\mu\nu}^2$  tensor structures. Now we use (4.4). It entails that the graviton three-point vertex does not generate the diffeomorphism invariant term  $R_{\mu\nu}^2$  although it has an overlap with it. This excludes  $R_{\mu\nu}^2$  as a relevant UV direction, which would otherwise be generated in all vertices. This statement only holds if we exclude non-trivial cancellations of which we have not seen any signature. Accordingly we set

$$f_{R_{\mu\nu}^2}^{(4)} \approx 0, \quad (4.5)$$

and conclude that this  $p^4$ -contribution or at least its UV-relevant part stems solely from  $R^2$ . It may be used to determine  $f_{R^2}^{(4)}$ .

In summary, the above statements about the momentum-dependencies are highly non-trivial and show that  $R^2$ -contributions are generated while  $R_{\mu\nu}^2$  and other higher derivative terms are strongly suppressed. These non-trivial findings also allow us to determine the most efficient way to project precisely onto the couplings of different invariants. This is discussed in Sec. 4.2.5.

We close this section with a brief discussion of the effect of higher derivative terms on perturbative renormalisability and the potential generation of massive ghost states. As already discussed in [82] in a perturbative setup, it is precisely the  $R_{\mu\nu}^2$  term that makes the theory perturbatively renormalisable. However, in this setup it gives rise to negative norm states. On the other hand, the  $R^2$  term neither ensures perturbative renormalisability, nor does it generate negative norm states. This is linked to the fact that the  $R^2$  term does not contribute to the transverse-traceless part of the graviton propagator. Consequently, the non-trivial suppression of  $R_{\mu\nu}^2$  tensor structures might be interpreted as a hint that we do not suffer from massive ghost states. However, a fully conclusive investigation requires the access to the pole structure of the graviton propagator, and hence a Wick rotation. Progress in the direction of real-time flows in general theories and gravity has been made e.g. in [299–302, 377–381].

### 4.2.3. Higher-order vertices and the background effective action

The results in the last section immediately lead to the question about the importance of the higher-order covariant tensor structures like e.g.  $f_{R^n}$  that have no overlap with the graviton  $n$ -point functions computed in this chapter. These are potentially relevant for the flows of  $G_5$  and  $G_6$ . These tensors have been dropped here, thus closing our vertex expansion. However, we may utilise previous results obtained within the background field approximation for estimating their importance: first we note that  $R^2$  gives rise to a new relevant direction, as we will show in Sec. 4.3.1. This has also been observed for the background field approximation [269, 271, 272, 274, 281]. There it has also been shown that the critical dimensions of the  $R^n$ -terms approximately follow their canonical counting [281]. Furthermore, our results so far have sustained the qualitative reliability of the background field approximation for all but the most relevant couplings. Indeed, it is the background field-dependence of the regulator that dominates the deviation of the background approximation from the full analysis for the low order vertices, and in particular the mass parameter  $\mu$  of the graviton. This field-dependence is less relevant for the higher order terms. Thus, we may qualitatively trust the background field approximation for higher curvature terms. This means that they are of sub-leading importance and can be dropped accordingly.

Finally, the above findings together with those from the literature suggest that an Einstein-Hilbert action is generating a diffeomorphism-invariant  $R^2$  term but not an  $R_{\mu\nu}^2$  term in the diffeomorphism-invariant background effective action  $\Gamma_k[g] = \Gamma_k[g, \phi = 0]$ . Moreover, no higher-derivative terms are generated if a non-trivial wave function renormalisation  $Z_h(p^2)$  and graviton mass parameter  $\mu = -2\lambda_2$  are taken into account. Note that this only applies for an expansion with  $p^2 < k^2$ . This is a very interesting finding as it provides strong non-trivial support for the semi-quantitative reliability of the background approximation in terms of an expansion in  $R$  for spectral values smaller than  $k^2$  subject to a resolution of the fluctuating graviton propagator:  $\mu$  and  $Z_h$  have to be determined from the flows of the fluctuation fields or in terms of the mNIs.

#### 4.2.4. Flow equations for the couplings

We obtain the flow equations for the couplings the  $n$ -point function, that are contracted with the projection operators as described in Sec. 3.4.2. The flow equations for the couplings up to graviton three-point function remain unchanged compared to the last chapter and the procedure how we obtain them is described in Sec. 3.4.3.

We have to emphasise again that the momentum dependence of the flow for  $g_3(p^2)$  is trivial, see Fig. 4.1. This allows for an easy extraction of the momentum dependence and as in the last chapter we use a bilocal projection between  $p = 0$  and  $p = k$ . From this we obtain an equation for  $g_3(k^2)$ . In contrast, the flow of the graviton four-point function exhibits a  $p^4$  contribution, implying a non-trivial  $g_4(p^2)$ . This makes the extraction of the momentum dependence more tricky. Still we obtain the flow equation for  $g_4(k^2)$  from a bilocal momentum projection at  $p^2 = 0$  and  $p^2 = k^2$ , but this uses a further approximation that relies on the fact that the coupling  $\lambda_4$  remains small. We refer to this equation as a bilocal equation. It is explicitly displayed in App. B.5, see equation (B.11). Within our setup this equation gives the best approximation of the vertex flows since it feeds back the most important momentum information into the flow. This further entails that the coupling  $g_4(k^2)$  includes information about the invariants  $R$  and  $R^2$ . In the next section we also show a trilocal momentum projection that disentangles the contribution from  $R$  and  $R^2$ , but consequently feeds less information about the vertex flow back.

The flow equation for  $\lambda_4$  is obtained from the momentum independent part of the graviton four-point function and is explicitly displayed in App. B.5

#### 4.2.5. Disentangling $R$ and $R^2$ tensor structures

In this section we present projection operators that disentangle contributions from  $R$  and  $R^2$  tensor structures to the flows of the couplings  $g_n(p^2)$ . In the present setup this only allows us to switch off the  $R^2$  coupling and thus to check the importance of the  $R^2$  coupling.

For the disentanglement, we have to pay attention to two things: First of all, a local momentum projection at  $p^2 = 0$  is very sensitive to small fluctuations and in consequence not very precise with regard to the whole momentum range  $0 \leq p^2 \leq k^2$ . This is explicitly shown in App. B.4. Hence, we have to rely on non-local momentum projections. Here the highest polynomial power of  $p^2$ , as indicated in (4.3), dictates the simplest way of projecting on the  $p^2$ -coefficient. The graviton three-point function is at most quadratic in the external momentum, and consequently it is enough to use a bilocal projection at  $p^2 = 0$  and  $p^2 = k^2$ . The resulting equation (B.12) can be found in App. B.5.

The graviton four-point function, on the other hand, has  $p^4$  as its highest momentum power, i.e. it is of the form

$$f(p^2) = b_0 + b_1 p^2 + b_2 p^4, \quad (4.6)$$

see also (4.3). Thus a bilocal momentum projection would not extract the  $p^2$  coefficient  $b_1$  alone. Instead, we use a trilocal momentum projection at  $p^2 = 0$ ,  $p^2 = k^2/2$ , and  $p^2 = k^2$  in order to solve the above equation for  $b_1$ . Consequently we solve a system of linear equations and obtain

$$b_1 = -3f(0) + 4f(k^2/2) - f(k^2). \quad (4.7)$$

The resulting flow equation (B.13) is again presented in App. B.5.

For even higher order momentum contributions we would have to use even more points of evaluation. These momentum projections together with the observation of (4.3) guarantee that we project precisely on the  $p^2$  coefficient in the whole momentum range  $0 \leq p^2 \leq k^2$ .

A natural upgrade of the current approximations amounts to the introduction of a second tensor structure that is orthogonal to the Einstein-Hilbert one in terms of these projections. Within our uniformity assumption this is considered to be sub-leading, and the momentum-dependence of  $g_4(p^2)$  takes care of the contribution of the  $R^2$  tensor structure  $f_{R^2}^{(4)}$ . While the orthogonal projection on the respective flow is simple, its back-feeding demands a two tensor structure approximation of the three- and four-graviton vertex in the flow, the implementation of which is deferred to future work.

Here, we only perform a further check of the relevance of the  $R^2$  tensor structure. This sustains the fact that the inclusion of the four-graviton vertex with its contribution of the  $R^2$  tensor structure leads to an additional UV-relevant direction. To that end we generalise our ansatz for the graviton four-point function such that we can extract a flow equation for both the Einstein-Hilbert tensor structure as well as for the  $R^2$  tensor structure. As already mentioned above, we cannot feed the generated coupling back into the flows, since they are given by vertices with Einstein-Hilbert tensor structures. Instead we compute the fixed point value that arises only from the Einstein-Hilbert tensor structures.

As the ansatz for the transverse-traceless graviton four-point function we choose

$$\Gamma_k^{(4)}(p^2) = Z_h^2(p^2) G_4 \left( C_{\Lambda_4}^{G_4} \Lambda_4 + C_{p^2}^{G_4} p^2 + C_{\Omega_4}^{G_4} \Omega_4 p^4 \right), \quad (4.8)$$

which is precisely the vertex that emerges from the sum of Einstein-Hilbert tensor structure and  $R^2$  tensor structure. The related generating diffeomorphism-invariant action for this four-graviton vertex is

$$S = S_{\text{EH}} + \frac{1}{16\pi G_N} \int d^4x \sqrt{g} \Omega R^2, \quad (4.9)$$

where  $S_{\text{EH}}$  is defined as in (3.4). The flow of  $\Omega_4$  is then obtained by the trilocal momentum projection described below (4.6). For  $b_2$  we obtain

$$b_2 = 2f(0) - 4f(k^2/2) + 2f(k^2). \quad (4.10)$$

The explicit form of the resulting flow equation (B.14) for the dimensionless coupling  $\omega_4 = \Omega_4 k^2$  is given in App. B.5. Note that in the present approximation, the flows do not depend on the coupling  $\omega_4$  since it does not feed back into the vertices.

#### 4.2.6. Computational details

The computations of correlation functions described in this section involve contractions of very large tensor structures. To give a rough estimate: the classical Einstein-Hilbert three-point vertex alone consists of around 200 terms, and the classical graviton propagator of 7 terms. For the box diagram of the flow of the graviton four-point function, displayed in [Fig. 3.1](#), this results in a total number of approximately  $200^4 \cdot 7^4 \approx 4 \cdot 10^{12}$  terms, if no intermediate simplifications are applied.

These contractions are computed with the help of the symbolic manipulation systems *FORM* [382, 383] and *Mathematica*. For individual tasks, we employ specialised *Mathematica* packages. In particular, we use *xPert* [384] for the generation of vertex functions, *DoFun* [385] to obtain symbolic flow equations, and the *FormTracer* [386] to create optimised *FORM* scripts to trace diagrams.

### 4.3. Asymptotic safety

In this section, we discuss the UV fixed point structure of our system. We first present our best result, which includes the tensor structures as presented in [Sec. 3.4.1](#) and in particular in [\(3.19\)](#) and [\(3.21\)](#). The underlying UV-relevant diffeomorphism invariants turn out to be  $\Lambda$ ,  $R$ , and  $R^2$ . The  $R^2$  coupling is included via the momentum dependence of the gravitational coupling  $g_4(p^2)$ , see [Sec. 4.2.2](#). As a main result we find an attractive UV fixed point with three attractive directions. The third attractive direction is related to the inclusion of the  $R^2$  coupling.

We further analyse the stability of this UV fixed point with respect to the identification of the higher couplings. We also analyse the previous truncation from [Chapter 3](#) and compare the stability of both truncations. Here we find that the improvement of the truncation increases the stability of the system. In particular, we find a rather large area in the theory space of higher couplings where the UV fixed point exists with three attractive directions throughout.

Lastly, we discuss the importance of the  $R^2$  coupling. In [Sec. 4.2.5](#) we have constructed projection operators that disentangle the contributions from  $R$  and  $R^2$  tensor structures. This allows us to switch off the  $R^2$  coupling and compare the stability of the reduced system to that of the full system. We find that the reduced system is significantly less stable, and that the area in the theory space of higher couplings where the fixed point exists is rather small. This highlights the importance of the  $R^2$  coupling.

#### 4.3.1. UV fixed point

In this section we display the UV fixed point structure of our full system. This means that we feed back the generated  $R^2$  coupling via the momentum dependence of the gravitational coupling  $g_4(p^2)$ , as discussed in [Sec. 4.2.2](#). Fixed points are by definition points where the flows of the dimensionless couplings vanish. In consequence, we look for the roots of the equations [\(B.7\)](#), [\(B.10\)](#), [\(B.12\)](#), and [\(B.11\)](#). We use the identification scheme  $g_6 = g_5 = g_4$  and  $\lambda_6 = \lambda_5 = \lambda_3$ . We find a UV fixed point at the values

$$(\mu^*, \lambda_3^*, \lambda_4^*, g_3^*, g_4^*) = (-0.45, 0.12, 0.028, 0.83, 0.57). \quad (4.11)$$

The fixed point values are similar to those of the previous truncation in the last chapter, see [\(3.30a\)](#). The biggest change concerns the graviton mass parameter, which is now less

negative and thus further away from its pole. Moreover, it is remarkable that the new couplings  $\lambda_4$  and  $g_4$  are close to their lower counterparts  $\lambda_3$  and  $g_3$ , but not at precisely the same values. Since we use the difference between these couplings to parameterise the breaking of diffeomorphism invariance, this is more or less what we expected. This issue is further discussed in the next section.

We do not have access to the full stability matrix of the UV fixed point due to the unknown flow equations of the higher couplings. For this reason, we discuss two different approximations of the stability matrix. The main difference between these two approximations concerns the order of taking the derivatives and identifying the higher couplings, which is explained in more detail in App. B.1. We argue that in a well converged approximation scheme the most relevant critical exponents should not depend on the approximation of the stability matrix. Thus, we can use the two different approximations to judge the quality of the current level of truncation. We define the critical exponents as minus the eigenvalues of the stability matrix. We call the critical exponents of the first approximation  $\bar{\theta}_i$ , and the ones of the second approximation  $\tilde{\theta}_i$ . The critical exponents using the first approximation are given by

$$\bar{\theta}_i = (4.7, 2.0 \pm 3.1i, -2.9, -8.0), \quad (4.12)$$

while the critical exponents using the second approximation are

$$\tilde{\theta}_i = (5.0, 0.37 \pm 2.4i, -5.6, -7.9). \quad (4.13)$$

Hence this fixed point has three attractive directions in both approximations of the stability matrix. The third attractive direction compared to the system of the graviton three-point function, cf. (3.30b), is related to the fact that the graviton four-point function has an overlap with  $R^2$ , which we feed back via the momentum dependence of the gravitational coupling  $g_4(p^2)$ . The  $R^2$  coupling has also been relevant in earlier computations with the background field approximation [269, 271, 272, 274, 281]. In addition, note that the most attractive eigenvalue is almost identical in both approximations of the stability matrix. This is a positive sign towards convergence since it is expected that the lowest eigenvalue is the first that converges, cf. App. B.1.

Furthermore, the anomalous dimensions at the UV fixed point read

$$(\eta_h^*(0), \eta_h^*(k^2), \eta_c^*(0), \eta_c^*(k^2)) = (0.56, 0.079, -1.28, -1.53), \quad (4.14)$$

where we have chosen to display the anomalous dimensions at the momenta that feed back into the flow. All anomalous dimensions stay well below the reliability bound  $\eta_{\phi_i}(p^2) < 2$ , which we will introduce later in Chapter 6.

### 4.3.2. Stability

In the following we investigate the UV fixed point from the previous section by varying the identification of the higher couplings. Again we look for the roots of the equations (B.7), (B.10), (B.12), and (B.11). These equations however still depend on the higher couplings  $g_5$ ,  $g_6$ ,  $\lambda_5$ , and  $\lambda_6$ . We have to identify these couplings with the lower ones or set them to constants in order to close the flow equations.

It is a natural choice to simply set these higher couplings equal to lower ones, e.g.  $g_6 = g_5 = g_3$  and  $\lambda_6 = \lambda_5 = \lambda_3$ , as done in the previous section. The couplings would

fulfil this relation exactly in a fully diffeomorphism invariant setup. However, such a diffeomorphism invariant setup is not at hand. In fact, we can parameterise the breaking of diffeomorphism invariance via these couplings, e.g. by writing  $g_n = g_3 + \Delta_{g_n}$ . Here we have designated  $g_3$  as a reference coupling since it is the lowest genuine gravitational coupling. For this reason, it is also the most converged gravitational coupling within this vertex expansion, thus justifying this choice. In general we expect  $\Delta_{g_n}$  to be small and in consequence we vary the identification of the higher couplings only in this part of the theory space of higher couplings. The quantity  $\Delta_{g_4}$  is indeed small at the UV fixed point presented in the last section, see (4.11). More precisely, it takes the value  $|\Delta_{g_4}/g_3| \approx 0.3$  at this UV fixed point.

In this analysis we choose to identify

$$g_5 = \alpha_1 g_3, \quad g_6 = \alpha_2 g_3, \quad (4.15)$$

and  $\lambda_6 = \lambda_5 = \lambda_3$  for simplicity, and investigate the existence of the UV fixed point as a function of the parameters  $\alpha_1$  and  $\alpha_2$ . In Fig. 4.2 the area where an attractive UV fixed point exists is displayed in blue. In the left panel, this is done for the previous truncation  $(\mu, \lambda_3, g_3)$ , see Chapter 3, and in the right panel for the current truncation  $(\mu, \lambda_3, \lambda_4, g_3, g_4)$ . At the border of the blue area the UV fixed point either vanishes into the complex plane or loses its attractiveness. Remarkably, both areas are rather large, suggesting that the existence of the UV fixed point is quite stable. Even more conveniently, the area increases with the improved truncation, suggesting that the system is heading towards a converging limit. Note that the number of attractive directions of the UV fixed point is constant throughout the blue areas, namely two in the left panel and three in the right panel.

We further analyse the fixed point values that occur within the blue area in the right panel of Fig. 4.2. Interestingly, the fixed point values are rather stable throughout the whole area where the UV fixed point exists. More precisely, they stay within the following intervals:

$$\begin{aligned} \mu^* &\in [-0.72, -0.19], & \lambda_3^* &\in [-0.018, 0.29], & \lambda_4^* &\in [-1.2, 0.12], \\ g_3^* &\in [0.22, 1.4], & g_4^* &\in [0.11, 0.97]. \end{aligned} \quad (4.16)$$

Hence, in particular the fixed point value of  $\lambda_3$  is already confined to a very small interval, and also a very small number. The latter is important since some of our approximations rely on the fact that the  $\lambda_n$  are small, see Sec. 4.2.2. The fact that  $\lambda_4^*$  is varying more strongly than  $\lambda_3^*$  is not surprising since we expect  $\lambda_3$  to be better converged, being a lower coupling. The fixed point values of  $g_3$  and  $g_4$  seem to try to compensate the change induced by the identification. Thus,  $g_3^*$  and  $g_4^*$  become larger towards the identification  $g_6 = g_5 = 0$  and smaller towards  $g_6 = g_5 = 2g_3$ . The shape of the area in the left panel in particular suggests the relation  $g_4^* < g_3^*$ , which is fulfilled by the improved truncation almost throughout the whole area where the fixed point exists. This is indeed a non-trivial prediction that has been fulfilled by our approximation scheme.

A further study of the dependence of the UV fixed point properties on the choice of identification is given in App. B.3.

### 4.3.3. Importance of the $R^2$ tensor structure

In the previous subsection we have fed back the  $R^2$  contributions to the flow via the momentum-dependent gravitational coupling  $g_4(p^2)$ . In order to check the quality of our

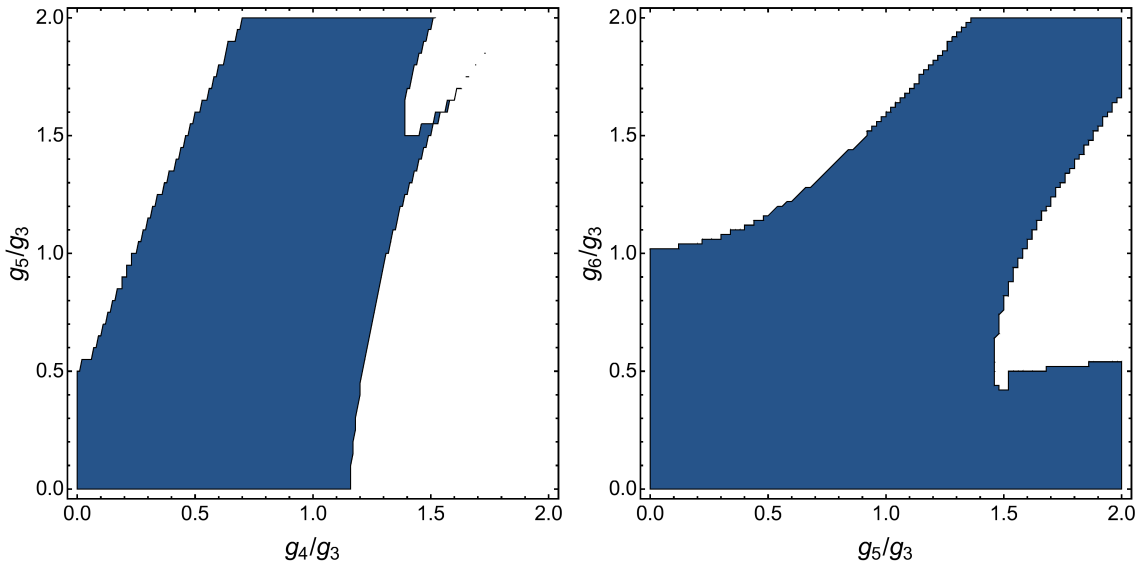


Figure 4.2.: Plots of the existence of an attractive non-trivial UV fixed point (blue) dependent on the higher couplings. Left: The system  $(\mu, \lambda_3, g_3)$ , see also [Chapter 3](#), dependent on the higher couplings  $g_4$  and  $g_5$ . Right: The system  $(\mu, \lambda_3, \lambda_4, g_3, g_4)$  dependent on the higher couplings  $g_5$  and  $g_6$ . The higher couplings  $\lambda_{n>n_{\max}}$  are always identified with  $\lambda_3$ . The blue area marks the region where an attractive UV fixed point was found. At the border of this area the fixed point either vanishes into the complex plane or loses its attractiveness. In both systems the area where the fixed point exists is rather large and contains the identification  $g_{n>n_{\max}} = g_3$ . Conveniently, the area increases for the better truncation, indicating that the system becomes more stable with an improvement of the truncation. The number of attractive directions is uniformly two in the left panel and three in the right panel.

approximation and to investigate the influence of the  $R^2$  tensor structure on the fixed point structure of the system, we switch off the  $R^2$  contribution in this section. We do the latter by projecting onto the  $p^2$  part of the flow via a trilocal momentum projection scheme, cf. [Sec. 4.2.2](#) and [Sec. 4.2.5](#). This is both an examination of the influence of  $R^2$  on the results presented in the previous subsections, as well as a proof of concept for disentangling the tensor structures of different invariants. Our analysis in this subsection suggests that leaving out the contribution of  $R^2$  leads to significantly less stable results.

In [Fig. 4.3](#) we display the result for the same analysis as in the previous section, but with the trilocal equation [\(B.13\)](#) for  $g_4$  instead. We find two fixed points with rather similar fixed point values. However, we are only interested in identifying the area in the theory space of the higher couplings where at least one UV fixed point exists. Thus, we unify both areas and obtain the blue area displayed in [Fig. 4.3](#). This area forms a rather narrow band whose total area is significantly smaller than for the momentum dependent gravitational coupling  $g_4(p^2)$ , cf. [Fig. 4.2](#). The identification  $g_6 = g_5 = g_3$  also does not lie within these regions, but just outside of them. Since we switched off the  $R^2$  contribution, a less stable fixed point structure was to be expected, and consequently these results highlight the importance of the  $R^2$  coupling.

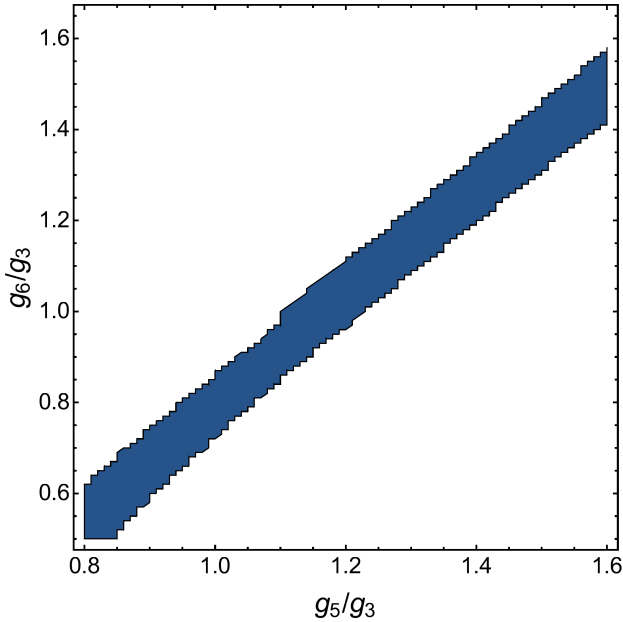


Figure 4.3.: Plot of the existence of an attractive non-trivial UV fixed point (blue) dependent on the higher couplings  $g_5$  and  $g_6$ . Here, the trilocal equation for the gravitational coupling  $g_4$  was used, which allows us to switch off the  $R^2$  coupling. We found two different fixed points with rather similar fixed point values. Each fixed point has its own area of existence in the theory space of the higher couplings. The blue area marks the unified area of both fixed points. Nevertheless, the area is significantly smaller than the areas displayed in Fig. 4.2. This reflects the importance of the  $R^2$  coupling.

#### 4.4. IR behaviour

In this section, we discuss the IR behaviour of the present theory of quantum gravity. We only consider trajectories that lie within the UV critical hypersurface, i.e. trajectories that are UV finite, and which end at the UV fixed point presented in (4.11) for  $k \rightarrow \infty$ . In this section we use the analytic flow equations given in App. B.6 for simplicity, and set the anomalous dimensions to zero, i.e.  $\eta_\phi = 0$ . This approximation gives qualitatively similar results, as discussed in App. B.4.

In the IR, it is particularly interesting to examine the background couplings  $\bar{g}$  and  $\bar{\lambda}$ . In the limit  $k \rightarrow 0$  the regulator vanishes by construction and the diffeomorphism invariance of the background couplings is restored. Hence they become observables of the theory. The flow equations for the background couplings are displayed in App. B.2.

In general we look for trajectories that correspond to classical general relativity in the IR. This implies that the quantum contributions to the background couplings vanish and in consequence that they scale classically according to their mass dimension. The classical scaling is described by

$$\bar{g}, g_3, g_4 \sim k^2, \quad \bar{\lambda}, \mu, \lambda_3, \lambda_4 \sim k^{-2}. \quad (4.17)$$

We use the classical scaling in the flow from the UV fixed point to the IR in order to set the scale  $k$  in units of the Planck mass  $M_{\text{Pl}}$ . We need to find a large enough regime where

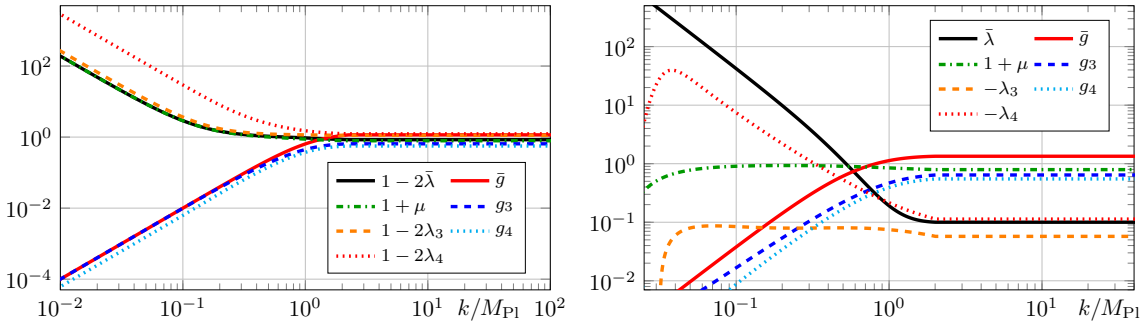


Figure 4.4.: Examples of UV finite trajectories from the UV fixed point (4.11) towards the IR. In the left panel all couplings scale classically below the Planck scale and reach their UV fixed point values shortly above the Planck scale. In the right panel some couplings show non-classical behaviour even below the Planck scale, which is triggered by the graviton mass parameter  $\mu$  flowing towards the pole of the graviton propagator at  $\mu = -1$ . However, in this case the numerics break down at  $k \approx 0.02M_{\text{Pl}}$  due to competing orders of the factor  $(1 + \mu)$  close to the singularity at  $\mu = -1$ . The trajectories in both panels correspond to theories that behave like classical general relativity in the IR. Note that some couplings are plotted shifted or with a minus sign in order to keep them positive over the whole range.

$\bar{g} \sim k^{-2}$ . This entails that Newton's coupling is a constant in this regime and sets the scale  $k$  via  $G_N = M_{\text{Pl}}^{-2} = \bar{g}k^{-2}$ .

In Fig. 4.4, two exemplary trajectories are displayed. In the left panel all couplings scale classically below the Planck scale and reach their UV fixed point values shortly above the Planck scale. All quantum contributions are suppressed simply by the fact that  $\mu \rightarrow \infty$ . In the right panel on the other hand some couplings exhibit a non-classical behaviour even below the Planck scale, which is triggered by the graviton mass parameter  $\mu$  flowing towards the pole of the graviton propagator at  $\mu = -1$ . This entails that the dimensionful graviton mass parameter  $M^2 = \mu k^2$  is vanishing in the IR. This IR behaviour is analogous to the one observed in [327], and recently also [301]. Remarkably, not only  $\mu$  is behaving non-classically but also  $\lambda_3$ , even though it is not restricted by any pole. However, in this scenario the numerics break down at  $k \approx 0.02M_{\text{Pl}}$  due to competing orders of the factor  $(1 + \mu)$  close to the singularity at  $\mu = -1$ .

In the left panel we have tuned the background couplings  $\bar{g}$  and  $\bar{\lambda}$  so that they are equal to the lowest corresponding fluctuation coupling in the IR, i.e.  $\bar{g} = g_3$  and  $\bar{\lambda} = \lambda_2 = -\mu/2$  for  $k \ll M_{\text{Pl}}$ . This is equivalent to solving a trivial version of the Nielsen identities (NIs). Since all quantum contributions are suppressed by the graviton mass parameter going to infinity in the IR,  $\mu \rightarrow \infty$ , the NI in (3.2) reduces to

$$\frac{\delta\Gamma[\bar{g}, h]}{\delta\bar{g}_{\mu\nu}} = \frac{\delta\Gamma[\bar{g}, h]}{\delta h_{\mu\nu}} \quad \text{for} \quad \mu \rightarrow \infty \quad \& \quad k \rightarrow 0. \quad (4.18)$$

In consequence, we should see that all couplings coincide in this limit,  $\bar{g} = g_n$  and  $\bar{\lambda} = \lambda_n$ . This is not the case in the left panel of Fig. 4.4 since we have only fine tuned the background couplings, and thus we have two further degrees of freedom that could be used for fine-tuning, stemming from the three dimensional UV critical hypersurface.

System	$\mu^*$	$\lambda_3^*$	$\lambda_4^*$	$g_3^*$	$g_4^*$	$\bar{\theta}_i$	$\tilde{\theta}_i$
$\mu, g_3, \lambda_3$	-0.57	0.095		0.62		$1.3 \pm 4.1 i$	-12
						7.3 -3.5	-7.4
$\mu, g_3, \lambda_3, g_4$	-0.53	0.086		0.74	0.67	$2.1 \pm 3.8 i$	-3.6 -11
						$0.75 \pm 1.5 i$	$-7.8 \pm 3.5 i$
$\mu, g_3, \lambda_3, \lambda_4$	-0.58	0.17	0.032	0.48		4.1	$0.35 \pm 2.6 i$
						6.2	1.8 -3.4 -8.8
$\mu, g_3, \lambda_3, g_4, \lambda_4$	-0.45	0.12	0.028	0.83	0.57	4.7	$2.0 \pm 3.1 i$
						5.0	$0.37 \pm 2.4 i$
							-2.9 -5.6 -7.9

Table 4.1.: Properties of the non-trivial UV fixed point for different orders of the vertex expansion scheme, computed for momentum dependent anomalous dimensions  $\eta_{\phi_i}(p^2)$  and bilocally projected Newton's couplings  $g_n(k^2)$ . The critical exponents  $\bar{\theta}_i$  and  $\tilde{\theta}_i$  stem from two different approximation of the stability matrix as discussed in App. B.1. The fixed points are computed with the identifications  $g_6 = g_5 = g_{\max}$  and  $\lambda_6 = \lambda_5 = \lambda_3$ . We observe that the fixed point values are only varying mildly between the different orders of the vertex expansion. Notably, if we compare the critical exponents of the two approximations of the stability matrix, we observe that the difference becomes smaller with an increasing order of the vertex expansion. This is precisely what one would expect of a systematic approximation scheme that is approaching a converging limit.

In summary, we find different types of trajectories that correspond to classical general relativity in the IR. The main difference lies in the behaviour of the graviton mass parameter  $\mu$ , which flows to infinity in one case and to minus one in the other case. Both scenarios are equivalent to general relativity in the end, in particular since only the background couplings become observables in the limit  $k \rightarrow 0$ .

## 4.5. Towards apparent convergence

In this section we discuss and summarise the findings of this chapter concerning apparent convergence. On the one hand, the order of our vertex expansion is not yet high enough to fully judge whether the system approaches a converging limit. Nevertheless, we have collected several promising first hints that we want to present in the following.

We have introduced two different approximations to the stability matrix, as presented in App. B.1. We have argued that in a well converged approximation scheme the most relevant critical exponents should not depend on the approximation of the stability matrix. In Tab.4.1 we display the UV fixed point properties for different orders of the vertex expansion. The first system is without the graviton four-point function and exactly the same as in Chapter 3. Then we look at systems where we add either only an equation for  $g_4(k^2)$  (cf. (B.11)), or only an equation for  $\lambda_4$  (cf. (B.10)). Lastly, we display our best truncation including all couplings up to the graviton four-point function, see Sec. 4.3.1. We observe that the fixed point values of the couplings vary only mildly with an improving truncation, although there is no clear pattern to those variations. The most important

piece of information is the difference between the critical exponents from the two different approximations of the stability matrix. While the difference is rather large in the truncation of the graviton three-point function, it is becoming smaller with each improvement of the truncation. At the level of the graviton four-point function, the critical exponents show only a small difference. This is precisely what we expect, and thus we interpret this as a sign that the system is approaching a converging limit.

Another important piece of information comes from the stability of the UV fixed point under different closures of the flow equation. In a well converged expansion scheme, the properties of the UV fixed point should be completely insensitive to the details of the closure of the flow equation. We have performed this analysis in Sec. 4.3.2. We observed that the area in which the UV fixed point exists in the theory space of higher couplings is indeed increasing with the improvement of the truncation. Furthermore, we saw that the UV fixed point values are confined to small intervals. We again interpret this as a sign that the system is approaching a converging limit.

In summary, we have already seen several signatures of apparent convergence although we are only at the level of the graviton four-point function within the present systematic expansion scheme. This suggests that we are on a promising path and that the present setup will eventually lead to a converging limit.

## 4.6. Summary

We have investigated quantum gravity with a vertex expansion and included propagator and vertex flows up to the graviton four-point function. The setup properly disentangles background and fluctuation fields and, for the first time, allows to compare two genuine Newton's couplings stemming from different vertex flows. Moreover, with the current truncation we have closed the flow of the graviton propagator: all vertices and propagators involved are computed from their own flows.

As a first non-trivial result we have observed that the vertex flows of the graviton three-point and four-point functions, in the sense of (4.3), are well described by a polynomial in  $p^2$  within the whole momentum range  $0 \leq p^2 \leq k^2$ . The projection used for the flows takes into account the  $R$ ,  $R^2$  and  $R_{\mu\nu}^2$  tensor structures as well as higher order invariants with covariant momentum dependencies. Importantly, it is orthogonal to the  $R^2$  tensor structure for the graviton three-point function, but includes it for the graviton four-point function. We have shown that the highest momentum power contributing to the graviton three-point function is  $p^2$ . Therefore,  $R_{\mu\nu}^2$  and higher derivative terms do not contribute to the graviton three-point function. Thus, in particular  $R_{\mu\nu}^2$  is excluded as a UV-relevant direction. On the other hand, the flow of the graviton four-point function shows  $p^4$  as its highest momentum power. Together with the three-point function result we infer that  $R^2$  is UV-relevant and contributes to the graviton four-point function. This is a very interesting and highly non-trivial result.

At the moment, we cannot make final statements about higher  $R^n$  terms directly from our analysis. Nonetheless, predictions can be made with a combination of the results presented here and previous ones obtained within the background field approximation as well as the vertex expansion: Firstly, this chapter sustains the qualitative reliability of background field or mixed approximations for all but the most relevant couplings. We have seen that the range of allowed Newton's couplings stemming from  $n$ -graviton vertices is growing with the level of the approximation. Moreover, in [2, 387] it has been shown

that already the substitution of the most relevant operator, the mass parameter  $\mu$ , in a mixed computation with that in the full vertex expansion stabilises the results in a particular gravity-matter system. Hence, this gives us some trust in the qualitative results for higher  $R^n$  terms in the background field approximation. In [281] the  $f(R)$ - potential has been computed polynomially up to  $R^{34}$ , and the relevance of these operators follows the perturbative counting closely. Accordingly it is quite probable that the higher  $R^n$  will turn out to be irrelevant in the full vertex expansion as well.

Based on the above observations we have also constructed projection operators that properly disentangle the contributions of different diffeomorphism-invariant tensor structures. This allowed us to switch off the  $R^2$  coupling in order to analyse its importance for the system. In this case, we are led to an unstable system, which highlights the importance of the  $R^2$  coupling for the asymptotic safety scenario. In this chapter we include the  $R^2$  contributions via the momentum dependence of the gravitational coupling  $g_4(p^2)$ , leading to a very stable system in the UV.

In the full system with  $R^2$  contributions we found an attractive UV fixed point with three attractive directions and two repulsive directions. The third attractive direction can be explained due to the overlap with  $R^2$ , and is in agreement with previous  $R^2$  studies in the background field approximation [269, 271, 272, 274, 281]. We investigated the stability of this UV fixed point with respect to changes of the identification of the higher couplings and compared it to the stability of the previous truncation without the graviton four-point function. We characterised the stability via the area of existence in the theory space of higher couplings, and remarkably this area increased with the improved truncation. We interpret this as a sign that the systematic approximation scheme is approaching a converging limit.

Furthermore, we investigated the IR behaviour and found trajectories that connect the UV fixed point with classical general relativity. In particular, we found two different types of such trajectories. In the first category all couplings, including background and fluctuation couplings, scale classically according to their mass dimension below the Planck scale. In consequence the Nielsen identities become trivial in this regime and we can solve them in the IR. In the second category, the graviton mass parameter and the coupling  $\lambda_3$  scale non-classically below the Planck scale, which is triggered by the graviton mass parameter flowing towards the pole of the graviton propagator  $\mu \rightarrow -1$ . In summary, the IR behaviour was found to be very similar to [327], and recently also [301].

Lastly, we discussed signs of apparent convergence in the present system by comparing the results to previous truncations. As mentioned before, we observed that the present system is more stable and less sensitive to the closure of the flow equation, which is expected from a converging system. We furthermore used two different approximations of the stability matrix and argued that the critical exponents belonging to the most attractive directions should not differ in a well converged expansion. Indeed we found that the difference of the critical exponents is decreasing with an improvement of the truncation. We interpret this as a sign towards apparent convergence.



# 5. Background curvature dependence in asymptotically safe quantum gravity

## 5.1. Introduction

In the last two chapters we have used the systematic vertex expansion to compute graviton correlation function on a flat Euclidean background up to the graviton four-point function. In these computations the flat background was a technically favourable choice since it allowed us to use standard Fourier representations for the correlation functions. This property is lost on generically curved backgrounds, as the covariant derivative and the Laplacian do not have a common eigenbasis anymore. Nonetheless, a computation about a curved background is highly desirable in particular if this background is a solution to the equation of motion. In the latter case convergence properties of the expansion scheme can be significantly enhanced.

In this chapter we take the setup from [Chapter 3](#) and extend it to curved backgrounds. We restrict ourselves to spherical backgrounds. For this purpose we construct an approximate momentum space that allows to use the previously developed techniques of correlation functions in momentum space. The key component for the construction is an approximation to angle between two spectral values of the covariant derivative. In this setup, all the dynamical couplings from the previous sections turn into functions of the background curvature. The algebraic fixed point equations turn into differential equations and they are solved with the input of the flat background solution. With the resulting curvature-dependent dynamical couplings we find viable UV fixed point functions for all curvatures of the spherical background considered. Interestingly these fixed point functions of the effective couplings are almost curvature independent: the couplings try to counterbalance the explicit curvature dependence and thus try to keep the fixed point curvature independent. The fixed point functions provide further evidence in favour of the asymptotic safety scenario. Since we feed back the full fixed point functions we obtain in the background a full fixed point potential  $f(R)$ .

Importantly, our setup allows for the computation and the distinction of the background and quantum equation of motion (EoM). We argue that these equations have a common solution at a vanishing infrared FRG cutoff scale  $k = 0$  due to background independence. In turn, the solutions to the background and quantum EoM do not agree at a finite cutoff scale  $k \neq 0$ , which signals the loss of background independence in the presence of the FRG-regulator. This is also seen in our explicit computations at the UV fixed point. We further argue that the quantum EoM, and *not* the background EoM, should be used to determine the self-consistent background at finite  $k$ .

Solutions to the background EoM appear as minimum in the background potential  $f(R)/R^2$ , which we compute for the first time from the dynamical background-dependent fluctuation couplings without a background field approximation. In the present work we compute the UV fixed point background potential  $f^*(R)$ . Interestingly, in the pure quantum gravity setting we do not find a solution to the background EoM, while a solution

appears at small positive curvature for Standard Model matter content. The quantum EoM on the other hand has a solution also in the pure quantum gravity setting.

## 5.2. General framework

In this chapter we do a qualitative step towards background independence and diffeomorphism invariance in asymptotically safe gravity by computing fluctuation correlation functions up to the three-point function as well as the full  $f(R)$ -potential of the background field. Within the categorisation of Sec. 3.2.1 we develop an approach in the class (2b). As already mentioned in the introduction, we compute the fixed point potential  $f^*(R)$  for  $k \rightarrow \infty$  but the present approach also allows for its computation in the physical limit  $k \rightarrow 0$ . This potential certainly has interesting applications in cosmology. The interplay of asymptotically safe gravity and cosmology is investigated in e.g. [288, 318, 388–409].

### 5.2.1. Quantum and background equation of motion

An important issue in quantum gravity is the background independence of physical observables. They are expectation values of diffeomorphism invariant operators, and hence do not depend on the gauge fixing. Examples for such observables are correlations of the curvature scalar. Another relevant example is the free energy of the theory,  $-\log Z[\bar{g}, J = 0]$ , with  $\delta Z[\bar{g}, J = 0]/\delta \bar{g}_{\mu\nu} = 0$ . These observables cannot depend on the choice of the background metric, which only enters via the gauge fixing. The latter fact is encoded in the NI for the effective action: The difference between background derivatives and fluctuation derivatives is proportional to derivatives of the gauge fixing sector,

$$\text{NI} = \frac{\delta \Gamma}{\delta \bar{g}_{\mu\nu}} - \frac{\delta \Gamma}{\delta h_{\mu\nu}} - \left\langle \left[ \frac{\delta}{\delta \bar{g}_{\mu\nu}} - \frac{\delta}{\delta \hat{h}_{\mu\nu}} \right] (S_{\text{gf}} + S_{\text{gh}}) \right\rangle = 0, \quad (5.1)$$

where  $S_{\text{gf}}$  is the gauge fixing term and  $S_{\text{gh}}$  is the corresponding ghost term, and  $h_{\mu\nu} = \langle \hat{h}_{\mu\nu} \rangle$ , see also Sec. 3.2. Note that (5.1) is nothing but the Dyson-Schwinger equation for the difference of derivatives w.r.t.  $\bar{g}_{\mu\nu}$  and  $h_{\mu\nu}$ . For the fully diffeomorphism-invariant Vilkovisky-deWitt or geometrical effective action the relation (5.1) is even more concise: the split is not linear and we have  $g_{\mu\nu} = \bar{g}_{\mu\nu} + f_{\mu\nu}(\bar{g}, h)$ , where  $f_{\mu\nu}(\bar{g}, h) = h_{\mu\nu} + \mathcal{O}(h^2)$  depends on the Vilkovisky connection. The NI then reads

$$\text{NI}_{\text{geo}} = \frac{\delta \Gamma_{\text{geo}}}{\delta \bar{g}_{\mu\nu}} - \mathcal{C}(\bar{g}, h) \frac{\delta \Gamma_{\text{geo}}}{\delta h_{\mu\nu}} = 0, \quad (5.2)$$

where  $\mathcal{C}(\bar{g}, h)$  is the expectation value of the (covariant) derivative of  $h(\bar{g}, g)$ , for a discussion in the present FRG setting see [188, 336, 338, 347].

The NIs, (5.1) and (5.2), entail that in both cases the effective action is not a function of  $g_{\mu\nu} = \bar{g}_{\mu\nu} + h_{\mu\nu}$  or  $g_{\mu\nu} = \bar{g}_{\mu\nu} + f_{\mu\nu}(\bar{g}, h)$  respectively. This property holds for general splits, and prevents the simple expansion of the effective action in terms of diffeomorphism invariants. Apart from this disappointing consequence of the NIs, it also entails good news: the effective action only depends on one field as background and fluctuation derivatives are connected.

An important property that follows from background independence is the fact that a solution of the background equation of motion (EoM)

$$\frac{\delta\Gamma[\bar{g}, h]}{\delta\bar{g}_{\mu\nu}} \bigg|_{\bar{g}=\bar{g}_{\text{EoM}}, h=0} = 0, \quad (5.3)$$

is also one of the quantum EoM,

$$\frac{\delta\Gamma[\bar{g}, h]}{\delta h_{\mu\nu}} \bigg|_{\bar{g}=\bar{g}_{\text{EoM}}, h=0} = 0. \quad (5.4)$$

see e.g. [365] for a discussion of this in Yang-Mills theories. In (5.3) and (5.4) we have already taken the standard choice  $h_{\mu\nu} = 0$  but the statement hold for general combinations  $\bar{g}_{\text{EoM}}(h)$  that solves either of the equations. The concise form (5.2) for the geometrical effective action makes it apparent that a solution of either EoM, (5.3) or (5.4), also entails a solution of the other one. Note that at  $h_{\mu\nu} = 0$  we have  $\mathcal{C}(\bar{g}, 0) = 1$ .

Even though less apparent, the same holds true for the effective action in the linear split: to that end we solve the quantum EoM (5.4) as an equation for  $\bar{g}_{\text{EoM}}(h)$ . As the current  $J$  in the generating functional simply is  $J = \delta\Gamma/\delta h_{\mu\nu}$ , the quantum EoM implies the vanishing of  $J$  and the effective action is given by  $\Gamma[\bar{g}_{\text{EoM}}(0), 0] = -\log Z[\bar{g}, J = 0]$ , the free energy. However, we have already discussed that  $\log Z[\bar{g}, 0]$  is background-independent and it follows that (5.3) holds.

The above properties and relations are a cornerstone of the background formalism as they encode background independence of observables. The NIs also link background diffeomorphism invariance to the Slavnov-Taylor identities (STIs) that hold for diffeomorphism transformations of the fluctuation field: the quantum deformation of classical diffeomorphism symmetry is either encoded in the expectation value of the gauge fixing sector or in the expectation value  $\mathcal{C}(\bar{g}, h)$ .

At finite  $k$ , the regulator term introduces a genuine dependence on the background field. Then  $\log Z_k[\bar{g}, 0]$  is not background independent. Consequently the STIs turns into modified STIs (mSTIs) and the NIs turn into modified NIs (mNIs). For the linear split, the mNI reads

$$\text{mNI} = \text{NI} - \frac{1}{2} \text{Tr} \left[ \frac{1}{\sqrt{\bar{g}}} \frac{\delta\sqrt{\bar{g}}R_k[\bar{g}]}{\delta\bar{g}_{\mu\nu}} G_k \right] = 0, \quad (5.5)$$

see [355, 356] for details and Chapter 8 for an application to gravity-matter systems. Importantly the right-hand side of (5.5) signals the loss of background independence. It is proportional to the regulator and vanishes for  $k \rightarrow 0$  where background independence is restored. A similar violation of background independence linear in the regulator is present in the geometrical approach, see [188, 336, 338, 347].

In summary this leaves us with non-equivalent solutions to the EoMs in the presence of the regulator: a solution of the quantum EoM (5.4) does not solve the background EoM (5.3). However, typically the asymptotically safe UV regime of quantum gravity is accessed in the limit  $k \rightarrow \infty$  as this already encodes the important scaling information in this regime. In this dissertation we also follow this strategy and hence we have to deal with different solutions of background and quantum EoMs, if they exist at all. Note that the right-hand side of the mNI is simply the expectation value of the background derivative of the regulator term. Accordingly it is the background EoM that is deformed directly by

the presence of the regulator while the quantum EoM feels its influence only indirectly. Therefore it is suggestive to estimate the physical UV-limit of the EoM in the limit  $k \rightarrow 0$  by the quantum EoM in the limit  $k \rightarrow \infty$ .

Studies in asymptotically safe quantum gravity have focused so far on finding solutions to (5.3). For instance in [288] they didn't find a solution to (5.3) in a polynomial expansion with the background field approximation. Other approaches with the background field approximation found a solution with the exponential parameterisation [286, 287] and within the geometrical approach [284, 291]. In this chapter we are for the first time able to disentangle (5.3) and (5.4) in a quantum gravity setting and look for separate solutions to the EoMs.

### 5.2.2. Background independence in non-perturbative expansion schemes

It is important to discuss the relations of the approaches described in Sec.3.2.1 in particular for future developments and the full resolution of *physical* background independence. This chapter extends a similar discussion from last chapter in the context of modified STIs for diffeomorphism transformations to NIs. Despite its importance one may skip this chapter for a first reading as its results are not necessary for the derivations and computations presented in this work.

We have technically very different options to access physical background independence of quantum gravity. Seemingly they have different advantages and disadvantages. For example, approach (1) via the NIs has the charm of directly implementing background independence. In turn, the results of (2b) may apparently not satisfy the NIs.

For resolving this issue it is instructive to discuss approach (2a). There the fluctuation correlation functions are computed for a specific background. Results for general backgrounds have then to be obtained with an expansion/extension of the results for the specific background. This could be done via the NIs in which case background independence is guaranteed. This procedure for guaranteeing STIs and NIs has been discussed in detail in [367] in the context of non-Abelian gauge theories, and in [3] for gravity. We briefly repeat and extend the structural argument presented there: First we notice that the functional equations for all correlation functions can be cast in the form

$$\Gamma^{(n,m)}[\bar{g}, h] = \text{FRG}_{n,m}[\{\Gamma^{(i \leq n, 2 \leq j \leq m+2)}[\bar{g}, h]\}, \bar{g}]. \quad (5.6)$$

Eq. (5.6) follows from integrating the functional renormalisation group equations for  $\Gamma^{(n,m)}$ , which have precisely the same structure for all theories: the flows of  $\Gamma^{(n,m)}$  are given by one-loop diagrams with full propagators and full vertices. The latter are given in terms of the correlation functions  $\{\Gamma^{(i \leq n, 2 \leq j \leq m+2)}\}$ , see e.g. [188, 367]. This also entails that the lowest fluctuation correlation function that contributes to the diagrams is the two-point function, i.e. the propagator.

In gravity (5.6) follows straightforwardly from (3.9) by integrating the flow equation and taking  $\bar{g}$ - and  $h$ -derivatives. As a side remark we note that the order of derivatives on the right-hand side is different within other functional approaches. For example, for Dyson-Schwinger equations (DSE) the right-hand side  $\text{DSE}_{n,m}$  for the  $\Gamma^{(n,m)}$  depends on  $\{\Gamma^{(i \leq n, j \leq m+r-2)}\}$  and contain up to  $r-2$ -loop diagrams. Here  $r$  is the highest order of the field in the classical action, see e.g. [188]. In typical examples of renormalisable theories we have  $r = 3, 4$ , but in gravity we have  $r = \infty$ . This singles out the flow equation for gravity as the only functional approach that only connects a finite order of correlation

functions in each equation. The coupling of the whole tower of equations then comes from the highest order correlation functions on the right-hand side. In turn, each DSE already contains all orders on the right-hand side of (5.6), that is  $2 \leq j$  without upper bound. Similar statements as for the DSE hold for 2PI or  $n$ PI hierarchies.

Importantly, for all functional approaches the right-hand side of (5.6) goes only up to the same order of background metric derivatives,  $i \leq n$ . This allows us to view (5.6) as functional relations for the highest order background metric correlation functions that have as an input  $\{\Gamma^{(n-1,m)}\}$ . Moreover, the NI relates a derivative w.r.t.  $\bar{g}$  to one w.r.t.  $h$ . For emphasising the similarities to the functional relations (5.6) we rewrite the NI. For simplicity we use the linear split NI, (5.1) and (5.5),

$$\Gamma^{(n,m)}[\bar{g}, h] = \Gamma^{(n-1,m+1)}[\bar{g}, h] + \mathcal{N}_{n,m}[G, \{\Gamma^{(i \leq n-1, j \leq m+1)}[\bar{g}, h]\}, \bar{g}], \quad (5.7)$$

where  $\mathcal{N}$  stands for the expectation value in (5.1), and additionally for the regulator loop in (5.5), and we have singled out the propagator  $G$  for elucidating the orders of the correlation functions on both sides. Importantly, (5.7) makes the fact apparent that for the NI, (5.1) and (5.5), the order of background derivatives is at most  $n-1$ . Note also that (5.7) is nothing but the difference of the Dyson-Schwinger equation for  $h$  and  $\bar{g}$  derivatives. In this difference the terms with the higher vertices with  $j \geq m+2$  drop out.

In summary this leaves us with two towers of functional relations. While the first one, (5.6) describes the full set of correlation functions, the second one, (5.7) can be used to iteratively solve the tower of mixed fluctuation-background correlations on the basis of the fluctuating correlation functions  $\{\Gamma^{(0,m)}\}$ . In both cases we can solve the system for the higher-order correlations of the background on the basis of the lower order correlations. If we use (5.7) with an iteration starting with the results from the flow equation for  $\{\Gamma^{(0,m)}[\bar{g}_{\text{sp}}, h]\}$  for a specific background  $\bar{g}_{\text{sp}}$ , this closure of the system automatically satisfies the NI. Accordingly, *any* set of fluctuation correlation functions  $\{\Gamma^{(0,m)}[\bar{g}_{\text{sp}}, h]\}$  can be iteratively extended to a full set of fluctuation-background correlation functions in an iterative procedure. Note that this procedure can be also applied to the case (2b).

While this seems to indicate that satisfying the symmetry identities is not relevant (it can be done for all inputs), it points at a more intricate structure already known from non-Abelian gauge theories. To that end let us assume we have derived a global unique solution of all correlation functions within this iterative procedure starting from the fluctuations correlation functions. If no approximation is involved, this solution automatically would satisfy the full set of functional relations for  $\{\Gamma^{(n,m)}\}$  that can be derived from the flow equation. However, in the presence of approximations these additional functional relations represent infinite many additional constraints on the iterative solution. These constraints are bound to fail in generic non-perturbative approximation schemes as any functional relation triggers specific resummations in given approximations. It is a priori not clear which of the functional relations are more important. Note also that typically the iterative solutions of the symmetry identities are bound to violate the locality constraints of local quantum field theories that are tightly connected to the unitarity of the theory. In conclusion it is fair to say that only a combination of all approaches is likely to provide a final resolution of *physical* background independence and diffeomorphism invariance in combination with unitarity.

### 5.3. Vertices in curved backgrounds

In this section we introduce a construction that allows for vertex flow on curved backgrounds. The curved backgrounds significantly enhance the difficulty of the computation and we discuss how we obtain an approximate momentum space that allows the use of the previously developed techniques in momentum space. With this technique we in particular upgrade the results from [Chapter 3](#) to constantly curved spherical backgrounds.

#### 5.3.1. Spectral decomposition

We extend our previous expansion schemes about the flat Euclidean background to one that allows for arbitrary constant curvatures. To that end we first discuss the procedure at the example of the propagators: propagators for non-trivial metrics  $\bar{g}$  with constant curvature can be written in terms of the scalar Laplacian  $\Delta_{\bar{g}} = -\bar{\nabla}^2$  and curvature terms proportional to the background scalar curvature  $\bar{R}$ ,

$$G = G(\Delta_{\bar{g}}, \bar{R}). \quad (5.8)$$

For the flat metric (5.8) reduces to  $G(p^2, 0)$ , where  $p^2$  are the continuous spectral values of the flat scalar Laplacian. In a spectral basis the propagator is diagonal and reads for general curvatures

$$\langle \varphi_\lambda | G | \varphi_\lambda \rangle|_{\lambda=p^2} = G(p^2, \bar{R}), \quad (5.9)$$

and  $\lambda = p^2$  are the discrete or continuous eigenvalues for the given metric, and  $\{|\varphi_{\lambda=p^2}\rangle\}$  is the orthonormal complete basis of eigenfunctions of the scalar Laplacian

$$\Delta_{\bar{g}} |\varphi_\lambda\rangle = \lambda |\varphi_{\lambda=p^2}\rangle, \quad (5.10)$$

see App. [C.1](#) for explicit expression for the propagator. The tricky part in this representation are the vertices, which are operators that map  $n$  vectors onto the real numbers. For example the three-point function can be written in a spectral representation in terms of an expansion in the tensor basis with eigenfunctions of  $\Delta_{\bar{g}}$ ,

$$\Gamma^{(3)} = \sum_{\lambda_1, \lambda_2, \lambda_3} \Gamma^{(3)}(\lambda_1, \lambda_2, \lambda_3, \bar{R}) \langle \varphi_{\lambda_1} | \otimes \langle \varphi_{\lambda_2} | \otimes \langle \varphi_{\lambda_3} |, \quad (5.11)$$

where the spectral values in general also depend on the curvature and  $\sum$  runs over discrete or continuous spectral values. Also,  $\sum$  may also include a non-trivial spectral measure weight  $\mu(\lambda)$ . The representation of the higher  $n$ -point functions follows straightforwardly from (5.11). Inserting this into the flow equation of the inverse propagator, we arrive at

$$\begin{aligned} \partial_t \Gamma^{(2)}(\lambda, \bar{R}) &= -\frac{1}{2} \sum_{\lambda_1} \Gamma^{(4)}(\lambda, \lambda, \lambda_1, \lambda_1, \bar{R}) (G \dot{R}_k G)(\lambda_1, \bar{R}) \\ &+ \sum_{\lambda_2, \lambda_3} \Gamma^{(3)}(\lambda, \lambda_2, \lambda_3, \bar{R}) G(\lambda_2, \bar{R}) (G \dot{R}_k G)(\lambda_3, \bar{R}) \Gamma^{(3)}(\lambda_3, \lambda_2, \lambda, \bar{R}), \end{aligned} \quad (5.12)$$

where we denoted  $\dot{R}_k = \partial_t R_k$ . The vertex functions  $\Gamma^{(n)}$  are complicated functions of  $\lambda_i$ .

On a flat background, the eigenfunctions of the Laplace operator are also eigenfunctions of the partial derivatives and the representation of the vertex functions follows trivially. On a curved background, however, the covariant derivatives do not commute with the Laplace operator and the representation of uncontracted covariant derivatives on the set of functions  $\{|\varphi_{\lambda=p^2}\rangle\}$  is complicated. One could tackle this problem with e.g. off-diagonal heat-kernel methods, but then a derivative expansion in momenta and curvature is necessary [328].

In this chapter we construct an approximate momentum space on a curved background, which facilitates computations considerably and allows for full momentum and curvature dependences. In order to derive the vertex functions, we first take functional derivatives with respect to the Einstein-Hilbert action on an arbitrary background. The result is a function depending on the Laplacian, products of covariant derivatives with respect to coinciding or different spacetime points and explicit curvature terms. In the expression for the vertex functions we symmetrise all covariant derivatives, which produces further  $\bar{R}$ -terms

$$\bar{\nabla}^\mu \bar{\nabla}^\nu = \frac{1}{2} \{ \bar{\nabla}^\mu, \bar{\nabla}^\nu \} + \bar{R}\text{-terms}. \quad (5.13)$$

In the curved momentum space approximation here, the product of symmetrised covariant derivatives acts on the set  $\{|\varphi_{\lambda=p^2}\rangle\}$  according to

$$\bar{\nabla}_1 \cdot \bar{\nabla}_2 = p_g \cdot q_g = \sqrt{p^2} \sqrt{q^2} x, \quad \text{with } x = \cos \theta_{\text{flat}}, \quad (5.14)$$

with an integration measure  $\int \sqrt{1 - \cos^2 \theta} d\cos \theta$ . The integration measure is chosen such that in the limit  $\bar{R} \rightarrow 0$  precisely the flat results are obtained. As a consequence, in this approximation  $\oint$  factorises into an angular integration and a sum/integration over the spectral values of  $\Delta_{\bar{g}}$ . According to (5.14), external spectral values are described by the angle to the internal one and their absolute values, which appear as parameters that can be treated as real numbers. We emphasise that this curved momentum space approximation has the correct flat background limit by construction and is correct for all terms that contain only Laplace operators. A comparison of the approximation as a function of the background curvature is detailed in App. C.3. With the above approximation associated with covariant derivatives, we arrive at a relatively simple flat-background-type representation of the flow equation in terms of angular integrals and spectral values  $p_i^2 = \lambda_i$

$$\begin{aligned} \partial_t \Gamma^{(2)}(\lambda, \bar{R}) &= -\frac{1}{2} \sum_{\lambda_1} \int d\Omega \Gamma^{(4)}(\lambda, \lambda_1, x, \bar{R}) (G \dot{R}_k G)(\lambda_1, \bar{R}) \\ &+ \sum_{\lambda_1} \int d\Omega \Gamma^{(3)}(\lambda, \lambda_1, x, \bar{R}) G(\lambda_1 + \lambda + \sqrt{\lambda \lambda_1} x, \bar{R}) (G \dot{R}_k G)(\lambda_1, \bar{R}) \Gamma^{(3)}(\lambda, \lambda_1, x, \bar{R}). \end{aligned} \quad (5.15)$$

The total  $\bar{R}$ -dependence of the flow equation enters via the explicit  $\bar{R}$ -terms in the vertex functions, the symmetrised covariant derivatives and the spectral values. The generalisation to flows of higher-order vertex functions is straightforward.

### 5.3.2. Vertex construction

The basic ingredients in the flow equations in Fig. 3.1 are the vertex functions  $\Gamma^{(n)}$ . We build on the parameterisation for vertex functions introduced in Chapter 3 but in contrast

to there, all quantities exhibit explicit  $\bar{R}$ -dependence. Hence, our ansatz is given by

$$\Gamma^{(\phi_1 \dots \phi_n)}(\mathbf{p}, \bar{R}) = \left( \prod_{i=1}^n Z_{\phi_i}^{\frac{1}{2}}(p_i^2, \bar{R}) \right) G_n^{\frac{n}{2}-1}(\bar{R}) S_{\text{EH}}^{(\phi_1 \dots \phi_n)}(\mathbf{p}; G_n(\bar{R}), \Lambda_n(\bar{R}), \bar{R}), \quad (5.16)$$

where  $\mathbf{p} = (p_1, \dots, p_n)$  is the collection of spectral values of the external legs.  $S_{\text{EH}}$  is the gauge-fixed Einstein-Hilbert action, cf. (3.4), and we choose to work with the gauge fixing parameters  $\alpha = \beta = 0$ .

The propagator is a pure function of  $\Delta_{\bar{g}}$  and  $\bar{R}$ , while the vertices with  $n > 2$  are functions of  $\Delta_{\bar{g}}$ ,  $\bar{\nabla}_\mu$ ,  $\bar{R}$ ,  $\bar{R}_{\mu\nu}$  and  $\bar{R}_{\mu\nu\rho\sigma}$ . Restricting ourselves to a background sphere, the dependence on the Ricci- and the Riemann-tensor reduces to a dependence on the constant background curvature  $\bar{R}$ . With the approximation constructed in the last section, we deal with the covariant derivatives  $\bar{\nabla}_\mu$  in the vertices. We set the anomalous dimensions  $\eta_{\phi_i}(p^2, \bar{R})$  throughout this chapter equal to zero. In the last chapters this approximation led to qualitatively reliable results. The graviton three-point function is evaluated at the point of symmetric spectral values,

$$p := |p_1| = |p_2|, \quad \theta_{\text{flat}} = 2\pi/3. \quad (5.17)$$

In this chapter we close the flow equations by setting the higher-order couplings to  $G_{n \geq 4} = G_3 =: G$  and  $\Lambda_4 = \Lambda_3$  as well as  $\Lambda_{n \geq 5} = 0$ . We also introduce the dimensionless variables

$$r := \bar{R}k^{-2}, \quad g := Gk^2, \quad \mu := -2\Lambda_2 k^{-2}, \quad \lambda_3 := \Lambda_3 k^{-2}. \quad (5.18)$$

From the graviton two-point function we extract the mass-parameter  $\mu(r)$ , while from the graviton three-point function we extract the gravitational coupling  $g(r)$  and the coupling of its momentum independent part  $\lambda_3(r)$ . In App. C.2 we give a derivation and display the flow equations.

### 5.3.3. Flow equations and trace evaluation

With the construction presented in the last sections, we are left with an explicit expression for the flow of the two- and the three-point function. The flow of the two-point is of the form (5.15) and the three-point function has a similar form according to the diagrammatic representation in Fig. 3.1. After projection the resulting flow equations take the form (C.13) and (C.14). In this chapter we are interested in the fixed point equations, which are differential equations with respect to  $r$  due to the dependence on the background curvature. According to the factorisation property of the approximate curved momentum space construction, we evaluate the angular integration in a straightforward manner in complete analogy to a flat background computation. We are then left with the evaluation of traces of the form

$$\sum_{\lambda} f(\lambda, r), \quad (5.19)$$

for functions of the curvature  $r$  and the spectral value  $\lambda$  as well as the couplings. In order to include the effects of the background curvature we perform a spectral sum over a four-sphere. On a four-sphere the spectrum and corresponding multiplicities of the scalar Laplacian are given by

$$\omega(\ell) = \frac{\ell(3+\ell)}{12}r, \quad m = \frac{(2\ell+3)(\ell+2)!}{6\ell!}, \quad (5.20)$$

with  $\ell$  taking integer values  $\ell \geq 0$ . Since we are left with only scalar spectral values we replace

$$\lambda \rightarrow \omega(\ell), \quad \sum_{\lambda} \rightarrow V^{-1} \sum_{\ell=2}^{\ell_{\max}} m(\ell), \quad (5.21)$$

where the exact sum is achieved for  $\ell_{\max} = \infty$  and we divide by the volume of a four sphere  $V = \frac{384\pi^2}{k^4 r^2}$ . Note, that we exclude the zero modes and start the spectral sum at  $\ell = 2$ . This does not affect the result for small curvature  $r$ . Performing the spectral sums one then obtains the traces. However, in most cases a closed form for the sums cannot be obtained and we have to resort to cutting the spectral sums off at a finite value  $\ell_{\max}$ . Nonetheless since each trace involves a regulator function that cuts modes off at order  $\omega(\ell) \approx k^2$  for non-zero  $r$  the spectral sum is only sensitive to the modes  $\omega(\ell) < k^2$ , which are finite in number. However, in the limit of vanishing curvature the spectral sum needs to be extended to infinite order, as all modes are only regulator suppressed for large  $r$  according to  $\exp(-\lambda_n r)$ , but become important once  $r \approx 1/\lambda_n$ . In fact, we need the limit  $r \rightarrow 0$  in order to set the boundary conditions of the fixed-point differential equations. It is obvious that there is only one physical initial conditions that fixes the solution of the fixed point differential equation uniquely, and that is the initial condition obtained from the flat background limit. In fact, a proper initial condition is also necessary from a mathematical point of view if one requires a finite derivative,  $g'(r) < \infty$ . One infers from (C.13) and (C.14), that the derivative of  $g(r)$  diverges in the limit  $r \rightarrow 0$  if the initial conditions are not chosen appropriately. However, as argued above, this limit cannot be calculated in practice with spectral sums as all modes contribute. In the small-curvature region the trace is evaluated by the early-time heat-kernel expansion where the leading order gives the flat-background momentum integrals. In this case we write the Laplace transform

$$\sum_{\lambda} f(\lambda, r) = \frac{1}{V} \int_0^{\infty} ds \operatorname{Tr}[e^{-s\Delta_g}] \tilde{f}(s, r), \quad (5.22)$$

and one expands the trace of the heat kernel in the scalar curvature  $r$  and the explicit dependence on  $r$  coming from  $\tilde{f}(s, r)$ . For small curvature the early-time heat-kernel expansion is given by

$$\frac{1}{V} \int_0^{\infty} ds \operatorname{Tr}[e^{-s\Delta_g}] \tilde{f}(s, r) = \frac{1}{(4\pi)^2} (Q_2[f] + Q_1[f] \frac{r}{6} + \dots), \quad (5.23)$$

where for  $n > 0$

$$Q_n[f] = \frac{1}{\Gamma(n)} \int d\lambda \lambda^{n-1} f(\lambda, r). \quad (5.24)$$

Using this heat-kernel expansion we translate the physical initial condition to finite  $r$  where we connect to the spectral sum. In particular we determine the curvature-dependent couplings as polynomials in the curvature  $r$ . The heat kernel provides the asymptotic limit  $r \rightarrow 0$  which can be reproduced by the spectral sum in the limit  $\ell_{\max} \rightarrow \infty$ . Thus, while the spectral sum with finite  $\ell_{\max}$  captures the large  $r$  behaviour of the trace, the heat kernel expanded to a finite order in  $r$  captures the small  $r$  behaviour. Both connect smoothly for finite but small  $r$ , for details see App. C.4.

## 5.4. Results

In this section we present the results of the given setup. First, we discuss the fixed point solutions of the beta functions related to the fluctuation field couplings. In our approach with curvature-dependent couplings, these solutions are fixed point functions. Subsequently, we analyse the background effective potential, which is calculated on the solution of the fluctuation field fixed point solution, with and without Standard Model matter content. Last we look for solution of the quantum EoM and compare to solutions of the background EoM.

### 5.4.1. Fixed point solutions

The beta functions for a coupling  $g_i(r)$  in the present framework are partial differential equations. Schematically, the equation a coupling  $g_i$  takes the form

$$\partial_t g_i(r) = g_i(r) A(g_j, \eta_h) + 2r g'_i(r) + \text{Flow}_{g_i}(g_j, r), \quad (5.25)$$

with a coefficient  $A$  that depends on the other scale-depend parameters  $g_j$ . For explicit expressions we refer to App. C.2. The fixed point equations are then obtained by setting  $\partial_t g_i(r) \equiv 0$  and we are left with a system of ordinary differential equations. The initial condition is imposed at  $r = 0$  and is chosen such that it matches the computation in a flat background from Chapter 3. For details see Sec. 5.3.3. The UV fixed point values for a flat background,  $g_i(r) = g_{i,0}$ , are given by

$$(g_0^*, \lambda_{3,0}^*, \mu_0^*) = (0.60, -0.12, -0.38). \quad (5.26)$$

with the critical exponents  $\theta$ , which are the negative eigenvalues of the stability matrix,

$$(\theta_{i,0}) = (2.0 \pm 2.1 i, -3.7). \quad (5.27)$$

These values differ slightly from, (3.30a) and (3.30b), since we use the gauge parameter  $\beta = 0$  and the exponential regulator, see (C.5). Taking these differences into account, the agreement is remarkable and highlights the insensitivity of our results with respect to the gauge and the regulator.

In order to display our results, it is convenient and meaningful to introduce effective couplings that include the explicit  $r$  dependence in the respective graviton  $n$ -point functions. According to (C.6) and (C.14), these are given by

$$g_{\text{eff}}(r) = g(r), \quad \mu_{\text{eff}}(r) = \mu(r) + \frac{2}{3}r, \quad \lambda_{3,\text{eff}}(r) = \lambda_3(r) + \frac{1}{6}r. \quad (5.28)$$

The interpretation and relevance of these effective couplings can be inferred for instance from the graviton two-point function. In terms of  $\mu_{\text{eff}}(r)$ , the transverse-traceless part of the graviton two-point function reads

$$\Gamma^{(0,2)} = (\Delta + \mu_{\text{eff}}(r)), \quad (5.29)$$

i.e. it comprises the non-kinetic part of the correlator. As an aside, we mention that one could define  $\lambda_{3,\text{eff}}$  alternatively via (C.13). The difference between the effective coupling for  $\lambda_3$  in (C.14) and (C.13) arises from the different tensor projections. We choose to define  $\lambda_{3,\text{eff}}$  via (C.14) since the flow equation for  $g$  is more important in this system.

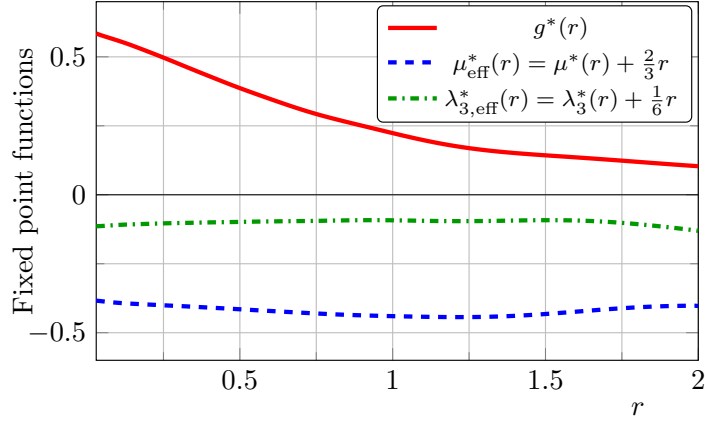


Figure 5.1.: Fixed point function solution for the system  $(g^*(r), \mu_{\text{eff}}^*(r), \lambda_{3,\text{eff}}^*(r))$  with the boundary condition from the first-order heat kernel. The solutions are stable in the whole investigated region. Note, that the effective couplings according to (5.28) are displayed.

The full,  $r$ -dependent fixed point solutions  $(g^*(r), \mu_{\text{eff}}^*(r), \lambda_{3,\text{eff}}^*(r))$  are displayed in Fig. 5.1. We find a fixed point solution with all desired properties. First of all, the fixed point solution is characterised by a positive gravitational coupling  $g(r) > 0$ , which decreases towards larger background curvatures. In order to get a feeling for the physical meaning of this behaviour, we consider the quantity  $G(R)R = g(r)r$ , i.e. the dimensionful Newton's coupling times the curvature. As this product is dimensionless, it can in principle be used to define an observable. In particular, we expect that this quantity is finite at the fixed point, which implies  $g^*(r) \sim 1/r$ . One might interpret our fixed solution  $g^*(r)$  as an onset of such a behaviour. The solutions for the mass-parameter  $\mu_{\text{eff}}(r)$  and  $\lambda_{3,\text{eff}}(r)$  are almost curvature independent, which implies that the implicit curvature dependence cancels with the explicit one. Consequently, the behaviour is not so different from the one of the computation on a flat background.

The full solution shown in Fig. 5.1 can be expanded in powers of the dimensionless curvature,  $g_i^*(r) = g_{i,0}^* + g_{i,1}^*r + \mathcal{O}(r^2)$ . The zeroth order is displayed in (5.26) and to linear order in  $r$  we find

$$(g_1^*, \lambda_{3,1}^*, \mu_1^*) = (-0.47, -0.10, -0.74). \quad (5.30)$$

with the critical exponents  $\theta$  given by

$$(\theta_{i,1}) = (-0.10 \pm 2.6i, -2.6). \quad (5.31)$$

Interestingly, we find that all new direction are UV repulsive. Further attractive directions of the UV fixed point that are linear in the background curvature were found in [328].

### 5.4.2. Background potential

In the previous section we have presented the fixed point solution for the fluctuation field couplings. All background quantities depend on these dynamical couplings and have to be evaluated on the above solution. Along these lines we calculate a background field potential at the fixed point. The flow of the background potential is completely determined by the

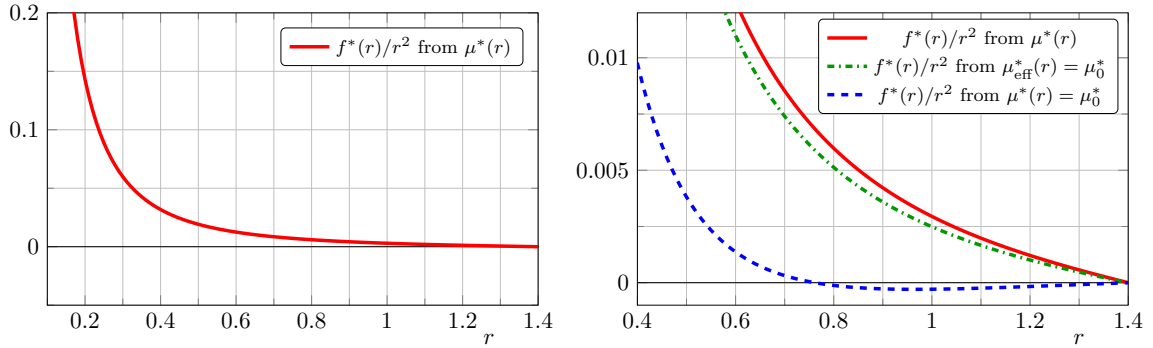


Figure 5.2.: Displayed are background potentials  $f^*(r)/r^2$  obtained from the fixed point solution  $\mu^*(r)$  (left and right panel) and from the approximations  $\mu_{\text{eff}}^*(r) = \mu_0^*$  and  $\mu^*(r) = \mu_0^*$  (right panel). All curves are obtained with the condition  $f^*(r = 1.4) = 0$ . Other conditions just shift the potential  $f^*(r)/r^2$  by a constant. The full solution does not contain a minimum, it becomes asymptotically flat. The approximation  $\mu_{\text{eff}}^*(r) = \mu_0^*$  is qualitatively very good, see also Fig. 5.1. The approximation  $\mu^*(r) = \mu_0^*$  corresponds to a pure Einstein-Hilbert computation. Here we find a minimum at  $r_0 = 0.97$ .

dynamical couplings of the two-point function, see (3.9). On a sphere, the background effective action is given by

$$\Gamma[\bar{g}, 0] = \int d^4x \sqrt{\bar{g}} k^4 f(\bar{R}/k^2) = \frac{384\pi^2}{r^2} f(r). \quad (5.32)$$

Denoting the right-hand side of (3.9) at vanishing fluctuation field by  $\mathcal{F}(r, \mu(r))$  we obtain a flow equation for the function  $f(r)$  given by

$$\frac{384\pi^2}{r^2} (\partial_t f + 4f(r) - 2rf'(r)) = \mathcal{F}(r, \mu(r)). \quad (5.33)$$

If we then look at the fixed point for  $f^*(r)$  we find

$$\frac{384\pi^2}{r^2} (4f^*(r) - 2rf^{*'}(r)) = \mathcal{F}(r, \mu^*(r)). \quad (5.34)$$

One then notes that the left-hand side is just the background EoM for  $f(r)$ -gravity on a constant curvature background. Thus when the function  $\mathcal{F}(r, \mu^*(r))$  vanishes we have a solution to the background EoM at the fixed point given by

$$\mathcal{F}(r_0, \mu^*(r_0)) = 0. \quad (5.35)$$

Equivalently we can look for a minimum of the function  $f(r)/r^2$ . In Fig. 5.2 we plot the background potential  $f(r)/r^2$  for our full solution (left panel) as well as in comparison with other approximations (right panel). There we use  $\mu_{\text{eff}}^*(r) = \mu_0^*$  and  $\mu^*(r) = \mu_0^*$  as given in (5.26). The first is seen to be a good approximation from Fig. 5.1 while the latter reduces our computation to an Einstein-Hilbert approximation. We observe that in the full solution and in the  $\mu_{\text{eff}}^*(r) = \mu_0^*$  approximation there are no solutions to the background EoM within the investigated curvature regime. This absence of a constant curvature solution is in agreement with studies of  $f(R)$  gravity in the background field

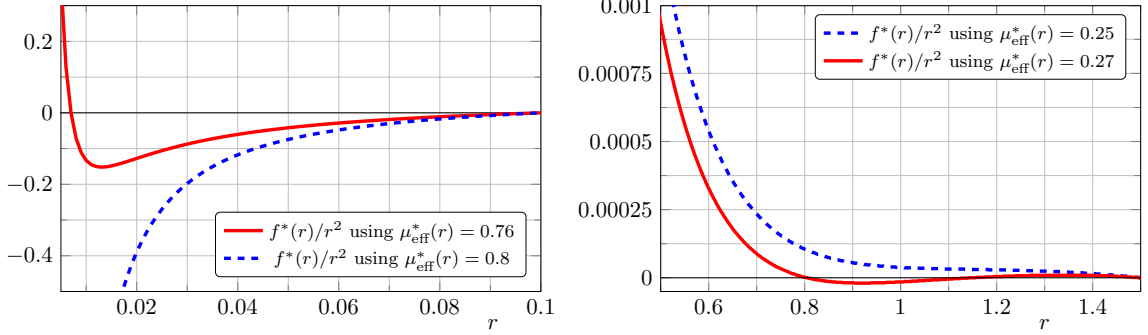


Figure 5.3.: Fixed point background potential for different constant input values of  $\mu_{\text{eff}}^*(r)$ .

The minimum that corresponds to the solution of the background equation of motion is at  $r > 0$  for  $\mu_{\text{eff}}^*(r) \lesssim 0.77$ , while for  $\mu_{\text{eff}}^*(r) \gtrsim 0.77$  it is at  $r < 0$  (left panel). For  $\mu_{\text{eff}}^*(r) \lesssim 0.25$  the minimum vanishes completely, while for  $\mu_{\text{eff}}^*(r) = 0.27$  the minimum is located at  $r_0 = 1.1$  (right panel).

approximation [288], although solutions have been found in calculations exploiting the exponential parameterisation [286, 287] and within the geometrical approach [284, 291]. For the approximation  $\mu^*(r) = \mu_0^*$ , which corresponds to a pure Einstein-Hilbert computation, we find a minimum at  $r_0 = 0.97$ . This is again in agreement with computations in the background field approximation [410, 411].

In a polynomial expansion around  $r = 0$  the background potential of the full solution would take the form

$$f(r) = 0.0065 - 0.0065 r + \mathcal{O}(r^2), \quad (5.36)$$

and consequently we obtain fixed point values of the background Newton's coupling and the background cosmological constant according to

$$\bar{g}^* = 3.0, \quad \bar{\lambda}^* = 0.50. \quad (5.37)$$

Note that  $\bar{\lambda} = \frac{1}{2}$  is not a pole in our computation: the pole is only present in the graviton mass parameter  $\mu(r)$ . Surprisingly the fixed point value of  $\bar{g}^*$  is rather large. We compare these values with the pure Einstein-Hilbert approximation, see blue dashed line in Fig. 5.2. We find

$$f_{\text{EH}}(r) = 0.0065 - 0.021 r + \mathcal{O}(r^2), \quad (5.38)$$

and consequently

$$\bar{g}_{\text{EH}}^* = 0.94, \quad \bar{\lambda}_{\text{EH}}^* = 0.15. \quad (5.39)$$

These values are comparable to standard Einstein-Hilbert computations in the background field approximation as well as in fluctuation computations. Thus the large values in (5.37) are indeed triggered by the non-trivial  $r$  dependence of the couplings.

We investigate the stability of the present results by treating  $\mu_{\text{eff}}^*(r)$  as a free parameter without curvature dependence. In this case,  $\mu_{\text{eff}}^*(r) = \mu_0^*$  is a good approximation for our best solution as discussed above. By varying this parameter we see for which values a solution to the background EoM exists. With reference to Fig. 5.3 we find that solutions

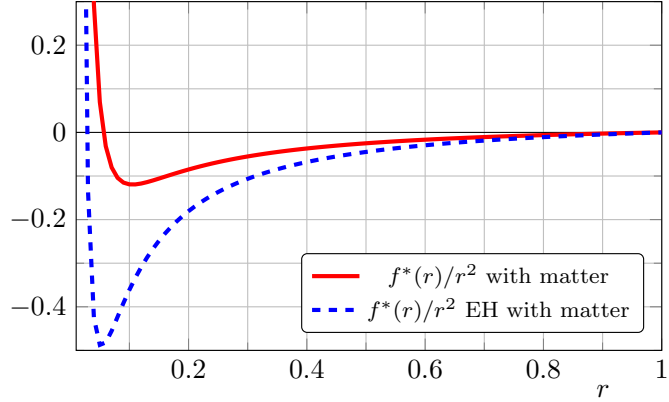


Figure 5.4.: Depicted is the fixed point background potential if Standard Model matter content is included. In the full solution as well as in the Einstein-Hilbert solution we find a minimum at small background curvature,  $r_0 = 0.11$  and  $r_{0,\text{EH}} = 0.05$ , respectively, which corresponds to the solution of the background equation of motion.

exist for positive curvature when  $0.255 \lesssim \mu_{\text{eff}}^* \lesssim 0.77$  and for negative curvature for  $\mu_{\text{eff}}^* \gtrsim 0.77$ . For  $\mu_{\text{eff}}^* \lesssim 0.255$  there are no solutions. The transition of the minimum from positive to negative curvature is depicted in the left panel of Fig. 5.3 while the full disappearance of the minimum is depicted in the right panel. The computed value of  $\mu_0^* = -0.38$ , see (5.26), is far away from the value where the solution appears. Thus we conclude that the absence of a minimum in the background potential in our full pure gravity computation is rather stable with respect to changes in the truncation.

### Dependence on matter

Matter can potentially have a significant influence on the properties of the UV fixed point, this will be detailed in the subsequent chapters of this dissertation. In this chapter matter influences the existence of a minimum in the background potential in two ways: On the one hand it has an influence on the fixed point values of the fluctuation couplings, where in particular the influence on  $\mu_{\text{eff}}^*(r)$  is important. On the other hand it has a direct influence on the background potential via the background matter loops. Both these effects will be studied in this dissertation in a fluctuation computation on a flat background, see Chapter 6 for scalars and fermions and Chapter 7 for gauge bosons. Consequently we adapt the analysis to curved backgrounds under the assumption that the effective graviton mass parameter  $\mu_{\text{eff}}(r)$  remains almost curvature independent in these extended systems, similar to the results displayed in Sec. 5.4.1. Combining the results of the two upcoming chapters for Standard Model matter content ( $N_s = 4$ ,  $N_f = 22.5$ , and  $N_v = 12$ ) gives a UV fixed point at

$$(g_0^*, \lambda_{3,0}^*, \mu_0^*)_{\text{SM}} = (0.17, 0.15, -0.71). \quad (5.40)$$

For the present analysis only the value  $\mu_{0,\text{SM}}^*$  is important since we now use  $\mu_{\text{eff}}^*(r) = \mu_{0,\text{SM}}^*$  as an input for the background potential. The matter content seemingly pushes  $\mu_{\text{eff}}^*$  in the wrong direction, cf. Fig. 5.3. However, the matter content has also a huge influence on the background equations. The combined result is displayed in Fig. 5.4. Indeed we find a

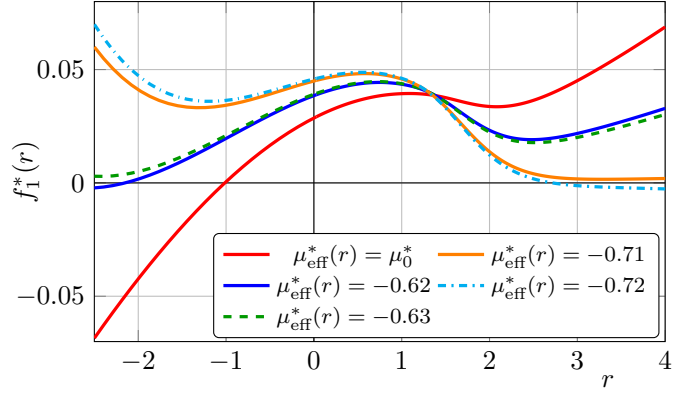


Figure 5.5.: Shown is the fixed point function  $f_1^*(r)$  for different constant input values of  $\mu_{\text{eff}}^*(r)$ . The zeros in these functions correspond to solutions to the quantum equations of motion (5.4). Our best result  $\mu_{\text{eff}}^*(r) = \mu_0^* = -0.38$  has a solution at negative curvature,  $r_0 = -1.0$ .

minimum in the background potential at small curvature,  $r_0 = 0.11$ . Also in the Einstein-Hilbert approximation, i.e.  $\mu^*(r) = \mu_{0,\text{SM}}^*$ , we find a minimum at  $r_{0,\text{EH}} = 0.05$ . With Standard Model matter content the full solution and the Einstein-Hilbert approximation are very similar. This comes as a surprise as the difference was rather significant without matter content, cf. Fig. 5.2.

#### 5.4.3. Quantum equation of motion

In this section we evaluate the graviton one-point function and thus look for solutions to the quantum EoM (5.4). As discussed in Sec. 5.2.1 the solution to this equation leads to self-consistent backgrounds that improve the convergence of the Taylor series. Moreover, it has been also argued there that the quantum EoM in the limit  $k \rightarrow \infty$  should be seen as an estimate for the solution of the UV EoM in the physical limit  $k \rightarrow 0$  where background and quantum EoM agree due to background independence.

Within the present setup the only invariant linear in the fluctuation field is given by  $f_1(r)h^{\text{tr}}$  with some function  $f_1$  that is determined by the fluctuation couplings. An invariant linear in the transverse traceless mode does not exist due to our restriction to a spherical background and thus the absence of terms like  $r^{\mu\nu}h_{\mu\nu}^{\text{tt}}$ . Consequently we evaluate (5.4) with a projection on the trace mode of the graviton.

In straight analogy to the background EoM (5.32) we parameterise the one-point function by

$$\Gamma^{(h_{\text{tr}})}[\bar{g}, 0] = \int d^4x \sqrt{\bar{g}} k^3 f_1(\bar{R}/k^2) = \frac{384\pi^2}{k r^2} f_1(r). \quad (5.41)$$

We denote again the right-hand side by  $\mathcal{F}_1(r, \mu(r))$ . This time, however, we obtain at a different differential equation for  $f_1$  due to the different mass-dimensions of  $\bar{g}$  and  $h$ . Thus  $f_1$  obeys the fixed point equation

$$\frac{384\pi^2}{r^2} (3f_1^*(r) - 2r f_1^{*\prime}(r)) = \mathcal{F}_1(r, \mu^*(r)). \quad (5.42)$$

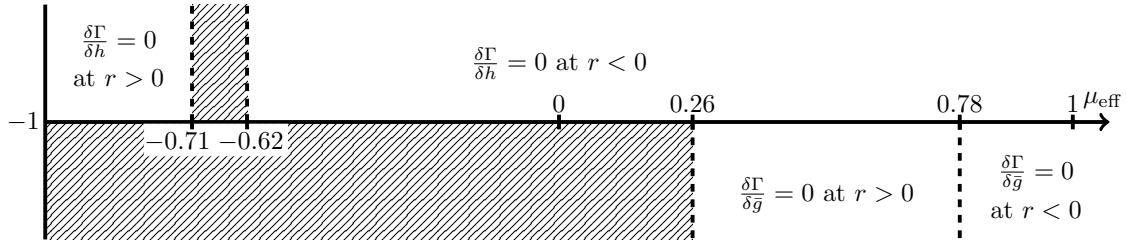


Figure 5.6.: Visualisation of the existence of a solution to the background and quantum equation of motion in dependence on the parameter  $\mu_{\text{eff}}$ . Solutions at positive curvature ( $r > 0$ ) and negative curvature ( $r < 0$ ) are distinguished.

We solve this equation with the initial condition that  $f_1^*(r)$  is finite at  $r = 0$ . Consequently we combine a heat kernel expansion around  $r = 0$  up to the order  $r^3$  with a spectral sum evaluation for large, positive curvature. For results at negative curvature we rely on the heat kernel expansion, but from a comparison of the heat kernel results with the spectral sum at positive curvature we can estimate the radius of convergence of the heat kernel. We estimate the latter by the range where the relative change is in the sub percent regime. We find that the radius of convergence is approximately given by  $r_{\text{conv}} \approx 1$ . The radius of convergence increases for larger  $\mu_{\text{eff}}^*(r)$ .

The resulting fixed point functions  $f_1^*(r)$  are shown in Fig. 5.5. For our best result  $\mu_{\text{eff}}^*(r) = \mu_0^* = -0.38$ ,  $f_1^*(r)$  has a root at negative curvature,  $r_0 = -1.0$ , which corresponds to a solution to the quantum EoM. The result lies within the radius of convergence of the heat-kernel expansion and thus we consider it trustworthy.

We again check the stability of the solution by treating  $\mu_{\text{eff}}^*(r)$  as a constant free input parameter. For more positive values,  $\mu_{\text{eff}}^* > \mu_0^*$ , the root of  $f_1^*(r)$  moves towards larger curvature, but always remains negative. In the limit  $\mu_{\text{eff}}^* \rightarrow \infty$  the root is located at  $r_0 = -0.42$ . For more negative values,  $\mu_{\text{eff}}^* < \mu_0^*$  the root of  $f_1^*(r)$  moves towards smaller curvature and eventually the root disappears at  $\mu_{\text{eff}}^* = -0.62$ , cf. Fig. 5.5. This result has to be taken very careful since at  $\mu_{\text{eff}}^* = -0.62$  the root is located at  $r_0 = -2.2$  and thus lies outside of the radius of convergence of heat kernel. At  $\mu_{\text{eff}}^* = -0.71$  a new solution appears at positive curvature,  $r_0 = 2.7$ . This root remains also for more negative values of  $\mu_{\text{eff}}^*$  until the pole at  $\mu_{\text{eff}}^* = -1$ . The roots at positive curvature are obtained with the spectral sum and thus do not rely on the radius of convergence of the heat kernel.

We have visualised the existence of a solution to the background and quantum EoM in Fig. 5.6. The quantum EoM has almost always a solution, only in the range  $-0.71 < \mu_{\text{eff}}^* < -0.62$  no solution exists. This range may even disappear with better truncations or an improved computation at large negative curvature. The background EoM on the other hand only allows for a solution for  $\mu_{\text{eff}}^* > 0.26$ , and thus in a region that is very unusual for pure gravity computations.

## 5.5. Summary

In this chapter we have developed an approach to asymptotically safe gravity with non-trivial backgrounds. As a first application of the novel approach we computed the  $f(R)$ -potential and discussed solutions of the equations of motion.

We have also given a discussion of functional approaches to quantum gravity that take

into account the necessary background independence of the theory. We have discussed, for the first time in quantum gravity, that background independence and diffeomorphism invariance can be achieved iteratively in *any* approximation scheme, based on a similar argument in non-Abelian gauge theories, see [Sec. 5.2.2](#). We have also emphasised the relevance of aiming for solutions that satisfy all functional relations. We have argued that this is tightly bound to the question of unitarity.

The approach is based on a vertex expansion of the effective action about non-trivial backgrounds, which at present are restricted to constantly-curved backgrounds. Our explicit results are based on a truncation that includes the flow of the graviton two- and three-point function and thus the couplings  $g$ ,  $\lambda_3$  and  $\mu$ . The construction of an approximate momentum space, cf. [\(5.14\)](#), allowed us to evaluate these couplings without a derivative expansion in momentum  $p$  or curvature  $r$ . In this chapter we focused on the curvature dependence and thus all couplings are functions of the curvature,  $g(r)$ ,  $\lambda_3(r)$  and  $\mu(r)$ . The flow equations for these coupling functions were obtained with spectral sums on a sphere. The results are smoothly connected to known results at vanishing background curvature with heat-kernel methods.

As one main result we found UV fixed point functions that confirm the asymptotic safety of the present system. Interestingly, the effective fixed point couplings,  $\lambda_{3,\text{eff}}^*(r)$  and  $\mu_{\text{eff}}^*(r)$ , cf. [\(5.28\)](#), turned out to be almost curvature independent over the investigated range: the couplings counterbalance the explicit curvature dependence of the  $n$ -point functions.

We have also discussed the background and the quantum equation of motion, [\(5.3\)](#) and [\(5.4\)](#), in [Sec. 5.2](#). At  $k = 0$ , their solutions agree due to background independence. In turn, at finite  $k$  the solutions to background and quantum equations of motion differ due to a regulator contribution to the modified Nielsen identity. This signals the breaking of background independence in the presence of the cutoff. We have argued in this chapter that at finite cutoff it is the solution of the quantum equation of motion that relates directly to the physical solution of the equation of motion at vanishing cutoff.

We explicitly evaluated both equations of motion with the UV fixed point functions and indeed found different solutions: The background equation of motion does not feature a solution. Only with Standard Model matter content a solution at small positive curvature is present. The quantum equation of motion exhibits already a solution at negative curvature without any matter content. We have checked the stability of these statements by scanning for solutions in the parameter  $\mu_{\text{eff}}^*$ . The background equation of motion without matter features a solution only for very large values of  $\mu_{\text{eff}}^*$ , far away from most values observed in pure quantum gravity truncations. On the other hand the quantum equation of motion has a solution for almost all  $\mu_{\text{eff}}^*$ . This indicates that the existence of a solution is robust to changes in the truncation. We have visualised this in [Fig. 5.6](#).

The discussion of the equation of motion leads us directly to a specific observable: the effective action, evaluated on the equation of motion. In standard quantum field theories this is the free energy, and it is gauge and parameterisation independent. For the present approach this is discussed in [Sec. 5.2.1](#). We therefore expect only a mild dependence on these choices within sensible approximations to the full effective action. Indeed, this has been observed in the background field approximation [\[258, 412\]](#). It would be interesting to see whether this property is also holds in the present approach that goes beyond the background field approximation. At finite cutoff this investigation can be done by studying the gauge and parameterisation independence of the effective action evaluated on the quantum equation of motion.



# 6. Towards combining the Standard Model with quantum gravity

## 6.1. Introduction

It is not sufficient to have a theory of quantum gravity, it must also incorporate all other degrees of freedom: the matter content of the universe, i.e. the Standard Model matter content and possible extensions of it. This medal has two sides: we know that gravity fluctuations become important beyond the Planck scale and thus it is of interest how the gravity contributions alter the running of the Standard Model couplings, for instance if it removes the Landau poles of the hypercharge and the quartic Higgs coupling large energies. But also matter fluctuations can influence the quantum gravity theory and one might hope to constrain the space of allowed matter theories by asking to which matter theory a viable quantum gravity theory can be constructed. This is can be seen in analogy to QCD with many quark flavours where asymptotic freedom is lost. One can even consider the possibility that a pure quantum gravity theory does not exist, only upon the inclusion of matter the theory becomes viable.

The inclusion of matter degrees of freedom poses different kinds of problems for different kind of quantum gravity theories. For example loop quantum gravity or spin foams are fundamentally discrete and thus the inclusion of fermions is a priori challenging. The asymptotic safety scenario has here the advantage of using standard QFT methods and consequently the treatment of matter is well understood. Nonetheless one faces technical challenges for example large tensor structures that need to be contracted, a large amount of diagrams per flow equation and, last but not least, that the pure quantum gravity sector is not yet under full control.

There has already been a plethora of results and developments in gravity-matter systems in asymptotically safe quantum gravity, see [120–122, 151, 152, 295, 376, 387, 413–440]. For a review of asymptotic safety on matter aspects see [441]. Most of the above works utilised the background field approximation and partially observed severe restrictions on the space of matter theories that are compatible with asymptotic safety see e.g. [416] or [424, 425] with a mixed approach, where the background field approximation for the couplings is augmented with dynamical anomalous dimensions. In these approximation it seemed that supersymmetric models are not compatible with asymptotic safety, while the Standard Model is compatible. Consequently this direction of research was dubbed with the catchy title 'matter matters'. These results have, however, be taken with care due to the background field approximation as we will show in upcoming chapters.

Concerning the other side of the medal, the influence of gravity fluctuation on the matter couplings, a lot of progress has been made recently. The impact of gravity can be parameterised via the graviton propagator and if the fluctuations become too strong, they trigger new divergences in the matter sector. This gives rise to a bound, called the weak gravity bound [387, 420, 432, 433]. Thus it is of great interest to get a quantitative handle on the strength of the graviton propagator.

$$\dot{\Gamma}_k[\bar{g}, \phi] = \frac{1}{2} \left( \text{double line loop} \right) - \left( \text{dotted line loop} \right) - \left( \text{solid line loop} \right) + \frac{1}{2} \left( \text{dashed line loop} \right)$$

Figure 6.1.: Flow equation for the scale dependent effective action  $\Gamma_k$  in diagrammatic representation. The double, dotted, solid and dashed lines correspond to the graviton, ghost, fermion and scalar propagators, respectively. The crossed circles denote the respective regulator insertions.

In the upcoming chapters of this dissertation we investigate the impact of matter fluctuations on the quantum gravity fixed point. The main difference compared to earlier works is that we go beyond the background field approximation and disentangle contributions from the fluctuation and the background field. We saw already in the previous chapters that the difference between these fields is potentially of qualitative nature. Indeed we will show that matter increases this qualitative difference and we find that large classes of matter models are compatible with asymptotically safe gravity. Thus we dubbed our research 'matter matters but gravity rules'.

In this chapter we analyse the influence of scalar and fermionic matter on the non-trivial UV fixed point of quantum gravity in the dynamical FRG setup put forward in [Chapter 3](#). The matter contributions to the quantum gravity system are extracted, for the first time, from the higher-order dynamical correlation functions. We analyse a system of vertex flows evaluated at flat Euclidean background. We also introduce a validity bound on the generic class of regulators used here, based on the size of the anomalous dimensions. This regime includes an arbitrary numbers of fermions, whereas it restricts the number of allowed scalars that can be discussed with the present generic class of regulators to a maximum  $\lesssim 20$ . Within this regime of validity we find that the UV-fixed point persists and remains UV stable. We also find that the UV fixed points for the dynamical couplings are significantly different from those of their associated background counterparts, once matter fields are included. In summary, the asymptotic safety scenario does not put constraints on the matter content of the theory within the validity bounds for the chosen generic class of regulators.

## 6.2. Functional renormalisation group

As in the previous chapter we use the functional renormalisation group approach. In the pure gravity context we detailed this setup in [Sec. 3.3](#). Here we focus on the additional terms that arise due to the matter contributions. The basic object is the scale-dependent effective action  $\Gamma_k[\bar{g}, \phi]$ , where the fluctuation superfield  $\phi$  contains now the fields

$$\phi = (h_{\mu\nu}, c_\mu, \bar{c}_\mu, \psi_i, \bar{\psi}_j, \varphi_l) . \quad (6.1)$$

The fermion fields  $(\bar{\psi}_i, \psi_j)$ , carrying the flavour indices  $i, j \in 1 \dots N_f$ , and the real scalars  $\varphi_l$  of flavour  $l = 1 \dots N_s$  constitute the matter contributions to  $\phi$ . The flow of the scale dependent action now also includes contributions from the matter fields, to wit

$$\partial_t \Gamma_k = \frac{1}{2} \text{Tr} [G_k \partial_t R_k]_{hh} - \text{Tr} [G_k \partial_t R_k]_{\bar{c}c} - \text{Tr} [G_k \partial_t R_k]_{\bar{\psi}\psi} + \frac{1}{2} \text{Tr} [G_k \partial_t R_k]_{\phi\phi} . \quad (6.2)$$

[Fig. 6.1](#) depicts equation (6.2) in terms of diagrams. We are again expanding the full scale-dependent effective action in powers of the fluctuation fields according to

$$\begin{aligned}\Gamma_k[\bar{g}, \phi] = \Gamma_k[\bar{g}, 0] + \Gamma_k^{(h)}[\bar{g}, 0]h + \frac{1}{2}\Gamma_k^{(hh)}[\bar{g}, 0]h^2 + \frac{1}{3!}\Gamma_k^{(hhh)}[\bar{g}, 0]h^3 + \frac{1}{2}\Gamma_k^{(\bar{c}c)}[\bar{g}, 0]\bar{c}c \\ + \frac{1}{2}\Gamma_k^{(\bar{\psi}\psi)}[\bar{g}, 0]\bar{\psi}\psi + \frac{1}{2}\Gamma_k^{(\varphi\varphi)}[\bar{g}, 0]\varphi^2 + \dots.\end{aligned}\quad (6.3)$$

$\Gamma_k[\bar{g}, \phi]$  is expanded about an, a priori, arbitrary fixed metric background  $\bar{g}_{\mu\nu}$ , but as in [Chapter 3](#) and [Chapter 4](#) we choose a flat Euclidean background, i.e.  $\bar{g}_{\mu\nu} = \delta_{\mu\nu}$ . In (6.3), the zero-point function  $\Gamma_k[\bar{g}, 0]$  and the one-point function  $\Gamma_k^{(h)}[\bar{g}, 0]$  are non-dynamical (background-) quantities that do not feed back into the flow of the dynamical  $n$ -point functions. Therefore we first focus on the computation of the latter ones and afterwards, in [Sec. 6.5](#), use the solution of the dynamical couplings for a self-consistent computation of the background couplings. Since the right hand side of the flow equation (6.2) contains second variations of the fields, the flows for the respective  $n$ -point functions contain  $n$ -point vertices up to order  $n + 2$ .

In straight analogy to [Sec. 3.4.1](#) we generate an ansatz for the vertices from a classical action and dress them according to (3.16). In this chapter the classical action  $S$  is given by the gauge-fixed Einstein-Hilbert action, see also [Sec. 3.3](#), added by covariant fermion and scalar kinetic terms according to

$$S = S_{\text{EH}} + \int d^4x \sqrt{g} \bar{\psi}_i \not{\nabla} \psi_i + \frac{1}{2} \int d^4x \sqrt{g} g_{\mu\nu} \partial^\mu \varphi_l \partial^\nu \varphi_l, \quad (6.4)$$

where we used the conventional slash-notation for the contraction of the spin-covariant derivative  $\nabla^\mu$  with gamma matrices. The covariant kinetic terms for the matter fields in (6.4) lead to minimal coupling between gravity and matter in the present truncation. In [Fig. 6.2](#) we show all dressed three-point vertices used in this chapter. For the formulation of fermions in curved spacetime we use the spin-base invariance formalism introduced in [\[442–444\]](#). This allows to circumvent possible ambiguities arising in the vielbein formalism and relies on spacetime dependent  $\gamma$ -matrices and the spin-connection  $\Gamma^\mu$ . As a result,  $\not{\nabla}$  reads

$$\not{\nabla} = g_{\mu\nu} \gamma(x)^\mu \nabla^\nu = g_{\mu\nu} \gamma(x)^\mu (\partial^\nu + \Gamma(x)^\nu), \quad (6.5)$$

if it acts on a spinor as in (6.4). In the following, we drop the explicit spacetime dependence of the latter quantities for a more convenient notation.

The vertex flows, that are derived by taking field derivatives from (6.2), carry spacetime and momentum indices. In order to obtain scalar flow equations for the couplings the appropriate projection of the flows is a crucial part of the present truncation and goes along the same lines as in [Chapter 3](#). It can be summed up in a three step procedure:

- (i) We decompose  $\mathcal{T}^{(n_h)}$ , where  $n_h$  is the number of variations with respect to  $h$ , into its momentum dependent and momentum independent part according to

$$\mathcal{T}^{(n_h)}(\mathbf{p}; \Lambda_{n_h}) = \mathcal{T}^{(n_h)}(\mathbf{p}; 0) + \Lambda_{n_h} \mathcal{T}^{(n_h)}(0; 1). \quad (6.6)$$

In (6.6), the first term on the right-hand side is quadratic in the external graviton momenta  $\mathbf{p}$  for the current truncation. The second term is momentum independent.

Figure 6.2.: Vertex dressing of all three-point vertices used in this chapter. The vertex dressing consist of the respective wave function renormalisations, couplings and tensor structures. The first line in the figure depicts all pure gravity three-point vertices while the second line shows the ones with gravity-matter-interactions.

- (ii) From (6.6) we take the dimensionless tensors  $\mathcal{T}^{(n_h)}(\mathbf{p}; 0)/\mathbf{p}^2$  and  $\mathcal{T}^{(n_h)}(0; 1)$  and separately multiply all spacetime-index pairs of both tensors with transverse-traceless projection operators  $\Pi_{tt}$ . This leaves us with the two tensors  $\mathcal{T}_{tt}^{(n_h)}(\mathbf{p}; 0)/\mathbf{p}^2$  and  $\mathcal{T}_{tt}^{(n_h)}(0; 1)$ , each of them carries  $2n_h$  spacetime indices.
- (iii) We contract the left and the right hand side of the vertex flow with these two tensors, in order to obtain Lorentz-scalar expressions. Hereby, the tensors  $\mathcal{T}_{tt}^{(n_h)}(\mathbf{p}; 0)/\mathbf{p}^2$  and  $\mathcal{T}_{tt}^{(n_h)}(0; 1)$  are used to project the tensorial flow onto the scalar flows of  $G_{n_h}$  and  $\Lambda_{n_h}$ , respectively.

The projection operators are also detailed in Sec. 3.4.3. In addition to the spacetime indices, the vertex flows carry spinor, flavour and colour indices. These however, can be trivially traced out after multiplying appropriately with  $\gamma$  and  $\mathbf{1}$ -matrices. After having traced out all discrete indices the resulting flow still depends on the external field momenta  $\mathbf{p}$ . As in Sec. 3.4.2 we choose the maximally symmetric configuration for the graviton three-point function.

Summarising the present truncation, we consider the renormalisation group flow for the  $n$ -point correlation functions in a system of minimally-coupled gravity and matter. To this end, we employ a vertex expansion of the scale dependent effective action about a flat metric background to derive flow equations for the  $n$ -point correlators up to order three. We derive the flows of the momentum-independent couplings  $G$ ,  $\Lambda_2$  and  $\Lambda_3$  as well as the momentum-dependent anomalous dimensions  $\eta_h(p^2)$ ,  $\eta_c(p^2)$ ,  $\eta_\psi(p^2)$  and  $\eta_\varphi(p^2)$ . The couplings  $G$  and  $\Lambda_3$  are computed from the transverse-traceless part of the graviton three-point function in the symmetric momentum configuration. Diffeomorphism invariant background couplings are computed on the solution of the dynamical couplings. Altogether, the present truncation yields the flow of the scale dependent parameters,

$$\bar{G}, \bar{\Lambda}, G, \Lambda_2, \Lambda_3, \eta_h(p^2), \eta_c(p^2), \eta_\psi(p^2), \eta_\varphi(p^2). \quad (6.7)$$

### 6.3. Flows of correlation functions

The properties of the given theory are completely determined by the flows of the respective correlation functions. Thus, the latter parameterise the non-trivial interplay between gravity and matter. Matter is known to have a significant impact on the UV-behaviour of

$$\partial_t \Gamma_{k, \text{matter}}^{(hh)} = N_s \left( -\frac{1}{2} \begin{array}{c} \text{---} \otimes \text{---} \\ \text{---} \text{---} \end{array} + \begin{array}{c} \text{---} \otimes \text{---} \\ \text{---} \text{---} \end{array} \right) - 2N_f \left( -\frac{1}{2} \begin{array}{c} \text{---} \otimes \text{---} \\ \text{---} \text{---} \end{array} + \begin{array}{c} \text{---} \otimes \text{---} \\ \text{---} \text{---} \end{array} \right)$$

$$\partial_t \Gamma_{k, \text{matter}}^{(hhh)} = N_s \left( -\frac{1}{2} \begin{array}{c} \text{---} \otimes \text{---} \\ \text{---} \text{---} \end{array} + 3 \begin{array}{c} \text{---} \otimes \text{---} \\ \text{---} \text{---} \end{array} - 3 \begin{array}{c} \text{---} \otimes \text{---} \\ \text{---} \text{---} \end{array} \right) - 2N_f \left( -\frac{1}{2} \begin{array}{c} \text{---} \otimes \text{---} \\ \text{---} \text{---} \end{array} + 3 \begin{array}{c} \text{---} \otimes \text{---} \\ \text{---} \text{---} \end{array} - 3 \begin{array}{c} \text{---} \otimes \text{---} \\ \text{---} \text{---} \end{array} \right)$$

Figure 6.3.: Diagrammatic representation of the matter induced flow of the graviton two- and three-point function. Double, single and dashed lines represent graviton, fermion and scalar propagators, respectively, filled circles denote dressed vertices. Crossed circles are regulator insertions.

quantum gravity. On the other hand, graviton fluctuations can lead to strong correlations among matter fields. The resulting mutual dependencies play a crucial rôle for the flow of the complete system and are discussed separately in the following sections.

### 6.3.1. Matter contributions to gravity flows

For the present analysis of quantum gravity, the gravity flows are extracted from the dynamical graviton two-point and three-point functions. The impact of matter manifests itself by matter loops in the diagrammatic representation of the flow. Fig. 6.3 depicts these contributions. The trace over the colour and flavour indices leads to weight factors of  $N_s$  and  $N_f$  for scalar and fermion loops, respectively. The matter contributions to  $\text{Flow}^{(hh)}$  and  $\text{Flow}^{(hhh)}$  are thus proportional to  $N_s$  or  $N_f$ .

From the transverse-traceless part of  $\text{Flow}^{(hh)}$  we extract the flow of the graviton mass parameter defined as  $M^2 := -2\Lambda_2$  and the graviton anomalous dimension  $\eta_h$ , just as in Sec. 3.4. The flow equation has the shape

$$\text{Flow}_{tt}^{(hh)}(p^2) = \frac{1}{32\pi} (\partial_t M^2 - \eta_h(p^2)(p^2 + M^2)) . \quad (6.8)$$

The matter contribution to  $\text{Flow}_{tt}^{(hh)}(p^2)$  are precisely the ones in Fig. 6.3. This equation is evaluated at two different momentum scales  $p^2$ . Subtracting these two equations from each other allows for an unambiguous extraction of  $\partial_t M^2$  and  $\eta_h(p^2)$ . We call this procedure bilocal momentum projection.

The matter contributions to the flow for the graviton three-point function parameterise the impact of matter on the dynamical gravitational couplings  $g$  and  $\lambda_3$ . The flow for  $G$  and  $\Lambda_3$  is extracted from the flow of the transverse-traceless three-graviton vertex, projected on the classical tensor structures as described in (6.6) and evaluated at the momentum symmetric point as described in (3.22). This yields equations of the type

$$\frac{2}{\sqrt{G}} \text{Flow}_{tt,i}^{(hhh)} = 2\mathcal{M}_i \partial_t \Lambda_3 - [\eta_G + 3\eta_h(p^2)] (\mathcal{N}_i p^2 + \mathcal{M}_i \Lambda_3) , \quad (6.9)$$

with  $i = G, \Lambda$ , for the projection on the tensor structures of  $G$  and  $\Lambda_3$ , respectively, and  $\eta_G = -\partial_t \ln G$ . The factors  $\mathcal{N}_i$  and  $\mathcal{M}_i$  arise from the tensor projection and they depend on the kinematic configuration. Note, that (6.9) is structurally very similar to (6.8). For the extraction of the flows for the couplings  $G$  and  $\Lambda_3$  we apply the bilocal momentum projection discussed before. Thus, we evaluate the flow of  $G$  at  $p^2 = k^2$  as well as at  $p^2 = 0$  and subtract both equations from each other. For the flow of  $\Lambda_3$  it is then sufficient

$$\begin{aligned}\dot{\Gamma}_k^{(\phi\phi)} &= -\frac{1}{2} \text{---} \text{---} \text{---} + \text{---} \text{---} \text{---} + \text{---} \text{---} \text{---} \\ \dot{\Gamma}_k^{(\psi\bar{\psi})} &= -\frac{1}{2} \text{---} \text{---} \text{---} + \rightarrow \text{---} \text{---} \text{---} + \rightarrow \text{---} \text{---} \text{---}\end{aligned}$$

Figure 6.4.: Diagrammatic representation of the gravitationally induced flows of the matter-two-point-functions. Double, single and dashed lines represent graviton, fermion and scalar propagators respectively, filled circles denote dressed vertices. Crossed circles are regulator insertions.

to evaluate (6.9) (with  $i = \Lambda$ ) at vanishing external momentum  $p^2 = 0$ . This prescription identical to the one in [Chapter 3](#) and the resulting flows with matter contributions are given in [App. D.1](#).

### 6.3.2. Gravity contributions to matter flows

In the matter sector, we consider the flows of the matter two-point functions. Since we do not admit matter self-interactions within the given truncation, these flows are driven solely by gravity-matter interactions. Furthermore, the matter fields are treated as massless, which is a good approximation for studies of the UV-behaviour of the theory. Consequently, the only quantities that are extracted here, are the matter anomalous dimensions. The effective action constructed from (6.4) is diagonal in both the colour and the flavour indices,  $i$  and  $k$ , respectively. We treat all scalars and all fermions on equal footing, providing them with one anomalous dimension for each of the field species,  $\eta_\varphi(p^2)$  and  $\eta_\psi(p^2)$ , respectively. This allows for an extraction of the matter anomalous dimension from one representative field, since  $\text{Flow}^{(\varphi_k\varphi_l)} = \delta_{kl} \text{Flow}^{(\varphi_k\varphi_k)}$  and  $\text{Flow}^{(\psi_i\psi_j)} = \delta_{ij} \text{Flow}^{(\bar{\psi}_i\psi_i)}$ . Consequently, we drop the colour and flavour indices in the flows of the scalar and fermion two-point functions.

[Fig. 6.4](#) depicts the flows of the matter two-point functions in diagrammatic representation, which constitute the respective right-hand sides of flow equation. From these flows we extract the matter anomalous dimensions. For the scalar fields the left-hand side is given by

$$\text{Flow}^{(\varphi\varphi)}(p^2) = -p^2 \eta_\varphi(p^2), \quad (6.10)$$

in complete analogy to the equation for the transverse-traceless graviton two-point function, (6.8). For the fermions we have the additional spinor structure that needs to be eliminated in order to obtain a Lorentz-scalar expression. The flow for the fermion two-point function reads

$$\text{Flow}^{(\bar{\psi}\psi)}(p^2) = -i \not{p} \eta_\psi(p^2). \quad (6.11)$$

By multiplying this expression with  $\not{p}$  and taking the trace over the spinor indices we obtain an expression, which is identical to (6.8) and (6.10) up to prefactors, to wit

$$\text{Tr} \left[ \not{p} \text{Flow}^{(\bar{\psi}\psi)}(p^2) \right] = -d i p^2 \eta_\psi(p^2). \quad (6.12)$$

Here  $d$  is the dimension of spinor space, which we set to  $d = 4$  throughout. Since (6.8), (6.10) and (6.12) are of the same form, we apply the same bilocal momentum projection for the extraction of the respective momentum dependent anomalous dimensions. This crucial procedure is discussed in more detail in the next section.

### 6.3.3. Anomalous dimensions

Each of the field species is equipped with an anomalous dimension  $\eta_{\phi_i}(p^2)$ . The latter are extracted from the flow of the respective field's two point function. In the context of heat-kernel methods, the anomalous dimensions are often referred to as 'RG improvement' [253, 254, 326, 424]. In this dissertation, they arise naturally from the truncation and we keep an approximated momentum dependence of the anomalous dimension.

The expressions (6.8), (6.10) and (6.12), together with the bilocal momentum projection lead to a coupled system of Fredholm integral equations for the anomalous dimensions  $\vec{\eta}_\phi = (\eta_h, \eta_c, \eta_\psi, \eta_\varphi)$ . It can be written as

$$\vec{\eta}_\phi(p^2) = \vec{A}(p^2, G, M^2, \Lambda_3) + \vec{B}(p^2, G, M^2, \Lambda_3)[\vec{\eta}_\phi], \quad (6.13)$$

where  $\vec{A}$  and  $\vec{B}$  are momentum-integral expressions. As the square brackets suggest,  $\vec{B}$  is a functional of  $\vec{\eta}_\phi(q^2)$ . Equation (6.13) can be solved iteratively which is, however, computationally very expensive since it is a coupled system of four equations. In order to get a handle on the solution of (6.13), we evaluate the anomalous dimension in  $\vec{B}$  at  $k^2$  and move  $\eta_\phi(k^2)$  in front of the integrals. This is a good approximation because all integrals of this type are sharply peaked around  $q = k$ . This feature arises due to the factor of  $q^3$  from the integral measure in  $d = 4$  dimensional spherical coordinates. Since  $\vec{B}$  is linear in  $\vec{\eta}_\phi$ , we can now write it as a matrix  $C$  multiplying the vector  $\vec{\eta}_\phi(k^2)$ . Hence, (6.13) simplifies to

$$\vec{\eta}_\phi(p^2) \approx \vec{A}(p^2, G, M^2, \Lambda_3) + C(p^2, G, M^2, \Lambda_3) \vec{\eta}_\phi(k^2). \quad (6.14)$$

We now evaluate the latter equation at  $p^2 = k^2$  in order to obtain an expression for  $\vec{\eta}_\phi(k^2)$ . The result  $\vec{\eta}_\phi(k^2)$  is substituted back into the momentum-dependent equation (6.14). This way, we obtain anomalous dimensions with an approximated momentum dependence. Note, that the latter approximation is considerably better than the assumption of momentum-independent anomalous dimensions, since we evaluate the functional dependence on  $\vec{\eta}_\phi$  at the peak position of the integrals. In particular, this procedure allows for a distinction of  $\vec{\eta}_\phi(k^2)$  and  $\vec{\eta}_\phi(0)$ , which is important since they both appear explicitly in the flow equations (D.1), due to the bilocal momentum projection. We show in Sec. 6.4.1 that our approximation is justified for the case without matter via comparison with the results from Chapter 3.

As an interesting fact, the scalar anomalous dimension  $\eta_\varphi(p^2)$  vanishes for the given gauge-fixing choice in the gravity sector. Generally, the scalar anomalous dimension comprises a term that is proportional to the scalar mass and one mass-independent term. The latter vanishes for the used harmonic gauge. The former term vanishes for massless scalars, which we consider here, leaving us with a vanishing scalar anomalous dimension  $\eta_\varphi(p^2) = 0$ . Note that this is only the case for the scalar anomalous dimension for the gauge fixing choice  $\beta = 1$  and  $\alpha = 0$ , for all other gauges  $\eta_\varphi(p^2)$  is not equal to zero.

### 6.3.4. Anomalous dimensions and bounds for the generic class of regulators

As part of the truncation, we choose a generic class of regulators  $R_k^\phi$ , that are proportional to the corresponding two-point function, i.e.

$$R_k^\phi(p^2) = \Gamma_k^{(\phi\phi)}(p^2) r_k^\phi(p^2) \Big|_{M^2=0}, \quad (6.15)$$

in momentum space, where  $r_k^\phi(p^2)$  is the regulator shape function. Since the effective graviton mass  $M^2$  is the only mass parameter in the present truncation the above definition implies that  $\Gamma_k^{(\phi\phi)}(p^2)|_{M^2=0}$  is either the full two-point function  $\Gamma_k^{(\phi\phi)}(p^2)$ , or, in case of the graviton field, its momentum-dependent part, i.e.  $\Gamma_{k,tt}^{(hh)}(p^2)|_{M^2=0} = (32\pi)^{-1}Z_h(p^2)p^2$ , see (6.8). This generic class covers the regulator choices in the literature, and implements the correct renormalisation group scaling of the effective action as discussed in [188, 327, 445]. It provides a RG-covariant infrared regularisation of the spectral values of the two-point function, and is hence called RG- or spectrally adjusted, [188, 445, 446]. It implies in particular, that the regulator is proportional to the corresponding field's wavefunction renormalisation via the dependence of  $R_k^\phi$  on the two-point function. Thus, the present choice leads to closed equations in terms of the anomalous dimensions. However, for large  $\eta_\phi$  the choice (6.15) leads to a peculiar RG-scaling of  $R_k^\phi$  in the UV. From the path integral point of view one expects a UV scaling with

$$\lim_{k \rightarrow \infty} R_k^\phi(p^2) \sim \lim_{k \rightarrow \infty} Z_\phi k^i \rightarrow \infty, \quad (6.16)$$

for all momenta  $p^2$ . In (6.16) we have  $i = 1$  for fermions and  $i = 2$  for all other fields. Equation (6.16) entails that the regulator diverges in the UV, and the related momentum modes in the path integral are suppressed. Since the wavefunction renormalisation behaves like  $Z_\phi \sim k^{-\eta_\phi}$  for large  $k$ , equation (6.16) is violated if the anomalous dimensions exceed the constraints

$$\eta_h < 2, \quad \eta_c < 2, \quad \eta_\varphi < 2, \quad \eta_\psi < 1. \quad (6.17)$$

Hence, if one of the bounds in (6.17) is violated, the respective regulator vanishes in the UV. In the spirit of the above path integral picture this may imply a decrease of the effective cutoff scale for the respective field, and hence a flow towards the IR. Note however, that this is far from being clear from the flow equation itself. For example, with the regulator (6.15) the transverse-traceless component of the graviton propagator is proportional to

$$\frac{1}{Z_h(p^2)} \frac{1}{(p^2(1+r_h) + M^2)}, \quad (6.18)$$

which implies a spectral, RG-covariant regularisation of the momentum modes of the full propagator, as discussed above. We conclude that if the bounds in (6.17) are exceeded, the regulator may not suppress field modes in the UV properly. Indeed, if the anomalous dimension are large enough, this does not only lead to a decreasing regulator, but also  $\partial_t R_k^\phi$  turns negative. This can be seen from the schematic expression

$$\partial_t R_k^\phi(p^2) \sim Z_\phi (\partial_t r_k^\phi(p^2) - \eta_\phi r_k^\phi(p^2)). \quad (6.19)$$

The second term in equation (6.19) exceeds the first one for  $p^2/k^2 \rightarrow 0$  exactly at the critical values given in (6.17). Still, this is not sufficient to change the sign of the respective diagrams, which involves an integration over all momenta. However, for an even larger anomalous dimensions,  $\eta_{\text{sign}} > 2$ , the sign of the respective diagrams changes. In the path integral interpretation introduced above this change of sign signals the global change from a UV-flow to an IR-flow for the respective diagram. Naturally, this bound depends on the shape function of the regulator. For the present approximation, the first diagrams

switch sign at  $\eta_{\text{sign}} = 4$ . This is already visible in the analytic, reduced, approximation derived later, see (D.1). Note also, that the sign of diagrams does not change for  $Z_h$ -independent regulators. Accordingly, for  $\eta_h > \eta_{\text{sign}}$  we have a regulator-dependence of the sign of diagrams, which has a qualitative impact on the physics under discussion. Hence, for  $\eta_h > \eta_{\text{sign}}$  the present approximation breaks down completely. In this dissertation, however, we resort to the stricter, shape-function-independent bound (6.17).

In summary, it is clear that if the bounds (6.17) are violated, additional investigations of the regulator-dependence, and hence of the reliability of the present approximation are required. Note however, that small anomalous dimensions, that obey (6.17), do by no means guarantee the convergence of the results with respect to an extension of the truncation. Such a convergence study requires the inclusion of higher order operators and detailed regulator studies and is deferred to future work.

## 6.4. Results

In this section, the results of the above presented setups are displayed. As a main result, within the validity bounds for the chosen generic class of regulators, we do not find an upper limit for the numbers of scalars and fermions that are compatible with the asymptotic safety scenario.

For the analysis we employ regulators of the type given in (6.15) and use a Litim-type shape function [372] that is,  $\sqrt{x}r(x) = (1 - \sqrt{x})\theta(1 - x)$  for fermions and  $xr(x) = (1 - x)\theta(1 - x)$  for all other fields. We close the flow equations with the identification  $\Lambda_5 = \Lambda_4 = \Lambda_3$  as well as  $G_5 = G_4 = G_3 \equiv G$ . We work with the dimensionless quantities

$$g := Gk^2, \quad \mu := M^2k^{-2}, \quad \lambda_3 := \Lambda_3k^{-2}. \quad (6.20)$$

### 6.4.1. Pure gravity

In order to study the UV behaviour of quantum gravity interacting with matter, we start from the UV fixed point of pure quantum gravity found in [Chapter 3](#) and study the deformation of this particular fixed point by the matter content. To that end, we rederive the results for the pure gravity case with the approximated momentum dependence of the anomalous dimensions discussed in [Sec. 6.3.3](#). We compare these findings with the results in [Chapter 3](#), where the full momentum dependence of the latter was considered. The fixed point values for the pure-gravity system in the present approximation read

$$(g^*, \mu^*, \lambda_3^*) = (0.62, -0.57, 0.095), \quad (6.21a)$$

with the critical exponents  $\theta_1$ ,  $\theta_2$  and  $\theta_3$  given by

$$(\theta_{1,2}, \theta_3) = (1.3 \pm 4.1i, -12). \quad (6.21b)$$

These fixed point values are in agreement with (3.30) within an error of 6% (15% for the critical exponents). This justifies the approximations described in [Sec. 6.3.3](#). The deformation of the fixed point (6.21) is calculated while successively increasing the number of scalars and fermions,  $N_s$  and  $N_f$ , respectively. This way, we analytically continue the fixed point of the pure gravity system towards a theory of quantum gravity and matter, which contains  $N_s$  scalars and  $N_f$  fermions. Although  $N_f$  and  $N_s$  are (half-)integers in the physical sense, we treat them as continuous deformation parameters for this analysis. With

this procedure we simulate the generic effect of gravity-matter interactions on gravity-theories. First, we analyse the influence of scalars and fermions separately before we briefly discuss combined system of both matter types.

#### 6.4.2. Scalars

We first consider the case  $N_f = 0$ ,  $N_s > 0$ , thus a theory of  $N_s$  scalars minimally coupled to gravity. Note again, that in the present approach, we neglect the influence of scalar self-interactions in the action (6.4). Detailed analyses of the potential impact of matter-matter couplings can be found in e.g. [121, 420, 423].

Before analysing the full numerical flow equations we try to anticipate the result from the analytic flow equations (D.1) without anomalous dimensions. For  $N_f = 0$ ,  $N_s > 0$  and  $\vec{\eta}_\phi = 0$  the latter equations read

$$\begin{aligned}\partial_t g &= +2g + \beta_{g_{\text{gravity}}} - \frac{43}{570\pi} g^2 N_s, \\ \partial_t \mu &= -2\mu + \beta_{\mu_{\text{gravity}}} + \frac{1}{12\pi} g N_s, \\ \partial_t \lambda_3 &= -2\lambda_3 + \beta_{\lambda_{3,\text{gravity}}} - \frac{1}{60\pi} \left(1 - \frac{43}{19}\lambda_3\right) g N_s.\end{aligned}\quad (6.22)$$

In this set of equation we have split the running of the dimensionless couplings into the canonical running, the contribution from graviton and ghost loops, and the contribution from scalar loops, in this ordering. In the following, we analyse whether the respective signs of the contributions potentially stabilise or destabilise the UV fixed point. A matter contribution to a given flow equation potentially destabilises the UV fixed point of the pure gravity system if it has the same sign as the canonical running. In this case, the contributions from graviton and ghost loops need to increase in to order to compensate for the matter contribution and, thus, allow for a gravity-matter fixed point. Conversely, if the canonical running and the matter contributions have the opposite sign we consider the matter contributions to potentially stabilise the fixed point. Further, we argue that the matter contribution to the running of  $\mu$  has the largest impact on the flow compared to the other equations of the system (6.22).

Using the above notion, the scalar contribution to  $\partial_t g$  potentially stabilises the fixed point, since the canonical running of  $g$  is positive and the  $N_s$ -dependent term has a negative sign. The positive sign of the  $N_s$ -term in  $\partial_t \mu$  potentially destabilises the fixed point, since we have found  $\mu^* < 0$  in the pure gravity case (see (6.21a)). Moreover, the contribution to  $\partial_t \lambda_3$  is potentially destabilising, since we consider a positive and small  $\lambda_3$  as in (6.21a). The behaviour is opposite for  $\lambda_3 > \frac{19}{43}$  and for  $\lambda_3 < 0$ .

We note that the flow equation for  $\mu$  has the largest impact on the complete system (6.22). For one, that is because  $\mu$  is the effective mass parameter of the graviton and, consequently, appears in all diagrams with graviton contributions in the loops. The second reason is that the fixed point value  $\mu^*$  for the pure gravity system is close to  $-1$ . The  $\mu$ -contributions to the flow equations generally take the form  $(1 + \mu)^{-n}$  with  $n \geq 1$ . Perturbations of  $\mu$  are therefore strongly amplified if  $\mu$  is close to  $-1$ . To see this we expand the general form of the  $\mu$ -contributions around  $-\frac{1}{2}$ , namely  $\mu = -\frac{1}{2} + \epsilon$ , which is approximately the fixed point value of the pure gravity system (see (6.21a)). The general

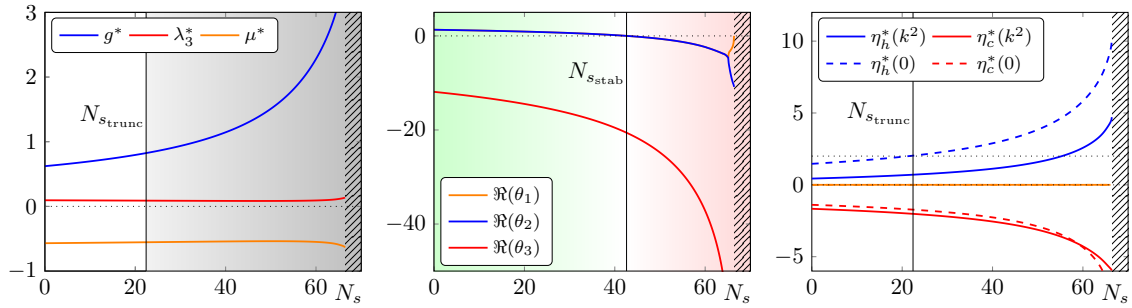


Figure 6.5.: Fixed point values (left), real parts of the critical exponents (middle), and the anomalous dimensions evaluated at  $p = k$  and  $p = 0$  (right) as functions of the number of scalars,  $N_s$ , respectively. The grey-shaded area in the left panel indicates where the regulator lies outside the reliability bounds defined in Sec. 6.3.4 due to a large graviton anomalous dimension (see right panel). The corresponding limiting number of scalars is given by  $N_{s_{\text{trunc}}}$ . The hatched regions in all three panels correspond to the  $N_s$ -regime where the UV fixed point does not exist. The green and red areas in the middle panel denote the region where the fixed point exhibits UV-attractive direction and the region where it is fully repulsive, respectively.  $N_{s_{\text{stab}}}$  is the corresponding critical number. The colours of the curves in the left panel indicate with which coupling of the left panel the corresponding eigenvector has the largest overlap. The anomalous dimension of the scalar  $\eta_\varphi$  (right panel) is zero due to the given graviton gauge.

form of the  $\mu$ -contributions is now given by

$$\frac{1}{(1+\mu)^n} = \frac{2^n}{(1+2\epsilon)^n} \approx 2^n(1-2n\epsilon), \quad (6.23)$$

which suggests that small perturbations of  $\mu$  around  $-\frac{1}{2}$  are amplified by a factor of  $2n$  compared to contributions of order one that appear linearly in the numerators. Using a Litim-type regulator we obtain terms of the latter type in  $\partial_t g$  up to  $n = 5$ . For these terms perturbations of  $\mu$  around  $-\frac{1}{2}$  are amplified by 10 compared to the linear quantities of order one. The impact of  $\mu$  on the flow (6.22) becomes even larger, the closer  $\mu$  is driven towards  $-1$ . For  $\partial_t \lambda_3$  this argument is additionally supported by the smaller scalar contribution to  $\partial_t \lambda_3$  compared to the respective contributions to  $\partial_t g$  and  $\partial_t \mu$ . This also compensates for the fact that the fixed point value in the pure gravity case is  $\lambda_3^* \approx \frac{1}{10}$  and therefore not of order one. For these reasons, the scalar contributions in the flow of  $\mu$  have the largest impact on the system (6.22).

In summary, we anticipate that the inclusion of scalar degrees of freedom potentially destabilises the UV fixed point. Hence, the gravity contributions in (6.22) must increase in order to compensate the destabilising  $N_s$ -contributions. This suggests that the couplings  $g^*$  and  $\lambda_3^*$  must increase with increasing  $N_s$ .

We now turn to the discussion of the UV fixed point for a varying number of scalars  $N_s$  in the full truncation. The left panel in Fig. 6.5 shows the fixed point values of the dynamical quantities of the system as a function of  $N_s$ . All fixed point values are continuous functions of the number of scalars in the regime  $0 \leq N_s \leq 66.4 =: N_{s_{\text{max}}}$ . Outside this regime (hatched area), the fixed point disappears, thus, spoiling asymptotic

safety of the corresponding theory. Below  $N_{s_{\max}}$ , the fixed point value of  $g$  increases with increasing  $N_s$ , as conjectured from the analytic equations (6.22). Both,  $\lambda_3^*$  and  $\mu^*$  remain almost constant, exhibiting only minor variations close to  $N_{s_{\max}}$ . The grey-shaded area in the left panel indicates where the regulator lies outside the reliability bounds defined in Sec. 6.3.4 due to a large graviton anomalous dimension. The corresponding limiting number of scalars is given by  $N_{s_{\text{trunc}}}$ .

The middle panel in Fig. 6.5 depicts the real parts of the critical exponents of the fixed point as functions of  $N_s$ . The colours of the curves are chosen such that the corresponding eigenvectors have the largest overlap with the coupling of the same colour in the left panel. All critical exponents decrease with increasing  $N_s$ . The real part of the complex conjugate pair of eigenvalues changes sign at  $N_{s_{\text{stab}}} = 42.6$ . Consequently, the green and red areas correspond to  $N_s$ -regimes where the fixed point exhibits attractive directions and regimes where it is fully UV repulsive, respectively. Furthermore, we observe that  $\theta_3$  takes large values for large  $N_s$ , which we see as further evidence for the insufficiency of the truncation in this regime [281, 282].

The right panel in Fig. 6.5 shows the anomalous dimensions of all involved fields evaluated at the fixed point and at the peak of the loop integrals,  $p^2 = k^2$ , as well as at vanishing momentum,  $p^2 = 0$ . As discussed in Sec. 6.3.3, the scalar anomalous dimension  $\eta_\varphi(p^2)$  is zero for all  $p^2$  within the chosen gravity-gauge. The graviton anomalous dimension increases with increasing  $N_s$  due to the increase of  $g^*$ . At  $N_{s_{\text{trunc}}} = 21.5$ ,  $\eta_h(0)$  exceeds the critical value of  $\eta_{h_{\text{crit}}} = 2$ , discussed in Sec. 6.3.3. Consequently, in the regime  $N_{s_{\text{trunc}}} \leq N_s \leq N_{s_{\max}}$ , the graviton anomalous dimension has exceeded the reliability bounds of the generic regulator class used here and we lose control over the suppression of graviton field modes by the regulator.

In summary, we draw the conclusion that within our truncation the inclusion of up to  $N_s \approx 21$  scalars is consistent with the asymptotic safety scenario of quantum gravity. We also find that beyond this limit, our truncation exhibits a large graviton anomalous dimension beyond the critical value defined in (6.17). This suggests that the truncation should be improved in order to draw definite conclusions about the regime  $N_s > N_{s_{\text{trunc}}}$ . Therefore, the limits  $N_{s_{\text{stab}}}$  and  $N_{s_{\max}}$  found above, should be treated with caution as they could be artefacts of the present truncation.

The  $N_s$ -dependence of the couplings shown in Fig. 6.5 is qualitatively different from that in [416, 424, 425]. This qualitative difference is also present in the fermion system discussed in the next section. A detailed comparison and evaluation of the reliability of the corresponding approximations is deferred to Sec. 6.5.

### 6.4.3. Fermions

In this section we discuss the effect of minimally coupled fermions, thus  $N_f > 0$  and  $N_s = 0$  in our notation. As before, matter-self interactions are neglected.

Again, we first analyse the generic behaviour of the system of analytic flow equations (see App. D.1) with the simplification  $\bar{\eta}_\phi = 0$ . To that end, we again divide the flow into canonical running, gravity- and ghost-loop contributions, and matter-loop terms. Consequently, the latter equations read

$$\begin{aligned}\partial_t g &= +2g + \beta_{g_{\text{gravity}}} - \frac{3599}{11400\pi} g^2 N_f, \\ \partial_t \mu &= -2\mu + \beta_{\mu_{\text{gravity}}} - \frac{8}{9\pi} g N_f,\end{aligned}$$

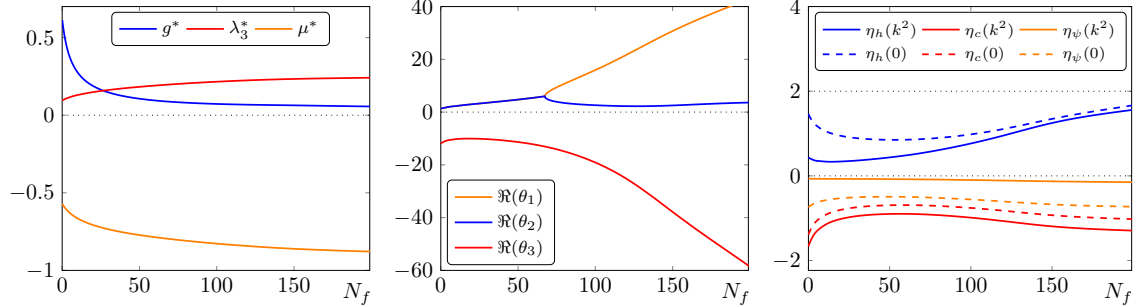


Figure 6.6.: Fixed point values (left), real parts of the critical exponents (middle), and the anomalous dimensions evaluated at  $p^2 = k^2$  and  $p^2 = 0$  (right) as functions of the number of fermions,  $N_f$ , respectively. The colours of the curves in the middle panel indicate with which coupling of the left panel the corresponding eigenvector has the largest overlap. All quantities remain well-behaved for any number of fermions. In particular, the fixed point stays attractive (middle panel) and the anomalous dimensions remain small (right panel).

$$\partial_t \lambda_3 = -2\lambda_3 + \beta_{\lambda_3, \text{gravity}} + \frac{1}{20\pi} \left( \frac{47}{7} + \frac{3599}{1140} \lambda_3 \right) g N_f. \quad (6.24)$$

Using the notion introduced in the last section, we conclude that the fermionic contributions to  $\partial_t g$  and  $\partial_t \mu$  potentially stabilise the UV fixed point since they have signs opposite to the respective canonical running. The fermionic contribution to  $\partial_t \lambda_3$ , by contrast, is potentially destabilising. As we argued in the last section, the matter contribution to  $\partial_t \mu$  is the most relevant one. Therefore, we expect that the fermion-gravity system remains stable under the increase of  $N_f$ .

We turn now to the full numerical equations with momentum dependent anomalous dimensions. The left panel in Fig. 6.6 shows the fixed point values of the dynamical quantities as functions of the number of fermions  $N_f$ . The fixed point value of  $g$  decreases with increasing  $N_f$  and approaches  $g^* \rightarrow 0$  asymptotically. At the same time,  $\mu^*$  decreases with increasing  $N_f$  and approaches  $\mu^* \rightarrow \mu_{\text{pole}} = -1$  for  $N_f \rightarrow \infty$ . The fixed point value of  $\lambda_3$  increases slightly with  $N_f$  and is driven towards an asymptotic value of  $\lambda_3^* \approx \frac{1}{4}$ . It is important to note that the crucial negative sign of the fermionic contribution to  $\partial_t \mu$ , which is the same as in the analytic equations (6.24), gives rise to an interesting stabilising effect: Since we start with a negative  $\mu^*$  for  $N_f = 0$  the negative fermionic contribution in  $\partial_t \mu$  drives  $\mu^*$  towards more negative  $\mu$  and therefore closer towards the propagator pole at  $\mu_{\text{pole}} = -1$ . This increases the contributions from graviton loops that have the opposite sign compared to the fermionic terms to  $\partial_t \mu$ . Thus, the latter contributions cancel each other and the system settles at small values of  $g^*$ .

The middle panel in Fig. 6.6 depicts the real parts of the critical exponents of the fixed point as functions of  $N_f$ . The colours are chosen such that the corresponding eigenvectors have the largest overlap with the coupling of the same colour in the left panel. The critical exponent of the repulsive direction  $\theta_3$  first increases slightly and then decreases to large values. The other two critical exponents  $\theta_{1,2}$  form a complex conjugate pair with an increasing real part until they reach  $N_f = 65.5$ . For  $N_f > 65.5$  all critical exponents are real. In this regime,  $\theta_1$  increases to larger values, while  $\theta_2$  remains almost constant. The large absolute values of the critical exponents  $\theta_1$  and  $\theta_3$  indicate, similar to the scalar case, the necessity to extend the given truncation. Large critical exponents appear in particular

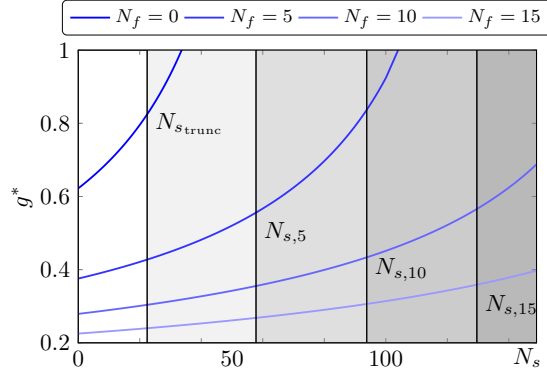


Figure 6.7.: Fixed point value  $g^*$  as a function of  $N_s$  for  $N_f = 0, 5, 10, 15$ . The vertical lines denote the numbers of scalars for which the graviton anomalous dimension exceeds its critical value in the UV, for the respective number of fermions.

for large numbers of fermions.

The right panel in [Fig. 6.6](#) shows the anomalous dimensions evaluated at the fixed point and at the momentum scales  $p^2 = 0$  and  $p^2 = k^2$ . Each anomalous dimension decreases at first and later increases slowly with increasing  $N_f$ . Nevertheless, all anomalous dimensions remain small. In particular, the graviton anomalous dimension stays below its critical value  $\eta_h < \eta_{h\text{crit}} = 2$ .

In summary, we find an attractive UV fixed point for all numbers of fermions. Thus, all numbers of fermions are compatible with the asymptotic safety scenario. We also note that, in contradistinction to the scalar case, the anomalous dimensions stay sufficiently small even for a large number of fermions. However, the appearance of large critical exponents is seen as an indicator for the necessity to improve the truncation.

As in the scalar case we find that the  $N_f$ -dependence of the couplings shown in [Fig. 6.6](#) is qualitatively different from that in [\[416, 424, 425\]](#). A detailed comparison and evaluation of the reliability of the corresponding approximations is deferred to [Sec. 6.5](#).

#### 6.4.4. Mixed scalar-fermion systems

In this section, we consider the fixed point behaviour of mixed systems of scalars and fermions. The gravity-fermion system is stable for all  $N_f$  in the present approximation. In turn, the gravity-scalar system exceeds the bounds [\(6.17\)](#) far before the fixed point first becomes unstable and finally disappears. Thus, it is interesting to study the effect of a fixed number of fermions on the  $N_s$ -regime of validity. As discussed in [Sec. 6.4.2](#), there exists a finite number of scalars  $N_{s\text{trunc}}$  for which  $\eta_h$  exceeds its critical value. In [Sec. 6.4.3](#) we observed that the inclusion of fermions leads to a decrease of  $g^*$ , which results in smaller anomalous dimensions. Therefore, we expect that the  $N_s$ -regime of validity is extended if we increase  $N_f$ .

In [Fig. 6.7](#) the fixed point value  $g^*$  is plotted as a function of  $N_s$  for different numbers of  $N_f$ . The vertical lines denote the numbers of scalars for which the graviton anomalous dimension exceeds its critical value in the UV. As displayed in the figure, the expected behaviour for the combined systems is indeed realised. Thus, the increase of  $N_f$  lowers the fixed point value  $g^*$  and extends the  $N_s$ -regime of validity. For  $N_f = 0, 5, 10$  and  $15$  the corresponding critical values  $N_{s\text{trunc}}, N_{s,5}, N_{s,10}$  and  $N_{s,15}$  are given by  $21.5, 57.9, 93.8$

and 129.6, respectively. The maximum number of scalars that defines the validity of the truncation increases almost linearly with  $N_f$ . Thus, every additional fermion stabilises the combined system such that  $\approx 7.1$  additional scalars are admitted. The ratio between these numbers suggests that fermions have a significantly stronger impact on the system than scalars. This is true for the complete truncation analysed here and can also be verified in the analytic equations by comparing the numerical values of the respective contributions (compare (6.22) and (6.24)). This imbalance between scalars and fermions was also observed in [424]. The increase of  $N_f$  also shifts the values of  $N_{s_{\text{sign}}}$  and  $N_{s_{\text{max}}}$  to larger values and extends the  $N_s$ -regime where a fixed point is found considerably. In summary, the inclusion of fermions stabilises the system and extends the  $N_s$ -regime of validity for the given truncation significantly.

#### 6.4.5. Independence on the approximation in the gravity sector

We close this section with a brief discussion of the impact of the approximation in the pure gravity sector on our results. Interestingly, the results agree qualitatively for all approximations in the pure gravity sector used in the literature. This includes the standard ones in the background field approximation which are discussed in the next section. We also note that the fixed point for our truncated system is also present, if all anomalous dimension are set to zero. It is interesting to note, however, that for  $N_s > 0$ ,  $N_f = 0$  the fixed point vanishes already for  $N_s \approx 45$  and therefore earlier than with anomalous dimensions. Thus, the anomalous dimensions stabilise the UV-behaviour of the system.

In order to combine the present matter contributions with the pure gravity systems in the geometrical framework [336], and with [327], we have to identify  $\lambda_3 = \lambda_2 \equiv -\mu/2$ . We find that the matter-contributions admit UV fixed points. Furthermore, we observe the same generic effect of scalars and fermions on the UV fixed point that was found for the present truncation. Hence, scalars drive the fixed point to larger values of  $g^*$ , while fermions lead to a decrease of  $g^*$  and  $\mu^*$ , where  $\mu^*$  approaches  $-1$ . In summary, our qualitative results are insensitive to the approximation in the pure gravity sector.

## 6.5. Background couplings and background field approximation

It is left to study the stability of the results under a change of the approximation scheme in the matter sector. This is even more important as the  $N_s$ - and  $N_f$ -dependencies of the couplings shown in Fig. 6.5 and Fig. 6.6 are qualitatively different from those in [416, 424, 425]. The latter works use the background field approximation for the computation of the flows for the couplings, which are augmented with dynamical anomalous dimensions in [424, 425]. Hence, we compare the present system of dynamical couplings with the standard flows in the background field approximation.

In perturbatively renormalisable quantum field theories, like the Standard Model, the gauge invariant background couplings in the limit  $k \rightarrow 0$  directly enter  $S$ -matrix computations. For  $k \rightarrow 0$  the regulator, which typically depends on the background field, vanishes. For these reasons, these couplings are observables of the theory. In direct analogy, we call the diffeomorphism-invariant background couplings of quantum gravity also observables in the limit  $k \rightarrow 0$ . Note that these quantities have a clear physical interpretation only in the limit  $k \rightarrow 0$ . For  $k > 0$ , on the other hand, the background couplings depend inherently on the background-field content via the non-vanishing regulator. In this case,

the couplings lose their clear physical meaning and their relation to observable quantities becomes unclear.

In this section we use the notation  $(g, \lambda_2, \lambda_3)$  for the dynamical couplings, where we reintroduced  $\lambda_2 = -1/2\mu$ . We also give a brief summary of the discussion in [188, 336, 337, 347, 352, 355, 356, 376, 447] on dynamical and background flows and the impact on the background field approximation: Standard approaches based on diffeomorphism invariant truncations use the background-field formalism for the definition of the truncated effective action. The corresponding flow equation, however, is not closed since it depends on the dynamical propagator. This is expressed schematically as

$$\partial_t \Gamma_k[\bar{g}, h] = F \left[ \frac{\delta^2 \Gamma_k[\bar{g}, h]}{\delta h^2}; \bar{g} \right], \quad (6.25)$$

where the separate dependence on  $\bar{g}$  stems from the regulator. In order to close (6.25) the background-field approach amounts to the identification of the propagators of fluctuating and background-fields, i.e.,

$$\frac{\delta^2 \Gamma_k[\bar{g}, h]}{\delta h^2} \approx \frac{\delta^2 \Gamma_k[\bar{g}, h]}{\delta \bar{g}^2}. \quad (6.26)$$

The latter identification is known to pose severe problems in QCD, for more details see [327, 376]. However, at least for pure quantum gravity the approximation (6.26) seems to work rather well, leading to a reliable UV-behaviour of the theory. In the more elaborate geometrical-effective action approach [448, 449], the differences between fluctuating and background propagators are encoded in the (modified) Nielsen-Identities [188, 347]. In [336] the latter identities together with a minimally consistent extension to the Einstein-Hilbert truncation were used to derive flow equations for the dynamical couplings  $(g, \lambda)$  and the background couplings  $(\bar{g}, \bar{\lambda})$  in the absence of matter. In the geometrical approach the flow equations for the background couplings read schematically

$$\partial_t \left( \frac{k^2}{\bar{g}} \right) = F_{R^1}(g, \lambda; N_s, N_f), \quad \partial_t \left( \frac{\bar{\lambda} k^4}{\bar{g}} \right) = F_{R^0}(g, \lambda; N_s, N_f), \quad (6.27)$$

for a theory with  $N_s$  scalars and  $N_f$  fermions. Note, that the right hand side of the latter equation only contains dynamical couplings. The dimensionful functions  $F_{R^1}$  and  $F_{R^0}$  correspond to the  $R^1$  and  $R^0$ -terms of the required heat-kernel expansion, respectively. With the identification of background and dynamical couplings  $(g, \lambda) = (\bar{g}, \bar{\lambda})$ , one retains the background-field approximation from the geometrical approach. Applying the derivatives in (6.27) leads us to

$$\frac{1}{\bar{g}} \left( 2 - \frac{\partial_t \bar{g}}{\bar{g}} \right) = f_{R^1}(g, \lambda; N_s, N_f), \quad \frac{\bar{\lambda}}{\bar{g}} \left( 4 + \frac{\partial_t \bar{\lambda}}{\bar{\lambda}} - \frac{\partial_t \bar{g}}{\bar{g}} \right) = f_{R^0}(g, \lambda; N_s, N_f), \quad (6.28)$$

where  $f_{R^i} := F_{R^i} k^{2(i-2)}$  is dimensionless. The equations (6.28) are now used to compare our flows for the dynamical couplings  $(g, \lambda_2, \lambda_3)$  with the standard background-field flows. Since both the standard background-field approximation and the geometrical effective action approach are based on diffeomorphism invariant truncations, they do not distinguish between the couplings of different-order graviton vertices. Hence, for the present analysis we set  $\lambda_3 \equiv \lambda_2$  and identify the remaining couplings  $(g, \lambda_2)$  with the running dynamical gravitational coupling and the dynamical cosmological constant in the geometrical

approach,  $(g, \lambda) = (g, \lambda_2)$ . We extract the expressions for  $f_{R^1}$  and  $f_{R^0}$  from the flow equations in [274, 424] reversing the identification of background and dynamical couplings. Explicit expressions for  $f_{R^i}$  are given in App. D.2.

In order to determine the fixed points of the flows (6.28), we set  $\partial_t \bar{g} = \partial_t \bar{\lambda} = 0$  and evaluate  $f_{R^i}$  at our fixed point values for the dynamical couplings,  $(g^*, \lambda_2^*)$ . This way, we arrive at simple fixed point equations for the background couplings, to wit

$$\bar{g}^* = \frac{2}{f_{R^1}(g^*, \lambda_2^*; N_s, N_f)}, \quad \bar{\lambda}^* = \frac{f_{R^0}(g^*, \lambda_2^*; N_s, N_f)}{2f_{R^1}(g^*, \lambda_2^*; N_s, N_f)}. \quad (6.29)$$

The fixed points provided by the latter equations are compared to the results from flows in the standard background-field approximation [274, 424].

First of all, we note that the matter-terms in the flows of the dynamical couplings  $(g, \lambda_2)$  have opposite signs relative to the respective contributions to the flows of background couplings. This can be seen most easily in the analytic equations with  $\vec{\eta}_\phi = 0$  where the matter contributions to  $(g, \lambda_2)$  can be written as

$$\partial_t g \sim -\frac{43}{570\pi} g^2 N_s - \frac{3599}{11400\pi} g^2 N_f, \quad \partial_t \lambda_2 \sim -\frac{1}{24\pi} g N_s + \frac{4}{9\pi} g N_f. \quad (6.30)$$

In [274, 424] the contributions to the flows of the background couplings  $\bar{g}$  and  $\bar{\lambda}$  read

$$\partial_t \bar{g} \sim +\frac{1}{6\pi} \bar{g}^2 N_s + \frac{1}{3\pi} \bar{g}^2 N_f, \quad \partial_t \bar{\lambda} \sim +\frac{1}{12\pi} (3 + 2\bar{\lambda}) \bar{g} N_s - \frac{1}{3\pi} (3 - \bar{\lambda}) \bar{g} N_f. \quad (6.31)$$

For  $\bar{\lambda} < 3$  every single term in (6.30) and (6.31) carries the respective opposite sign.

Still, the signs of the matter contributions for the background flows are trivially the same. Accordingly, we expect the explicit  $N_s, N_f$  scalings in the flows of the background couplings to dominate the qualitative behaviour of the background fixed points. The implicit dependence of the fixed points  $(g^*, \lambda_2^*)$  on  $N_s, N_f$  is expected to be sub-leading, resulting in a similar behaviour of the fixed points of our background quantities and those from studies in background-field approximation.

### 6.5.1. Background fixed points in the full system

The left panel in Fig. 6.8 shows the fixed point for the dynamical quantities  $(g, \lambda_2)$  (solid lines) and that of their corresponding background counterparts  $(\bar{g}, \bar{\lambda})$  (dashed lines) calculated from (6.29) as a function of  $N_s$ . The fixed point values of the background couplings have similar values compare to the fixed points for the dynamical couplings at  $N_s = 0$ . However, both quantities evolve very differently under the inclusion of scalars. In particular,  $\bar{g}$  and  $\bar{\lambda}$  increase quickly with increasing  $N_s$ . At  $N_{s_{\text{pole}}} = 25.8$ ,  $\bar{\lambda}$  crosses the propagator pole, which is impossible in the background-field approximation. Here, however, we do not identify background and dynamical couplings, i.e.  $\bar{\lambda} \neq \lambda_2$ , and in consequence crossing of the pole does not pose a problem. The background couplings diverge for  $N_s = 60.8$ , resulting in an invalid fixed point for  $N_s > 60.8$  (dotted area). The latter divergence, however, is *not* present for the dynamical couplings. It merely results from the fact, that  $f_{R^1}$  becomes zero at this point, leading to divergent expressions for  $(\bar{g}, \bar{\lambda})$  in (6.29). Consequently, the fixed point for the background couplings does in fact exist beyond  $N_s = 60.8$  until the dynamical fixed point is lost (hatched area). Since  $f_{R^1}$  has, however, changed sign in this regime  $\bar{g}^*$  is negative and, therefore, clearly unphysical.

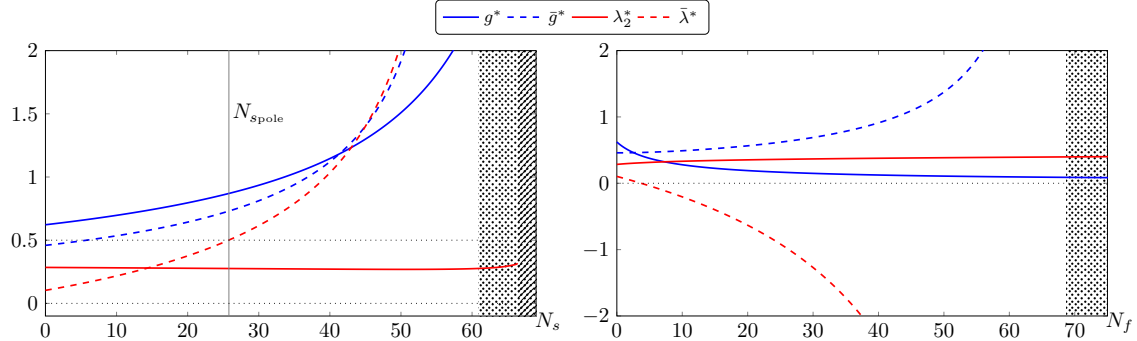


Figure 6.8.: Fixed point values of the dynamical couplings  $(g, \lambda_2)$  (solid lines) in comparison with their corresponding background counterparts  $(\bar{g}, \bar{\lambda})$  (dashed lines) as functions of the number of scalars  $N_s$  (left panel) and the number of fermions  $N_f$  (right panel). The fixed point values of the background couplings diverge for  $N_s = 60.8$  (left panel) and  $N_f = 68.6$  (right panel). The dotted regions denote the regimes beyond the latter divergences.  $N_{s\text{pole}}$  denotes the number of scalars at which  $\bar{\lambda}$  would run into the propagator pole, if the identification  $\lambda_2 = \bar{\lambda}$ , common in the background approximation, is applied.

The right panel in Fig. 6.8 compares the fixed points for the dynamical couplings and the background couplings as a function of  $N_f$ . Starting at similar values at  $N_f = 0$ , the fixed point for the background couplings again exhibits a very different behaviour from that of the corresponding dynamical fixed points under the inclusion of fermions. While  $g^*$  decreases with increasing  $N_f$ ,  $\bar{g}$  increases strongly. Similarly,  $\bar{\lambda}^*$  is quickly driven to large negative values, changing sign at  $N_f = 3.7$ , whereas the dynamical  $\lambda_2^*$  remains almost constant. The fixed point for the background quantities diverges for  $N_f = 68.6$ . The dotted region denotes the regime where the background fixed point is invalid. Again, the divergence appears only for the background quantities. The dynamical couplings remain well behaved for all  $N_f$ .

In summary, the fixed points for the background couplings behave very differently from their dynamical counterparts under the inclusion of matter fields. In particular, the latter exhibit divergences which are not present for the dynamical couplings. The dynamical couplings calculated in this chapter are the ones which are relevant for probing the consistency of gravity as a quantum field theory in the UV. Thus, the above analysis suggests that divergences or the disappearance of fixed points for the background couplings do not reflect actual divergences of the dynamical couplings. It is therefore indispensable, to distinguish between background and dynamical couplings in order to study the UV behaviour of quantum gravity, once matter fields are included.

### 6.5.2. Comparison to background fixed points in the literature

We now compare the fixed points for the background quantities, that we obtained from the equations (6.29), with the ones obtained from a background-field approximation as reported in [424]. In our analysis, we disregard the use of different regulators in the different approaches. Hence, we assume that the generic behaviour of the approaches is independent of this choice.

The left panel in Fig. 6.9 depicts fixed points for background couplings as functions

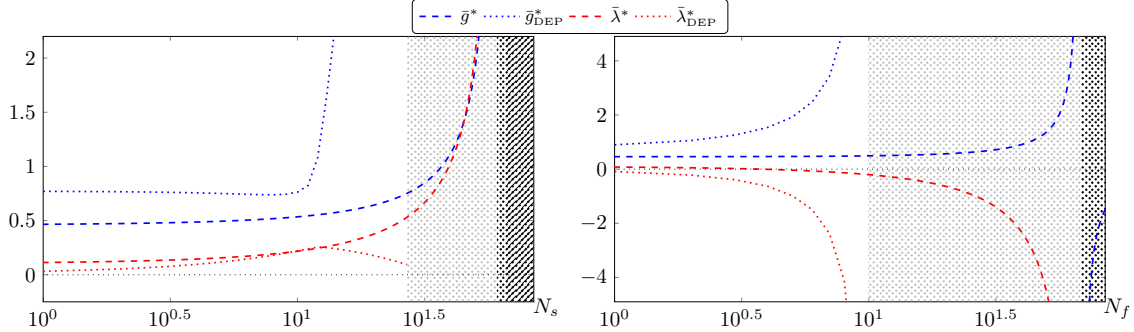


Figure 6.9.: Logarithmic plot of the fixed point values of the background field couplings  $(\bar{g}, \bar{\lambda})$  as a function of the number of scalars  $N_s$  (left) and as a function of the number of fermions  $N_f$  (right) in comparison with results in background-field approximation from [424] (DEP). Our background couplings behave very similarly to the couplings in [424]. The grey and black-shaded area denote the regimes, where the fixed point for the couplings in [424] and for our couplings is lost, respectively.

of  $N_s$ . The dotted curves represent fixed points of flows determined in background-field approximation in [424] (DEP) and the dashed curves denote our background couplings, which are calculated from the dynamical couplings (identical to the respective curves in Fig.6.8). The fixed point value for the gravitational coupling  $\bar{g}_{\text{DEP}}^*$  increases with increasing  $N_s$  and eventually diverges at  $N_s \approx 27$ . For  $N_s > 27$  no UV fixed point exists, which is indicated by the grey dotted area in the plot. Note, that due to the identification of background and dynamical couplings the graviton-propagator pole is located at  $\bar{\lambda} = 0.5$ . This limit cannot be intersected by  $\bar{\lambda}_{\text{DEP}}^*$ . In consequence,  $\bar{\lambda}_{\text{DEP}}^*$  first increases but exhibits a characteristic kink at  $N_s \approx 16$  and then decreases again until the fixed point ceases to exist at  $N_s \approx 27$ .

For small numbers of  $N_s$ , the fixed points from the background-field approximation  $(\bar{g}_{\text{DEP}}^*, \bar{\lambda}_{\text{DEP}}^*)$  show a behaviour, which is similar to that of our background couplings  $(\bar{g}^*, \bar{\lambda}^*)$ . For larger values of  $N_s$  the value of  $\bar{\lambda}_{\text{DEP}}^*$  is driven closer to the propagator pole and the flow equations receive growing contributions from the graviton loops, which is not the case for our background couplings. Here, the implicit dependence of the fixed point on  $N_s$  is large and we observe large deviations between our background couplings and those in [424] in the regime  $N_s \gtrsim 10$ .

The right panel in Fig.6.9 depicts the fixed points for background couplings as functions of  $N_f$ . The notation for the curves in the right panel is the same as in the left one described above. The fixed point value  $\bar{g}_{\text{DEP}}^*$  strongly increases with increasing  $N_f$  and runs into a divergence for  $N_f \approx 10$ . For  $N_f > 10$  the fixed point does not exist anymore, which is indicated by the grey dotted area in the plot. The value for  $\bar{\lambda}_{\text{DEP}}^*$  starts at small negative values and decreases quickly with increasing  $N_f$  until the fixed point ceases to exist at  $N_f \approx 10$ .

For small numbers of  $N_f$ , our background couplings  $(\bar{g}^*, \bar{\lambda}^*)$  show again a similar behaviour to the fixed points in the background-field approximation. For larger  $N_f$ , we observe large deviations, though the generic behaviour of the fixed points is the same. An important common feature is the existence of a singularity for the fixed point for a finite number of fermions. As discussed in the previous section, this divergence has no influence

on the asymptotic safety of the theory since it is clearly independent from the physical dynamical couplings. Again, the divergence of the background fixed point is due to the fact that  $f_{R^1}$  in (6.29) passes zero. Beyond this divergence the background fixed point still exists but has changed sign. This can be observed for  $\bar{g}^*$  in the lower right corner of the right panel of Fig. 6.9.

In summary, for sufficiently small  $N_f, N_s \lesssim 10$  the couplings in the background-field approximation (DEP) behave similarly to the background-field couplings of the full dynamical system computed here. Note, that both computations show divergences in the background coupling for a finite number of scalars and fermions. These divergences are not reflected in the dynamical couplings and the current analysis strongly suggests their absence at  $k = 0$ . We conclude that the background-field approximation provides an adequate qualitative picture of the behaviour of the physical background couplings for  $N_f, N_s \lesssim 10$ . The relevant quantities for studies of the UV behaviour of quantum gravity are, however, the dynamical couplings. In turn, for  $N_f, N_s \gtrsim 10$  the background field approximation fails, and it is necessary to compute dynamical flows and couplings.

## 6.6. Summary

We have presented the first genuine calculation of dynamical gravitational couplings based on a vertex flow in gravity-matter systems with an arbitrary number of scalars and fermions. We have calculated the matter contributions to the dynamical graviton two- and three-point functions and included momentum-dependent gravity and matter anomalous dimensions. The UV behaviour of the resulting theory has been analysed under the influence of  $N_s$  scalars and  $N_f$  fermions.

In the scalar sector the increase of  $N_s$  leads to an increasing Newton's coupling at the UV fixed point and thus to a strengthening of graviton fluctuations at high energies. For large numbers of scalars  $N_s > 21.5$  the present generic class of regulators violates the bounds (6.17) due to a large graviton anomalous dimension, i.e.  $\eta_h > 2$  in this regime. Deep in this regime the UV fixed point first becomes repulsive and finally is lost, which requires further investigation.

In the fermion sector the UV fixed point exists and is stable for all  $N_f$ . Also, all fixed point values remain small, and the anomalous dimensions stay below the bounds (6.17), i.e.  $\eta_h, \eta_c, \eta_\varphi < 2$  and  $\eta_\psi < 1$ , for all  $N_f$ . Similar to the scalar case the increase of  $N_f$  enhances graviton fluctuations. Here however, the enhancement is due to the shift of the graviton-mass parameter towards the propagator pole.

In summary, we always find an attractive UV fixed point in the presence of a general number of scalars and fermions within the validity bounds for the generic class of regulators used here. Finally we have discussed and embedded previous results in the literature within our extended setting. In particular we have also compared the present results within the full dynamical system to results that partially rely on the background field approximation. Interestingly, we find the signs of the matter contributions to the flows of our dynamical couplings to be opposite to those of flows in background-field approximation. This is in sharp contrast to the pure gravity flows whose signs agree in all approximations. We have also computed the fixed points of the background couplings in the present approach. We have shown that the latter agree qualitatively with the fixed point couplings in the background-field approximation for  $N_f, N_s \lesssim 10$ . In turn, for  $N_f, N_s \gtrsim 10$  the background field approximation fails, and it is necessary to compute dynamical flows and couplings.

## 7. UV dominance of gravity over matter fluctuations

### 7.1. Introduction

In the last chapter we have started to couple Standard Model matter content to asymptotically safe quantum gravity. We found in the scalar sector inconclusive results on how many scalar fields are compatible with asymptotic safety and further saw qualitative differences between results with and without background field approximation. We now turn to Yang-Mills theories coupled to quantum gravity. The impact of quantised gravity on gauge theories has already been investigated within perturbation theory [450–455] by treating gravity as an effective field theory [456], and within the asymptotic safety scenario [376, 419, 457]. Modulo gauge and scheme dependences, all studies find the same negative sign for the Yang-Mills beta function ( $\beta < 0$ ) in support of asymptotic freedom. The reason for this was uncovered in [376, 457]: Due to an important kinematical identity, related to diffeomorphism- and gauge invariance,  $\beta < 0$  follows automatically, and irrespective of the gauge or regularisation. We will comment on this in more detail later in this chapter.

In this chapter we want to understand the prospect for asymptotic safety of quantum gravity coupled to matter. To that end, we combine general, formal considerations with detailed and explicit studies in the framework of the systematic vertex expansion of the functional renormalisation group. A main new addition is a formal line of reasoning, which explains why and how gravitons dominate the high-energy behaviour, largely independently of the matter fields as long as these remain sufficiently weakly coupled. This argument is based on successively integrating out first the matter fields and then gravity, which is well controlled due to the weak coupling of the matter fields. The argument fully applies in the absence of marginal couplings, and covers the results in the literature. However, the marginal couplings, being related to  $R^2$  and  $R_{\mu\nu}^2$ , play a special rôle as they carry the only direct dependence on the number of matter fields. This number of matter field is henceforth called flavour in a slight abuse of notation.

For the explicit computation we work on the example of  $SU(N_c)$  Yang-Mills-theory coupled to gravity. In an expansion about a flat Euclidean backgrounds, explicit results for beta functions, fixed points, universal exponents, and scaling solutions are given. Systematic approximations exploiting running propagators, the three-graviton- and the graviton-gauge-vertices are performed up to including independent couplings for gauge-gravity and pure gravity interactions, and for the background couplings. Care is taken to distinguish fluctuating and background fields. Invariably, we find that the gauge coupling becomes asymptotically free while the gravitational sector becomes asymptotically safe. The dependence on matter field multiplicities is weak. We also investigate the scheme dependence, which is found to more pronounced, and explain how it can be handled without changing the physics. This allows us to offer a new interpretation of many earlier results and to lift some of the tensions amongst previous findings.

## 7.2. From asymptotic freedom to asymptotic safety

In this section, we provide our main line of reasoning for why matter fields, which are free or sufficiently weakly coupled in the UV – such as in asymptotic freedom – entail asymptotic safety in the full theory including gravity. Throughout, Yang-Mills theory serves as the principle example.

### 7.2.1. Yang-Mills coupled to gravity: the setup

Any correlation function computation to gravity works within an expansion of the theory about some generic metric. The necessity of gauge fixing forces the introduction a background metric into the approach. Hence, we use a background field approach in the gauge sector, giving us a setting with a combined background  $\bar{g}_{\mu\nu}$  and  $\bar{A}_\mu^a$ . Background independence is then ensured with the help of Nielsen or split Ward identities and the accompanying Slavnov-Taylor identities (STIs) for both the metric fluctuations and the gauge field fluctuations. The superfield  $\phi$  comprises all fluctuations or quantum fields with

$$A_\mu = \bar{A}_\mu + a_\mu, \quad g_{\mu\nu} = \bar{g}_{\mu\nu} + \sqrt{G} h_{\mu\nu}, \quad \phi = (h_{\mu\nu}, c_\mu, \bar{c}_\mu, a_\mu, c, \bar{c}), \quad (7.1)$$

with the dynamical fluctuation graviton  $h_{\mu\nu}$  and gauge field  $a_\mu$ . In (7.1),  $c_\mu$  and  $c$  are the gravity and Yang-Mills ghosts, respectively. Note that throughout this chapter we use a slightly different notation for the split of the metric. We now explicitly display the prefactor  $\sqrt{G}$  in front of the fluctuation field  $h_{\mu\nu}$ . In the previous and in the next chapters we included this prefactor via the vertex dressing, see (3.16). The notation here puts more emphasis on the fact that the fluctuation field has the mass dimension one.

The classical Euclidean action of the Yang-Mills–gravity system is given by the sum of the gauge-fixed Yang-Mills and Einstein-Hilbert actions,

$$S_{\text{cl}}[\bar{g}, \bar{A}; \phi] = S_{\text{gauge}}[\bar{g}, \bar{A}; \phi] + S_{\text{gravity}}[\bar{g}, \bar{A}; \phi], \quad (7.2)$$

where the two terms  $S_{\text{gauge}} = S_A + S_{A,\text{gf}} + S_{A,\text{gh}}$  and  $S_{\text{gravity}} = S_{\text{EH}} + S_{g,\text{gf}} + S_{g,\text{gh}}$  are the fully gauge fixed actions of Yang-Mills theory and gravity respectively. The Yang-Mills action reads

$$S_A[g, A] = \frac{1}{2} \int d^4x \sqrt{g} g^{\mu\mu'} g^{\nu\nu'} \text{tr} F_{\mu'\nu'} F_{\mu\nu}, \quad (7.3)$$

where the trace in (7.3) is taken in the fundamental representation, and

$$F_{\mu\nu} = \frac{i}{g_s} [D_\mu, D_\nu], \quad D_\mu = \partial_\mu - i g_s A_\mu, \quad \text{tr} t^a t^b = \frac{1}{2}. \quad (7.4)$$

The classical Yang-Mills action (7.3) only depends on the full fields  $g_{\mu\nu}$  and  $A_\mu$  and induces gauge-field–graviton interactions via the determinant of the metric as well as the Lorentz contractions and derivatives. The gauge fixing is done in the background Lorentz gauge  $\bar{D}_\mu a_\mu = 0$  with  $\bar{D} = D_\mu(\bar{A})$ . The gauge fixing and ghost terms read

$$S_{A,\text{gf}} = \frac{1}{2\xi} \int d^4x \sqrt{\bar{g}} (\bar{g}^{\mu\nu} \bar{D}_\mu a_\nu)^2, \quad S_{A,\text{gh}} = \int d^4x \sqrt{\bar{g}} \bar{g}^{\mu\nu} \bar{c} \bar{D}_\mu D_\nu c, \quad (7.5)$$

where we take the limit  $\xi \rightarrow 0$ . The gauge fixing and ghost terms only depend on the background metric and hence do not couple to the dynamical graviton  $h_{\mu\nu}$ . The gauge-fixed Einstein-Hilbert action is identical to Sec. 3.3.

### 7.2.2. Asymptotic freedom in Yang-Mills with gravity

Gauge theories with gauge group  $U(N)$  or  $SU(N)$  describe the electroweak and the strong interactions, and form the basis of the Standard Model of particle physics. A striking feature of non-Abelian gauge theories is asymptotic freedom, meaning that the theory is governed by a Gaussian fixed point in the UV, which implies that gluon interactions weaken for high energies and that perturbation theory is applicable. In fact, the great success of the Standard Model is possible only due to the presence of such a Gaussian fixed point, which allows us to neglect higher order operators in the high energy limit. The weakening of interactions is encoded in the energy dependence of the Yang-Mills coupling, which in turn is signalled by a strictly negative sign of the beta function. However, it is well known that fermions contribute with a positive sign to the running of the Yang-Mills coupling,

$$\frac{\beta_{\alpha_s}^{\text{1-loop}}}{\alpha_s^2} \equiv \mu \frac{\partial \alpha_s}{\partial \mu} \frac{1}{\alpha_s^2} = -\frac{1}{4\pi} \left( \frac{22}{3} N_c - \frac{4}{3} N_f \right), \quad (7.6)$$

where we have displayed only the one-loop contributions with  $N_c$  and  $N_f$  denoting the number of colours and fermion flavours, and  $\alpha_s = g_s^2/(4\pi)$ . One can see that there is a critical number of fermion flavours  $N_f^{\text{crit}} = \frac{11}{2} N_c$  above which the one-loop beta function changes sign. This implies that asymptotic freedom is lost. It has been noted recently that gauge theories with matter and without gravity may very well become asymptotically safe in their own right [146, 147, 458–461].

Returning to gravity, it has been shown in [376, 419, 450–455, 457] that graviton fluctuations lead to an additional negative term  $\beta_{\alpha_s,h}$  in  $\beta_{\alpha_s} \rightarrow \beta_{\alpha_s,a} + \beta_{\alpha_s,h}$  where  $\beta_{\alpha_s,a}$  is the pure gauge theory contribution (7.6). The graviton contribution has a negative sign,

$$\beta_{\alpha_s,h} \leq 0. \quad (7.7)$$

Due to the lack of perturbative renormalisability this term is gauge- and regularisation-dependent. However, it has been shown that it is always negative semi-definite, [376, 457], based on a kinematic identity related to diffeomorphism invariance. Hence, asymptotic freedom in Yang-Mills theories is assisted by graviton fluctuations. In the case of  $U(1)$  they even trigger it. This result allows us to already get some insight into the coupled Yang-Mills–gravity system within a semi-analytic consideration in an effective theory spirit: In this chapter we consider coupled Yang-Mills–gravity systems within an expansion of the pure gravity part in powers of the curvature scalar as well as taking into account the momentum dependence of correlation functions. In the Yang-Mills sub-sector we consider an expansion in  $\text{tr } F^n$  and  $(\text{tr } F^2)^n$ , the lowest non-classical terms being

$$w_2 (\text{tr } F^2)^2, \quad v_4 \text{tr } F^4. \quad (7.8)$$

Asymptotic freedom allows us to first integrate out the gauge field. This sub-system is well-described by integrating out the gauge field in a saddle point expansion within a one-loop approximation. Higher-loop orders are suppressed by higher powers in the asymptotically free gauge-coupling. This leads us to the effective action

$$\Gamma[\bar{g}, \bar{A}, \phi] = S_{\text{gravity}}[\bar{g}; \phi] + S_{\text{gauge}}[\bar{g}, \bar{A}; \phi] - \frac{1}{2} \text{Tr} \ln \left[ \Delta_1 \delta_{\mu\nu} + \left( 1 - \frac{1}{\xi} \right) \nabla_\mu \nabla_\nu \right]_{k_a^{\text{IR}}}^{k_a^{\text{UV}}}, \quad (7.9)$$

where  $\Delta_1$  represents the spin-one Laplacian and  $k_a^{\text{IR}}, k_a^{\text{UV}}$  indicate diffeomorphism preserving IR and UV regularisations of the one-loop determinant. Most conveniently this is

achieved by a proper-time regularisation, for a comprehensive analysis within the FRG framework see [356, 462]. In any case both regularisations depend on the metric  $g_{\mu\nu}$  and the respective scales  $k_a^{\text{IR}}, k_a^{\text{UV}}$ . The computation can be performed with standard heat-kernel methods.

The IR sector of the theory is not relevant for the present discussion of the fate of asymptotic safety in the UV. Note also that Yang-Mills theory exhibits an IR mass gap with the scale  $\Lambda_{\text{QCD}}$  due to its confining dynamics. In covariant gauges as used in the present dissertation this mass gap results in a mass gap in the gluon propagator, for a treatment within the current FRG-approach see [368, 463] and references therein. This dynamical gaping may be simulated by simply identifying the IR cutoff scale with  $\Lambda_{\text{QCD}}$ .

Moreover, even though integrating out the gauge field generates higher order terms such as (7.8) in the UV, they are suppressed by both, powers of the UV cutoff scale as well as the asymptotically free coupling. Accordingly, we drop the higher terms in the expansion of the Yang-Mills part of the effective action (7.9). Note that they are present in the full system as they are also generated by integrating-out the graviton. This is discussed below.

It is left to discuss the pure gravity terms that are generated by UV gluon fluctuations in (7.9). They can be expanded in powers and inverse powers of the UV-cutoff scale  $k_a = k_a^{\text{UV}}$ . This gives an expansion in powers of the Ricci scalar  $R$  and higher order invariants. From the second line of (7.9) we are led to

$$(N_c^2 - 1) \left[ c_{g,a} k_a^2 \int d^4x \sqrt{g} (2c_{\lambda,a} k_a^2 - R) + c_{R^2,a} \int d^4x \sqrt{g} (R^2 + z_a R_{\mu\nu}^2) \ln \frac{R + k_a^{\text{IR}}}{k_a^2} \right] + \mathcal{O}\left(\frac{R^3}{k_a^2}\right), \quad (7.10)$$

where we suppressed potential dependences on  $\Delta_g$  and  $\nabla_\mu$ , in particular in the logarithmic terms. The logarithm also could contain further curvature invariants such as  $R_{\mu\nu}^2$ . In the spirit of the discussion of the confining IR physics we may substitute  $k_a^{\text{IR}} \rightarrow \Lambda_{\text{QCD}}$  in a full non-perturbative analysis. In (7.10) the coefficients  $c_{g,a}, c_{\lambda,a}, c_{R^2,a}$  and  $z_a$  are regularisation-dependent and lead to contributions to Newton's coupling, the cosmological constant, as well as generating an  $R^2$ -term and potentially an  $R_{\mu\nu}^2$  term. In the present Yang-Mills case  $c_{g,a}$  is positive for all regulators. For fermions and scalars the respective coefficients  $c_{g,\psi}, c_{g,\phi}$  are negative. In summary this leaves us with an asymptotically free Yang-Mills action coupled to gravity with redefined couplings

$$G_{\text{eff}} = \frac{G}{1 + (N_c^2 - 1)c_{g,a} k_a^2 G}, \quad \frac{\Lambda_{\text{eff}}}{G_{\text{eff}}} = \frac{\Lambda}{G} + (N_c^2 - 1)c_{g,a} c_{\lambda,a} k_a^4. \quad (7.11)$$

The coupling parameters  $G$  and  $\Lambda$  should be seen as bare couplings of the Yang-Mills-gravity system and chosen such, that the (renormalised) couplings  $G_{\text{eff}}$  and  $\Lambda_{\text{eff}}$  are  $k_a$ -independent. This corresponds to a standard renormalisation procedure (introducing the standard RG scale  $\mu_{\text{RG}}$ ) and leads to  $G(N_c, k_a)$  and  $\Lambda(N_c, k_a)$ . Note that demanding  $k_a$ -independence of the effective couplings also eliminates their  $N_c$ -running. For example for the effective Newton's coupling

$$(N_c^2 - 1)\partial_{(N_c^2 - 1)} \ln G_{\text{eff}} = k_a^2 \partial_{k_a^2} \ln G_{\text{eff}} = 0, \quad (7.12)$$

holds in a minimal subtraction scheme where the renormalisation scale  $\mu_{\text{RG}}$  does not introduce further  $N_c$ -dependencies, most simply done with  $\mu_{\text{RG}}$ -independent couplings  $G$  and  $\Lambda$ .

We also have to include  $g_{R^2} R^2$  and  $g_{R_{\mu\nu}^2} R_{\mu\nu}^2$  terms in the classical gravity action in order to renormalise also these couplings,

$$\begin{aligned} g_{R^2,\text{eff}} &= g_{R^2} + (N_c^2 - 1)c_{R^2,a} \ln \frac{k_a^{\text{IR}^2}}{k_a^2}, \\ g_{R_{\mu\nu}^2,\text{eff}} &= g_{R_{\mu\nu}^2} + (N_c^2 - 1)c_{R^2,a} z_a \ln \frac{k_a^{\text{IR}^2}}{k_a^2}. \end{aligned} \quad (7.13)$$

Here, the minimal subtraction discussed above requires  $g_{R^2}(N_c, \ln k_a/k_a^{\text{IR}})$  as well as  $g_{R_{\mu\nu}^2}(N_c, \ln k_a/k_a^{\text{IR}})$ . This leaves us with a theory, which includes all UV quantum effects of the Yang-Mills theory. Accordingly, in the UV its effective action (7.9) resembles the Einstein-Hilbert action coupled to the classical Yang-Mills action with appropriately redefined couplings. It also has  $R^2$ - and  $R_{\mu\nu}^2$ -terms. However, the latter terms are generated in any case by graviton fluctuations so there is no structural difference to standard gravity with the Einstein-Hilbert action coupled to the classical Yang-Mills.

The only relevant  $N_c$ -dependence originates in the logarithmic curvature dependence of the marginal operators  $R^2$  and  $R_{\mu\nu}^2$  leading e.g. to

$$(N_c^2 - 1) c_{R^2,a} \int d^4x \sqrt{g} R^2 \ln \left( 1 + \frac{R}{k_a^{\text{IR}^2}} \right). \quad (7.14)$$

These terms are typically generated by flows towards the IR, for a respective computation in Yang-Mills theory see [464]. Such a running cannot be absorbed in the pure gravity part without introducing a non-local classical action. From its structure the logarithmic running in (7.13) resembles the one of the strong coupling in many flavour QCD: the rôle of the gravity part here is taken by the gluon part in many flavour QCD and that of the Yang-Mills part here is taken by the many flavours. Accordingly a fully conclusive analysis has to take into account these induced interactions. This is left to future work, here we concentrate on the Einstein-Hilbert part. The respective truncation to matter-gravity systems have been studied at length in the literature, and the arguments presented here fully apply. Note also that the current setup (and the results in the literature) can be understood as a matter-gravity theory, where the respective terms are removed by an appropriate classical gravity action that includes e.g.  $R^2 \ln R$ -terms. The discussion of these theories is also linked to the question of unitarity in asymptotically safe gravity.

If we do not re-adjust the effective couplings within the minimal subtraction discussed above they show already the fixed point scaling to be expected in an asymptotically safe theory of quantum gravity, see (7.11) and (7.13). This merely reflects the fact that Yang-Mills theory has no explicit scales. If we only absorb the  $k_a$  running of the couplings while leaving open a general  $\mu_{\text{RG}}$ -dependence, the effective Newton's coupling  $G_{\text{eff}}$  scales with  $1/N_c^2$ , while the effective cosmological constant scales with  $N_c^0$ .

In any case we have to use  $G_{\text{eff}}$  for the gravity scale in the Yang-Mills-gravity system instead of  $G$ . For example, the expansion of the full metric  $g_{\mu\nu}$  in a background and a fluctuation then reads

$$g_{\mu\nu} = \bar{g}_{\mu\nu} + \sqrt{G_{\text{eff}}} h_{\mu\nu}, \quad (7.15)$$

with the dimension-one field  $h_{\mu\nu}$  in the  $d = 4$  dimensional Yang-Mills-gravity system.

### 7.2.3. Asymptotic safety in gravity with Yang-Mills

It is left to integrate out graviton fluctuations on the basis of the combined effective action where the pure gravity part is of the Einstein-Hilbert type. The couplings of the pure gravity sector, in particular Newton's coupling and the cosmological constant only receive quantum contributions from pure gravity diagrams, while pure gauge and gauge-graviton couplings only receive contributions from diagrams that contain at least one graviton line. This system is asymptotically safe in the pure gravity sector and assists asymptotic freedom for the minimal gauge coupling, see (7.6) and (7.7), and leads to graviton-induced higher-order coupling such as (7.8). In summary we conclude that Yang-Mills–gravity systems are asymptotically safe. The flow of this system and its completeness is discussed in Sec. 7.7.

The present analysis is also important for the evaluation of general matter-gravity systems: we have argued that asymptotic freedom of the Yang-Mills theory allows us to successively integrate out the degrees of freedom, starting first with the Yang-Mills sector. Evidently, this is also true for matter-gravity systems with free matter such as treated in the last chapter and in e.g. [424]. In [424] fermions and scalars were found to be unstable for a large flavour numbers while in the last chapter fermions were shown to be stable. For scalars the situation was inconclusive as the anomalous dimension of the graviton was exceeding an upper bound,  $\eta_h < 2$ , beyond which a regulator of the form  $R_{h,k}(p^2) \propto Z_h R_{h,k}^{(0)}(p^2)$  with  $R_{h,k}^{(0)}(0) = k^2$  is no longer a regulator with the cutoff scale  $k$ :

$$\lim_{k \rightarrow \infty} R_{h,k}(0) \propto (k^2)^{1-\eta_h/2} \rightarrow 0, \quad \text{for } \eta_h > 2. \quad (7.16)$$

While the differences in the stability analysis can be partially attributed to the different approximations (see last chapter for a discussion), we come to conclude here, that both (and all similar ones) analyses lack the structure discussed above. This calls for a careful reassessment of the UV flows of matter-gravity systems also in the view of relative cutoff scales. The latter is since long a well-known problem in quantum field theoretical applications of the FRG, in particular in boson-fermion systems. For example, in condensed matter systems it has been observed that exact results for the three-body scattering (STM), see [465], can only be obtained within a consecutive integrating out of degrees of freedom in local approximations. If identical cutoff scales are chosen, the three-body scattering only is described approximately. For a recent analysis of relative cutoff scales in multiple boson and boson-fermion systems see [466].

In summary the gravitationally coupled free-matter–gravity systems, Yang-Mills–gravity systems or more generally asymptotically free gauge-matter–gravity systems are asymptotically safe, independent of the number of matter degrees of freedom if this holds for one degree of freedom or more generally if this holds for the minimal number of degrees of freedom that already has the most general interaction structure of the coupled theory. Phrased differently: simple large  $N$ -scaling cannot destroy asymptotic safety, with  $N$  being the number of gauge-matter degrees of freedom.

We emphasise that the analysis of such a minimal system as defined above is necessary. It is not sufficient to rely on the fact that the matter or gauge part can be integrated out first as gravity necessarily induces non-trivial matter and gauge self-interactions at an asymptotically safe gravity fixed point [121, 122, 420, 432, 433]. If these self-interactions do not destroy asymptotic safety, the systems achieve asymptotic safety for a general number of matter or gauge fields by guaranteeing the UV dominance of graviton fluctuations.

It also suggest a natural scaling hierarchy for the cutoff scales  $k_h, k_a$  in the gravity and

Yang-Mills sector respectively: while gravity feels the effective Newton's coupling  $G_{\text{eff}}$  and hence graviton fluctuations and gravity scales should be measured in  $G_{\text{eff}}$ , the Yang-Mills field generates contributions to the (bare) Newton's coupling  $G$ . This leads us to

$$G_{\text{eff}} k^2 \simeq G k_a^2, \quad (7.17)$$

for the respective cutoff scales  $k_h = k$  in the gravity subsystem and  $k_a$  in the Yang-Mills-subsystem. With this scale hierarchy the  $N_c$ -dependence of the coupled system disappears and, within an appropriate fine-tuning of the relation (7.17) the fixed point values of Newton's coupling and the cosmological constant show no  $N_c$ -dependence at all. In short such a rescaling always guarantees the dominance of graviton fluctuations over gauge or matter fluctuations in the coupled system if the gauge-matter system is asymptotically free. We close this section with some remarks:

- (1) The naturalness of the rescaling (7.17) is finally decided by taking into account momentum or spectral dependencies of the correlation functions. This is at the root of the question of stability and instability of matter-gravity systems. It is here where the marginal, logarithmically running, terms such as (7.14) come into play. They are not affected by this rescaling, which also shows their direct physics relevance.
- (2) Within the above rescaling the fixed point of the gravity-induced gauge couplings such as  $w_2$  and  $v_4$ , see (7.8), are of order  $g^{*4}$  of the pure gravity fixed point coupling  $g^*$ . Note however, that this value can be changed by re-adjusting the rescaling (7.17).
- (3) Note that within the dynamical re-adjustment of the scales the fixed point Newton's coupling gets weak,  $g^* \propto 1/N_c^2$ . In other words, gravity dominates by getting weak. This is in line with the weak-gravity scenario advocated recently [387, 432, 433]. However, its physical foundation is different.
- (4) For a sufficiently large truncation the theory should be insensitive to a relative rescaling of the cutoff scales  $k_{\text{gravity}}$  and  $k_{\text{matter}}$  and to other changes of the regularisation scheme. This is partially investigated in Sec. 7.7. Moreover in all of the following renormalisation group computations we do not resort to the rescaling (7.17) but use identical cutoff scales  $k_{\text{gravity}} = k_{\text{matter}}$ .

In the following analysis we will refer to the present section for an evaluation of our results.

### 7.3. Functional renormalisation group in the gravity–Yang-Mills system

In this section we quantise the Yang-Mills–gravity system within the functional renormalisation group approach. As in the previous chapters we use a vertex expansion of the effective action and obtain flow equations for the correlation functions by functional derivatives of the Wetterich equation. For the current field content (7.1) the Wetterich equation is given by

$$\partial_t \Gamma_k[\bar{g}, \bar{A}; \phi] = \frac{1}{2} \text{Tr} [G_k \partial_t R_k]_{hh} + \frac{1}{2} \text{Tr} [G_k \partial_t R_k]_{aa} - \text{Tr} [G_k \partial_t R_k]_{\bar{c}c}. \quad (7.18)$$

with the propagator  $G_k = (\Gamma_k^{(2)} + R_k)^{-1}$  and where the  $\bar{c}c$ -term includes graviton and gauge ghosts. We compute the flow of the two- and three-point functions,  $\partial_t \Gamma^{(aa)}$ ,  $\partial_t \Gamma^{(hh)}$ ,

$\partial_t \Gamma^{(\bar{c}c)}$ ,  $\partial_t \Gamma^{(hhh)}$  and  $\partial_t \Gamma^{(aah)}$ . For this we expand the effective action in vertex functionals in straight analogy to the pure gravity case (3.10). The pure gravity vertices are the same as in (3.10). For the Yang-Mills and the mixed Yang-Mills-gravity  $n$ -point functions we expand according to

$$\begin{aligned} \Gamma[\bar{g}, \bar{A}; \phi] \Big|_{\text{YM \& mixed}} &= \Gamma^{(a)}[\bar{g}, \bar{A}; 0]a + \Gamma^{(ah)}[\bar{g}, \bar{A}; 0], ah + \frac{1}{2}\Gamma^{(ahh)}[\bar{g}, \bar{A}; 0]ah^2 \\ &+ \frac{1}{2}\Gamma^{(aa)}[\bar{g}, \bar{A}; 0]a^2 + \frac{1}{2}\Gamma^{(aah)}[\bar{g}, \bar{A}; 0]a^2h + \frac{1}{4}\Gamma^{(aahh)}[\bar{g}, \bar{A}; 0]a^2h^2 \\ &+ \frac{1}{12}\Gamma^{(aahhh)}[\bar{g}, \bar{A}; 0]a^2h^3 + \mathcal{O}(a^3h, ah^3). \end{aligned} \quad (7.19)$$

As we consider also correlation functions of the background gluon, we need the expansion of the fluctuation vertices in (7.19) in the background field, i.e.

$$\Gamma^{(ah)}[\bar{g}, \bar{A}; 0] = \Gamma^{(ah)}[\bar{g}, 0; 0] + \Gamma^{(\bar{A}ah)}[\bar{g}, 0; 0]\bar{A} + \mathcal{O}(\bar{A}^2), \quad (7.20)$$

in an expansion about vanishing background gauge field. In the following we choose the backgrounds  $\bar{g} = \delta$  and  $\bar{A} = 0$  for the metric and the gauge field. In these backgrounds the terms of the order  $\mathcal{O}(a^3h, ah^3)$  do not enter the flow equations of the propagators nor that of the three-point functions. This is the reason why they have not been displayed explicitly in (7.19). Note that with this background choice the terms linear in  $a$  in (7.19) vanish. We would like to emphasise two structures that facilitate the present computations:

- (1) As we consider the flow equations for the two- and three-point functions, only the terms quadratic in  $a_\mu$  in (7.19) contribute to the graviton-gluon interactions in the flow equations. The non-Abelian parts in the  $F^2$ -term do not contribute since they are of order three and higher. Hence, modulo trivial colour factors  $\delta^{ab}$ , the vertices defined above are identical for  $SU(N)$  and  $U(1)$  gauge theories.
- (2) In principle, the derivatives in  $F^{\mu\nu}$  are covariant derivatives with respect to the Levi-Civita connection. However, since  $F^{\mu\nu}$  is asymmetric, and the Christoffel-symbols symmetric in the paired index, the latter cancel out and the covariant derivatives can be replaced by partial derivatives.

We dress the classical  $n$ -point functions with wave function renormalisations and promote the classical couplings to level- $n$  couplings in order to obtain a parameterisation for the  $n$ -point function of the effective action. This is in straight analogy to (3.17) and for the present chapter the classical action is given by the combined gauge-fixed Einstein-Hilbert and Yang-Mills action. Each graviton  $n$ -point function,  $\Gamma^{(h_1 \dots h_n)}$ , depends on the dimensionless parameters

$$g_n \equiv g_{h^n} = G_n k^2, \quad \lambda_n \equiv \lambda_{h^n} = \Lambda_n / k^2, \quad (7.21a)$$

and a mixed gauge-graviton  $(n+2)$ -point function on

$$g_{a^2 h^n} = G_{a^2 h^n} k^2. \quad (7.21b)$$

In this chapter we are using mostly the uniform approximation with one Newton's coupling. We identify

$$g_{a^m h^n} = g_3 =: g, \quad \lambda_{n>2} = \lambda_3, \quad \lambda_2 = -\frac{1}{2}\mu. \quad (7.22)$$

$$\text{Flow}_h^{(aa)} = -\frac{1}{2} \text{Diagram} + \text{Diagram} + \text{Diagram}$$

Figure 7.1.: Diagrammatic depiction of gravitational contributions to the flow of the Yang-Mills propagator. The wiggly lines are gluon propagators, and the double line represent graviton propagators.

Later in Sec. 7.7.2 we will also distinguish the Newton's couplings from the three-graviton vertex and the one from the graviton-gluon vertex. There we identify

$$g_{a^m h^{n>0}} = g_a, \quad g_n = g_3 =: g, \quad \lambda_{n>2} = \lambda_3, \quad \lambda_2 = -\frac{1}{2}\mu. \quad (7.23)$$

In the end, we are interested in the gravitational corrections to the Yang-Mills beta function, and the Yang-Mills contributions to the running in the gravity sector. The beta functions of the pure gravity section have been discussed in great detail in the last chapters. In the Yang-Mills sector, we make use of the fact that the wave function renormalisation  $Z_A$  of the background gluon is related to the background (minimal) coupling by

$$Z_{\alpha_s} = Z_A^{-1}, \quad (7.24)$$

which is derived from background gauge invariance of the theory. The latter can be related to quantum gauge invariance with Nielsen identities, see [188, 336, 347, 355, 467] in the present framework. This also relates the background minimal coupling to the dynamical minimal coupling of the fluctuation field. Note that this relation is modified in the presence of the regulator, in particular for momenta  $p^2 < k^2$ . There the interpretation of the background minimal coupling requires some care. The running of the background coupling is then determined by

$$\partial_t \alpha_s = \beta_{\alpha_s} = \eta_A \alpha_s, \quad (7.25)$$

with the gluon anomalous dimension

$$\eta_A := -\partial_t \ln Z_A. \quad (7.26)$$

Note that in general all these relations carry a momentum-dependence as  $Z_A(p^2)$  carries a momentum-dependence. This will become important in the next section for the physics interpretation of the results.

## 7.4. Graviton contributions to Yang-Mills

In this section we compute the gravitational corrections to the running of the gauge coupling. The key question is if graviton-gluon interactions destroy or preserve the property of asymptotic freedom in the Yang-Mills sector. The running of the gauge coupling can be calculated from the background gluon wave function renormalisation. Its flow equation is derived from (7.18) with two functional derivatives w.r.t.  $\bar{A}$ . Schematically it reads

$$\partial_t \Gamma^{(\bar{A}\bar{A})}(p) = \text{Flow}_A^{(\bar{A}\bar{A})}(p) + \text{Flow}_h^{(\bar{A}\bar{A})}(p), \quad (7.27)$$

where the first term contains only gluon fluctuations and the second term is induced by graviton-gluon interactions. The diagrammatic form of the second term is displayed in [Fig. 7.1](#). This split is reflected in a corresponding split of the anomalous dimension

$$\eta_A(p^2) = \eta_{A,A}(p^2) + \eta_{A,h}(p^2). \quad (7.28)$$

Note that in the present approximation we have  $\eta_{A,h} = \eta_{a,h}$ . This originates in the fact that the fluctuation graviton only couples to gauge invariant operators.

Asymptotic freedom is signalled by a negative sign of the gluon anomalous dimension as the beta function for the coupling is proportional to  $\eta_A$ . We know that the pure gluon contributions  $\eta_{A,A}$  are negative. Hence, the question whether asymptotic freedom is preserved in the Yang-Mills–gravity system boils down to the sign of the gravity contributions  $\eta_{A,h}$ , and we arrive at

$$\eta_{A,h} \leq 0 \iff \text{asymptotic freedom}. \quad (7.29)$$

The anomalous dimension in [\(7.29\)](#) depends on both, cutoff and momentum scales. For small momentum scales  $p^2/k^2 \rightarrow 0$  the regulator induces a breaking of quantum-gauge and quantum-diffeomorphism invariance: the respective STIs of the fluctuation field correlation functions are modified. This necessitates also a careful investigation of the background observables, which only carry physics due to the relation of background gauge- and diffeomorphism invariance.

Note that asymptotic freedom as defined in [\(7.29\)](#) only applies to the minimal coupling. Higher order fluctuation couplings are not necessarily vanishing. Indeed it has been shown that the asymptotically safe fixed points of general matter and gauge fields coupled to gravity can not be fully asymptotically free in the matter and gauge field sector, see [\[122, 387, 420, 432, 433\]](#). This leads to  $a^4$ -vertices from higher order invariants such as  $(\text{Tr } F^2)^2$  and  $\text{Tr } F^4$  with fixed point values proportional to  $g_a^2/(1+\mu)^3$  with  $g_a = g$  in our approximation. Moreover these vertices generate a tadpole diagram that contribute to the gluon propagator. Apart from shifting the Gaussian fixed point of higher order operators in the Yang-Mills sector to an interacting one, see [\[432\]](#) for the  $U(1)$ -case, it also deforms the gluon contribution to the Yang-Mills beta function. Its qualitative properties will be discussed later, as it is important for the large  $N_c$  behaviour of the fixed point.

#### 7.4.1. Background observables

The discussion of physics content of background observables and its relation to gauge- and diffeomorphism invariance has been initiated for the Yang-Mills–gravity system in [\[376, 457\]](#). There it has been shown that  $\eta_{a,h} = 0$  vanishes for

$$\frac{r_a}{1+r_a} \frac{1}{1+r_h} = 0. \quad (7.30)$$

due to a non-trivial kinematic identity. This identity relates angular averages of one- and two-graviton–two-gluon scattering vertices in the absence of a gluon regulator  $r_a$ , see [Fig. 7.2](#). In other words, for a combination of regulators that satisfy [\(7.30\)](#) the quantum-gauge and quantum-diffeomorphism symmetry violating effects of the regulators do not effect the kinematic identity that holds in the absence of the regulator.

This structure requires some care in the interpretation of the running of background observables for  $k \rightarrow \infty$ : while the physics properties of the dynamical fluctuation fields

$$\langle \text{Diagram with } T_{\mu\nu\delta\lambda} \text{ and } \Omega_p \rangle = \frac{1}{2} \langle \text{Diagram with } T_{\mu\nu\delta\lambda} \text{ and } \Omega_p \rangle$$

Figure 7.2.: Kinematic identity for the one- and two-graviton–two-gluon scattering vertices for  $r_a = 0$  and  $\Gamma_A^{(2)} \simeq S_A^{(2)}$ , taken from [376, 457].

should not depend on the choice of the regulators, background observables do not necessarily display physics in this limit. By now we know of many examples for the latter deficiency ranging from the beta function of Yang-Mills theory, see [355], to the behaviour of the background couplings in pure gravity, see the discussions in the previous chapters. Moreover, we have already argued that the relation between the dynamical and the background minimal coupling only holds without modifications for sufficiently large momenta.

In summary this implies the following for the interpretation of background observables: we either choose pairs of regulators that satisfy (7.30) or we evaluate background observables for momentum configurations that are not dominantly affected by the breaking of quantum-gauge and diffeomorphism invariance. Here we pursue the latter option that gives us more freedom in the choice of regulators. For the computation of the graviton contribution to the running of the Yang-Mills background coupling this implies that we have to evaluate the flow of the two-point function for sufficiently large external momenta,

$$p^2 \gtrsim k^2. \quad (7.31)$$

For these momenta the three-point function diagrams effectively satisfy (7.30) and the anomalous dimension  $\eta_{a,h}(p^2)$  carries the information about the graviton contribution of the beta function of the background coupling.

#### 7.4.2. Gravity supports asymptotic freedom

The results of the discussion on background observables allow us to access the question of asymptotic freedom of the minimal Yang-Mills coupling. With the construction of the effective action (7.19), we obtain a flow equation for  $\partial_t \Gamma^{(aa)}$ , which is projected with the transverse projection operator  $\Pi_T$ . The graviton-induced contributions to the resulting flow equation take the form

$$\begin{aligned} \Pi_T^{\mu\nu}(p) \partial_t \Gamma_{\mu\nu}^{(aa)}(p) &= k^2 \text{Flow}_h^{(aa)}(p^2) \\ &= Z_a(p^2) g k^2 \int_q \left( (\dot{r}(q^2) - \eta_a(q^2)r(q^2)) f_a(q, p, \mu) + (\dot{r}(q^2) - \eta_h(q^2)r(q^2)) f_h(q, p, \mu) \right), \end{aligned} \quad (7.32)$$

where the terms on the right-hand side originate from diagrams with a regulator insertion in the gluon and graviton propagator, respectively. The left-hand side is simply given by

$$\Pi_T^{\mu\nu}(p) \partial_t \Gamma_{\mu\nu}^{(aa)}(p) = p^2 \partial_t Z_a(p^2). \quad (7.33)$$

Dividing by  $Z_a(p^2)$ , one obtains an inhomogeneous Fredholm integral equation of the second kind for the gluon anomalous dimension,

$$\eta_a(p^2) = f(p^2) + g \int \frac{d^4 q}{(2\pi)^4} K(p, q, \mu, \eta_h) \eta_a(q^2). \quad (7.34)$$

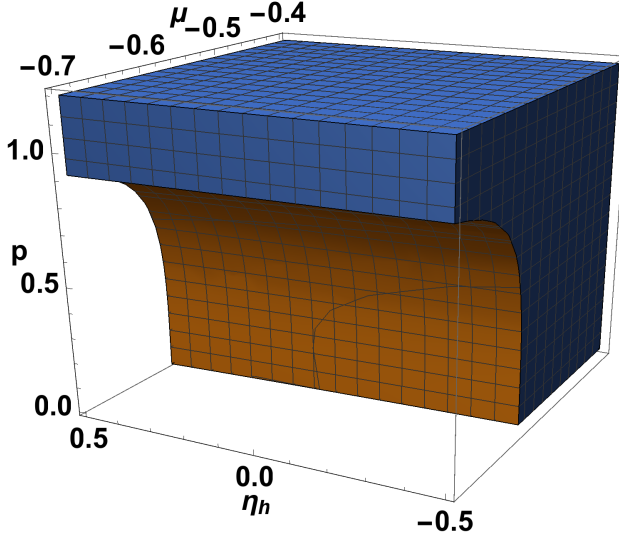


Figure 7.3.: Sign of the graviton contributions to the gluon anomalous dimension  $\eta_{a,h}$  as a function of  $\eta_h$ ,  $\mu$ , and  $p$ . The coloured region indicates  $\text{sgn } \eta_{a,h} < 0$ . At  $p = k$  the whole displayed region supports asymptotic freedom.

This integral equation can be solved using the resolvent formalism by means of a Liouville-Neumann series. In this chapter we approximate the full momentum dependence by evaluating the anomalous dimension in the integrand in (7.34) at  $q^2 = k^2$ . This is justified since the integrand is peaked at  $q \approx k$  due to the regulator. With this approximation (7.34) can be evaluated numerically for all momenta. This approximation was already used in the previous chapters and lead to results in good qualitative agreement with the full momentum dependence. With the approximation to (7.34) we investigate the sign of the graviton contributions to the gluon propagator. These contributions are functions of the gravity couplings, which in turn depend on the truncation. It is therefore interesting to evaluate  $\eta_{a,h}$  with a parametric dependence on the gravity couplings, in order to obtain general conditions under which asymptotic freedom is guaranteed.

The gluon anomalous dimension is of the form  $\eta_a(p^2, g, \mu, \eta_h)$ . In order to avoid the unphysical regulator dependence potentially induced by the violation of the kinematical identity (7.30) we choose the momentum  $p^2 = k^2$  in order to satisfy (7.31). In summary this provides us with a minimal coupling  $\alpha_s$ ,

$$\partial_t \alpha_s = \beta_{\alpha_s} = \eta_a(k^2) \alpha_s. \quad (7.35)$$

As a main result in the present section we conclude that

$$\beta_{\alpha_s} \leq 0 \quad \text{for} \quad \mu > -1 \quad \& \quad \eta_h(k^2) \leq 2. \quad (7.36)$$

The restriction to  $\eta_h \leq 2$  is also the bound on the anomalous dimension advocated in [2]. To be more precise  $\eta_h > 2$  only changes the sign of the Yang-Mills beta function in the limit  $\mu \rightarrow -1$ . For other values of  $\mu$  very large values of  $\eta_h$  are necessary in order to destroy asymptotic freedom, e.g. for  $\mu = -0.4$  the bound is  $\eta_h \approx 50$ . The precise bound is displayed in Fig. 7.4, where the red region indicates  $\beta_{\alpha_s} > 0$ .

Despite the necessary restriction to momenta  $p^2 \gtrsim k^2$  for its relation to the physical background coupling, we have also evaluated  $\eta_{a,h}$  for more general momentum configura-

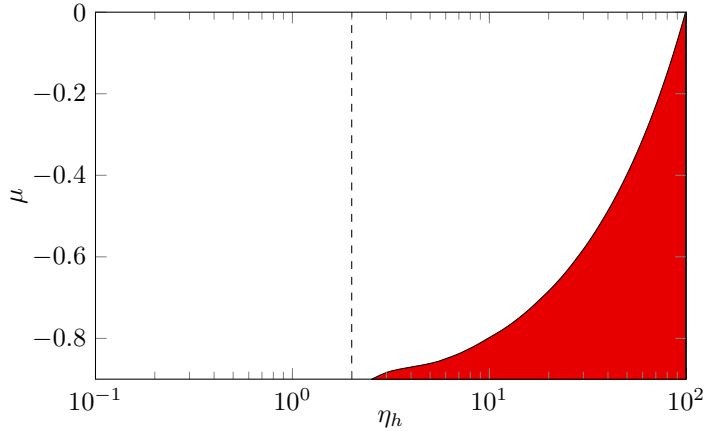


Figure 7.4.: Sign of the graviton contributions to the gluon anomalous dimension  $\eta_{a,h}(k^2)$  as a function of  $\eta_h$  and  $\mu$ . The red region indicates  $\text{sgn } \eta_{a,h}(k^2) > 0$  and the loss of asymptotic freedom. The dashed line marks  $\eta_h = 2$ .

tions and a range of gravity parameters  $\mu$  and  $\eta_h$ : In Fig. 7.3 the sign of the graviton-induced part of the gluon anomalous dimension  $\eta_{a,h}$  is plotted in the momentum range  $0 \leq p^2 \leq k^2$ . For small momenta  $\eta_{a,h}$  changes sign for  $\mu \rightarrow -1$ . Again it can be shown that this does not happen for regulators with (7.30).

In order to understand the patterns behind Fig. 7.3 and Fig. 7.4 it is illuminating to examine  $\eta_{a,h}(p^2 = 0)$  for flat regulators (E.1) with a  $p^2$  derivative. It reads

$$\eta_{a,h} = -\frac{g}{8\pi} \left( \frac{8 - \eta_a}{1 + \mu} - \frac{4 - \eta_h}{(1 + \mu)^2} \right). \quad (7.37)$$

The first term on the right hand side stems from  $\partial_t R_{k,a}$  and is positive for  $\eta_a < 8$ . The second stems from  $\partial_t R_{h,k}$ . It is non-vanishing for  $\eta_h = 0$  and hence already contributes at one-loop order. Its very presence reflects the breaking of the non-trivial kinematical identity depicted in Fig. 7.2 as it is proportional to it. The interpretation of  $\eta_{a,h}$  as the graviton-induced running of the Yang-Mills background coupling crucially hinges on physical quantum gauge invariance: it is important to realise that only with the relation between the auxiliary background gauge invariance and quantum gauge invariance the latter carries physics. In turn, in the momentum regime where the kinematical identity is violated, physical gauge invariance is not guaranteed, and background gauge invariance reduces to an auxiliary symmetry with no physical content. Accordingly, one either has to evaluate  $\eta_{a,h}(p^2)$  for sufficiently large momenta  $p^2 \gtrsim k^2$  or utilises regulators that keep the kinematical identity Fig. 7.2 at least approximately for all momenta.

In summary, Fig. 7.3 and Fig. 7.4 entail that  $\text{sgn}(\eta_{a,h}) < 0$  holds for physically relevant momenta and values of the gravity couplings. Thus asymptotic freedom is preserved. We have argued that (7.35) provides the correct definition for the beta function of the minimal coupling of Yang-Mills theory with  $\text{sgn}(\beta_{\alpha_s}) \leq 0$ . Hence we conclude that an UV fixed point in the spirit of the asymptotic safety scenario is compatible with asymptotic freedom of the minimal coupling in Yang-Mills theories.

$$\text{Flow}_a^{(2h)} = -\frac{1}{2} \begin{array}{c} \text{Diagram 1} \\ \text{Diagram 2} \end{array} + \begin{array}{c} \text{Diagram 3} \\ \text{Diagram 4} \end{array}$$

$$\text{Flow}_a^{(3h)} = -\frac{1}{2} \begin{array}{c} \text{Diagram 5} \\ \text{Diagram 6} \end{array} + 3 \begin{array}{c} \text{Diagram 7} \\ \text{Diagram 8} \end{array} - 3 \begin{array}{c} \text{Diagram 9} \\ \text{Diagram 10} \end{array}$$

Figure 7.5.: Diagrammatic depiction of the gluon contributions to the flow of the graviton propagator and the graviton three-point function. The wiggly lines are gluon propagators, and the double line represent graviton propagators.

## 7.5. Yang-Mills contributions to gravity

This section is concerned with the impact of gluon fluctuations on the gravity sector. The fully coupled system is analysed subsequently in [Sec. 7.6](#).

### 7.5.1. General structure

For the question of asymptotic safety we have to investigate the gluon contributions to the graviton propagator as well as to the graviton three-point function. This allows us to compute the corrections to the running of the gravity couplings  $(\mu, g, \lambda_3)$  due to gluon fluctuations.

The gluon corrections to the graviton two- and three-point function split analogously to the graviton corrections to Yang-Mills theory in the preceding section, since for any graviton  $n$ -point function the structure is given by

$$\text{Flow}^{(nh)} = \text{Flow}_h^{(nh)} + \text{Flow}_a^{(nh)}, \quad (7.38)$$

with graviton and gluon contributions denoted by  $\text{Flow}_h^{(nh)}$  and  $\text{Flow}_a^{(nh)}$  respectively. For example, the gluon contributions to the flow of the graviton two- and three-point function are depicted in [Fig. 7.5](#). All these diagrams contain a closed gluon loop and hence all the factors in the above equations with an index  $a$  are proportional to  $N_c^2 - 1$ .

### 7.5.2. Contributions to the graviton propagator

The gluon contribution to the graviton propagator has been studied in a derivative expansion around  $p^2 = 0$  in [\[457\]](#) where it was shown that this projection is insufficient due to the non-trivial momentum-dependence of the flow. The latter is characterized by a peak at  $p^2 \approx k^2$ . We have rederived the momentum dependence of  $\text{Flow}_a^{(2h)}(p^2)$ , see the left panel of [Fig. 7.6](#).

For the projection at  $p^2 = 0$  and flat regulators [\(E.1\)](#), we rederive the result of [\[457\]](#) and obtain for the momentum-independent part

$$\text{Flow}_a^{(2h)}(p^2 = 0) = g Z_h (N_c^2 - 1) \frac{1}{60\pi} \eta_a. \quad (7.39)$$

Surprisingly, this contribution is proportional to  $\eta_a$ . This happens due to a cancellation between both diagrams displayed in [Fig. 7.5](#). Note that this cancellation only occurs for

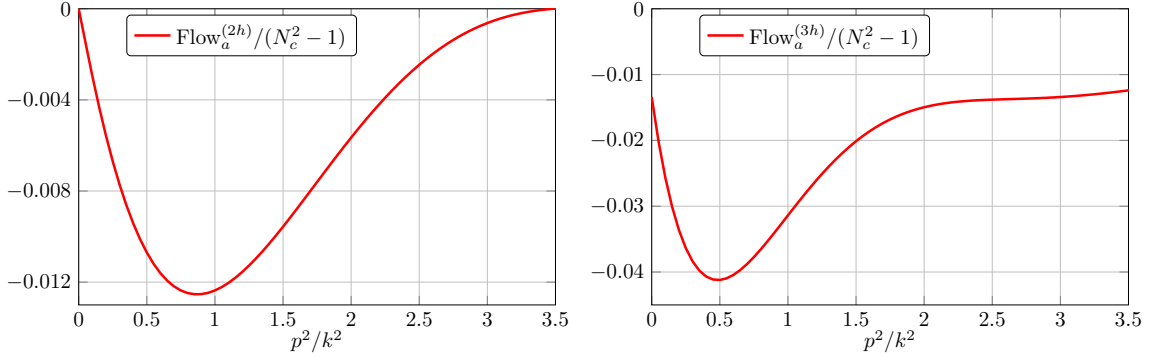


Figure 7.6.: The momentum dependence of  $\text{Flow}_a^{(2h)}/(N_c^2 - 1)$  (left) and  $\text{Flow}_a^{(3h)}/(N_c^2 - 1)$  (right) for  $g = 1$  and  $\eta_a = 0$  on the right-hand side of the flow.

the flat regulator. For other regulators the contribution can be either positive or negative. This is discussed in App. E.2 and will play a crucial rôle in the later analysis.

For the computation of the graviton anomalous dimension we resort to a finite difference projection, which is of the general form

$$\frac{\text{Flow}_a^{(2h)}(p_1^2) - \text{Flow}_a^{(2h)}(p_2^2)}{p_1^2 - p_2^2} = g Z_h (N_c^2 - 1) (\alpha + \beta \eta_a), \quad (7.40)$$

where  $\alpha$  and  $\beta$  depend only on  $p_1$  and  $p_2$ . This is rooted in the fact that there are only internal gluon propagators and graviton-gluon vertices and these do not depend on  $\lambda_3$  and  $\mu$  as discussed in the last section. For  $p_2 = 0$  and  $p_1 \rightarrow p_2$ , i.e. a  $p^2$ -derivative at  $p^2 = 0$ , we obtain

$$\alpha = \beta = -\frac{1}{12\pi} \approx -0.027. \quad (7.41)$$

For a finite difference with  $p_1^2 = k^2$  and  $p_2 = 0$  we obtain

$$\alpha \approx -0.012, \quad \beta \approx -0.0033. \quad (7.42)$$

(7.41) and (7.42) display the gluon contribution to  $-\eta_h$  thus the gluon contribution to  $\eta_h$  is positive independent of the momentum projection scheme. Note however that (7.41) and (7.42) display a qualitatively different behaviour, and (7.42) is the correct choice due to the momentum-dependence of the flow. This has already been observed in the pure gravity computations in [325, 327] and in the previous chapters and emphasises the importance of the momentum-dependence. In this chapter we use a finite difference between  $p_1^2 = p^2$  and  $p_2^2 = -\mu k^2$  for the equation of  $\eta_h(p^2)$ .

### 7.5.3. Contributions to the three-point function

The contributions to the graviton three-point function enter the beta function of the Newton's coupling  $g$  and the beta function of  $\lambda_3$ . The diagrammatic representation of these contributions is shown in Fig. 7.5. Here the contribution to  $\partial_t g$  is the momentum dependent part and the contribution to  $\partial_t \lambda_3$  in the momentum independent part to the graviton three-point function. For the projection on the couplings  $g$  and  $\lambda_3$  we use precisely

the same projection operators as in [Sec. 3.4.3](#). These are different projection operators for  $g$  and  $\lambda_3$  and we mark this with an index  $G$  and  $\Lambda$  in the following.

We have seen in the previous sections, that the momentum dependence of the flow plays a crucial rôle, and key properties may be spoiled if non-trivial momentum-dependence is not taken into account properly. Therefore we resolve the momentum dependence of the contributions  $\text{Flow}_{G,a}^{(3h)}(p^2)$ , which is shown in the right panel of [Fig. 7.6](#). Interestingly, the contribution is peaked at  $p^2 = \frac{1}{2}k^2$  and is not well described by  $p^2$  in the region  $0 \leq p^2 \leq k^2$ . Due to this non-trivial structure the contribution to  $\partial_t g$  depends on the momenta where it is evaluated. For general momenta  $p_1^2$  and  $p_2^2$  we obtain

$$\frac{\text{Flow}_{G,a}^{(3h)}(p_1^2) - \text{Flow}_{G,a}^{(3h)}(p_2^2)}{p_1^2 - p_2^2} = g^{\frac{3}{2}} Z_h^{\frac{3}{2}} (N_c^2 - 1) (\gamma + \delta \eta_a), \quad (7.43)$$

where  $\gamma$  and  $\delta$  again only depend on  $p_1^2$  and  $p_2^2$ . Evaluated as derivatives, i.e.  $p_2^2 = 0$  and  $p_1^2 \rightarrow 0$  we arrive at

$$\gamma = -\frac{7}{30\pi} \approx -0.074, \quad \delta = -\frac{1}{570\pi} \approx -0.00056. \quad (7.44)$$

With  $p_1^2 = k^2$  and  $p_2^2 = 0$  they are given by

$$\gamma \approx -0.018, \quad \delta \approx -0.0014. \quad (7.45)$$

As in the case of the gluon propagator the sign of the derivative definition agrees with the bi-local one but they differ strongly in their magnitude. We use (7.45). The contribution to  $\lambda_3$  is always evaluated at vanishing momentum. We obtain

$$\text{Flow}_{\Lambda,a}^{(3h)}(p^2 = 0) = g^{\frac{3}{2}} Z_h^{\frac{3}{2}} (N_c^2 - 1) \frac{3 - \eta_a}{60\pi}. \quad (7.46)$$

#### 7.5.4. Mixed graviton-gluon coupling

So far we have only considered pure gluon and pure graviton correlation functions in the coupled Yang-Mills-gravity system. Indeed, the results that will be presented in [Sec. 7.6](#) are based on precisely these correlation functions and other couplings are identified according to (7.22). In [Sec. 7.7](#) we discuss the stability of the results under extensions of the truncation. In particular, we take a look at the inclusion of a flow equation for the graviton–two-gluon–coupling  $g_a$ .

The flow equation for  $g_a$  is derived analogously to the  $g_3$  coupling from three-graviton vertex: we build the projection operator from the classical tensor structure  $S^{(haa)}$  with a transverse traceless graviton and two transverse gluons. This projection operator is contracted with both sides of the flow equation for this specific vertex. The equation is further evaluated at the momentum symmetric point (3.22). The resulting  $p^2$ -part gives the flow equation for  $g_a$ . We obtain an analytic flow equation for  $g_a$  by a  $p^2$ -derivative at  $p^2 = 0$ . The resulting flow equation is given in [App. E.4](#).

For the computations in [Sec. 7.7](#) we use the preferred method of finite differences. In particular we choose the evaluation points  $p^2 = k^2$  and  $p^2 = 0$ . With this method we do not obtain analytic flows but we take more non-trivial momentum dependences into account. The computation is simplified by the fact that the present flow is actually vanishing at  $p^2 = 0$ . Consequently the finite difference equals to an evaluation at  $p^2 = k^2$  and the momentum derivative gives the same result as a  $1/p^2$ -division.

### 7.5.5. Momentum locality

We close this section with a remark on the momentum locality introduced in Sec. 3.5.1 as a necessary condition for well-defined RG-flows. It was shown to be related to diffeomorphism invariance of the theory. It entails that flows should not change the leading order of the large momentum behaviour of correlation functions. The asymptotics of the diagrams for the graviton two-point function, ordered as displayed in Fig. 7.5, are

$$\text{Diag}_1^{(2h)}(p^2 \rightarrow \infty) = -g \frac{8 - \eta_a}{12\pi}, \quad \text{Diag}_2^{(2h)}(p^2 \rightarrow \infty) = g \frac{8 - \eta_a}{12\pi}, \quad (7.47)$$

while the asymptotics for the graviton three-point function, again ordered as displayed in Fig. 7.5, are

$$\begin{aligned} \text{Diag}_1^{(3h)}(p^2 \rightarrow \infty) &= -g^{3/2} \frac{8 - \eta_a}{19\pi}, & \text{Diag}_2^{(3h)}(p^2 \rightarrow \infty) &= g^{3/2} \frac{4(8 - \eta_a)}{19\pi}, \\ \text{Diag}_3^{(3h)}(p^2 \rightarrow \infty) &= -g^{3/2} \frac{3(8 - \eta_a)}{19\pi}. \end{aligned} \quad (7.48)$$

Consequently we again have a highly non-trivial cancellation between different diagrams, which leads to the property of momentum locality. In summary, we assert

$$\lim_{p^2/k^2 \rightarrow \infty} \frac{\partial_t \Gamma^{(2h,3h)}(p^2)}{\Gamma^{(2h,3h)}(p^2)} = 0, \quad (7.49)$$

in the transverse traceless mode. Hence, the full flows of the graviton two- and three-point functions including Yang-Mills corrections are momentum local.

## 7.6. Asymptotic safety of Yang-Mills–gravity

In this section we provide a full analysis of the UV fixed point of the coupled Yang-Mills–gravity system. It is characterised by the non-trivial fixed point of Newton’s coupling  $g$ , the coupling of the momentum-independent part of the graviton three-point function  $\lambda_3$  and the graviton mass parameter  $\mu$  while the minimal gauge coupling vanishes,  $\alpha_s = 0$ .

### 7.6.1. Finite $N_c$

The fully coupled fixed point shows some remarkable features. The fixed point values are displayed in the left panel of Fig. 7.7. The fixed point value of the graviton mass parameter remains almost a constant as a function of  $N_c$ . The Newton’s coupling is approaching zero, while  $\lambda_3^*$  becomes slowly smaller and crosses zero at  $N_c^2 \approx 166$ . This behaviour can be understood from the equations: the leading contribution from Yang-Mills to  $\partial_t \mu$  cancels out and only a term proportional to  $\eta_a$  remains, see (7.39). The latter is small at the fixed point and hence the effect on  $\partial_t \mu$  is strongly suppressed. The fall off of  $g^*$  and  $\lambda_3^*$  is explained by the respective contribution in the flow equations, see (7.45) and (7.46).

The critical exponents of the fixed point, which are given by minus the eigenvalues of the stability matrix, are displayed in the central panel of Fig. 7.7. They remain stable over the whole investigated range. Two critical exponents form a complex conjugated pair. The real part of this pair is positive and thus corresponds to two UV attractive directions. The third critical exponent is real and negative and corresponds to a UV repulsive direction.

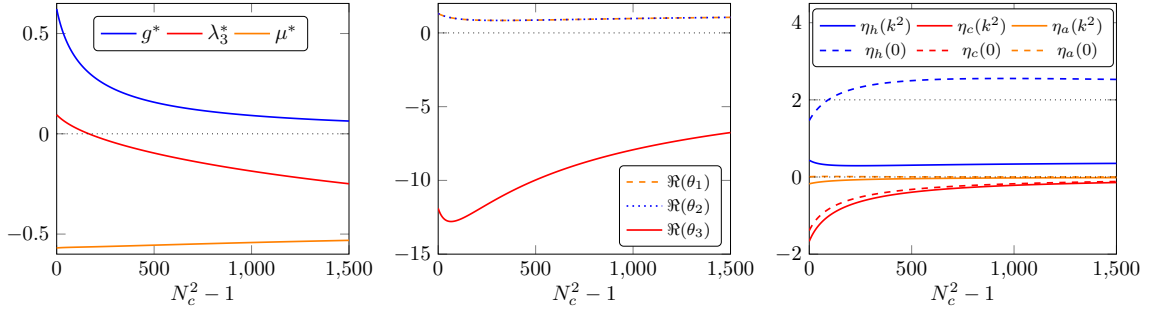


Figure 7.7.: Properties of the UV fixed point as a function of  $N_c^2 - 1$  in the uniform approximation with one Newton's coupling. Displayed are the fixed point values (left panel), the critical exponents (central panel), and the anomalous dimensions (right panel).

The eigenvector belonging to the latter exponent points approximately in the direction of  $\lambda_3$ , which is in accordance with pure gravity results from [Chapter 3](#).

In the right panel of [Fig. 7.7](#) we show the anomalous dimensions at the fixed point, evaluated at  $p^2 = 0$  and  $p^2 = k^2$ . The ghost and gluon anomalous dimensions tend towards zero for increasing  $N_c$ . Most importantly  $\eta_a(k^2)$  is always negative, which is a necessary condition for asymptotic freedom in the Yang-Mills sector. The graviton anomalous dimension does not tend towards zero. At  $p^2 = k^2$  it is getting smaller with an increasing  $N_c$  despite the positive gluon contribution (7.42). The reason is that the anomalous dimension is also proportional to  $g^*$ , which is decreasing and this effect dominates over the gluon contribution. At  $p^2 = 0$  on the other hand the gluon contribution is also positive but larger in value, see (7.41), and consequently dominates over the decrease in  $g^*$ .  $\eta_h(0)$  is increasing, crosses the value 2 and starts to decrease again for large  $N_c$ . As mentioned in (7.16),  $\eta < 2$  is a bound on regulators that are proportional to the respective wave function renormalisation. In our case  $\eta_h(0)$  exceeds the value 2 just slightly, and remains far from the strict bound, which is  $\eta_h < 4$ , see [Sec. 6.3.4](#) for details.

The fixed point values of the background couplings are displayed in [Fig. 7.8](#). The equations for the pure gravity part are identical to the ones in [Chapter 4](#) and the gluon part is identical to the one in [421]. In this setting the background couplings behave very similar to the dynamical ones. The background Newton's coupling goes to zero with  $1/N_c^2$  while the background cosmological constant goes to a constant for large  $N_c$ . Interestingly the background coupling reach their asymptotic behaviour much faster than the dynamical ones.

### 7.6.2. Large $N_c$ scaling

In the limit  $N_c \rightarrow \infty$  the couplings approach the fixed point values

$$g^* \rightarrow \frac{89}{N_c^2} + \frac{8.0 \cdot 10^4}{N_c^4}, \quad \mu^* \rightarrow -0.45 - \frac{3.3 \cdot 10^2}{N_c^2}, \quad \lambda_3^* \rightarrow -0.71 + \frac{2.4 \cdot 10^3}{N_c^2}. \quad (7.50)$$

As expected the 't Hooft coupling  $g^* N_c^2$  is going to a constant in the large  $N_c$ -limit. This behaviour is also displayed in [Fig. 7.8](#) for finite  $N_c$ . Remarkably,  $\mu^*$  and  $\lambda_3^*$  remain finite. In the  $\lambda_3$  equation this originates from a balancing of the gluon contribution with the

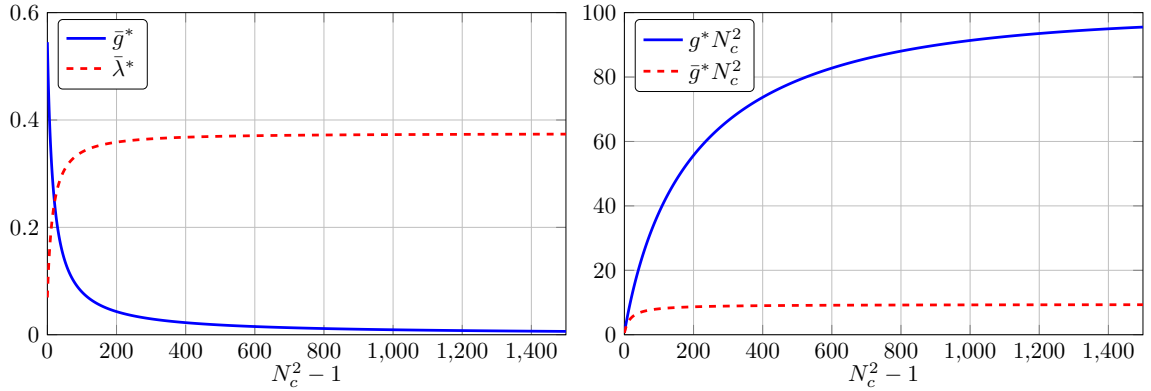


Figure 7.8.: Displayed are the background couplings  $\bar{g}^*$  and  $\bar{\lambda}^*$  (left) as well as the 't Hooft couplings  $g^*N_c^2$  and  $\bar{g}^*N_c^2$  as a function of  $N_c^2 - 1$  evaluated at the UV fixed point displayed in Fig. 7.7. The coupling  $\bar{g}^*$  is going to zero with  $\frac{1}{N_c^2}$  and  $\bar{\lambda}^*$  goes to the constant 0.38, see (7.52). The 't Hooft couplings reach the asymptotic values  $g^*N_c^2 \rightarrow 89$  and  $\bar{g}^*N_c^2 \rightarrow 9.4$ , see (7.50) and (7.52).

canonical term. In the  $\mu$  equation on the other hand all contributions go to zero in leading order and the fixed point value of  $\mu$  follows from the second order contributions. The asymptotic anomalous dimensions follow as

$$\begin{aligned} \eta_h(0) &\rightarrow 2 + \frac{2.7 \cdot 10^3}{N_c^2}, & \eta_h(k^2) &\rightarrow 0.36 + \frac{2.9 \cdot 10^2}{N_c^2}, \\ \eta_c(0) &\rightarrow -\frac{1.3 \cdot 10^2}{N_c^2}, & \eta_c(k^2) &\rightarrow -\frac{1.5 \cdot 10^2}{N_c^2}, \\ \eta_a(0) &\rightarrow -\frac{8.7}{N_c^2}, & \eta_a(k^2) &\rightarrow -\frac{22}{N_c^2}, \end{aligned} \quad (7.51)$$

which satisfy the bounds  $\eta_i \leq 2$  necessary for the consistency of the regulators that are proportional to  $Z_h, Z_c, Z_a$ . Note that only the graviton anomalous dimension is non-vanishing in this limit. Importantly the gluon anomalous dimension approaches zero from the negative direction, which means that it supports asymptotic freedom in the Yang-Mills sector. The asymptotic value  $\eta_h(0) = 2$  follows directly from the demand that all contributions in the  $\mu$  equation have to go to zero in leading order, as discussed in the last paragraph. The critical exponents are given by

$$\theta_{1,2} \rightarrow 1.2 \pm 2.1i + \frac{(1.1 \mp 5.6i) \cdot 10^3}{N_c^2}, \quad \theta_3 \rightarrow -2.3 - \frac{14 \cdot 10^3}{N_c^2}. \quad (7.52)$$

The fixed point has two attractive and one repulsive direction for all colours. Remarkably the values of the critical exponents remain of order one. The background couplings approach the values

$$\bar{g}^* \rightarrow \frac{9.4}{N_c^2} - \frac{1.3 \cdot 10^2}{N_c^4}, \quad \bar{\lambda}^* \rightarrow 0.38 - \frac{1.4}{N_c^2}. \quad (7.53)$$

Again, the background 't Hooft coupling  $\bar{g}^*N_c^2$  remains finite in the large  $N_c$ -limit, which is also displayed in Fig. 7.8.

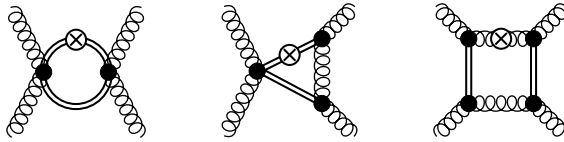


Figure 7.9.: Diagrammatic depiction of the graviton induced higher order gluon interactions. The wiggly lines are gluon propagators, and the double line represent graviton propagators.

In summary we have found a stable UV fixed point with two attractive directions. The fixed point values, the critical exponents and the anomalous dimensions are of order one. In Fig. 7.7 we display this behaviour up to  $N_c^2 = 1500$  and in this section we have augmented this with a solution for  $N_c \rightarrow \infty$ . Consequently we conclude that the system is asymptotically safe in the gravity sector and asymptotically free in the Yang-Mills sector for all  $N_c$ .

### 7.6.3. Decoupling of gravity-induced gluon self-interactions

It has been advocated in [420] that interacting matter-gravity systems necessarily contain self-interacting matter fixed points. This has been investigated in scalar, fermionic and Yukawa systems in e.g. [122, 387, 433].

Recently, also a Yang-Mills-gravity system with an Abelian  $U(1)$  gauge group has been investigated [432]. It was found that the coupling of the fourth power of the field strength,  $F^4$ , takes a finite fixed point value, while the minimal coupling that enters the covariant derivative can be asymptotically free. As already mentioned before in Sec. 7.4, the same happens in Yang-Mills-gravity systems. In particular we are led to

$$w_2^* (\text{tr} F_{\mu\nu}^2)^2 + v_4^* \text{tr} F_{\mu\nu}^4, \quad (7.54)$$

with  $w_2^* \neq 0$  and  $v_4^* \neq 0$  without non-trivial cancellations. A quantitative computations of these fixed point couplings is deferred to future work. Here we simply discuss their qualitative behaviour: even if not present in the theory, the couplings  $w_2$  and  $v_4$  are generated by diagrams with the exchange of two gravitons, see Fig. 7.9. In leading order these diagrams are proportional to

$$\frac{g^2}{(1+\mu)^3} \propto \frac{1}{N_c^4} \rightarrow 0, \quad (7.55)$$

and vanish in the large  $N_c$  scaling of (7.50). It is simple to show that the further diagrams in the fixed point equations of  $w_2, v_2$  proportional to  $w_2, v_2$  decay even faster when using (7.55) for the diagrams.

Finally, we get additional gluon tadpole contributions proportional to  $w_2^*$  and  $v_4^*$  for the running of the Yang-Mills beta function. In leading order these contributions are proportional to  $N_c^2$  due to a closed gluon loop. Together with the fixed point scaling of  $w_2^*$  and  $v_4^*$  in (7.55) this leads to a  $1/N_c^2$ -decay of these contributions. They have the same large  $N_c$ -scaling as the pure gravity contributions but also share the same negative sign supporting asymptotic freedom, see [432] for a study in  $U(1)$ -theories.

We close this section with a qualitative discussion of the stability for the interacting fixed point: As  $\omega_2$  and  $v_2$  do not couple into the pure gravity subsystem, the stability matrix is

skew-symmetric, and the eigenvalues are computed in the respective sub-systems. Both, the gravity as well as the  $\omega_2$  and  $v_4$  sub-systems are stable in the limit  $g \rightarrow 0$ .

This concludes our analysis of the large  $N_c$ -behaviour of quantum gravity with the flat regulator and the identification (7.22). As expected, Newton's coupling  $g$  shows the  $1/N_c^2$ -behaviour discussed in Sec. 7.2.

## 7.7. UV dominance of gravity

### 7.7.1. Dynamical scale fixing

In Sec. 7.6 we used the identifications of all Newton's couplings (7.22). In the present section we discuss the general case without this identification. We provide a comprehensive summary of results and the underlying structure, more details can be found in App. E.3. While we have argued in Sec. 7.2 that the present Yang-Mills-gravity system, as well as all free-matter-gravity systems are asymptotically safe, the interesting question is how and if at all in the present approximation this is dynamically observed.

Within the iterative procedure in Sec. 7.2 we arrived at a fixed point action that is identical to that of the pure gravity sector with fixed point values for  $g_n^*$ ,  $\lambda_n^*$ , and  $\mu^*$ . We also have  $g_a = g_3$  due to the expansion of the metric  $g_{\mu\nu} = \bar{g}_{\mu\nu} + \sqrt{Z_h g_3} k h_{\mu\nu}$  with  $k = k_h$ . Note also that in such a two-scale setting with  $k_h$  and  $k_a$  the latter rather is to be identified with  $k_a^{\text{UV}}$  and not with  $k_a^{\text{IR}}$ . As the effect of the latter has been absorbed in a renormalisation of Newton's coupling prior to the integrating-out of graviton fluctuations (or rather their suppression with  $k_h \rightarrow \infty$ ), this sets the graviton cutoff scale  $k_h = k$  as the largest scale in the system. This leads to (7.17) that effectively induces

$$k^2 \simeq N_c^2 k_a^2, \quad (7.56)$$

in the large  $N_c$  limit. Note that with a rescaling of our unique cutoff scale in Sec. 7.6 with  $N_c^2$  we already arrive at the  $N_c$ -independent fixed point values (7.50). The large values come from dropping the  $N_c$ -independent prefactor in the ratio  $G/G_{\text{eff}}$ . The latter fact signals the unphysical nature of fixed point values, which within this two-scale setting also extends to the product  $g^* \lambda^*$ , typically used in the literature as a potentially rescaling-invariant observable.

Despite (7.17) being a natural relative scale setting, without any approximation the full system of flow equations with  $k_h = k_a$  should adjust itself dynamically to this situation with  $g_a^* \sim g_c^* \sim g^*$  and with  $g^* \propto 1/N_c^2$  in the large  $N_c$ -limit. In the present approximation this can happen via two mechanisms that both elevate the graviton fluctuations to the same  $N_c$ -strength as the gluon fluctuations: the graviton propagator acquires a  $N_c$ -scaling

$$k^2 G_h(p^2 = 0) = \frac{1}{Z_h} \frac{1}{1 + \mu} \propto N_c^2, \quad (7.57)$$

after an appropriate rescaling of the couplings, for more details see App. E.3. We proceed by discussing the two dynamical options that the system has to generate the  $N_c$ -scaling in (7.57):

- (1) Evidently, (7.57) can be achieved via

$$\mu^* \propto -1 + c_+/N_c^2, \quad (7.58)$$

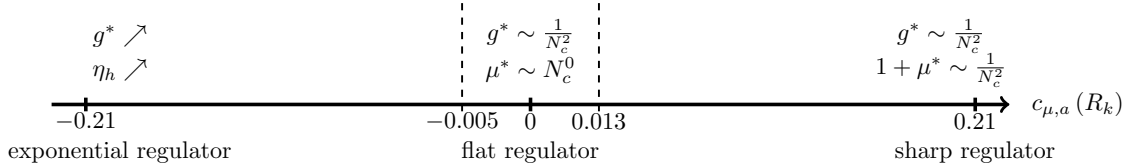


Figure 7.10.: Schematic picture of the dynamical scale re-adjustment mechanisms as a function of the coefficient  $c_{\mu,a}(R_k)$ .

with a positive constant  $c_+$ . Note that (7.58) is not present in the fixed point results in Sec. 7.6. Accordingly adding the fixed point equation for  $g_a$  has to trigger this running. Below we shall investigate this possibility in more detail.

(2) The  $N_c$ -scaling can also be stored in  $1/Z_h$ . As we have chosen regulators that are proportional to  $Z_h$  this leads to an effective elimination of  $Z_h$  from the system, its only remnant is the anomalous dimension  $\eta_h$  in the cutoff derivative. Since  $1/Z_h \propto (k^2)^{\eta_h/2-1}$ , the anomalous dimension  $\eta_h$  has to grow large and positive in order to effectively describe the  $N_c$ -scaling in (7.57):

$$\eta_h \rightarrow \infty. \quad (7.59)$$

In the present setting with  $R_{h,k} \propto Z_h$  this option cannot be investigated as (7.59) violates the bound

$$R_{h,k} \propto Z_h \quad \Rightarrow \quad \eta_h < 2, \quad (7.60)$$

for the regulator. For  $\eta_h > 2$  the regulators of type (7.60) cannot be shown to suppress UV degrees of freedom anymore in the limit  $k \rightarrow \infty$  as  $\lim_{k \rightarrow \infty} R_k(p^2) \rightarrow 0$  for  $\eta_h > 2$ . This bound was introduced in Sec. 6.3.4, where  $\eta_h$  grows beyond this bound for a large number of scalars. It was stated there that the stability of the scalar-gravity system could not be investigated conclusively since the regulator cannot be trusted anymore. In the light of the present results and discussion we know that the free-matter system is asymptotically safe. Then, the growing  $\eta_h$  signals that the system wants to accommodate (7.57) with a growing  $1/Z_h$ .

We emphasise that the physics of both options, (1) and (2), is captured by (7.57) and is identical. Which part of the scaling of the propagator is captured by  $\mu$  and which one by  $Z_h$  is determined by the projection procedure. Note that the latter is also approximation dependent.

In summary the coupled Yang-Mills–gravity system approaches the large  $N_c$  limit via (7.57). Whether or not this is seen in the current approximation with the cutoff choice (7.60) is a technical issue. If the approximation admits option (1) then the fixed point can be approached, if (2) or a mixture of (1) and (2) is taken then the fixed point cannot be seen due to the regulator bound in our setup. We emphasise again that this does not entail the non-existence of the fixed point, which is guaranteed by the analysis of Sec. 7.2. The analysis here evaluates the capability of the approximation to capture this fixed point. The understanding of this structure and guaranteeing this capability of the approximation is of chief importance when evaluating the stability of more complex matter-gravity systems with genuine matter self-interaction: No conclusion concerning the stability of

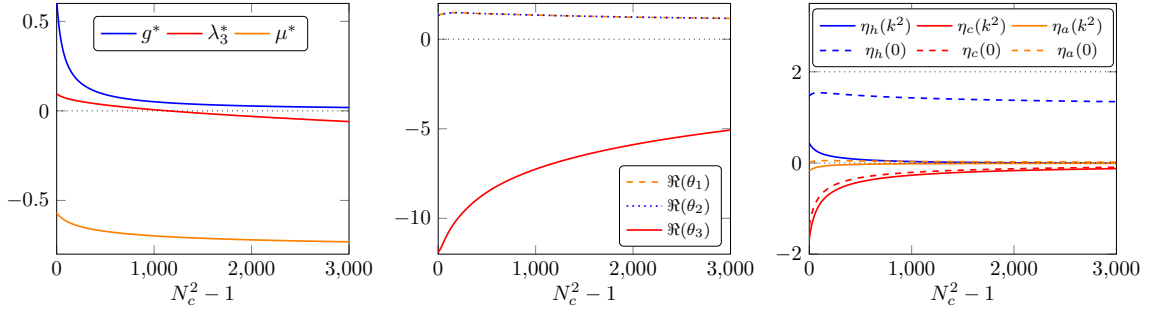


Figure 7.11.: Properties of the UV fixed point as a function of  $N_c^2 - 1$  in the uniform approximation with one Newton's coupling and with  $c_{\mu,a} = \frac{1}{24\pi} \approx 0.0133$ . Displayed are the fixed point values (left panel), the critical exponents (central panel), and the anomalous dimensions (right panel).

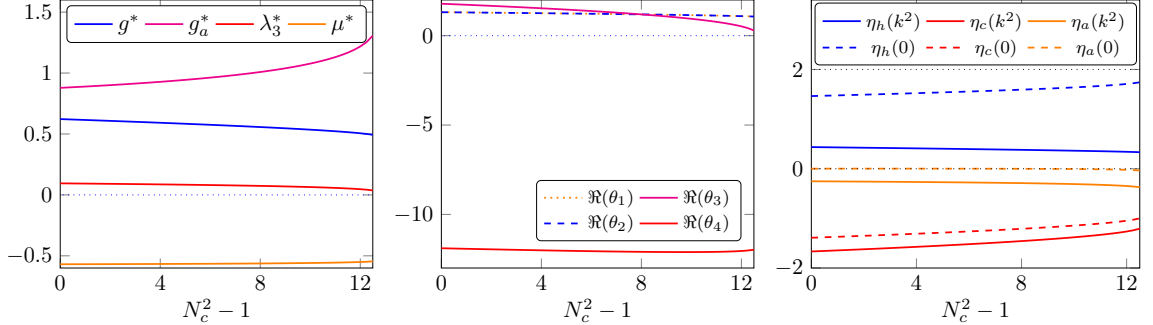


Figure 7.12.: Properties of the UV fixed point as a function of  $N_c^2 - 1$  in the approximation with two Newton's couplings and with the flat regulator,  $c_{\mu,a} = 0$ . Displayed are the fixed point values (left panel), the critical exponents (central panel), and the anomalous dimensions (right panel).

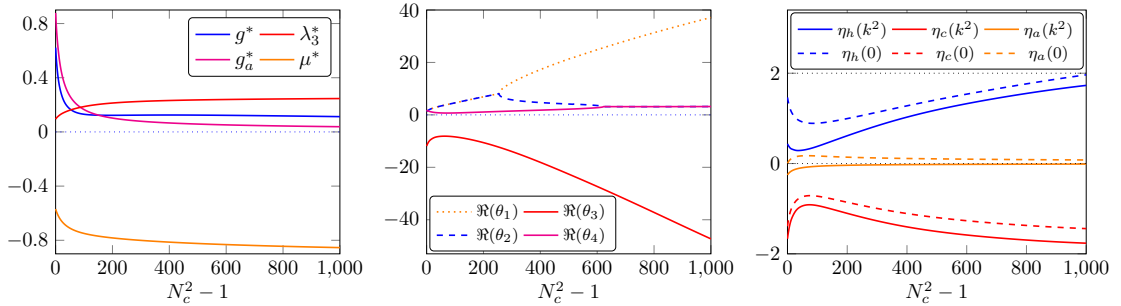


Figure 7.13.: Properties of the UV fixed point as a function of  $N_c^2 - 1$  in the approximation with two Newton's couplings and with  $c_{\mu,a} = \frac{1}{4\pi} \approx 0.08$ . Displayed are the fixed point values (left panel), the critical exponents (central panel), and the anomalous dimensions (right panel).

these systems can be drawn if the capability problem for the free-matter–gravity systems is not resolved. Moreover, even if the fixed points exist, their physics may be qualitatively biased by this problem.

### 7.7.2. Results in the extended approximation

In the following analysis we concentrate on the  $g_a$  fixed point equation and keep  $g_c = g$ . Before we extend the approximation to this case, let us re-evaluate the results with  $g_a = g$  in the light of the last Sec. 7.7.1. There it has been deduced that a consistent  $N_c$ -scaling requires  $g^* \propto 1/N_c^2$  and either (7.58) or (7.59), or both. Fig. 7.7 shows the consistent large  $N_c$ -scaling for Newton's coupling but neither (7.58) nor (7.59). This comes as a surprise as the system is asymptotically safe and the large  $N_c$ -limit in the approximation  $g = g_a$  is seemingly stable. To investigate this stability we examine the regulator-dependence of the coefficients of the flow equations. To that end we notice that the coefficients in the  $\mu$  equation (and the  $g_3, g_a$ -equations) are of crucial importance for the stability of the system. The coefficient  $c_{\mu,a} = -1/(60\pi)\eta_a$  of the Yang-Mills contribution to the graviton mass parameter is proportional to the gluon anomalous dimension  $\eta_a$ : the leading coefficient vanishes, see (E.10) and (E.16). Indeed, choosing other regulators, the leading order term is non-vanishing with

$$-0.2 \lesssim c_{\mu,a}(R_k) \lesssim 0.2, \quad (7.61)$$

see App. E.2. Typically, it supersedes the  $\eta_a$ -dependent term, and the flat regulator appears to be a very special choice. If  $c_{\mu,a} \gtrsim 0.013$  we indeed find a solution, which is consistent with (7.58), see Fig. 7.11 for  $c_{\mu,a} = \frac{1}{24\pi} \approx 0.0133$ . In turn, for  $c_{\mu,a} \lesssim -0.005$  we find solutions with growing  $\eta_h$ , hence in the class (7.59). Accordingly, this solution is not trustworthy with  $\eta_h$  beyond the bound (7.60). Its failure simply is one of the approximation (within this choice of regulator) rather than that of asymptotic safety.

In summary this leads us to a classification of the regulators according to the large  $N_c$ -limit: they either induce the dynamical re-adjustment of the scales via (7.58) or via (7.59) or they fall in between such as the flat cutoff. Within the current approximation it is required that the re-adjustment happens via (7.58).

Now we are in the position to discuss the general case with  $g_a \neq g$ . An optimal scenario would be that the inclusion of the  $g_a$  equation already stabilises the system such that it enforces the dynamical re-adjustment via (7.58) for all regulators proportional to  $Z_h$ . However, as we shall see, the general scheme from the uniform approximation persists with this upgrade of the approximation.

#### No apparent $N_c$ -scaling for $\mu$ and $\eta_h$

In the uniform approximation with one Newton's coupling (7.22) this scenario was taken with regulators with  $-0.005 \lesssim c_{\mu,a} \lesssim 0.013$ . A typical regulator in this class is the flat regulator used in this chapter. This scenario does not enhance the graviton propagator and hence does not fulfil (7.57). The stability of the results in the large  $N_c$ -limit in the uniform approximation must thus rather be considered a mere coincidence. Indeed in the extended truncation with  $g \neq g_a$  the enhancement of the graviton propagator is not triggered by the included  $g_a$  equation and consequently the flat regulator does not have a stable large  $N_c$ -limit anymore. The fixed point values, critical exponents and the anomalous dimensions in this approximation are shown in Fig. 7.12. The fixed point values show a marginal  $N_c$ -dependence up to the point where the fixed point vanishes into the complex plane at  $N_c^2 \approx 13.5$ , which is signalled by one of the critical exponents going towards zero. The vanishing critical exponent can be associated with  $g_a$ . Typically this is interpreted as a sign for the failure of asymptotic safety. Here it is evident that the truncation cannot

accommodate the dynamical re-adjustment of the scales that takes place in the full system. This could also signal an over-complete system:  $g$  and  $g_a$  are related by diffeomorphism invariance. In any case the failure of the approximation can either lead to the divergence of the couplings (related to (7.59)), or in complex parts of the fixed point values. For the flat regulator the latter scenario is taken.

### Scenario with $1 + \mu \propto 1/N_c^2$

This scenario requires regulators with  $c_+ < c_{\mu,a} < c_{\max}$ . A typical regulator in this class is the sharp regulator, see (E.2) and Fig. 7.10. Here we do not present a full analysis of this case but only change the coefficient  $c_{\mu,a}$  accordingly. This is justified in terms of linear small perturbations of the system:  $c_{\mu,a}$  is the only leading order coefficient in the system that exhibits a qualitative change when changing the regulator away from the flat regulator. Note however, that this change ceases to be small for large  $N_c$  as  $c_{\mu,a}$  is multiplied by  $N_c^2$ . If accompanied by a respective change of the relative cutoff scales  $k_h/k_a$  this factor could be compensated. Then, however, we are directly in the stable regulator choice with (7.17). Here we are more interested in the dynamical stabilisation and we refrain from the rescaling. The system exhibits the  $1/N_c^2$ -scaling in the Newton's couplings,  $g^*$  and  $g_a^*$ , as well as the mass parameter  $\mu^*$ , see Fig. 7.13 for  $c_{\mu,a} \approx 0.08$ . However, with this choice the critical exponents of the fixed point become rather large. We determined the constant  $c_+ \approx 0.07$ .

### Scenario with $\eta_h$ growing large

This scenario requires regulators with  $-c_{\min} < c_{\mu,a} < -c_-$ . A typical regulator in this class is the exponential regulator, see (E.2) and Fig. 7.10. For this class of regulators both couplings grow large and we have the scenario with (7.59) bound to fail to provide fixed point solutions beyond a maximal  $N_c$  due to the failure of the approximation scheme.

### 7.7.3. Resumé: Signatures of asymptotic safety of Yang-Mills–gravity systems

In summary with the choice of the regulator we can dial the different scenarios that all entail the same physics: the dynamical re-adjustment of the respective scales in the gauge and gravity subsystems and the asymptotic safety of the combined system. The two different scenarios are described in Sec. 7.7.2 and Sec. 7.7.2. Both scenarios entail the same physics mechanism: the enhancement of the graviton propagator, see (7.57). This triggers the dominance of gravity in the UV, which is clearly visible in the consecutive integrating-out of degrees of freedom discussed in Sec. 7.2. The crucial property for the validity of this structure is the asymptotic freedom of the Yang-Mills system, and hence the existence of the gauge system in a given background. This property is trivially present in systems with free matter coupled to gravity, and hence the present analysis extends to these cases.

This leaves us with the question of how to re-evaluate the existing results on matter–gravity system in the light of the present findings. We first notice that the helpful peculiarity of the Yang-Mills–gravity system that allowed us to easily access all the different scenarios, is the possibility to choose the sign of  $c_{\mu,a}$  with the choice of the regulator. Clearly, the gauge contribution to the running of the graviton mass parameter plays a

pivotal rôle for how the enhancement of the graviton propagator in (7.57) is technically achieved. In the other matter-gravity system this parameter has a definite sign, which is why one sees a specific scenario for typical regulators. Collecting all the results and restricting ourselves to truncations that resolve the difference between fluctuation and background fields we find:

- (1) Fermion-gravity systems: they fall into the class [Sec. 7.7.2](#), and the asymptotic safety of the system can be accessed in the approximation. The required large flavour  $N_f$  pattern with (7.58) is visible in the results.
- (2) Scalar-gravity systems: they fall into the class [Sec. 7.7.2](#), and for large enough number of scalars  $N_s$  the fixed point seemingly disappears due to the fixed point coupling  $g^*$  and anomalous dimension  $\eta_h$  growing too large.
- (3) Vector-gravity/Yang-Mills-gravity systems: this system has been discussed here and it falls into all classes, [Sec. 7.7.2](#), [Sec. 7.7.2](#) and [Sec. 7.7.2](#). This also includes the  $U(1)$ -system.
- (4) Self-interacting gauge-matter-gravity systems: these systems only fall into the pattern described in [Sec. 7.7.2](#), [Sec. 7.7.2](#) and [Sec. 7.7.2](#) if the gauge-matter system is itself UV stable. For example, one flavour QED exhibits a UV-Landau pole and is stabilised by gravity, which makes the combined system asymptotically safe, for a comprehensive analysis see [432, 435]. Adding more flavours potentially destabilises the system, however such an analysis has to avoid the interpretation of the seeming failure of asymptotic safety described here. One possibility to take this into account is the scale-adjustment (7.17). This discussion also carries over to general gauge-matter-gravity systems including the Standard Model and its extensions.

In summary this explains the results obtained in gravitationally interacting gauge-matter-gravity systems, which are the basis of general gauge-matter-gravity system. While it suggests the use of relative cutoff scales such as (7.17) it still leaves us with the task of devising approximations that are capable of capturing the dynamical re-adjustment of scales that happens in gravitationally interacting gauge-matter-gravity systems. In particular, the marginal operator  $R^2 \ln(1 + R/k_a^{\text{IR}})$ , cf. (7.14), has to be included as discussed in [Sec. 7.2.2](#).

Besides this task the present analysis also requires a careful re-analysis of phenomenological bounds on UV fixed point couplings. It is well-known that the values of the latter are subject to re-scalings and only dimensionless products of couplings such as  $g^* \lambda^*$  possibly have a direct physical interpretation. We have argued here that the dynamically adjusted or explicitly adjusted relative cutoff scales ask for a reassessment also of these dimensionless products.

## 7.8. Summary

We have investigated the prospect for asymptotic safety of gravity in the presence of general matter fields. A main new addition are general arguments, which state that if matter remains sufficiently weakly coupled in the UV, or is even asymptotically free, then asymptotic safety for the combined matter-gauge-gravity theory follows, in essence, from asymptotic safety of pure gravity, cf. [Sec. 7.2](#). Ultimately, the UV dominance of gravitons

relates to the fact that integrating out UV free matter fields only generates local counter terms in the gravitational sector. This argument assumes the absence of marginal terms in the full theory such as  $R^2 \ln R$ , in line with assumptions commonly used in the study of matter-gauge-gravity systems. Interestingly, this setup can now be understood as a consistent matter-gauge-gravity theory, which *does* contain marginal terms in the classical gravity action. It is the renormalisation of the latter that removes the flavour dependence.

Our reasoning has been tested comprehensively for Yang-Mills theory coupled to gravity. Using identical cutoffs for gravity and matter, we invariably find that asymptotic safety arises at a partially interacting fixed point with asymptotic freedom in the Yang-Mills and asymptotic safety in the gravity sector. Fluctuations of the gravitons dominate over those by matter fields including in the asymptotic limit  $N_c \rightarrow \infty$ , where we were able to provide explicit results, see Sec. 7.6.2. Interestingly, the UV dominance of gravity can materialise itself in different manners, see Fig. 7.11, 7.12 and 7.13, strongly depending on technical parameters of the theory such as the gauge, the regularisation, and the momentum cutoff. We have visualised this in Fig. 7.10. The overall physics, the UV dominance of gravity fluctuations, is not affected. This pattern is reminiscent of how confinement arises in gauge-fixed continuum formulations of QCD. It is also worth noting that the observed  $N_c$ -independence with identical cutoffs follows automatically, if, instead, "relative cutoff scales" for matter- and gravity-fluctuations are adopted, following (7.17). This may prove useful for practical studies of gravity-matter systems in set approximations. The necessity for "relative cutoff scales" is well-understood in condensed matter systems, albeit for other reasons [465, 466].

There are several points that would benefit from further study in the future. While we explained in general terms how findings extend to more general matter sectors, see Sec. 7.7, it would seem useful to further substantiate this in explicit studies. Also, our study highlighted the appearance of logarithmic terms such as  $R^2 \ln R$ , and similar, see Sec. 7.2. These classically marginal terms are of relevance for the question of unitarity of asymptotically safe gravity. It remains to be seen whether they affect the observed  $N_c$ -independence of gravity-matter fixed points in any significant manner, see Sec. 7.7. Finally, our findings offer a natural reinterpretation of earlier results, as the ones from the previous chapter. It is important to confirm whether this is sufficient to remove a tension amongst previous findings based on different implementations of the renormalisation group, namely with and without background field approximation.



# 8. Effective universality in quantum gravity

## 8.1. Introduction

The discussions and the results from the last chapters have put emphasis on the fact that disentangling background and fluctuation field is a necessary task. This is related to keeping track of diffeomorphism invariance and background independence. In the present chapter we address two questions that are ultimately linked to these key properties:

The first question concerns the dynamical couplings of gravity-matter systems. Gauge theories feature different *avatars* of the gauge coupling, a prominent example being the different avatars of the running gauge couplings in the Standard Model. For instance, in QED the running electric coupling can be extracted from the wave function of the photon or from the running of the electron-photon vertex. This relation can be derived from the Ward identities in QED. In QCD the running of the gauge coupling can be extracted from different combinations of vertex and propagator scalings including, e.g., the three-gluon vertex and the quark-gluon vertex. Again this can be derived from the identities following from the gauge symmetry, in this case the Slavnov-Taylor identities.

In these examples the respective couplings are marginal and exhibit two-loop universality. This facilitates the identification. In gravity the above universality holds for the (marginal)  $R^2$  and  $R_{\mu\nu}^2$  couplings. However, the couplings in the classical Einstein-Hilbert action and the minimal couplings to matter are dimensionful and universality is not expected anymore on the quantum level. Still, the multi-graviton couplings related to Taylor expansions of the terms in the classical action, e.g.  $\sqrt{g}R$  and  $\sqrt{g}\Lambda$  agree on the classical level and are related by Slavnov-Taylor identities in quantum gravity. It is an intriguing physics question and of paramount technical importance, whether for all practical purposes these relations nevertheless facilitate an identification, for example, between all *avatars* of the minimal coupling in gravity, the Newton's coupling  $G_N$ . We call this scenario *effective universality*, which is detailed in the next section. In this chapter we investigate this question focusing on the dynamical pure gravity coupling and the dynamical gravity-scalar coupling. We stress that due to the dimensionful nature of the couplings, different *avatars* of the Newton's coupling could agree if evaluated within the same scheme, but depend of course e.g. on the choice of regulator in the context of an FRG setup. Here, universality is not to be understood in the sense of scheme-independence at the two-loop level.

Indeed, we find that the fixed point values and the leading coefficients of the above two couplings agree on a semi-quantitative level as a function of the number of minimally coupled scalars. These computations of dynamical couplings in a vertex expansion about a flat background extend the works of the previous chapters, in particular [Chapter 6](#).

The second question concerns the couplings of the background metric. These couplings are related via Ward-identities. Additionally, they are related to the dynamical couplings discussed above via Nielsen identities or split Ward identities. Importantly, these identities also carry the background independence of quantum gravity. In this chapter we also investigate the question to what extent the *avatars* of the background couplings can be

identified with that of the fluctuation couplings. We emphasise that this identification is at the root of the background field approximation whose background independence stands or falls with the validity of this identification.

In this chapter we do not only critically compare the avatars of the background Newton's coupling to that of the fluctuation coupling, we also further improve the background coupling to a level-one coupling with the explicit use of a Nielsen identity. We find that the effective universality, that exists between the dynamical couplings, is not present for the background and the level-one couplings. However, general qualitative features of the flow equations, such as as the sign of the scalar contribution, are preserved for all couplings but the background cosmological constant in comparison to the graviton mass parameter.

## 8.2. Avatars of couplings and effective universality

In this section we explain the origin of different avatars of couplings in the effective action of matter-gravity systems. We further discuss their relation via the modified symmetry relations, STIs and Nielsen-identities, that are derived from the underlying diffeomorphism invariance and its breaking in the presence of cutoff terms. In short, effective universality is the notion that these complicated symmetry identities are well approximated by Ward-identities, that is a diffeomorphism-invariant approximation of the effective action, for more details see [Sec. 8.2.2](#).

### 8.2.1. Avatars of couplings in matter-gravity systems

Asymptotically safe matter-gravity systems and their physics can be described in terms of the effective action  $\Gamma[\bar{g}, \phi]$ . In [Sec. 3.3.2](#) we have expanded this effective action in correlation  $n$ -point functions. Each of these  $n$ -point vertices is equipped with a coupling  $G_{\vec{n}}$ , where the vector  $\vec{n}$  consists of the numbers of the different dynamical fields, in the present scalar-gravity setting  $\phi = (h_{\mu\nu}, c_\mu, \varphi, \dots)$ , that take part in the process,

$$\vec{n} = (n_h, n_c, n_\varphi, \dots). \quad (8.1)$$

The couplings  $G_{\vec{n}}$  are avatars of the gravitational self-coupling  $G_N$ . In the present study we focus on gravity-scalar couplings. This leaves us with couplings labelled by two indices

$$G_{(n_h, n_\varphi)}. \quad (8.2)$$

In this chapter we denote dimensionless versions of Newton's coupling by capital letters, e.g. as above  $G_{(n_h, n_\varphi)}$ , and dimensionful versions with an additional over-bar, such as  $\bar{G}_{(n_h, n_\varphi)}$ . The fluctuation couplings  $G_{(n_h, n_\varphi)}$  defined in [\(8.2\)](#) are related to the expansion coefficients in an expansion in powers of  $h_{\mu\nu}$  and  $\varphi$ , the couplings  $G_{(n_{\bar{g}}, n_\varphi)}$  are related to those in an expansion in powers of  $\bar{g}_{\mu\nu}$  and  $\varphi$ . The respective vertices are given by

$$\Gamma^{(n, m, l)}(p_1, \dots, p_{n+m+l}) = \frac{\delta^{n+m+l} \Gamma[\bar{g}, h, \varphi]}{\delta \bar{g}^n(p_1, \dots) \delta h^m(\dots, p_i, \dots) \delta \varphi^l(\dots, p_{n+m+l})}, \quad (8.3)$$

where we suppress the indices on  $\bar{g}_{\mu\nu}$  and  $h_{\mu\nu}$  for brevity of notation. The couplings [\(8.2\)](#) can now be defined by [\(8.3\)](#) at selected kinematic configurations. In this chapter, we focus on  $G_{(3,0)}$  and  $G_{(1,2)}$  defined at the momentum symmetric point. The former coupling relates to the scattering of three gravitons, and is derived from the pure gravity part of

the effective action. The coupling  $G_{(1,2)}$  relates to the scattering of one graviton and two scalars, and is derived from the kinetic term of the scalars. This coupling is also present in the free -no self-interaction- scalar theory and can be considered the fundamental coupling of scalar fields to gravity.

Evidently these couplings cannot be defined uniquely and depend on the given kinematical limit. Note that this even holds for dimensionless couplings beyond one loop, despite their universal RG running. Accordingly, the evaluation of, e.g., scattering processes with different momentum configurations requires an analysis of the corresponding  $n$ -point vertex as a function of all its independent momenta, i.e., a simple function of one momentum cannot capture the full dynamics adequately. If dealing with an approximation to the theory at hand that does not maintain the full momentum-dependence of vertices, a typical choice is the symmetric point, for higher-order vertices a symmetric point. Using these momentum configurations can lead to semi-quantitative agreement with the full results even in strongly-correlated systems, see [Chapter 3](#) and for a resent work in QCD see [\[463\]](#). For a related interesting discussion in the effective field theory approach to gravity see [\[468\]](#). Keeping this caveat in mind, we proceed with our evaluation whether avatars of the Newton's coupling, defined using the symmetric momentum configuration of various three-point vertices, show semi-quantitative agreement.

With the dynamical vertices [\(8.3\)](#) and the dynamical propagators we can compute the background vertices, that is the  $S$ -matrix elements. This leads to further avatars of the Newton's coupling, this time being directly related to S-matrix elements for the selected momentum configuration. In this chapter we consider the avatar of the Newton's coupling of the background curvature term in the action. It is distinguished from the  $G_{\vec{n}}$  by two properties: first it is the prefactor of a diffeomorphism invariant term in the action. Second, as a pure background quantity it does not drive the RG flow of the system, which is driven by the fluctuation field and its couplings. In this chapter, we refer to its dimensionless version as  $\bar{G}$  and the dimensionful version as  $G_N$ .

### 8.2.2. Effective universality

Already one diffeomorphism-invariant operator at the classical level, for example the curvature scalar  $\sqrt{g} R$  leads to infinitely many different couplings at the quantum level: These are obtained by taking the  $n$ th  $h_{\mu\nu}$ -derivative of  $\sqrt{g} R$  and projecting  $\Gamma^{(n)}$  (given a complete basis) on this tensor structure. While still being related by STIs they do not agree. In the presence of the regularisation these STIs turn into mSTIs.

The situation is slightly different for the  $n$ th order background couplings: they even agree at the full quantum level as they are related by Ward identities due to background diffeomorphism invariance. This property even survives the introduction of the regularisation. However, the computation of their beta functions requires the knowledge of the fluctuation vertices. They are related to the background vertices by the Nielsen or split Ward identities, which turns the Ward identities into the STIs. In the presence of the regularisation we have modified NIs as we have mSTIs.

This leaves us with the technical challenge of computing all these coupling avatars related to a given operator, in the present example the avatars of the Newton's coupling. Specifically, the challenge lies in the need to close a given system of flow equations for correlation functions that depend on the higher-order correlation functions. To that end one has to provide an ansatz for higher-order couplings for which the flow is not computed.

The canonical choice is their classical value. For standard QFTs this leads to vanishing higher-order couplings. In quantum gravity this canonical choice leads to an identification of all higher-order couplings derived from a given operator with the lowest order one, effectively restoring diffeomorphism invariance. This we call *effective universality*.

For example, let us assume for a moment that we only compute the flow of one avatar of the Newton's coupling. Then the canonical choice leads to the identification of all higher-order Newton's couplings with the lowest order one. If we apply this concept to the dynamical system, effective universality can be summarised by

$$G_{(n_h, n_\varphi)} \approx G, \quad n_h, n_\varphi \in \mathbb{N}, \quad (8.4)$$

with a unique Newton's coupling for a suitably chosen momentum configuration. One of the main aims of this chapter is to compare the scale dependence of these couplings under the impact of quantum fluctuations of the metric and of  $N_s$  scalar fields.

In its maximal version for both, background couplings and fluctuation couplings it can be summarised in a concise form of the effective action,

$$\Gamma[\bar{g}_{\mu\nu}, h_{\mu\nu}, \varphi] = \Gamma_{\text{diff}}[\bar{g}_{\mu\nu} + h_{\mu\nu}, \varphi] + \Delta\Gamma_{\text{gauge}}[\bar{g}_{\mu\nu}, h_{\mu\nu}, \varphi]. \quad (8.5)$$

with a diffeomorphism-invariant action  $\Gamma_{\text{diff}}[g]$  and

$$\Delta\Gamma_{\text{gauge}}[\bar{g}_{\mu\nu}, h_{\mu\nu}, \varphi] \approx S_{\text{gf}}[\bar{g}_{\mu\nu}, h_{\mu\nu}] + S_{\text{gh}}[\bar{g}_{\mu\nu}, h_{\mu\nu}, c_\mu], \quad (8.6)$$

with gauge fixing and ghost action,  $S_{\text{gf}}$  and  $S_{\text{gh}}$ , respectively, see [99, 469]. Furthermore, only the regulator terms would carry the breaking of background independence. This approximation is called the background field approximation, which has been predominantly used in the RG approach to quantum gravity as well as being paramount to effective field theory applications in quantum gravity.

In summary the quest for effective universality is directly related to the task of finding an efficient (rapidly convergent) expansion of the quantum effective action of matter-gravity systems in diffeomorphism-invariant operators. While this task is seemingly a technical one it is -in disguise- the quest for the dominating physics and phenomena that govern quantum gravity systems.

### 8.3. RG for scalar-gravity systems

We aim to shed light on the above issues and specifically explore in which settings effective universality may emerge in simple approximations. To that end we compare two avatars of the dynamical Newton's coupling. The first is defined from the three-graviton vertex, as in [Chapter 3](#), and its dimensionless version is called  $G_{(3,0)}$ . The second one is defined from the graviton-two-scalar vertex as in [429, 436], and is called  $G_{(1,2)}$ .

The computation of the flow equations is in analogy to the previous chapters. The classical action is given by the gauge-fixed Einstein-Hilbert action (3.4) and a kinetic part for the scalars,

$$S = S_{\text{EH}} + \frac{1}{2} \sum_{i=1}^{N_s} \int d^4x \sqrt{g} g^{\mu\nu} \partial_\mu \varphi^i \partial_\nu \varphi^i. \quad (8.7)$$

From this action we generate the ansatz for the  $n$ -point functions according to (3.16).

We compute flows up to the third order in the fluctuation field. In total we evaluate the coupled flow equations of the scale dependent dimensionless quantities

$$\bar{\lambda}, \bar{G}, \mu, \lambda_3, G_{(3,0)}, G_{(1,2)}, \eta_h(p^2), \eta_\varphi(p^2), \eta_c(p^2). \quad (8.8)$$

The background couplings  $\bar{\lambda}$  and  $\bar{G}$  do not enter the flow and thus do not affect the fluctuation couplings. Their flow equations are analytic and derived using the York-decomposition [81, 470] with field redefinitions [247, 413]. The explicit pure gravity flow equation for our gauge is displayed in [262] and App. B.2. The  $N_s$ -dependent part is gauge independent and thus equal to, e.g. [424] and App. D.2. The flow equations for  $\mu$  and  $\lambda_3$  are also analytic and are given in App. B.6 and D.1 (the coupling  $G_{(1,2)}$  has to be disentangled from  $G_{(3,0)}$  in the appropriate terms). The momentum dependence of the Newton's couplings,  $G_{(3,0)}$  and  $G_{(1,2)}$ , and the anomalous dimensions is of importance, see App. B.4, and thus, it is preferable to evaluate these at finite momentum, which does not allow for analytic equations. Nevertheless the analytic version of these flows leads to qualitatively reliable results. The analytic and momentum dependent versions of  $G_{(3,0)}$ ,  $\eta_h$ , and  $\eta_\varphi$  agrees with the ones in Chapter 6. Again  $G_{(1,2)}$  has to be distinguished from  $G_{(3,0)}$ . The analytic version of  $G_{(1,2)}$  is the same as in [436] while the momentum dependent version is derived here for the first time.

The  $\beta$ -function prescriptions for the Newton's couplings are given by

$$\begin{aligned} \beta_{G_{(3,0)}} &= (2 + 3\eta_h(k^2)) G_{(3,0)} - \frac{24}{19} (\eta_h(k^2) - \eta_h(0)) \lambda_3 G_{(3,0)} \\ &\quad + (32\pi)^2 \frac{64}{171} G_{(3,0)}^{1/2} \left( \text{Flow}_{tt,G_{(3,0)}}^{(hhh)}(k^2) - \text{Flow}_{tt,G_{(3,0)}}^{(hhh)}(0) \right), \\ \beta_{G_{(1,2)}} &= (2 + \eta_h(k^2) + 2\eta_\varphi(k^2)) G_{(1,2)} + \frac{8}{3} G_{(1,2)}^{1/2} \text{Flow}_{tt,G_{(1,2)}}^{(h\varphi\varphi)}(k^2). \end{aligned} \quad (8.9)$$

The notation is just as in (3.23). We used a bilocal projection for both couplings, but note that due to the shift symmetry in the scalar sector,  $\text{Flow}_{tt,G_{(1,2)}}^{(h\varphi\varphi)}(0) = 0$ .

## 8.4. Effective universality for the dynamical couplings

To address our first key question, we compare the beta functions and fixed point results for the dynamical system including  $G_{(3,0)}$ ,  $G_{(1,2)}$ ,  $\mu$  and  $\lambda_3$ . Note however that the  $\lambda_n$  and in particular  $\mu = -2\lambda_2$  take a special rôle due to the convexity of the effective action. To see this consider the effective action for classical gravity. It is the double Legendre transform of the classical action. Accordingly, for positive cosmological constant it only agrees with the classical action for large enough curvature. Thus, even for a diffeomorphism-invariant action the  $\lambda_n$  are not necessarily the same. In summary, in the reduced system under investigation effective universality may only hold directly for  $G_{(3,0)}$  and  $G_{(1,2)}$  even in case it is fully present. This leaves us with the two avatars of the Newton's coupling while  $\mu$  and  $\lambda_3$  should be evaluated in dependence of  $G_{(3,0)}$  and  $G_{(1,2)}$  on a given trajectory.

Note also that effective universality is necessarily broken at a finite cutoff scale as the regulators break diffeomorphism invariance. Accordingly it cannot hold quantitatively for all cutoff scales. It may hold at  $k \rightarrow 0$ , and potentially at  $k \rightarrow \infty$ . While the former physical case is evident, the latter case deserves some explanation: in the physics limit at  $k = 0$  and for momentum scales  $p \gg M_{\text{Pl}}$  we are in the scaling regime about the UV fixed

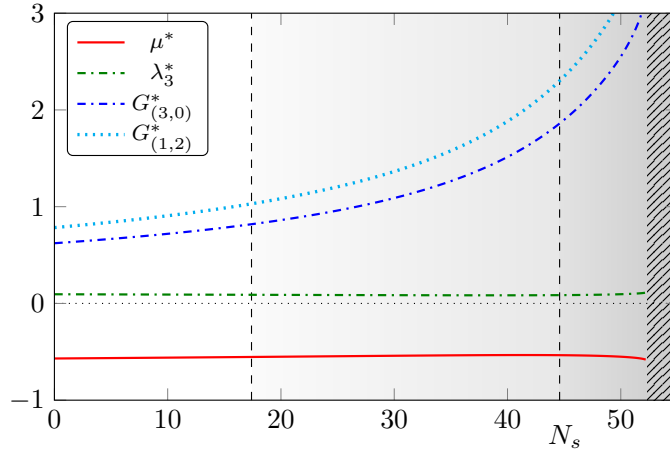


Figure 8.1.: Fixed-point values for the fluctuation couplings as a function of  $N_s$ . The vertical lines at  $N_s \approx 17.5$  and  $N_s \approx 44.6$  show where  $\eta_h(0)$  and  $\eta_h(k^2)$  exceed the value two, respectively.

point. If effective universality holds for  $k = 0$ , we have in particular  $G_{(3,0)}(p^2) \approx G_{(1,2)}(p^2)$ . If we now increase the cutoff scale, the scaling couplings are only changed for  $p^2 \approx k^2$ . Moreover, self-similarity in the scaling regime entails that  $k$ -scaling and  $p$ -scaling agree. Hence, *physical* effective universality at  $k = 0$  translates into effective universality of the cutoff-dependent couplings in the scaling regime.

We shall see that  $G_{(3,0)}$  and  $G_{(1,2)}$  indeed feature a quantitative effective universality on scaling trajectories close to the fixed point.

### 8.4.1. Effective universality at the fixed point

We solve the flow equations of the fully coupled fluctuation system,  $G_{(3,0)}$ ,  $G_{(1,2)}$ ,  $\mu$  and  $\lambda_3$  identifying all higher-order gravity couplings with  $G_{(n \geq 3,0)} = G_{(3,0)}$  and  $\lambda_{n \geq 3} = \lambda_3$ , and all graviton-scalar couplings with  $G_{(n,m \geq 2)} = G_{(1,2)}$ . The  $\beta$ -functions of the Newton's couplings are given schematically in (8.9).

The resulting fixed point values are shown in Fig. 8.1. We observe that both Newton's couplings have similar fixed point values that increase with  $N_s$ . The couplings  $\mu$  and  $\lambda_3$  remain approximately constant as a function of  $N_s$ . This already shows a qualitative effective universality for  $G_{(3,0)}$  and  $G_{(1,2)}$  that supports the reliability of computations where this property is used. The similar behaviour of the two avatars of the Newton's coupling for all  $N_s$  and the  $N_s$ -independence of  $\mu$  and  $\lambda_3$  suggests to first perform a detailed analysis at a fixed  $N_s$  and then a subsequent one of the  $N_s$ -dependence. For the first part of the analysis we choose  $N_s = 0$ . This is in complete analogy of the quenched approximation in QCD, where one drops all closed quark loops. In the present case it amounts to dropping all closed scalar loops.

### 8.4.2. Quenched quantum gravity

In the quenched limit with  $N_s = 0$ , a quantitative self-consistency analysis reveals an even more interesting property than the mere similarity observed in Fig. 8.1. To that end we remind ourselves that the bilocal projection used in the present fixed point computation

is based on observations in the pure gravity system in Sec. 4.2.2 for  $G_{(3,0)}$  and  $G_{(4,0)}$ . It was shown that the momentum dependence of the flow of the coupling  $G_{(3,0)}$  and  $G_{(4,0)}$  related to the curvature term  $R$  is quantitatively given by a linear  $p^2$ -dependence. The four-graviton vertex has an additional  $p^4$ -dependence related to the  $R^2$ -term, no higher order momentum-dependence is present. These properties are based on non-trivial cancellations between diagrams based on diffeomorphism invariance. It also hints already at effective universality. This situation suggests the following self-consistency analysis of effective universality for  $G_{(3,0)}$  and  $G_{(1,2)}$ : assume for the moment that effective universality works quantitatively at the fixed point, that is

$$G_{\vec{n}} = G \quad \text{with} \quad G = G_{(3,0)}, \quad (8.10)$$

for all avatars of the Newton's coupling. The self-consistency of (8.10) is tested quantitatively by evaluating the momentum-dependent  $\beta$ -functions  $\beta_{G_{(3,0)}}$  and  $\beta_{G_{(1,2)}}$  on (8.10) and the approximately  $N_s$ -independent fixed point values  $\mu^*$  and  $\lambda_3^*$ . Solving the momentum-dependent  $\beta$ -functions for the momentum-dependent couplings on the bilocal fixed point  $G^*$ ,  $\mu^*$  and  $\lambda_3^*$  leads us to

$$\begin{aligned} p^2 \sqrt{G_{(3,0)}(p^2)} &\simeq -\frac{64}{171} (32\pi)^2 \frac{\text{Flow}^{(3,0)}(p^2) - \text{Flow}^{(3,0)}(0)}{2 + 3\eta_h(p^2)} \Big|_{G^*, \mu^*, \lambda_3^*}, \\ p^2 \sqrt{G_{(1,2)}(p^2)} &\simeq -\frac{8}{3} \frac{\text{Flow}^{(1,2)}(p^2)}{1 + \eta_h(p^2) + 2\eta_\varphi(p^2)} \Big|_{G^*, \mu^*, \lambda_3^*}. \end{aligned} \quad (8.11)$$

Note that  $\eta_\varphi(p^2) = 0$  in the chosen gauge  $\beta = 1$  and  $\alpha = 0$ . The momentum-dependent fixed-point couplings are shown in Fig. 8.2. In the left panel we have shifted  $G_{(1,2)}(p^2)$  by its value at  $p^2 = k^2$  in order to make the quantitatively coinciding linear dependence for  $p^2 \gtrsim 0.2 k^2$  apparent. This coincidence is a non-trivial consequence of the different contributions of  $\mu$  and  $\lambda_3$  to both  $\beta$ -functions. It entails effective universality on the quantitative level. The deviation from effective universality at small momenta may have two different sources: first we expect that the regulator-induced breaking of effective universality is maximal at low momenta in comparison to the cutoff scale. A second source of the deviation may be the graviton mass scale in the graviton propagators, and could be related to the convexity-enforcement at work in the effective action.

The highly non-trivial result in Fig. 8.2 of quantitative effective universality also suggests to discuss different analytic schemes based on local and bilocal approximations that accommodate the momentum dependence of the couplings and reflect effective universality.

### Quantitative bilocal schemes

The full momentum dependence of the couplings is approximated best in bilocal approximations by using the bilocal result for the three-graviton coupling,  $G_{\text{bl},(3,0)}$ , also for the scalar-graviton coupling with an additional analytic interpolating piece,

$$p^2 \sqrt{G_{(1,2)}^{\text{quant}}(p^2)} := p^2 \sqrt{G_{(3,0)}^{\text{bl}}} + k^2 \sqrt{\Delta G_{(1,2)}(p^2)}, \quad (8.12a)$$

with

$$\sqrt{\Delta G_{(1,2)}(p^2 \gtrsim 0.2 k^2)} = \sqrt{G_{(1,2)}(k^2)} - \sqrt{G_{(3,0)}^{\text{bl}}},$$

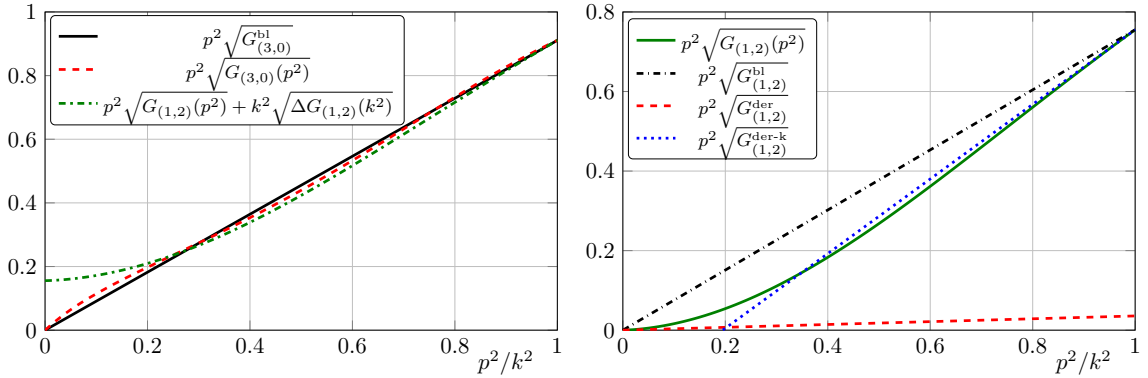


Figure 8.2.: Momentum dependent Newton's couplings and approximations to it, evaluated on the bilocal fixed point using effective universality for the momentum-independent couplings, (8.10). Left:  $p^2 \sqrt{G_{(3,0)}(p^2)}$  and  $p^2 \sqrt{G_{(1,2)}(p^2)} - k^2 \sqrt{\Delta G_{(1,2)}(k^2)}$ , see (8.12). The black line guides the eye and corresponds to the bilocal approximation to the flow. Right: Local and bilocal approximations of  $p^2 \sqrt{G_{(1,2)}(p^2)}$ .

$$\Delta G_{(1,2)}(0) = 0, \quad (8.12b)$$

and  $\Delta G_{(1,2)}(p^2)$  interpolates between these two values in the interval  $0 \leq p^2 \lesssim 0.2 k^2$ , see Fig. 8.2. Note that the accurate determination of this interpolation at small momenta  $p^2 \lesssim 0.2 k^2$  is numerically irrelevant as these momenta are suppressed in loops due to the  $p^3$ -factor from the measure.

We can make maximal use of the numerical irrelevance of the low momentum regime with  $p^2 \lesssim 0.2 k^2$  and drop the non-linear piece altogether. This amounts to

$$\sqrt{\Delta G_{(1,2)}(p^2)} = \sqrt{G_{(1,2)}(k^2)} - \sqrt{G_{(3,0)}^{\text{bl}}}, \quad (8.13)$$

see also Fig. 8.2. In this approximation of the vertex  $p^2 \sqrt{G_{(1,2)}(p^2)}$  does not vanish at  $p^2 = 0$ , which breaks shift symmetry. However, the approximation scheme never uses this information, which effectively restores shift symmetry.

### Qualitative bilocal schemes

An even simpler approximation is dropping  $\Delta G_{(1,2)}$  completely,  $\Delta G_{(1,2)} \equiv 0$ . With (8.12a) this leads to

$$G_{(1,2)}^{\text{qual}} = G_{(3,0)}^{\text{bl}}, \quad (8.14)$$

for the respective coupling see Fig. 8.2. This leads to explicit shift symmetry in (8.12) but also triggers up to a  $\sim 20\%$  deviations in the results for the respective loops proportional to  $G_{(1,2)}$ .

The final variant of the bilocal scheme is the standard bilocal approximation for  $G_{(1,2)}$ . Using shift symmetry with  $p^2 \sqrt{G_{(1,2)}(p^2)} \Big|_{p^2=0} = 0$ , we are led to

$$G_{(1,2)}^{\text{bl}} = G_{(1,2)}(k^2), \quad (8.15)$$

for the respective coupling see [Fig. 8.2](#). It is up to  $\sim 20\%$  bigger than  $G_{(1,2)}(p^2)$  in the numerically relevant regime with  $p^2 \gtrsim 0.2 k^2$ . Accordingly, it has a quantitative error of about this size but maintains explicit shift symmetry. Note also that it is  $\sim 20\%$  smaller than the *slope* of  $p^2 \sqrt{G_{(1,2)}(p^2)}$  for  $p^2 \gtrsim 0.2 k^2$  where effective universality takes place.

This approximation has been used with  $\Delta G_{(n,m)} = 0$  for all  $n, m$  in [\(8.12\)](#) in matter-gravity systems in the last two chapters, and the respective results there are now sustained further by effective universality in the scalar-gravity system. We also use it here, and a more quantitative analysis is provided in [Sec. 8.4.4](#).

### Derivative expansions

A derivative expansion is a local expansion in momenta. The expansion point is either chosen for analytic and numerical convenience or in order to optimise the convergence with the full result. Analytic convenience singles out  $p^2 = 0$  as this allows for analytic flow equations for specific regulators such as the flat or Litim regulator, [\[372, 373\]](#) or the sharp cutoff.

Best convergence is achieved for an expansion at the momentum value at which the integrands in the flow peak. This typically is a momentum close to the cutoff scale,  $p^2 \approx k^2$ , leading to

$$\sqrt{G_{(1,2)}^{\text{der-k}}} = \sqrt{G_{(1,2)}(k^2)} + p^2 \frac{\partial \sqrt{G_{(1,2)}(p^2)}}{\partial p^2} \bigg|_{p^2=k^2}. \quad (8.16)$$

In the present case this has the additional benefit that it also includes a good estimate of the linear piece of the  $G_{(1,2)}$  avatar of the Newton's coupling, see [Fig. 8.2](#). From its quantitative nature it is in the same ballpark as the quantitative bilocal approximation with [\(8.13\)](#) described in [Sec. 8.4.2](#).

It is left to discuss the standard derivative expansion with the expansion point  $p^2 = 0$

$$G_{(1,2)}^{\text{der}} = G_{(1,2)}(0). \quad (8.17)$$

We note that the non-trivial momentum dependence of the vertex  $p^2 \sqrt{G_{(1,2)}(p^2)}$  at small momenta  $p^2 \rightarrow 0$  casts some further doubt on the naive use of derivative expansions in quantum gravity. Moreover, the analysis of the momentum space expansion about  $p^2 = 0$  also applies to curvature expansions as used in the background field approximation. Hence the current reliability discussion translates one to one to computations within the background field approximation.

Clearly, approximating  $G_{(1,2)}$  by the derivative of  $p^2 \sqrt{G_{(1,2)}(p^2)}$  at  $p^2 = 0$  leads to a significant deviation (factor  $\sim 20$ ) of the resulting coupling from the correct result in the numerically relevant regime for  $p^2 \gtrsim 0.2 k^2$ . This issue is also discussed in [App. B.4](#) for pure quantum gravity, where the deviation is smaller. This is already visible from the full momentum-dependence of  $G_{(3,0)}$  in [Fig. 8.2](#). Still this scheme captures all qualitative aspects of the current systems.

### 8.4.3. Unquenching quantum gravity

The quantitative self-consistency analysis in [Sec. 8.4.2](#) above was done at  $N_s = 0$ . Now we study the  $N_s$ -derivative at  $N_s = 0$ . This gives us a sum of the different terms that

show up with a linear  $N_s$ -dependence that comes from a closed scalar loop. If this sum again shows a behaviour as seen in [Fig. 8.2](#) this indicates the persistence of quantitative effective universality for all  $N_s$ . A global analysis for large  $N_s$  is hampered by the strongly rising Newton's couplings: we hit the reliability bounds of the approximation before the  $N_s$ -effects become dominant. In conclusion the current local analysis is as good as it gets in the approximation used here.

The  $N_s$ -derivative of the vertices evaluated on the fixed point read for the three-graviton coupling

$$\partial_{N_s} p^2 \sqrt{G_{(3,0)}(p^2)} = p^2 \sqrt{G_{(3,0)}(p^2)} \left\{ \frac{\partial_{N_s} [\text{Flow}^{(3,0)}(p^2) - \text{Flow}^{(3,0)}(0)]}{\text{Flow}^{(3,0)}(p^2) - \text{Flow}^{(3,0)}(0)} - 3 \frac{\partial_{N_s} \eta_h(p^2)}{2 + 3\eta_h(p^2)} \right\}, \quad (8.18a)$$

and for the minimal scalar-graviton coupling

$$\partial_{N_s} p^2 \sqrt{G_{(1,2)}(p^2)} = p^2 \sqrt{G_{(1,2)}(p^2)} \left\{ \frac{\partial_{N_s} \text{Flow}^{(1,2)}(p^2)}{\text{Flow}^{(1,2)}(p^2)} - \frac{\partial_{N_s} \eta_h(p^2)}{2 + \eta_h(p^2)} \right\}, \quad (8.18b)$$

where the respective second terms on the right-hand sides of [\(8.18a\)](#) and [\(8.18b\)](#) take care of the  $Z^{n/2}$  dressing of the  $n$ -point vertices. The terms in the respective flow contributions from  $\partial_{N_s} \text{Flow}^{(n,m)}$  read

$$\partial_{N_s} \text{Flow} = \frac{\partial}{\partial N_s} \bigg|_{G, \eta_h} \text{Flow} + [\partial_{N_s} \eta_h(k^2)] \partial_{\eta_h} \text{Flow} + \frac{3}{2} \frac{\partial_{N_s} G}{G} \text{Flow}. \quad (8.19)$$

The first term on the right-hand side of [\(8.19\)](#) simply counts the number of scalars in closed scalar loops, which rises linear with  $N_s$ . This term vanishes for  $G_{(1,2)}$  as its flow has no diagram with a closed scalar loop. The second term takes into account the  $N_s$ -dependence of the graviton propagator as well as that of the wave function renormalisations in the vertices. With the present RG-adjusted graviton regulator that is proportional to  $Z_h$  this dependence is stored solely in the  $\eta_h$ -dependence of the scale derivative of the regulator. The anomalous dimension  $\eta_h$  has a linear  $N_s$ -dependence proportional to the closed scalar loop for the graviton propagator. Together with the closed scalar loop for  $G_{(3,0)}$  it gives the  $N_s$ -dependence on one-loop. For universal couplings such as the gauge couplings in the Standard Model these terms provide the universal  $N_s$ -dependence of the couplings.

The additional terms arrange for the typical resummations present in FRG computations: the  $\partial_{N_s} \eta_h$  derivative takes into account the  $N_s$ -dependence of the anomalous dimension and the third term takes into account the  $N_s$ -dependence of the fixed point coupling from the prefactor  $G^{3/2}$  in all the diagrams. Further terms are present that take into account the  $N_s$ -dependence of  $\mu$  and  $\lambda_3$ , which are dropped in the present analysis as they are approximately  $N_s$ -independent at the fixed point, see [Fig. 8.1](#).

If we simply evaluate the  $N_s$ -dependence of the flow for given  $N_s$ -independent couplings, these additional resummation terms from  $\partial_{N_s} G$  are missing. This is displayed in the left panel of [Fig. 8.3](#). We see a qualitatively similar momentum-dependence of both,  $\partial_{N_s} p^2 \sqrt{G_{(3,0)}(p^2)}|_G$  and  $\partial_{N_s} p^2 \sqrt{G_{(1,2)}(p^2)}|_G$  evaluated at the fixed point. Moreover, their absolute values are one/two orders of magnitude smaller than in the quenched system in [Fig. 8.2](#). Accordingly, scalars can only change the system qualitatively for  $N_s \gtrsim 10 - 10^2$ . This is seen in [Fig. 8.1](#): the system is basically unchanged for  $N_s \lesssim 20$ . From there on

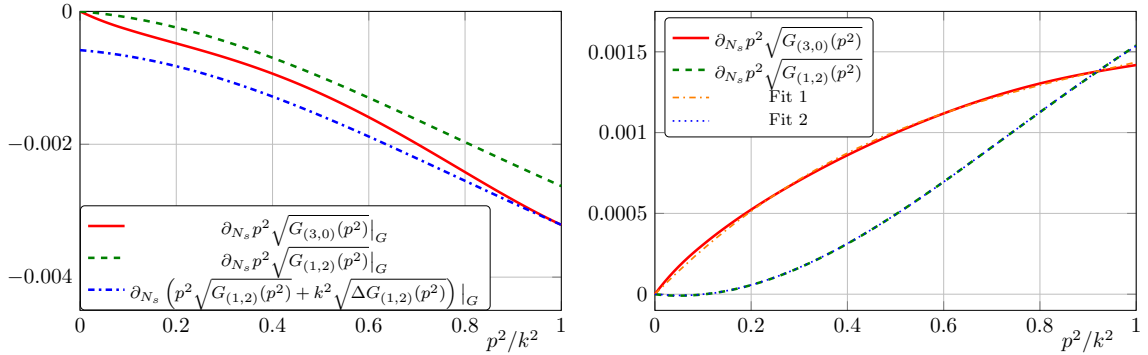


Figure 8.3.:  $N_s$ -derivative of the momentum-dependent Newton's couplings  $\partial_{N_s} p^2 \sqrt{G_{(3,0)}(p^2)}$  and  $\partial_{N_s} p^2 \sqrt{G_{(1,2)}(p^2)}$ . Left/right: without/with resumming the  $N_s$ -dependence of  $G^*$ . The fits are given in (8.20).

the approximation violates reliability bounds for the regulator with  $\eta_h < 2$  and should be taken with a grain of salt.

In the left panel of Fig.8.3 we see that the contributions are negative, and hence the part of the fixed point equations for the two avatars of  $G_N$  under consideration proportional to  $G^{\frac{3}{2}}$  decreases. This results in an increase of  $G^*$ . This increase should be visible if taking into account the  $N_s$ -dependences of the fixed point value of  $G^*$  in (8.18). This leads us to the right panel of Fig.8.3, which displays the full  $N_s$ -derivative of the fixed point couplings  $p^2 \sqrt{G_{(3,0)}}$  and  $p^2 \sqrt{G_{(1,2)}}$ .

This momentum dependence encodes a very interesting structure. First of all the quantitative effective universality present in Fig.8.2 is not found. Still, the  $N_s$ -dependences have the same size, which explains the similar growth in Fig.8.1. Note that this similarity is even better for the momentum regime relevant in the loop integrals with  $p^2 \approx k^2$ , so fully momentum-dependent or bilocal approximations take account of this fact. Nonetheless the momentum-dependence in Fig.8.3 is not covered well by a linear function in  $p^2$ . This suggests that higher-order terms are triggered by the unquenching terms. We have applied polynomial fits to the results, leading to

$$\begin{aligned} \partial_{N_s} p^2 \sqrt{G_{(3,0)}} &\approx 10^{-3} (3.0 p^2 - 2.5 p^4 + 0.86 p^6) , \\ \partial_{N_s} p^2 \sqrt{G_{(1,2)}} &\approx 10^{-3} (-0.34 p^2 + 3.4 p^4 - 1.6 p^6) , \end{aligned} \quad (8.20)$$

see also Fig.8.3. Now we relate the momentum dependences with diffeomorphism-invariant terms in the action as suggested by effective universality. Then the  $p^2$ -terms stand for the curvature scalar  $\sqrt{g}R$  and kinetic term  $\sqrt{g}\varphi\Delta\varphi$  respectively. The  $p^4$ -terms relate to  $R_{\mu\nu}^2$ , and  $\sqrt{g}R_{\mu\nu}\varphi\nabla_\mu\nabla_\nu\varphi$  terms. This observation is very much in line with the observation that within asymptotically safe gravity the fixed-point action necessarily features shift-symmetric higher-order interactions [420]. For a recent study of the  $\sqrt{g}R_{\mu\nu}\varphi\nabla_\mu\nabla_\nu\varphi$ -coupling see [436]. Note also that our projection has no overlap with  $R^2$ , as discussed in Sec. 3.4.1. For the same reasoning, there is no overlap with  $\sqrt{g}R\varphi\Delta_g\varphi$ . We emphasise that the  $R_{\mu\nu}^2$  coupling triggered by the Einstein-Hilbert truncation is compatible with zero, see also Fig.8.2. The present finding suggest that the unquenching effects due to the closed scalar loops do trigger corrections to the  $G_{(3,0)}$  coupling as well as the generation  $R_{\mu\nu}^2$  coupling of a comparable size. The latter is very interesting as it is not generated

in a quenched scalar-gravity system. In turn, no contribution to  $G_{(1,2)}$  is triggered by the unquenching effects: the coefficient of the  $p^2$ -term in (8.20) is an order of magnitude smaller than the other terms and thus might be well covered by the systematic error of our approximation. In contrast, the coefficients of the higher-order terms in (8.20) have both the same order of magnitude, which matches the size of the coefficients for the  $N_s$ -dependence of  $G_{(3,0)}$ .

This is also very interesting in the light of the results in the last chapter. While it should be possible to absorb the  $N_s$  dependence of  $G_{(3,0)}$  and  $\eta_h$  in an appropriate redefinition of  $G_{(3,0)}$ , this does not hold for that of the marginal couplings. Note that after re-normalising  $G_{(3,0)}$ , there is no potential  $N_s$ -dependence left in  $G_{(1,2)}$  as its flow does not feature closed scalar loops. We argued in the last chapter that in a sufficiently rich approximation this renormalisation should occur dynamically. In this context we remark that in general this would also require a re-normalisation of  $\mu$  and  $\lambda_3$ . It is highly non-trivial that neither of them shows an  $N_s$ -dependence, which can be understood as part of such a potential dynamical mechanism. The suppression of the  $N_s$ -dependence of  $G_{(1,2)}$  adds some further non-trivial evidence for such a dynamical mechanism.

In summary this offers the exciting possibility of a dynamical stabilisation of scalar-gravity systems for all  $N_s$ . We rush to add that far more work is required to solidify this, the next step being an analysis with  $R^2, R_{\mu\nu}^2, \sqrt{g}R\varphi\Delta\varphi, \sqrt{g}R_{\mu\nu}\varphi\nabla_\mu\nabla_\nu\varphi$  terms.

#### 8.4.4. Effective universality beyond the fixed point

The intriguing result displayed in Fig. 8.2 has shown that effective universality holds quantitatively at the fixed point within the  $N_s$ -range of validity of the current approximation. As argued in the beginning of Sec. 8.4, we expect effective universality to only hold in the vicinity of the fixed point, that is on given trajectories for  $k \rightarrow \infty$ , and, if present, for all momenta at  $k \rightarrow 0$ .

Such a scenario suggests an approximation that utilises effective universality also for finite cutoffs as the related error disappears at  $k = 0$  and  $k \rightarrow \infty$ . Here we investigate the question how it fares away from the fixed point. For the sake of simplicity we do not resort to the quantitative bilocal scheme described in Sec. 8.4.2, but to the qualitative bilocal scheme described in Sec. 8.4.2 with (8.15). If evaluating the  $\beta$ -functions on (8.10) and on the fixed point values of  $\mu$  and  $\lambda_3$  we obtain

$$\begin{aligned} \beta_{G_{(3,0)}} \Big|_{\mu^*, \lambda_3^*} &= 2G - (3.4 - 0.013N_s)G^2 + \mathcal{O}(G^3), \\ \beta_{G_{(1,2)}} \Big|_{\mu^*, \lambda_3^*} &= 2G - (2.7 - 0.0085N_s)G^2 + \mathcal{O}(G^3). \end{aligned} \quad (8.21)$$

We have simply used the fixed-point values of  $\mu$  and  $\lambda_3$  at  $N_s = 0$ , as they are almost  $N_s$ -independent (cf. Fig. 8.1). The coefficients of the  $\beta$ -functions in (8.21) are not universal. This is caused by the missing offset in (8.12) at momenta  $p^2 \gtrsim 0.2k^2$  required for the quantitative agreement, as explained in Sec. 8.4.1.

As our further investigation of effective universality is based on the  $\beta$ -functions in (8.21) we confirm here that the qualitative nature of the present approximation scheme discussed in Sec. 8.4.2 below (8.15) already explains all the deviations in (8.21). The  $N_s$ -independent terms should be subject to underestimating the slope of  $p^2 G_{(1,2)}$  in the regime  $p^2 \gtrsim 0.2k^2$  where effective universality takes place, see Fig. 8.2. Accordingly, this part of  $\beta_{G_{(1,2)}}$  should

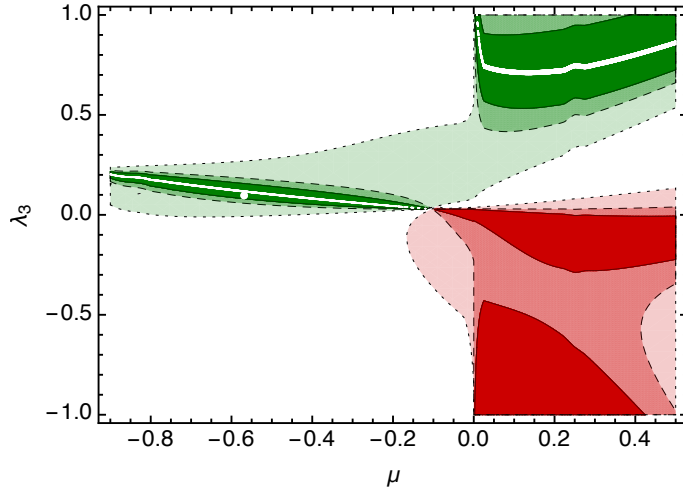


Figure 8.4.: The regions in which  $\epsilon < \frac{1}{5}$  ( $\epsilon < \frac{1}{3}$ ;  $\epsilon < \frac{3}{4}$ ) is marked in dark (light, dashed contour; lighter, dotted contour) colours for  $N_s = 1$  and  $G \rightarrow 0$ . The green (red) colour indicates  $\Delta\beta_G < 0$  ( $\Delta\beta_G > 0$ ). The two green regions are centred around thin bands where  $\epsilon < \frac{1}{100}$  (white). The UV fixed point value is indicated by the white dot. The area is almost  $N_s$  independent, as are the fixed point values of  $\mu$  and  $\lambda_3$  (cf. Fig. 8.1).

be  $\sim 20\%$  smaller than that of  $\beta_{G_{(3,0)}}$  and their ratio should be  $\sim 0.8$ . From (8.21) we get  $2.7/3.4 = 0.79$ . For the  $N_s$ -dependent terms the situation is not that clear.

In summary (8.21) fully reflects the quantitative universality in the given bilocal approximation precisely by its semi-quantitative or qualitative pattern. This has to be kept in mind if evaluating deviations from effective universality within this approximation.

Now we proceed with this evaluation by devising a measure of the breaking of effective universality. It is a property of the anomalous part  $\Delta\beta$  of the  $\beta$ -functions,

$$\Delta\beta_{G_{(i,j)}} = \beta_{G_{(i,j)}} - 2G. \quad (8.22)$$

As a measure of effective universality we use the relative error between the scaling of two avatars of the coupling evaluated under the assumption of universality, that is  $G_{\vec{n}} = G$  for the avatars of the Newton's coupling. In the present case this reads

$$\epsilon(G, \mu, \lambda_3, N_s) = \left| \frac{\Delta\beta_{G_{(3,0)}} - \Delta\beta_{G_{(1,2)}}}{\Delta\beta_{G_{(3,0)}} + \Delta\beta_{G_{(1,2)}}} \right|_{G_{\vec{n}}=G}. \quad (8.23)$$

In the simplest case of effective universality  $\epsilon$  is zero. Note however, that in the present non-trivial realisation we have a breaking pattern for small momenta, see again Fig. 8.2. In the presence of such a breaking  $\epsilon = 0$  does indeed indicate a small violation of effective universality. Further patterns are, that for  $\epsilon < 1$  the anomalous parts of the beta functions have the same sign, and  $\epsilon > 1$  for different signs. In the limit  $G \rightarrow 0$  we precisely compare the  $G^2$ -terms as displayed in (8.21). The definition (8.23) also allows to separately compare the gravity and scalar contributions by taking the limits  $N_s \rightarrow 0$  and  $N_s \rightarrow \infty$ , respectively. It does, however, not distinguish between anomalous parts of a  $\beta$ -function that allow for a UV fixed point ( $\Delta\beta < 0$ ) and that do not ( $\Delta\beta > 0$ ).

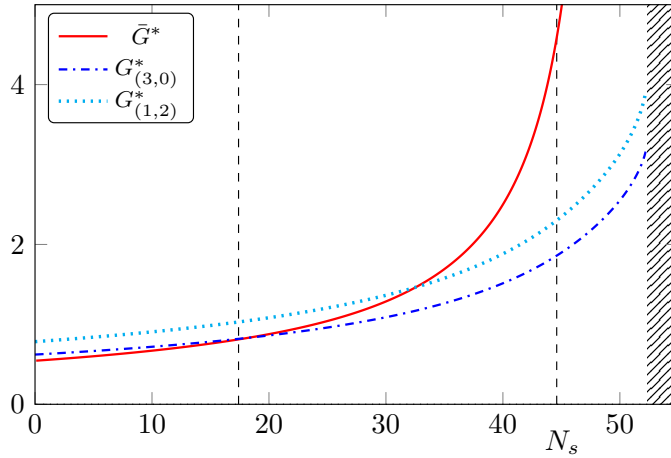


Figure 8.5.: Displayed are the fixed-point values for three Newton's couplings: the background coupling (red continuous line), the three-graviton coupling (blue dot-dashed line) and the graviton-scalar-coupling (light blue dotted line).

In Fig. 8.4 we show the regions in the  $(\mu, \lambda_3)$ -plane where effective universality is realised for the coupling  $G_{(3,0)}$  and  $G_{(1,2)}$ . In particular we display the regions in which  $\epsilon < \frac{1}{5}$  and  $\epsilon < \frac{1}{3}$  for  $N_s = 1$  and  $G \rightarrow 0$ . We further distinguish between regions that allow for a UV fixed point ( $\Delta\beta < 0$ , green colour) and regions that don't ( $\Delta\beta > 0$ , red colour). We observe that effective universality and a UV fixed point is only allowed in two regions: this first is for negative  $\mu$  and small  $\lambda_3 \approx 0.1$ . In fact fixed point values for  $\mu$  and  $\lambda_3$  lie in this region of effective universality. In Fig. 8.4 it is marked with a star. The other region is at positive  $\mu$  and large  $\lambda_3 > 0.5$ . At positive  $\mu$  and negative  $\lambda_3$  there is another region that allows for effective universality but not for a UV fixed point. Fig. 8.4 highlights that the common realisation of effective universality and a UV fixed point is highly non-trivial.

## 8.5. Effective universality for the background-fluctuation system

### 8.5.1. Effective universality for the background Newton's coupling

We now address our second key question and explore whether effective universality is also present on the level of the background Newton's coupling.

The flow of  $\bar{G}$  and  $\bar{\lambda}$  is driven exclusively by the fluctuation couplings and thus we can simply evaluate their flow equation on the computed fixed point values of the fluctuation couplings, displayed in Fig. 8.1. We observe that the fixed point values of  $\bar{G}^*$  track those of the fluctuation system at the qualitative level, cf. Fig. 8.5. A similar conclusion can be drawn by comparing the  $\beta$ -function for  $\bar{G}$  that reads

$$\beta_{\bar{G}} = 2\bar{G} - (3.64 - 0.057 N_s) \bar{G}^2, \quad (8.24)$$

again evaluated on the fixed point for  $N_s = 1$ , thereby neglecting an additional  $N_s$ -dependence of these coefficients. The pure-gravity coefficient differs by 6% in comparison to  $\beta_{G_{(3,0)}}$ , cf. (8.21), and the  $N_s$ -dependent coefficient by a factor 4.4. Both signs agree with those in the fluctuation system. The substantial deviation of the  $N_s$ -dependent coefficient leads to a larger gap between the fluctuation and the background avatars at large  $N_s$ .

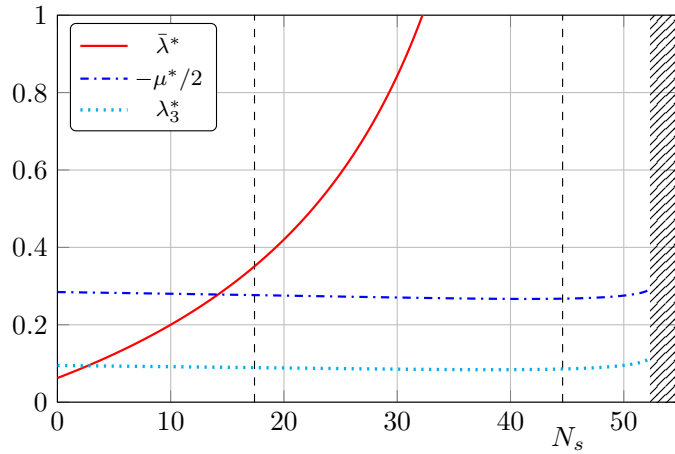


Figure 8.6.: Displayed are the fixed-point values for  $\bar{\lambda}$ ,  $\mu$  and  $\lambda_3$  as a function of  $N_s$ . We use the fluctuation system as input on the right-hand side of the Wetterich equation.

Nevertheless, the  $N_s$ -dependent fixed point values for all avatars of the Newton's coupling agree on the qualitative level.

### 8.5.2. The fate of effective universality in commonly used approximations

#### Background field approximation

While it is the fluctuation-field propagator that drives the flow, we are ultimately interested in the background effective action  $\Gamma_{k \rightarrow 0}[\bar{g}_{\mu\nu} = g_{\mu\nu}, h_{\mu\nu} = 0]$  to read off the physics. A commonly used approximation thus consists in inserting  $\Gamma_k^{(2,0)}[\bar{g}_{\mu\nu} = g_{\mu\nu}, h_{\mu\nu} = 0]$  on the right-hand side of the Wetterich equation and thereby letting the background couplings drive the flow. In a system with fully intact symmetries, this approximation would of course be exact. Although this leads to a semi-quantitative agreement with the full results at  $N_s = 0$ , the approximation fails to capture even the qualitative  $N_s$  dependence correctly. While this might in principle improve in extended approximations, it casts some doubt on the use of the background field approximation for gravity-matter systems at least in the case of scalar matter.

For the background Newton's coupling, the flow equation in the background field approximation, i.e., at  $\eta_h = -2$ , evaluated at  $\bar{\lambda} = 0$  reads

$$\beta_{\bar{G}} = 2\bar{G} - \left( \frac{79}{4} - N_s \right) \frac{\bar{G}^2}{6\pi} \approx 2\bar{G} - (1.05 - 0.053N_s) \bar{G}^2, \quad (8.25)$$

where the signs of the coefficients still agree with those of the fluctuation system. The failure of the background field approximation to correctly capture the  $N_s$  dependence is a consequence of the difference between  $\mu$  and  $\bar{\lambda}$ . While  $\mu^*$  stays approximately constant with increasing  $N_s$ ,  $\bar{\lambda}^*$  is driven towards larger values, thereby enhancing gravity fluctuations and suppressing the effect of scalar-matter fluctuations. The background cosmological constant in the full system is displayed in Fig. 8.6, together with the fluctuation couplings  $\mu$  and  $\lambda_3$ . It is worth to note that  $-\mu/2$  cannot cross the value 1/2 as this is the pole of the graviton propagator. The couplings  $\bar{\lambda}$  and  $\lambda_3$  on the other hand can

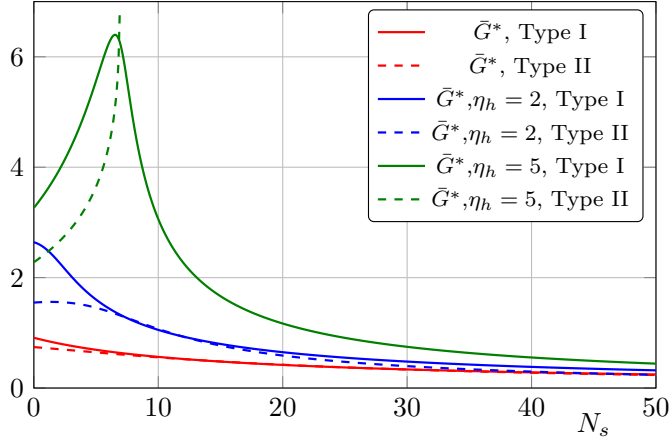


Figure 8.7.: Fixed-point values of the background Newton's coupling for a type-I and a type-II regulator with the background field approximation ( $\eta_h = -2$ , red lines), and in hybrid cases with  $\eta_h = 2$  (blue lines) and  $\eta_h = 5$  (green lines).

cross this value and for  $\bar{\lambda}$  this indeed happens for large  $N_s$ . In summary this results highlights the necessity that at least the coupling  $\mu$  needs to be computed from a fluctuation computation, at least at the present level of approximation.

### Hybrid scheme for $\eta_h$

In a hybrid scheme, put forward in [326] and employed in the analysis of gravity-matter systems in [424], the graviton anomalous dimension is distinguished from the anomalous dimension of the background Newton's coupling. While  $\eta_h$  is evaluated as a function of the background couplings  $\bar{G}$  and  $\bar{\lambda}$  in this hybrid, it can deviate from the background-value  $\eta_h = -2$ , and thereby partially account for the non-trivial anomalous dimension of the graviton.

Within such a hybrid setup, a behaviour qualitatively closer to that of the full fluctuation system was observed, [424], i.e. the fixed-point value for Newton's coupling rose as a function of  $N_s$ . This can be traced back to a growth of the anomalous dimension, cf. Fig. 8.7. A strong growth of the anomalous dimension has to be considered carefully: the usual choice of regulators is  $R_k \sim Z_h$ , implying a bound on the anomalous dimensions  $\eta < 2$  (for bosonic fields), see Sec. 6.3.4. As  $Z_h \sim k^{-\eta_h}$  in the fixed-point regime,  $\eta_h > 2$  destroys the UV behaviour of the regulator that should suppress all modes in the limit  $k \rightarrow \infty$ . For  $\eta_h > 4$  signs of diagrams in beta functions start to flip. Furthermore a large anomalous dimension can be interpreted as a hint at large relative cutoff scales between the different fields of the theory, see the discussions in the last chapter.

We demonstrate the transition between the  $N_s$  dependence of  $\bar{G}^*$  in the strict background field approximation and the hybrid scheme by setting the anomalous dimension to fixed successively increasing values, cf. Fig. 8.7. We investigate type-I and type-II regulators [274]. Indeed the background Newton's coupling with a type-II regulator rises as soon as  $\eta_h > 4$  and the diagrams in the beta function have flipped. For the type-I regulator this happens at  $\eta_h > 6$ , as it features higher powers of  $(1 - 2\lambda)$  in the denominator, which flip their sign only at  $\eta_h > 6$ .

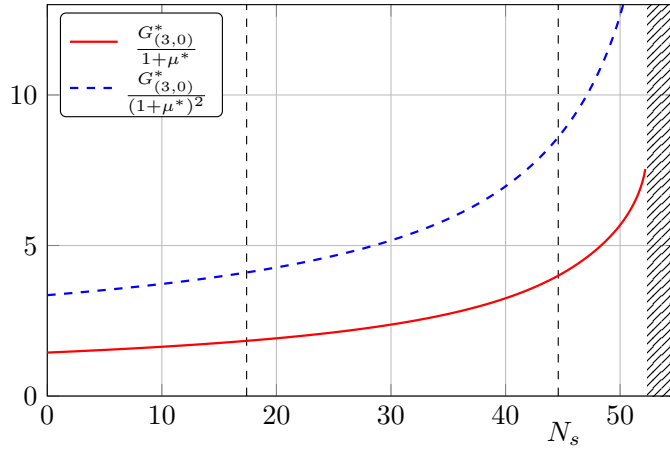


Figure 8.8.: We plot the effective gravitational couplings  $G_{(3,0)}^*/(1 + \mu^*)$  and  $G_{(3,0)}^*/(1 + \mu^*)^2$ . The former/latter stems from propagators without/with the regulator insertion  $\partial_t R_k$ . The factor  $G^*$  stems from adjoint vertices.

### 8.5.3. Effective gravitational coupling

Ultimately, we are interested in the strength of the metric propagator, as this is a crucial quantity to determine the quantum-gravity effects on matter [120, 152, 433, 441].

Metric fluctuations enter the diagrams with a propagator of the form  $\frac{G_{(n,m)}}{1+\mu} = g_{\text{eff},1}$  and  $\frac{G_{(n,m)}}{(1+\mu)^2} = g_{\text{eff},2}$ , which we define as the two effective gravitational couplings. The first/second is the effective coupling associated to a graviton propagator without/with an insertion of  $\partial_t R_k$ . For the flow of matter vertices, these are the two dominant combinations of  $G_{(n,m)}$  and  $\mu$  that enter the flow – a higher power of the denominator can appear due to a derivative expansion.

Effective universality allows us to use  $G_{(3,0)}$  exclusively. In our fully coupled system, cf. Fig. 8.1,  $\mu$  stays approximately constant, while all Newton's couplings were increasing as a function of  $N_s$ . Consequently we find that  $g_{\text{eff},1/2}$  increase as well, cf. Fig. 8.8.

In summary we observe an enhancement of the graviton propagator when we increase the number of scalar flavours. This is in line with the arguments in the last chapter that such systems as minimally coupled scalars should be dominated by gravity in the UV via an enhancement of the propagator if the marginal terms as  $R^2$  and  $R_{\mu\nu}^2$  are neglected as they are in this dissertation. Here we find an enhancement of the graviton propagator via the wave function renormalisation and consequently the graviton anomalous dimension crosses the regulator bound  $\eta_h < 2$  at  $N_s \approx 17$ . Accordingly, we are still unable to observe the dynamical readjustment mechanism that according to the last chapter should take place in the present scalar-gravity system within the approximation used (no  $R^2$ - and  $R_{\mu\nu}^2$ -terms). This mechanism makes all flavour numbers of minimally coupled scalars compatible with asymptotically safe gravity.

It is of great interest to determine whether the graviton propagator grows with the number of scalar flavours, in view of indications for a weak-gravity bound in asymptotic safety [120, 387, 432, 441], where gravity fluctuations trigger new divergences in the matter sector if they are too strong. In this chapter we have used a parameterisation where the graviton propagator is indeed enhanced. Yet, within the current truncation (no  $R^2$ - and

$R_{\mu\nu}^2$ -terms) there is at least one regularisation scheme where the graviton propagator is independent of the number of scalar flavours. Thus a final assessment of the strength of the graviton propagator requires a full coupling of the matter interactions with the present system and the inclusion of the marginal couplings  $R^2$  and  $R_{\mu\nu}^2$ . A study of such a system appears to be highly worthwhile and we defer it to future work.

## 8.6. Level-one improvement

It is desirable to find a simple approximation of the system that ideally does not require the separate calculation of both background and fluctuation flows. Therefore we study whether the background field approximation can qualitatively or even quantitatively reproduce the behaviour of the full system if upgraded to a level-one system by using the modified split Ward identity.

### 8.6.1. Nielsen or split Ward identity and its applications

We exploit the Nielsen identity (NI) or split Ward identity (sWI) to improve upon the background field approximation. Related derivations and applications in the present context can be found in [188, 336, 347, 355, 356, 471]. Split Ward identities have also been discussed in [333–335, 337–343, 352, 472, 473].

With the introduction of a background field, the effective action becomes a functional of both the dynamical fluctuation field  $\Phi$  and the auxiliary background field  $\bar{\Phi}$

$$\Gamma_k = \Gamma_k[\bar{\Phi}, \Phi]. \quad (8.26)$$

In the present case of a scalar-gravity system the background and fluctuation fields read

$$\bar{\Phi} = (\bar{g}_{\mu\nu}, 0, 0, \bar{\phi}), \quad \Phi = (h_{\mu\nu}, c_\mu, \bar{c}_\mu, \varphi), \quad (8.27)$$

respectively, where the full metric and scalar fields are given by

$$g_{\mu\nu} = \bar{g}_{\mu\nu} + h_{\mu\nu}, \quad \phi = \bar{\phi} + \varphi. \quad (8.28)$$

In scalar theories there is no need to choose the cutoff to depend on the background field. Thus the flowing action is only a function of the full field  $\phi = \bar{\phi} + \varphi$ . For purposes of illustration, we introduce a dependence of the cutoff on  $\bar{\phi}$  artificially. The effective action at  $k = 0$  is a functional of the full field  $\phi = \bar{\phi} + \varphi$  only. This is due to the fact that the classical action has this property,  $S_{\text{cl}}[\bar{\phi}, \varphi] = S_{\text{cl}}[\bar{\phi} + \varphi]$ . The shift symmetry is broken by the cutoff term  $R_k = R_k[\bar{\phi}]$ . The resulting difference in the dependence on the two fields is sourced only by the cutoff term and expressed by the NI/sWI, [355]

$$\frac{\delta\Gamma_k}{\delta\bar{\phi}} - \frac{\delta\Gamma_k}{\delta\varphi} = \frac{1}{2} \text{Tr} \left[ \frac{\delta R_k[\bar{\phi}]}{\delta\bar{\phi}} G_k[\bar{\phi}, \varphi] \right]. \quad (8.29)$$

This equation is derived in straight analogy to the flow equation itself, which is reflected in the structural similarities [355]. We again use the shorthand  $G_k$  for the regularised propagator of the fluctuation field. For flows towards the infrared where the regulator vanishes, (8.29) suggests to use the background field approximation

$$\Gamma_k[\bar{\phi}, \varphi] \approx \Gamma_k[\bar{\phi} + \varphi, \varphi = 0], \quad (8.30)$$

which is exact for  $k = 0$  in the present example of scalar theories. However, for flows towards the UV ( $k \rightarrow \infty$ ) the background field approximation is spoiled by power-counting leading terms in the effective action. This is a consequence of the mass-like nature of the cutoff, which makes it UV relevant. In the following, we do not include the scalar background field into the regulator, thus the right-hand side of (8.29) is zero and we focus on the NI for the graviton.

In gravity, and gauge theories in general, the situation is even more complicated. In this case there are two sources for the background dependence of the effective action. In addition to the regulator term, the second source of background dependence comes from the gauge fixing sector  $S_{\text{gauge}} = S_{\text{gf}} + S_{\text{gh}}$ . Both the gauge fixing term  $S_{\text{gf}}$  and the ghost term  $S_{\text{gh}}$  have to depend on the background field if background gauge invariance is demanded. Thus the motivation for introducing the background field, namely background gauge invariance, leads to a genuine background dependence of the effective action. For our gravity-matter system the NI (8.29) turns into

$$\frac{\delta\Gamma_k}{\delta\bar{g}_{\mu\nu}} - \frac{\delta\Gamma_k}{\delta h_{\mu\nu}} = \frac{1}{2} \text{Tr} \left[ \frac{1}{\sqrt{\bar{g}}} \frac{\delta\sqrt{\bar{g}}R_k[\bar{g}]}{\delta\bar{g}_{\mu\nu}} G_k[\bar{g}, h] \right] + \left\langle \frac{\delta S_{\text{gauge}}[\bar{g}, h]}{\delta\bar{g}_{\mu\nu}} - \frac{\delta S_{\text{gauge}}[\bar{g}, h]}{\delta h_{\mu\nu}} \right\rangle, \quad (8.31)$$

where the regulator  $R_k$  is now a matrix in field space. The second line in (8.31) originates from the background field dependence of the gauge fixing sector, and it survives in the limit  $k \rightarrow 0$  if the effective action is evaluated off-shell, but vanishes on the solution of the equations of motion [365]. Here we approximate (8.31) and use

$$\lim_{k \rightarrow \infty} \left( \frac{\delta\Gamma_k}{\delta\bar{g}_{\mu\nu}} - \frac{\delta\Gamma_k}{\delta h_{\mu\nu}} \right) \simeq \frac{1}{2} \text{Tr} \left[ \frac{1}{\sqrt{\bar{g}}} \frac{\delta\sqrt{\bar{g}}R_k[\bar{g}]}{\delta\bar{g}_{\mu\nu}} G_k[\bar{g}, h] \right], \quad (8.32)$$

where we have dropped the second line with the gauge fixing contributions. Two arguments underlie our choice to focus on the cutoff term: First at the present level of truncation it is actually possible to effectively subsume changes in the gauge fixing under changes of the regulator: Specifically we concentrate on momenta  $p^2 \lesssim k^2$  and a given gauge fixing  $S_{\text{gf}}^2(p^2)$ . In this regime we can utilise the generality of the regulator to effectively re-adjust it

$$R_k \rightarrow R_k - S_{\text{gf}}^2(p^2) r(p^2/k^2) + S_{\text{gf,diff}}^2(p^2) r(p^2/k^2), \quad (8.33)$$

where  $S_{\text{gf,diff}}^2$  is a general gauge fixing term. Hence, with (8.33) we have effectively changed the gauge fixing term for momenta  $p^2 \lesssim k^2$ . If applying this procedure to the ghost, it is only possible to change its propagator and the interaction of the ghost with the background graviton  $\bar{G}_{\mu\nu}$ , but not that with the dynamical graviton  $h_{\mu\nu}$ . As the ghost terms do not take a leading rôle in the flows this is negligible. In the background field approximation, and using the standard expansion in powers of the curvature, the above mapping strictly holds. In summary, for the study of different gauge fixing terms it suffices in the present approximation to study the regulator-dependence of the flow for momenta  $p^2 \lesssim k^2$ . Note however, that here we refrain from exploiting this freedom in practice.

Second if one compares the contributions of the cutoff term and the gauge fixing sector to the UV flow, a counting argument suggests that the cutoff term dominates. This is because it couples to all fluctuation modes of the graviton, while the contributions of the gauge fixing sector couple directly only to the longitudinal modes. Hence the transverse-traceless approximation, which focuses on the spin-2 mode of the graviton, is only affected by the regulator term (8.32).

Finally we are interested in the relation between background and fluctuation field two-point functions. To that end we apply  $(\delta/\delta\bar{g}_{\rho\sigma} + \delta/\delta h_{\rho\sigma})$  to (8.32), which yields

$$\frac{\delta^2\Gamma_k}{\delta\bar{g}_{\mu\nu}\delta\bar{g}_{\rho\sigma}} - \frac{\delta^2\Gamma_k}{\delta h_{\mu\nu}\delta h_{\rho\sigma}} \simeq \frac{1}{2} \left( \frac{\delta}{\delta\bar{g}_{\rho\sigma}} + \frac{\delta}{\delta h_{\rho\sigma}} \right) \text{Tr} \left[ \frac{1}{\sqrt{\bar{g}}} \frac{\delta\sqrt{\bar{g}}R_k[\bar{g}]}{\delta\bar{g}_{\mu\nu}} G_k[\bar{g}, h] \right]. \quad (8.34)$$

In the example of Yang-Mills theory [355, 356], the analogous fluctuation field derivative of the term in the square brackets on the right-hand side of (8.34) gives sub-leading contributions. We test a similar assumption and thereby arrive at the final approximation for the fluctuation two-point function, which we use in order to close the flow equation,

$$\frac{\delta^2\Gamma_k}{\delta h_{\mu\nu}\delta h_{\rho\sigma}} \approx \frac{\delta^2\Gamma_k}{\delta\bar{g}_{\mu\nu}\delta\bar{g}_{\rho\sigma}} - \frac{1}{2} \frac{\delta}{\delta\bar{g}_{\rho\sigma}} \text{Tr} \left[ \frac{1}{\sqrt{\bar{g}}} \frac{\delta\sqrt{\bar{g}}R_k}{\delta\bar{g}_{\mu\nu}} G_k \right]. \quad (8.35)$$

This approximation has been used in gravity in [336, 471]. Apart from the standard background two-point function it contains a second, regulator-induced term. Specifically, this tests the assumption that the effective action as written in (8.5) simplifies to

$$\Gamma_k[\bar{g}, h, \varphi] = \Gamma_{k,\text{diff}}[g, \varphi] + \Delta\Gamma_{k,\text{gauge}}[\bar{g}], \quad (8.36)$$

where  $\Delta\Gamma_{k,\text{gauge}}$  does only depend on the background field. This would be the simplest case for the background-field dependence. The effective universality that we observe for the fluctuation system motivates us to test a simple structure as in (8.36). For this form, (8.35) becomes an equality. If the deviation from a diffeomorphism invariant action in (8.36) contains further terms that depend on  $h_{\mu\nu}$  separately, we will see indications of this as (8.35) will not yield a level-two propagator in agreement with the fluctuation propagator.

The computation of the trace-term in (8.35) is the challenging part. For this we first expand the propagator in orders of background curvature

$$\begin{aligned} \text{Tr} \left[ \frac{1}{\sqrt{\bar{g}}} \frac{\delta\sqrt{\bar{g}}R_k}{\delta\bar{g}_{\mu\nu}} G_k \right] &= \frac{1}{2} \bar{g}^{\mu\nu} \text{Tr} [R_k G_k] + \text{Tr} \left[ \frac{\delta R_k}{\delta\bar{g}_{\mu\nu}} G_k(\bar{R} = 0) \right] \\ &\quad + \bar{R} \text{Tr} \left[ \frac{\delta R_k}{\delta\bar{g}_{\mu\nu}} G'_k(\bar{R} = 0) \right] + \mathcal{O}(\bar{R}^2). \end{aligned} \quad (8.37)$$

For the terms in the second line we use that

$$\begin{aligned} \frac{\delta R_k(\bar{\Delta})}{\delta\bar{g}_{\mu\nu}} G_k(\bar{\Delta}, \bar{R} = 0) &= \frac{\delta\bar{\Delta}}{\delta\bar{g}_{\mu\nu}} \frac{\partial R_k(\bar{\Delta})}{\partial\bar{\Delta}} G_k(\bar{\Delta}, \bar{R} = 0) \\ &= \frac{\delta}{\delta\bar{g}_{\mu\nu}} \int_0^{\bar{\Delta}} dx' \frac{\partial R_k(x')}{\partial x'} G_k(x', \bar{R} = 0), \end{aligned} \quad (8.38)$$

and define the latter integral as

$$F_{\text{RG}}(x) = \int_0^x dx' \frac{\partial R_k(x')}{\partial x'} G_k(x', \bar{R} = 0), \quad (8.39)$$

where we have restricted ourselves to IR-finite regulators. We manipulate the trace term with  $G'$  in (8.37) in straight analogy. However these terms only contribute at order  $\bar{R}^2$

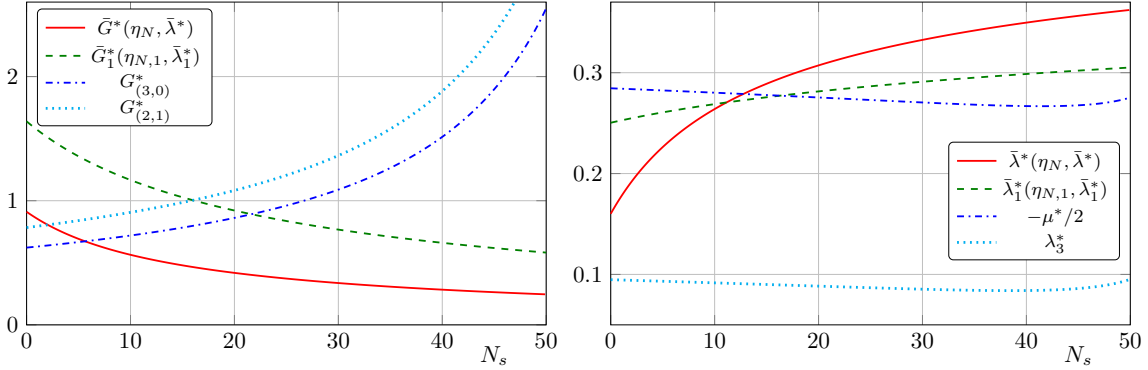


Figure 8.9.: We show the fixed point values as a function of  $N_s$  in the background field approximation (red continuous lines), in the level-one approximation (green dashed lines) and for the fluctuation system (blue dot-dashed and light blue dotted lines).

and are thus not relevant for the present work. More details and the flow equations for the level-one couplings can be found in App. F.2 and F.3.

Consequently (8.37) can straightforwardly be computed with heat-kernel methods. For UV flows, power counting suggests that the cutoff terms yield leading contributions to relevant operators such as the two-, three-, and four-point functions. In terms of diffeomorphism invariant objects this relates to the running of cosmological constant  $\Lambda$ , curvature scalar  $R$ , curvature scalar squared  $R^2$  and Ricci-tensor squared  $R_{\mu\nu}R^{\mu\nu}$ , superpositions of which form the presumably minimal set of three relevant operators in asymptotically safe quantum gravity [276].

### 8.6.2. Fixed-point results for level-one couplings

Our procedure provides us with a set of beta functions for the dimensionless level-one couplings,  $\bar{G}_1$  and  $\bar{\lambda}_1$ , which are displayed in App. F.2 while the technical details of the computation are given in App. F.3. We now analyse whether the level-one improvement leads to a system that reproduces the fluctuation results more closely than the background field approximation.

In Fig. 8.9 we display the fixed-point values of the fluctuation, the level-one, and the background system. The input on the right-hand side of the Wetterich equation is fluctuation, level-one, and background couplings, respectively. In Fig. 8.10 we present the corresponding real parts of the relevant critical exponents. The background and the level-one system each contain exactly two couplings. Both of them are relevant and their associated critical exponents form a complex conjugated pair. The fluctuation system has four dynamical couplings and four non-dynamical background couplings (background and level-one couplings). Of the four dynamical couplings three are relevant and one is irrelevant. Two relevant critical exponents form a complex conjugated pair and their real part is displayed in Fig. 8.10 since one can associate them with the couplings  $\mu$  and  $G_{(3,0)}$  by means of the largest overlap of the corresponding eigenvector. Finally in Fig. 8.11 we display the fixed-point values of the background, level-one, and fluctuation couplings with the full fluctuation system as input on the right-hand side of the Wetterich equation.

We observe that in pure gravity, the level-one improvement leads to critical exponents that agree better with the fluctuation results than the background field approximation,

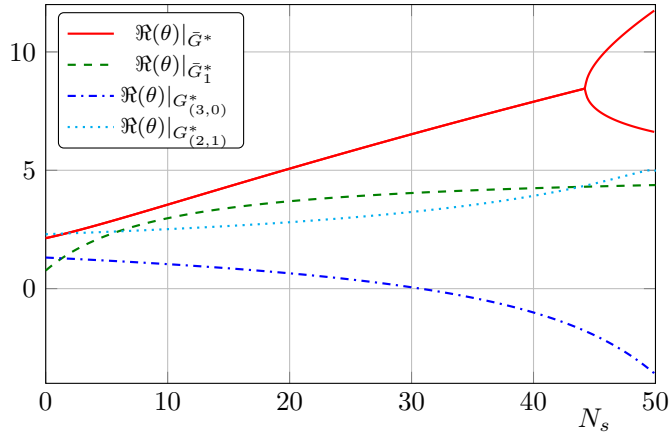


Figure 8.10.: We show the real part of the relevant critical exponents as a function of  $N_s$  in the background field approximation (red continuous line), in the level-one approximation (green dashed line) and for the fluctuation system (blue dot-dashed and light blue dotted lines).

cf. Fig. 8.10. As a function of  $N_s$  the fluctuation results shows a qualitatively different behaviour than the background and the level-one results. The real parts of critical exponents of the latter are increasing as a function of  $N_s$  while they are decreasing in the fluctuation case and even become irrelevant at  $N_s \approx 31$ . Nevertheless the level-one critical exponents are growing slower than the background ones and thus we observe a slight improvement.

For the fixed-point values of the Newton's couplings the level-one approximation tracks the background-approximation in its qualitative dependence on  $N_s$ : they are both decreasing as a function of  $N_s$  while the fluctuation Newton's couplings are increasing. However the quantitative difference between  $G_{(3,0)}^*$  and  $\bar{G}_1^*$  is smaller than the quantitative difference between  $G_{(3,0)}^*$  and  $\bar{G}^*$ , cf. Fig. 8.9. In the sector of the cosmological constants or momentum-independent parts of the  $n$ -point functions, the level-one improvement is more clearly visible. While the background cosmological constant increases strongly and approaches the pole at  $\bar{\lambda} = \frac{1}{2}$ , the level-one coupling remains almost constant and increases only slightly. The fluctuation coupling  $-\mu/2$  also remains almost constant but decreases slightly with  $N_s$ .

In summary the level-one approximation might be considered a slight improvement on the background field approximation. We have observed slight improvements in the critical exponents and in the fixed point values of the Newton's couplings and the cosmological constants. Considering however its failure to adequately capture the fluctuation results, a level-one approximation seems hardly justified in view of the significantly increased computational effort—at least based on the results in our truncation.

Last but not least we consider the fixed-point results when all couplings, including the background and the level-one coupling, are evaluated with the fluctuation couplings on the right-hand side of the Wetterich equation, cf. Fig. 8.11. We observe that the level-one approximation even appears to break the effective universality that was observed for Newton's coupling: the qualitative and quantitative dependence of  $\bar{G}_1^*$  on  $N_s$  does not match that of the other couplings as it first decreases with  $N_s$  and then strongly increases. For the ‘cosmological constants’, we make the opposite observation: while the background cosmological constant deviates strongly from the  $N_s$ -dependence of the graviton mass parameter,

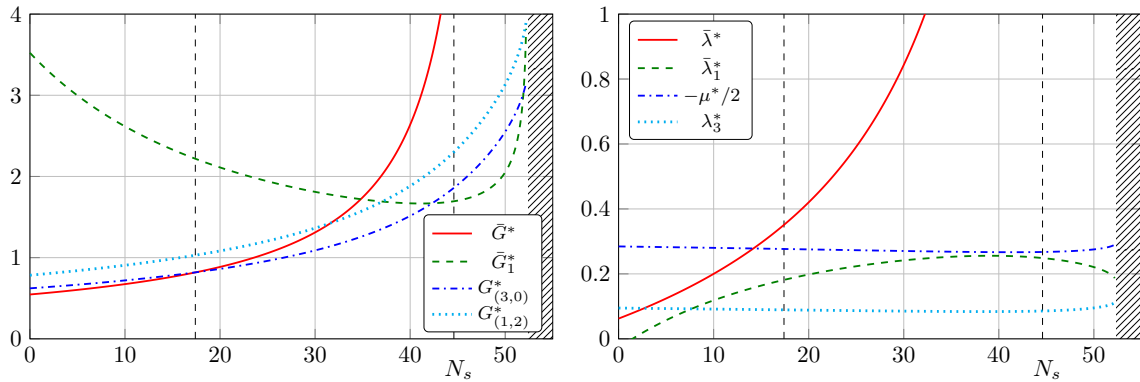


Figure 8.11.: Comparison of different level- $n$  gravitational couplings (left panel) and 'cosmological constants' (right panel). All couplings were evaluated with the input of the full fluctuation system on the right-hand side. While the gravitational couplings behave qualitatively similar, the level- $n$  'cosmological constants' display significant differences in their behaviour.

the level-one cosmological constant approaches it towards larger  $N_s$ . For the canonically most relevant coupling in the truncation, the step from the background coupling to the level-one coupling is therefore a significant step towards effective universality.

## 8.7. Summary

Universality guarantees the uniqueness of the one- and two-loop coefficients of the running of the marginal couplings in perturbatively renormalisable gauge theories irrespective from which vertex the running is read off. We investigated an analogous concept for non-marginal couplings such as the Newton's coupling in gravity-matter systems. For such couplings not even the one-loop coefficient is universal and breaking of diffeomorphism invariance and background independence due to the regularisation scheme further complicate computational tasks. Nonetheless an effective form of universality would be highly desirable, in particular with regard to the closure of the flow equations: all applications to asymptotically safe gravity need to close the flow equations in a truncation. For instance an effective universality in the Newton's coupling would be a key step towards a quantitative reliable closure of the system of flow equations for the  $n$ -point functions.

In this chapter we have critically discussed this effective universality of couplings in asymptotically safe gravity. This is of paramount importance, as it is at the root of all systematic expansion schemes used in the approach. We have critically examined and compared several common approximations based on effective universality, namely the single metric background field approximation, the level-one approximation to the fluctuation computation. In the latter effective universality is only used for the highest-order couplings. We focus on systems in the presence of  $N_s$  minimally coupled scalar fields, and include the effect of their quantum fluctuations.

Indeed we found an effective universality between the two Newton's couplings  $G_{(3,0)}$  and  $G_{(1,2)}$  in the scaling regime of the UV fixed point. This effective universality was semi-quantitative in quenched quantum gravity with the bilocal projection scheme that we used throughout this dissertation. If we took into account the full momentum dependence, see Fig. 8.2, we even found a quantitative effective universality in the relevant momentum

range  $p^2 \gtrsim 0.2k^2$ .

In the unquenched system we saw a violation of the effective universality, see [Fig. 8.3](#). While the bilocal momentum projections actually give almost the same  $N_s$  dependence of the Newton's couplings, the actual full momentum dependence behaves differently: the  $p^2$ -parts of the flows have different signs and the higher-order momentum dependences are non-negligible, which is in strong contrast to the situation in the quenched system. This hints at the fact that higher-order scalar-gravity operators need to be included, such as  $\sqrt{g}R^{\mu\nu}\varphi\nabla_\mu\nabla_\nu\varphi$  [\[436\]](#).

We investigated how the semi-quantitative effective universality of the bilocal approximation persists away from the UV fixed point by studying the size of the one-loop coefficients in the  $(\mu, \lambda_3)$ -plane, cf. [Fig. 8.4](#). Indeed we observed there that the effective universality is only fulfilled in a very small region of the parameter space. The UV fixed point lies in this small region, underlining that the occurrence of effective universality is highly non-trivial.

We searched for suitable simple truncations that imitate the behaviour of the fluctuation system. For this we used the Nielsen identity or split Ward-identity to upgrade the background couplings to level-one couplings. We thereby aim at deriving an upgrade to the single-metric approximation so that the improved background system can be derived without the need to separately evaluate the fluctuation system and insert it on the right-hand side of the Wetterich equation. This specifically tests if we can write the effective action as a diffeomorphism invariant and a gauge part, where the latter is independent of the fluctuation field, cf. [\(8.36\)](#). This would be the easiest case of possible dependences for the gauge part and it is motivated by the non-trivial effective universality that we observed. Unfortunately, our results of the level-one couplings do not sustain such an ease functional dependence. We saw a slight improvement of the level-one couplings towards the fluctuation system compared to the background system. We saw however still a discrepancy and in conclusion the improvement does not justify the increased computational effort. Nonetheless the non-trivial effective universality hints strongly towards a simple form of the effective action.

In summary this chapter provided first non-trivial hints that different avatars of the Newton's coupling show an effective universality in the scaling regime around the UV fixed point. This result is a cornerstone for future truncations and the quest for a consistent closure of the flow equation.

## 9. Summary and outlook

In this dissertation we went on a journey from low to high energy scales in search of a UV completion of the Standard Model of particle physics. The topics ranged from electroweak baryogenesis at small energy scales of the order of TeV to asymptotically safe quantum gravity at energy scales beyond the Planck scale. A further focus was put on the couplings of quantum gravity to the Standard Model, which is the basis of a possible UV completion.

In [Chapter 2](#) we investigated measurable consequences of electroweak baryogenesis. In the Standard Model the electroweak phase transition is of second order and electroweak baryogenesis is not possible. It can be triggered with appropriate beyond the Standard Model physics. In these cases the electroweak phase transition becomes a strong first-order phase transition. Here we parameterised wide classes of beyond the Standard Model physics via polynomial and non-polynomial modifications of the Higgs potential. Importantly, the non-polynomial modifications cannot be Taylor expanded around a vanishing field value. We determined that the typical energy scale of these modifications should be in the TeV range such that they can influence the order of the electroweak phase transition. Next, we clearly identified three different regimes in which the measured value of the Higgs self-couplings can fall into. If the cubic Higgs self-coupling is too small ( $\lambda_{H^3}/\lambda_{H^3,0} < 1.5$ ) electroweak baryogenesis is not possible within the limits of the presented setup. If the cubic Higgs self-coupling is big enough ( $\lambda_{H^3}/\lambda_{H^3,0} > 2$ ) we have strong hint that electroweak baryogenesis can take place. In the intermediate range ( $1.5 < \lambda_{H^3}/\lambda_{H^3,0} < 2$ ) the results are not conclusive and a study of the underlying microscopic model would be necessary. Importantly the cubic Higgs self-coupling will be measured precisely enough in the planned high-luminosity run of the LHC. We determined analogous regimes for the quartic Higgs self-coupling. A quantitative measurement of the quartic Higgs self-coupling is however only in the far future possible. These results allow for a search for beyond Standard Model physics guided by the phenomenology of the baryon asymmetry.

In [Chapter 3](#) we significantly increased the energy scale to beyond Planck scale energies and presented the asymptotic safety approach to quantum gravity. We presented the minimal setup that contains a genuine fluctuation Newton's coupling: the setup that includes the flow of the graviton two- and three-point function. With this truncation we have shown that Wilsonian RG is well defined in the sense that all computed correlation functions are momentum-local due to non-trivial cancellations between different diagrams. We further confirmed the existence of the interacting UV fixed point in this truncation that renders the high energy behaviour of all couplings finite. This UV fixed point had two relevant directions corresponding to the diffeomorphism invariant operators  $\sqrt{g}$  and  $\sqrt{g} R$ . From this basic setup we expanded in the subsequent chapters in different directions.

The first improvement of the minimal setup is described in [Chapter 4](#), where we tried to go towards quantitative precision or even towards apparent convergence by extending the setup to higher-order vertex functions. In particular we extended the setup to the graviton four-point function. This setup included two genuine fluctuation Newton's couplings, which also allowed for comparisons and extensive studies of different closures of the flow equations. We found an UV fixed point with three relevant directions in this extended

truncation. We made further observations: With the inclusion of the graviton four-point function we found for the first time a non-vanishing  $p^4$ -contribution in the flow of a graviton  $n$ -point function. Such contributions come from  $R^2$  or  $R_{\mu\nu}^2$  tensor structures. We were able to determine, that the  $R_{\mu\nu}^2$  tensor structures are non-trivially suppressed while the  $R^2$  tensor structures are dynamically generated and are responsible for the  $p^4$ -contribution. Due to this overlap we associated the third relevant directions of the UV fixed point with  $R^2$ . Considering the convergence of the system we indeed observed that the existence of the fixed point and the values of the critical exponents became less sensitive with respect to changes of the closure of the flow equations compared to the previous truncation.

The next improvement, also based on the minimal setup is the inclusion of background curvature dependence. In an idealistic setup one would like to keep a generic curved background and expand in the fluctuation field about this generic background. Due to technical limitations this is unfeasible and in most chapters of this dissertation we expanded about the flat background. In [Chapter 5](#) we constructed an approximate momentum space that allowed for the evaluation of vertex flows on constantly curved backgrounds. The fixed point couplings turned into functions of the background curvature. We confirmed the existence of these fixed point functions, which provided further evidence in favour of the asymptotic safety scenario. The setup further allowed to set up the equations of motion and find solutions to them. Solutions to the equations of motion are of great interest as they provide self-consistent backgrounds and an expansion around these backgrounds potentially improves the convergence properties of the expansion. For the first time we were able to distinguish between the background and the quantum equation of motion. The former stems from a derivative with respect to the background field while the latter stems from a derivative with respect to the fluctuation field. In the full quantum effective action with vanishing regulator, these two equation yield compatible solutions, but in the usual asymptotic safety regime ( $k \rightarrow \infty$ ) they are manifestly different. We argued that in this case the quantum equation of motion is the relevant one. In the literature mainly the background equation of motion was investigated and in agreement with the literature we found that it did not yield a solution in the pure quantum gravity setup. Only with Standard Model matter content a solution at small positive curvature appeared. For the more important quantum equation of motion we found a solution at negative background curvature. We checked that our results were stable with respect to changes of the truncation.

In the remaining chapters of this dissertation we focused on the inclusion of Standard Model matter content into the asymptotic safety scenario. This task is of particular importance as any theory of quantum gravity must be able to connect to the full Standard Model in the IR, including all its measurements. We started with the inclusion of  $N_s$  minimally coupled scalars and  $N_f$  minimally coupled fermions in [Chapter 6](#). We investigated the UV fixed point as a function of  $N_s$  and  $N_f$ . We observed that fermions are generally stabilising the UV fixed point and we found compatibility with asymptotic safety for all  $N_f$ . For scalars we couldn't draw any final conclusion. The reason for this was a validity bound on commonly used regulators that we introduced: if one chooses the regulator proportional to the two-point function and thus also proportional to the wave function renormalisation, then one finds that the anomalous dimension should stay below a certain value, for the graviton anomalous dimension  $\eta_h < 2$ . In the scalar sector this bound was violated at  $N_s \approx 21$  scalars. We further found significant qualitative differences between our results and results using the background field approximation [\[424\]](#). This emphasised

the importance of going beyond the background field approximation in gravity-matter systems.

In [Chapter 7](#) we coupled Yang-Mills theory to quantum gravity. We manifested and confirmed previous results that the gravity contribution to Yang-Mills theory can only support asymptotic freedom in the minimal coupling of the gauge sector. More importantly we carefully reassessed the physics of all gravitationally coupled gravity-matter systems. This includes the scalar-fermion-gravity systems from [Chapter 6](#) and also asymptotically free gauge-matter-gravity systems. We provided a formal argument that a successive integration of first the matter and gauge degrees of freedom and then the gravity degrees of freedom provides a well controlled environment where the resulting asymptotically safe UV fixed point does not have any dependence on the number of matter or gauge fields as long as  $R^2$  and  $R_{\mu\nu}^2$  terms are neglected. The latter terms were neglected in all gravity-matter-gauge computations within asymptotically safe quantum gravity so far. In consequence, in all truncations considered so far, the existence of the UV fixed point should not depend on the number of matter or gauge fields. If it does, as in the scalar case of [Chapter 6](#), it is just an artefact of the truncation. In the remaining parts of [Chapter 7](#) we explicitly tested the Yang-Mills–gravity system with respect to these findings. We indeed found that  $SU(N_c)$  Yang-Mills theory is compatible with asymptotic safety for all  $N_c$  and we could provide explicit results in the limit  $N_c \rightarrow \infty$ . We found a strong scheme dependence, but the underlying physics remained unchanged. The gravity system had two possibilities to dynamically adjust itself to the presence of the gauge fields: Either the graviton mass parameter moved towards its pole ( $\mu \rightarrow -1$ ) or the wave function renormalisation increased. Both possibilities increased the graviton propagator and thus counterbalanced the impact of the gauge fields. Which choice was taken depended on the choice of regulator shape function. This is a unique situation for Yang-Mills theory, because fermions always move the graviton mass parameter towards its pole while scalars always fall in the category of increasing wave function renormalisation. The latter remained inaccessible due to the above mentioned regulator bound,  $\eta_h < 2$ . In summary this chapter classified different matter fields according to their impact on the graviton propagator and showed that the underlying physics is just identical. Furthermore it pointed out that the inclusion  $R^2$  and  $R_{\mu\nu}^2$  tensor structures is necessary in order to obtain a true dependence of the UV fixed point on the number of matter or gauge fields.

In [Chapter 8](#) we investigated the concept of effective universality for gravity-matter systems. This concept is analogous to two-loop universality for marginal couplings of perturbatively renormalisable theories. In gravity, for instance, not even the one-loop coefficient of the flow for Newton’s coupling is unique. Nonetheless we revealed an effective universality in the scaling regime of the UV fixed point for the fluctuation couplings. Effective universality means that different avatars of the Newton’s coupling are quantitative similar, irrespective from which vertices they are read off. This effective universality only seems to hold in the IR for vanishing regulator and in the scaling regime of the UV fixed point. This result is thus a key stone for further truncation as it provides a guiding principle for the closure of flow equations. Motivated by these surprising results we advocated a simple form for the effective action: a diffeomorphism invariant part and a gauge part that is independent of the fluctuation field. We tested this scenario by upgrading a flow from the background field approximation with the use of a Nielsen identity to a level-one flow. We found, however, that the level-one flow is not in agreement with the fluctuation results and thus this simple form of the effective action is a too strong approximation.

Nonetheless the non-trivial effective universality hints strongly towards a simple form of the effective action.

There are many possible improvements of the work in dissertation:  
 In the area of electroweak baryogenesis it would be interesting to check the influence of a full inclusion of the weak Standard Model sector. In this work the weak sector was mimicked by a fiducial coupling, which work well over larger orders of magnitudes at vanishing temperature compared to the full running in the Standard Model [74]. A huge deviation is thus not to be expected but is still necessary for improved quantitative precision. Furthermore we have restricted ourselves to a certain set of modifications of the Higgs potential, namely polynomial, logarithmic and exponential modifications where the latter are not Taylor-expandable about vanishing field value. These are all standard choices for modifications and one can ask what would happen if we all kinds of numerical modifications are allowed. Maybe this would increase the range of values for the Higgs self-couplings that are compatible with electroweak baryogenesis. In some sense we have so far investigated natural choices of modifications. Straight forward connected to this question is the link between the different modifications and the underlying microscopic new physics. We have so far not investigated from which new degrees of freedom the presented modifications can arise. In general, a stronger link between beyond the Standard Model physics and Higgs potential modifications could provide a guideline for restricting the space of possible modifications and thus in the end provide a stronger bound on the Higgs self-couplings that are compatible with electroweak baryogenesis.

In the pure gravity sector an obvious improvement would be the inclusion of higher  $n$ -point functions. However, the computational effort for flows of higher  $n$ -point functions grows factorially and thus such extensions of the truncation become soon not worth the effort. It would be much more worthwhile to broaden the lower  $n$ -point functions to larger tensor structures. For example the  $R^2$  and the  $R_{\mu\nu}^2$  tensor structures have already been included in the graviton two-point function in [294]. This work also raised the question of one-loop universality of classically marginal couplings in gravity fluctuation computations: it did not obtain the usual universal one-loop coefficient of the beta-functions of the marginal  $R^2$  and  $R_{\mu\nu}^2$  couplings. A combination of the increased tensor space with a high-order vertex computation thus appears to be highly worthwhile in order to clarify this question. It can shed further light on the number of relevant operators in asymptotically safe quantum gravity. Recently there has been no full agreement [3, 293–295] and the number of relevant operators ranges from two to four, with a slight preference for three. In most computation  $\sqrt{g}$ ,  $\sqrt{g}R$  and  $\sqrt{g}R^2$  are the relevant operators and  $\sqrt{g}R_{\mu\nu}^2$  is irrelevant.

Throughout this dissertation we have worked with the linear split of the metric  $g_{\mu\nu} = \bar{g}_{\mu\nu} + h_{\mu\nu}$ . Other splits of the metric are possible, such as the exponential split  $g_{\mu\nu} = \bar{g}_{\mu\rho} (e^h)^\rho_\nu$  [259, 262, 349–351, 426]. Such a choice of split influences the vertices generated from the underlying classical action and consequently also directly the flow equation of the couplings, if one works in a truncation. Changing the split can thus provide a tool to check the stability of a truncation. Similarly varying the gauge fixing parameters can provide such a tool. Here in particular the dependence on the gauge fixing parameter  $\beta$  is interesting, since the Landau gauge  $\alpha = 0$  is clearly preferred due to the fixed point of the RG flow [366] and since it maximally disentangles physical modes and gauge modes [474]. Such investigations have been performed so far on the level of the background field approximation [245, 262, 263] but hardly at the level of fluctuation computations [328].

The caveat is of course that keeping the general dependence on the split and on the gauge parameters further complicates the computation and thus one will not be able to perform a high-order computation compared to a setup with fixed split and gauge parameters.

In the gravity-matter sector the next important step inevitably involves the inclusion of  $R^2$  and  $R_{\mu\nu}^2$  tensor structures. According to [Chapter 7](#) the running the corresponding couplings are the only ones that can generate a dependence of the fixed point values on the number of matter or gauge fields that is not scheme dependent. With the inclusion of such operators one will be able to asses whether the graviton propagator grows or shrinks with the number of matter or gauge fields. This in particular interesting in view of indications for a weak-gravity bound in asymptotic safety [\[120, 387, 432, 441\]](#), where gravity fluctuations trigger new divergences in the matter sector if they are too strong.

The quantitative precision that this dissertation has aimed at is also inherently necessary for postdictions of the Standard Model. Recently for instance the top mass was approximately postdicted with a background field approximation in the quantum gravity sector [\[120\]](#). It will be intriguing to see how this postdiction persists in an extended truncation that includes a dependence on the number of matter or gauge fields of the graviton propagator that is not scheme dependent due to the inclusion of  $R^2$  and  $R_{\mu\nu}^2$  tensor structures.

In overall summary this dissertation provides valuable contributions to the UV-completion of the Standard Model. Electroweak baryogenesis is soon to be tested with the measurement of the Higgs self-coupling at the LHC, which will serve a guidance for the search of beyond the Standard Model physics. In quantum gravity we have provided many conceptual advancements that aim towards apparent convergence, quantitative precision and background independence of the approach. The results contribute to the significant evidence for the existence of the UV fixed point and thus the non-perturbative renormalisability of quantum gravity. We further have laid down the basis for future computation of gravity-matter-gauge systems by establishing the compatibility of weakly coupled matter with the asymptotic safety scenario and by revealing an effective universality between different avatars of Newton's coupling.



# A. Electroweak baryogenesis

This Appendix belongs to [Chapter 2](#).

## A.1. Flow equations

The set of couplings in our setup consists of the  $SU(3)$  coupling  $g_3$ , a fiducial coupling  $g_F$  that simulates the  $SU(2)$  and the  $U(1)$  sector, the top-Yukawa coupling  $y_t$ , and the full Higgs potential  $V(\phi)$  [\[74\]](#). For the  $SU(3)$  coupling it suffices to consider one-loop running, since higher-order or threshold corrections have little impact on the phase transition. The one-loop beta function is given by

$$\beta_{g_3} = -\frac{g_3^3}{(4\pi)^2} \left( 11 - \frac{2}{3} n_f \right), \quad (\text{A.1})$$

with  $n_f = 6$ . We fix the  $SU(3)$  coupling through  $g_3(1 \text{ TeV}) = 1.06$ , so the scale-dependent  $SU(3)$  coupling is known analytically. We approximate its temperature dependence by replacing  $k \rightarrow \sqrt{k^2 + \pi T^2}$ ,

$$g_3(k, T) = \left( \frac{7}{8\pi^2} \ln \frac{\sqrt{k^2 + \pi T^2}}{1 \text{ TeV}} + \frac{1}{1.06^2} \right)^{-1/2}. \quad (\text{A.2})$$

The logarithmic running of the  $U(1)$  and  $SU(2)$  couplings is sufficiently slow to be negligible for our purpose [\[74\]](#). We model it as a fiducial coupling  $g_F$  that is a constant as a function of the RG scale and thus also a constant as a function of the temperature. At finite temperature, this simplified treatment must be ameliorated by a thermal mass generated by fluctuations from the electroweak sector. According to the high- $T$  expansion of the one-loop thermal potential it is given by

$$V_{\text{thermal mass}}(\phi, T) = \frac{1}{16} \left( 3g^2 + g'^2 \right) \frac{T^2 \phi^2}{2}, \quad (\text{A.3})$$

where  $g = 0.65$  and  $g' = 0.36$  are the  $SU(2)$  and  $U(1)$  gauge couplings, respectively.

To derive beta functions for the Higgs potential and the top-Yukawa coupling we introduce the renormalised dimensionless field  $\rho$  and the dimensionless potential  $u$

$$\rho = \frac{\phi^2}{2k^2 Z_\phi}, \quad u(\rho) = \frac{V(\phi(\rho))}{k^4}. \quad (\text{A.4})$$

The wave function renormalizations of the fields appear in the beta functions only via their anomalous dimension

$$\eta_\phi = -\frac{d \log Z_\phi}{d \log k}, \quad \eta_\psi = -\frac{d \log Z_\psi}{d \log k}. \quad (\text{A.5})$$

Written in terms of threshold functions, the beta function for the top Yukawa coupling agrees with that from [74, 180–182], see e.g. Eq.(C8) of [74]. However, we use a spatial regulator as described below and temperature-dependent threshold functions. The spatial regulator changes some prefactors, which is compensated by the different definition of the threshold functions. The beta function is given by

$$\begin{aligned}
\frac{dy_t^2}{d \log k} = & y_t^2 (\eta_\phi + 2\eta_\psi) \\
& - \frac{y_t^4}{\pi^2} \left( 3\kappa u''(\kappa) + 2\kappa^2 u^{(3)}(\kappa) \right) l_{1,2}^{(FB)4} (\kappa y_t^2, u'(\kappa) + 2\kappa u''(\kappa); \eta_\psi, \eta_\phi; T) \\
& + \frac{y_t^4}{2\pi^2} \left( l_{1,1}^{(FB)4} (\kappa y_t^2, u'(\kappa) + 2\kappa u''(\kappa); \eta_\psi, \eta_\phi; T) \right. \\
& \quad \left. - 2\kappa y_t^2 l_{2,1}^{(FB)4} (\kappa y_t^2, u'(\kappa) + 2\kappa u''(\kappa); \eta_\psi, \eta_\phi; T) \right) \\
& + \frac{3}{\pi^2} \frac{(N_c^2 - 1)}{2N_c} g_3^2 y_t^2 \left( 2\kappa y_t^2 l_{2,1}^{(FB)4} (\kappa y_t^2, 0; \eta_\psi, \eta_A; T) - l_{1,1}^{(FB)4} (\kappa y_t^2, 0; \eta_\psi, \eta_A; T) \right) \\
& - \frac{c_y g_F^2 y_t^2}{16\pi^2 \left( 1 + \left( \frac{80}{246} \right)^2 \kappa \right)}, \tag{A.6}
\end{aligned}$$

where  $c_y = 97/30$  and  $N_c = 3$ . It depends on the position of the renormalised dimensionless minimum  $\kappa$  of the potential, the anomalous dimensions of the fields, as well as on regulator-dependent threshold functions specified below. Here, we have employed the same projection scheme onto the Yukawa flow as in [74] for reasons of comparison. In principle, there exists an improved scheme [240] more adequately capturing higher-order contributions to the Yukawa flow for the present model [242], possibly improving the fixing of initial conditions on the 5% level. In either case, working in the symmetric regime with  $\kappa = 0$  and neglecting the additional  $\eta$  dependence in the threshold functions reproduces the universal one-loop beta functions, as it should.

The beta function for the Higgs potential at vanishing temperature has been computed in [74, 180–182], see e.g. Eq.(E1) of [74]. As for the beta function of the Yukawa coupling, the present finite temperature beta function for the Higgs potential agrees with the  $T = 0$  one in terms of the threshold functions

$$\begin{aligned}
\frac{du(\rho)}{d \log k} = & -4u(\rho) + (2 + \eta_\phi)\rho u'(\rho) \\
& + \frac{1}{4\pi^2} \left( l_0^{(B)4} (u'(\rho) + 2\rho u''(\rho); \eta_\phi; T) - 4N_c l_0^{(F)4} (y_t^2 \rho; \eta_\psi; T) \right) \\
& + \frac{c_l}{2\pi^2 \left( 1 + \frac{g_F^2 \rho}{2} \right)}, \tag{A.7}
\end{aligned}$$

where  $c_l = 9/16$  and again  $N_c = 3$ .

Finally, we need expressions for the anomalous dimensions of the Higgs field and the top-quark: the first two terms in (A.6) are integral parts of the universal one-loop contribution. In terms of the threshold functions the anomalous dimension of the top quark agrees with the  $T = 0$  one in Eq.(C8) of [74], and the anomalous dimension of the scalar field has the

same form as in Eq.(16) of [180–182]. With the thermal threshold functions of the present work this means

$$\begin{aligned}\eta_\phi &= \frac{2}{3\pi^2} N_c y_t^2 \left( m_4^{(F)4}(\kappa y_t^2; \eta_\psi; T) - \kappa y_t^2 m_2^{(F)4}(\kappa y_t^2; \eta_\psi; T) \right) \\ &\quad + \frac{1}{3\pi^2} \kappa \left( 3u''(\kappa) + 2\kappa u^{(3)}(\kappa) \right)^2 m_4^{(B)4} (u'(\kappa) + 2\kappa u''(\kappa); \eta_\phi; T) , \\ \eta_\psi &= \frac{1}{6\pi^2} y_t^2 m_{1,2}^{(FB)4} (\kappa y_t^2, u'(\kappa) + 2\kappa u''(\kappa); \eta_\phi; T) \\ &\quad + \frac{1}{2\pi^2} \frac{(N_c^2 - 1)}{2N_c} g_3^2 \left( m_{1,2}^{(FB)4}(\kappa y_t^2, 0; \eta_\psi, 0; T) - \tilde{m}_{1,1}^{(FB)4}(\kappa y_t^2, 0; \eta_\psi, 0; T) \right) .\end{aligned}\quad (\text{A.8})$$

The beta functions found above are expressed in terms of regulator-dependent and temperature-dependent threshold functions. Here we provide explicit analytic results for these threshold functions for one specific regulator. The analyticity of the threshold function is rooted in the use of a Litim-type regulator [373] that only regularises the spatial momenta. The dimensionless bosonic and fermionic propagators are regularised as

$$\begin{aligned}G_\phi(\omega_n^2, \vec{p}^2, m_\phi^2) &= (\omega_n^2 + \vec{p}^2/k^2(1 + r_B(\vec{p}^2/k^2)) + m_\phi^2)^{-1} , \\ G_\psi(\nu_n^2, \vec{p}^2, m_\psi^2) &= (\nu_n^2 + \vec{p}^2/k^2(1 + r_F(\vec{p}^2/k^2)) + m_\psi^2)^{-1} ,\end{aligned}\quad (\text{A.9})$$

with the bosonic Matsubara frequency  $\omega_n = 2\pi n T/k$  and the fermionic Matsubara frequency  $\nu_n = 2\pi(n + \frac{1}{2})T/k$ . Note that  $m_\phi$  and  $m_\psi$  are dimensionless mass-like arguments. The bosonic and fermionic regulator shape functions read [373]

$$r_B(x) = (x^{-1} - 1) \Theta(1 - x) , \quad r_F(x) = \left( x^{-1/2} - 1 \right) \Theta(1 - x) , \quad (\text{A.10})$$

where  $x = \vec{p}^2/k^2$ . In the following, we express the threshold functions in terms of the bosonic and fermionic distribution functions,

$$n_{F,B}(m_{\psi,\phi}^2, T) = \left( \exp \left( \frac{k}{T} \sqrt{1 + m_{\psi,\phi}^2} \right) \mp 1 \right)^{-1} . \quad (\text{A.11})$$

The set of threshold functions we need in our calculation includes

$$\begin{aligned}l_0^{(B)d}(m_\phi^2; \eta_\phi; T) &= \frac{2}{d-1} \left( 1 - \frac{\eta_\phi}{d+1} \right) \mathcal{B}_{(1)}(m_\phi^2; T) , \\ l_0^{(F)d}(m_\psi^2; \eta_\psi; T) &= \frac{2}{d-1} \left( 1 - \frac{\eta_\psi}{d} \right) \mathcal{F}_{(1)}(m_\psi^2; T) , \\ l_{n,m}^{(FB)d}(m_\psi^2, m_\phi^2; \eta_\psi, \eta_\phi; T) &= \frac{2}{d-1} \left( n \left( 1 - \frac{\eta_\psi}{d} \right) \mathcal{FB}_{(n+1,m)}(m_\psi^2, m_\phi^2; T) \right. \\ &\quad \left. + m \left( 1 - \frac{\eta_\phi}{d+1} \right) \mathcal{FB}_{(n,m+1)}(m_\psi^2, m_\phi^2; T) \right) , \\ m_4^{(B)d}(m_\phi^2; \eta_\phi; T) &= \mathcal{B}_{(4)}(m_\phi^2; T) , \\ m_2^{(F)d}(m_\psi^2; T) &= \mathcal{F}_{(4)}(m_\psi^2; T) ,\end{aligned}$$

$$\begin{aligned}
m_4^{(F)d}(m_\psi^2; \eta_\psi; T) &= \mathcal{F}_{(4)}(m_\psi^2; T) + \frac{1 - \eta_\psi}{d - 3} \mathcal{F}_{(3)}(m_\psi^2; T) \\
&\quad - \frac{1}{2} \left( \frac{1 - \eta_\psi}{d - 3} + \frac{1}{2} \right) \mathcal{F}_{(2)}(m_\psi^2; T), \\
m_{1,2}^{(FB)d}(m_\psi^2, m_\phi^2; \eta_\psi, \eta_\phi; T) &= \left( 1 - \frac{\eta_\phi}{d} \right) \mathcal{FB}_{(1,2)}(m_\psi^2, m_\phi^2; T), \\
\tilde{m}_{1,1}^{(FB)d}(m_\psi^2, m_\phi^2; \eta_\psi, \eta_\phi; T) &= \frac{2}{d - 2} \left( \left( 1 - \frac{\eta_\phi}{d} \right) \mathcal{FB}_{(1,2)}(m_\psi^2, m_\phi^2; T) \right. \\
&\quad + \left( 1 - \frac{\eta_\psi}{d - 1} \right) \mathcal{FB}_{(2,1)}(m_\psi^2, m_\phi^2; T) \\
&\quad \left. - \frac{1}{2} \left( 1 - \frac{\eta_\psi}{d - 1} \right) \mathcal{FB}_{(1,1)}(m_\psi^2, m_\phi^2; T) \right). \quad (\text{A.12})
\end{aligned}$$

All threshold functions are expressed in terms of

$$\begin{aligned}
\mathcal{F}_{(1)}(m_\psi^2; T) &= \frac{T}{k} \sum_{n \in \mathbb{Z}} G_\psi(\nu_n, m_\psi^2), & \mathcal{B}_{(1)}(m_\phi^2; T) &= \frac{T}{k} \sum_{n \in \mathbb{Z}} G_\phi(\omega_n, m_\phi^2), \\
\mathcal{FB}_{(1,1)}(m_\psi^2, m_\phi^2; T) &= \frac{T}{k} \sum_{n \in \mathbb{Z}} G_\psi(\nu_n, m_\psi^2) G_\phi(\omega_n, m_\phi^2). \quad (\text{A.13})
\end{aligned}$$

At finite temperature for the flat regulators in (A.10) they are given by

$$\begin{aligned}
\mathcal{F}_{(1)}(m_\psi^2; T) &= \frac{1}{\sqrt{1 + m_\psi^2}} \left( \frac{1}{2} - n_F(m_\psi^2, T) \right), \\
\mathcal{B}_{(1)}(m_\phi^2; T) &= \frac{1}{\sqrt{1 + m_\phi^2}} \left( \frac{1}{2} + n_B(m_\phi^2, T) \right), \\
\mathcal{FB}_{(1,1)}(m_\psi^2, m_\phi^2; T) &= \left[ \frac{\frac{1}{2} + n_B(m_\phi^2, T)}{2\sqrt{1 + m_\phi^2}} \left( \left( m_\psi^2 + 1 - \left( i\pi T/k + \sqrt{1 + m_\phi^2} \right)^2 \right)^{-1} \right. \right. \\
&\quad + \left( m_\psi^2 + 1 - \left( i\pi T/k - \sqrt{1 + m_\phi^2} \right)^2 \right)^{-1} \left. \right) \\
&\quad + \frac{\frac{1}{2} - n_F(m_\psi^2, T)}{2\sqrt{1 + m_\psi^2}} \left( \left( m_\phi^2 + 1 - \left( i\pi T/k + \sqrt{1 + m_\psi^2} \right)^2 \right)^{-1} \right. \\
&\quad + \left. \left. \left( m_\phi^2 + 1 - \left( i\pi T/k - \sqrt{1 + m_\psi^2} \right)^2 \right)^{-1} \right) \right]. \quad (\text{A.14})
\end{aligned}$$

They obey the relations

$$\frac{\partial \mathcal{F}_{(n)}}{\partial m_\psi^2} = -n \mathcal{F}_{(n+1)}, \quad \frac{\partial \mathcal{B}_{(n)}}{\partial m_\phi^2} = -n \mathcal{B}_{(n+1)},$$

$$\frac{\partial \mathcal{FB}_{(m,n)}}{\partial m_\psi^2} = -m \mathcal{FB}_{(m+1,n)}, \quad \frac{\partial \mathcal{FB}_{(m,n)}}{\partial m_\phi^2} = -n \mathcal{FB}_{(m,n+1)}. \quad (\text{A.15})$$

The notation and the threshold functions agree with [240]. Note, that the  $T \rightarrow 0$  limit of the threshold functions does not agree with the ones given in [180–182], since we use a spatial regulator while [180–182] uses a covariant regulator. This concludes the list of threshold functions and relations necessary in order to numerically evaluate the previously given beta functions.

## A.2. Grid approach and benchmarking

We solve the functional differential equation for the Higgs potential, (A.7), using a grid code. This means that the potential  $u(\rho)$  and its derivative  $u'(\rho)$  are discretised on a grid in the field invariant  $\rho$ . The discretisation converts the partial differential equation for  $u(\rho)$  into a large set of coupled ordinary differential equations. The grid code has to manage a numerical integration from  $k = \Lambda$ , where we initialise the flow, down to  $k = k_{\text{IR}} \approx 100$  GeV. At this IR value all physical relevant quantities are frozen out and only convexity-generating processes take place.

The grid code also has to cover a large range of values in the scalar field  $0 \leq \phi \leq c\Lambda$ , where we typically choose  $c = \mathcal{O}(1 \dots 10)$ . To resolve both, large field values and the minimum of the potential at small field values, we employ an exponential distribution of the grid points  $\rho_i = \phi_i^2/2$  with  $i \in 0, \dots, N - 1$  according to

$$\rho_i = \rho_a + \frac{\exp\left(\frac{i}{c_{\text{grid}}}\right) - 1}{\exp\left(\frac{(N-1)}{c_{\text{grid}}}\right)} \rho_b, \quad (\text{A.16})$$

where  $N$  is the number of grid points,  $c_{\text{grid}}$  a grid parameter that governs the distributions of the grid points, and  $\rho_a$  and  $\rho_b$  the smallest and largest included field value, respectively.

We introduce a grid for the potential  $u(\rho_i)$  as well as for the derivative of the potential  $u'(\rho_i)$ , and we match the second and third derivative of the potential in between the grid points [475]. This is augmented by a differential equation for the top-Yukawa coupling, while the  $SU(3)$  coupling is already integrated out and the fiducial coupling for  $SU(2)$  and  $U(1)$  remains constant. Consequently, we obtain a system of  $2N + 1$  coupled differential equations for a grid consisting of  $N$  points, which is solved with an iterative Runge-Kutta-Fehlberg method with an adaptive step size.

At the IR scale and at vanishing temperature, we match the output of the grid code with the physically known observables, see (2.12). This is implemented on the level of the variables of the grid code and in particular we demand that the errors fulfil  $\Delta\rho_{\text{min}} \leq 20$  GeV $^2$ ,  $\Delta\lambda_4 \leq 0.002$  and  $\Delta y_t \leq 0.0014$ . Expressed in the quantities of (2.12) these errors correspond to  $\Delta v \leq 0.08$  GeV,  $\Delta m_H \leq 0.28$  GeV, and  $\Delta m_t \leq 0.23$  GeV. It is important to determine the vacuum expectation value more precisely since its error directly influences the error on the Higgs and the top mass.

To achieve this precision we tune the parameters  $\mu$ ,  $\lambda_4$  and  $y_t$  at the UV scale, which is done by a secant method in  $\mu$  and a two-dimensional bisection method in  $\lambda_4$  and  $y_t$ . The grid code might exhibit other systematic errors and in particular the measurement of the Higgs mass is challenging since it is related to the second derivative of the potential.

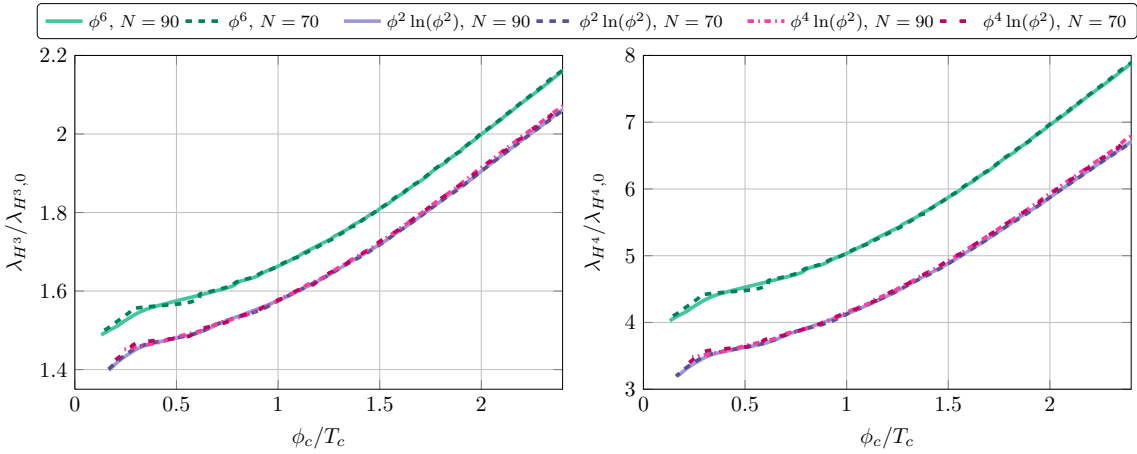


Figure A.1.: Modification of the self-couplings  $\lambda_{H^3}/\lambda_{H^3,0}$  (left) and  $\lambda_{H^4}/\lambda_{H^4,0}$  (right) as a function of  $\phi_c/T_c$  for polynomial and logarithmic modifications of the UV potentials, cf. (2.11). We compare results for  $N = 70$  and  $N = 90$  grid points.

Hence we conservatively estimate the total accuracy of the IR values with

$$\Delta v \leq 0.2 \text{ GeV}, \quad \Delta m_H \leq 1.5 \text{ GeV}, \quad \Delta m_t \leq 0.5 \text{ GeV}. \quad (\text{A.17})$$

The tuning process is performed at vanishing temperature and the tuned initial values are subsequently used as initial values for all finite-temperature computations. For each temperature we initialise the flow in this way and determine the position of the minimum at the IR scale  $k_{\text{IR}}$ . The critical temperature is obtained with a bisection method where we demand an accuracy of  $\Delta T_c \leq 0.2$  MeV. This high accuracy is necessary for a precise value of  $\phi_c$ , which is in turn given by the position of the minimum at the temperature just below  $T_c$ . From the grid code, it is difficult to get a clear signature distinguishing between second-order phase transitions and weak first-order phase transitions. Within our numerical accuracy, a reliable distinguishing signature is not available for  $\phi_c \lesssim 20$  GeV. For finite temperature computations we slightly increase the number of grid points, since the exponential functions in the bosonic and fermionic distribution functions make these computations technically more challenging.

We test our numerical results by first comparing the observables for two different numbers of grid points. The necessary number varies with our choice of cutoff and the modification of the Higgs potential. For example, more grid points are necessary for the exponential modifications of the potential. For polynomial and logarithmic modifications and a cutoff  $\Lambda = 2$  TeV, we use typically  $N = 90$  grid points, while for exponential modifications with the same cutoff we use  $N = 150$  grid points. In Fig. A.1 we display results for polynomial and logarithmic modifications. In particular we show the correlation between the strength of first-order phase transition and the Higgs-self couplings. In Fig. A.2 we show the same correlation but for exponential modifications and for  $N = 130$  and for  $N = 150$  grid points. The results for  $N = 90$  and for  $N = 150$  are identical with those displayed in Fig. 2.7.

To make our analysis more quantitative we also display the relative change of the correlation for polynomial and logarithmic modifications in Fig. A.3. The results do not change significantly when we increase the number of grid points. In case of polynomial and logarithmic modifications the amount of wiggles in the region of a weak first-order

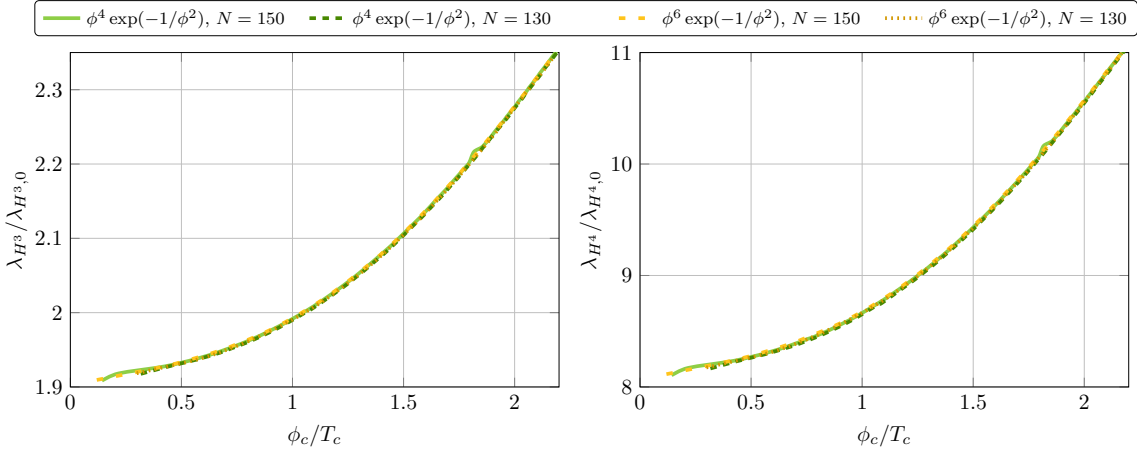


Figure A.2.: Modification of the self-couplings  $\lambda_{H^3}/\lambda_{H^3,0}$  (left) and  $\lambda_{H^4}/\lambda_{H^4,0}$  (right) as a function of  $\phi_c/T_c$  for exponential modifications of the UV potentials, cf. (2.11). We compare results for  $N = 130$  and  $N = 150$  grid points.

phase transition, which originates from numerical uncertainties, is further reduced. In the region of a weak first-order phase transition we have a relative change of less than 2%, while in the region of a strong first-order phase transition we have a relative change of less than 0.5%. This is sufficient for our analysis, since we are only interested in the latter case. In case of the exponential modifications the change is hardly visible. The relative change is globally less than 0.02%. These results illustrate that our findings are indeed numerically stable.

Finally, we can compare our functional renormalization group results to other methods, for instance to the mean-field-like methods of [52]. To perform a meaningful comparison, we have to take into account the slightly different setup: while we modify the microscopic potential, [52] implements the modifications directly at the level of the effective potential. This means that in our setup a  $\phi^6$  modification of the microscopic potential generates finite higher-order modifications through quantum fluctuations, which in the weak coupling regime are similar to the one-loop determinant. These additional terms do not appear in [52].

For our comparison we therefore adjust the parameter  $\lambda_6$  such that the  $T = 0$  effective potentials of both setups agree. Due to the impact of quantum fluctuations, different values of  $\Lambda$  require slightly different initial conditions for  $\lambda_6$  in our setup. With a cutoff  $\Lambda = 1$  TeV it turns out that this is the case for  $\lambda_6 \approx 0.21$ , while for a cutoff  $\Lambda = 0.6$  TeV we find  $\lambda_6 \approx 0.19$ . The difference in values of  $\lambda_6$  is accounted for by the RG flow between the two choices of cutoff scale. With these values we can then compare  $T_c$  and  $\phi_c/T_c$ . As expected, we indeed find good qualitative agreement. For instance, for  $\Lambda = 0.6$  TeV we find  $\phi_c/T_c = 2.7$  and  $T_c = 83$  GeV vs  $\phi_c/T_c = 2.8$  and  $T_c = 75$  GeV from [52]. We emphasize that a more precise agreement cannot be expected: the modification of the microscopic and the effective Higgs potential are necessarily different, as our setup accounts for quantum fluctuations, in particular affecting  $\lambda_6$  between the microscopic scale and the IR.

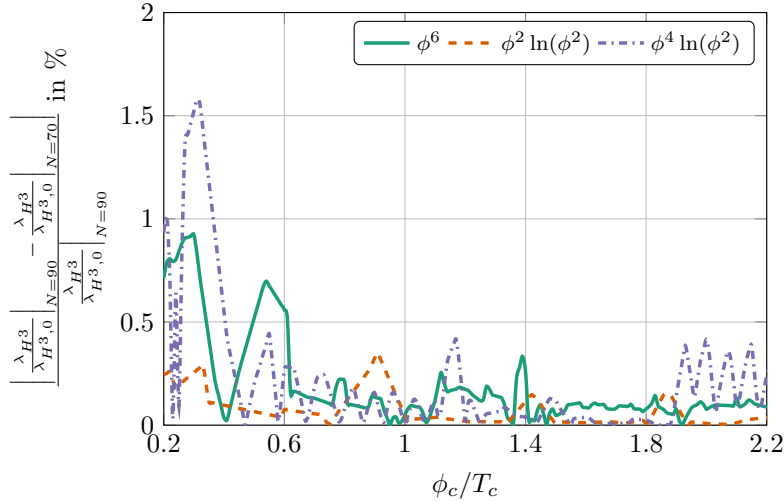


Figure A.3.: Relative change of  $\lambda_{H^3}/\lambda_{H^3,0}$  with different numbers of grid points as a function of  $\phi_c/T_c$  for polynomial and logarithmic modifications of the UV potentials, cf. (2.11). In the regime of interest of  $\phi_c/T_c \geq 1$ , the relative difference between  $N = 70$  and  $N = 90$  is in the sub-percent regime,  $\leq 0.5\%$ .

### A.3. Finite temperature mean-field approximation

In this Appendix we display the computation of the effective Higgs potential with a mean-field approximation. The mean-field analysis is numerically by far less demanding than the grid code but still gives global information of the potential as long as the system is weakly coupled. However, as displayed in Fig. 2.2 this approximation is only sufficient for polynomial modifications of the Higgs potential.

The mean-field approximation entails that only the fermion determinant drives the flow of the potential: neither Higgs fluctuations nor gauge boson fluctuations do contribute to the flow. Furthermore the top-Yukawa coupling does not flow at all. The potential at scale  $k$  is thus given by

$$V_k^{\text{MF}}(\phi) = V_{k=\Lambda}(\phi) - \frac{1}{\Omega} \ln \det_{\Lambda,k} (i\partial + \frac{i}{\sqrt{2}}y_t\phi), \quad (\text{A.18})$$

where  $\Omega$  denotes the spacetime volume. This results for our truncation in

$$V_k^{\text{MF}}(\phi) = V_{k=\Lambda}(\phi) - \frac{1}{2} \text{Tr} \ln \frac{(\phi + R_{F,k})^2 + y_t^2\phi^2/2}{(\phi + R_{F,\Lambda})^2 + y_t^2\phi^2/2}. \quad (\text{A.19})$$

Again we regularise only the spatial directions and thus, after performing the angular integration

$$V_k^{\text{MF}}(\phi) = V_{k=\Lambda}(\phi) - \frac{T}{\pi^2} \sum_{n \in \mathbb{Z}} \int dp p^2 \ln \frac{p^2(1 + r_{F,k})^2 + \nu_n^2 k^2 + y_t^2 \phi^2/2}{p^2(1 + r_{F,\Lambda})^2 + \nu_n^2 k^2 + y_t^2 \phi^2/2}, \quad (\text{A.20})$$

with the fermionic Matsubara frequencies  $\nu_n = 2\pi(n + \frac{1}{2})T/k$ . In order to evaluate the Matsubara sums we use the identities

$$\ln((2n+1)^2\pi^2 + \omega^2/T^2) = \int_1^{\omega^2/T^2} \frac{d\theta^2}{\theta^2 + (2n+1)^2\pi^2} + \ln(1 + (2n+1)^2\pi^2),$$

$$\sum_{n \in \mathbb{Z}} \frac{1}{(2n+1)^2 \pi^2 + \theta^2} = \frac{1}{\theta} \left( \frac{1}{2} - \frac{1}{e^\theta + 1} \right), \quad (\text{A.21})$$

from [476]. Consequently we get the expression

$$\begin{aligned} V_k^{\text{MF}}(\phi) &= V_{k=\Lambda}(\phi) - \frac{T}{\pi^2} \sum_{n \in \mathbb{Z}} \int dp p^2 \int_{(p^2(1+r_{F,\Lambda})^2+y_t^2\phi^2/2)/T^2}^{(p^2(1+r_{F,k})^2+y_t^2\phi^2/2)/T^2} \frac{d\theta^2}{\theta^2 + (2n+1)^2 \pi^2} \\ &= V_{k=\Lambda}(\phi) - \frac{T}{\pi^2} \int dp p^2 \int_{(p^2(1+r_{F,\Lambda})^2+y_t^2\phi^2/2)/T^2}^{(p^2(1+r_{F,k})^2+y_t^2\phi^2/2)/T^2} \frac{d\theta^2}{\theta} \left( \frac{1}{2} - \frac{1}{e^\theta + 1} \right) \\ &= V_{k=\Lambda}(\phi) - \frac{T}{\pi^2} \int dp p^2 \left( 2 \ln(1 + e^{\frac{\sqrt{p^2(1+r_{F,k})^2+y_t^2\phi^2/2}}{T}}) - \frac{\sqrt{p^2(1+r_{F,k})^2+y_t^2\phi^2/2}}{T} \right. \\ &\quad \left. - 2 \ln(1 + e^{\frac{\sqrt{p^2(1+r_{F,\Lambda})^2+y_t^2\phi^2/2}}{T}}) + \frac{\sqrt{p^2(1+r_{F,\Lambda})^2+y_t^2\phi^2/2}}{T} \right). \quad (\text{A.22}) \end{aligned}$$

For  $k = 0$  this reduces to

$$\begin{aligned} V_{k=0}^{\text{MF}}(\phi) &= V_{k=\Lambda}(\phi) - \frac{T}{\pi^2} \int_0^\Lambda dp p^2 \left( 2 \ln(1 + e^{\frac{\sqrt{p^2+y_t^2\phi^2/2}}{T}}) - \frac{\sqrt{p^2+y_t^2\phi^2/2}}{T} \right. \\ &\quad \left. - 2 \ln(1 + e^{\frac{\sqrt{\Lambda^2+y_t^2\phi^2/2}}{T}}) + \frac{\sqrt{\Lambda^2+y_t^2\phi^2/2}}{T} \right). \quad (\text{A.23}) \end{aligned}$$

All but the first integral can be performed analytically. The result is

$$\begin{aligned} V_{k=0}^{\text{MF}}(\phi) &= V_{k=\Lambda}(\phi) \\ &\quad + \frac{1}{8\pi^2} \left( \Lambda \left( y_t^2 \phi^2/2 - \frac{2}{3} \Lambda^2 \right) \sqrt{\Lambda^2 + y_t^2 \phi^2/2} + \frac{y_t^4 \phi^4}{4} \ln \left( \frac{\sqrt{y_t^2 \phi^2/2}}{\sqrt{\Lambda^2 + y_t^2 \phi^2/2} + \Lambda} \right) \right) \\ &\quad + \frac{2T}{\pi^2} \left( \frac{1}{3} \Lambda^3 \ln \left( e^{\frac{\sqrt{\Lambda^2+y_t^2\phi^2/2}}{T}} + 1 \right) - \int_0^\Lambda dp p^2 \ln \left( 1 + e^{\frac{\sqrt{p^2+y_t^2\phi^2/2}}{T}} \right) \right). \quad (\text{A.24}) \end{aligned}$$

It is possible to improve this by adding a thermal mass term to the potential. This however doesn't change the qualitative behaviour.

## B. Towards apparent convergence

This Appendix belongs to [Chapter 3](#) and [Chapter 4](#).

### B.1. Approximations of the stability matrix

The stability matrix  $B$  is defined as the Jacobi matrix of the flow equations for all couplings  $\alpha_i$ . It is given by

$$B_{ij} = \partial_{\alpha_j} \partial_t \alpha_i. \quad (\text{B.1})$$

The critical exponents of a fixed point are defined as minus the eigenvalues of the stability matrix evaluated at this fixed point. In our setup, the stability matrix is infinite dimensional since it is spanned by all couplings  $\lambda_n$  and  $g_n(p^2)$ . Note that one momentum dependent coupling alone is enough to render the stability matrix infinite dimensional.

In this dissertation, only couplings up to order six appear in the flow. We furthermore do not resolve the full momentum dependence of the couplings. Thus, we have already rendered the stability matrix finite. Nevertheless, the full stability matrix is not known since the flows of the fifth- and sixth order couplings are unknown and depend itself on further higher couplings. In consequence, we have to make an approximation of the stability matrix to obtain the critical exponents. Note that we also have to make an approximation of the flow itself to close it. Naturally, these approximations are related.

We next present two different approximations of the stability matrix. We further argue that these approximations should give approximately the same values for the most relevant critical exponents if the expansion scheme is well converged. In almost all chapters of this dissertation we use the first approximation. In [Chapter 4](#) we compare both methods.

The approximation of the flow is related to its closure and describes how the higher-order couplings are identified with the lower ones. We call this process identification scheme and denote it by  $|_{\text{id.}}$ . The two different approximations of the stability matrix are distinguished by the sequence of taking the derivatives and applying this identification scheme. In the first approximation, the identification is performed *before* taking the derivatives:

$$\bar{B}_{ij} = \partial_{\alpha_j} (\partial_t \alpha_i |_{\text{id.}}). \quad (\text{B.2})$$

The critical exponents that correspond to this approximation represent the critical exponents that belong to the computed phase diagram of the theory.

In the second approximation, the identification is performed *after* taking the derivatives

$$\tilde{B}_{ij} = (\partial_{\alpha_j} \partial_t \alpha_i) |_{\text{id.}}. \quad (\text{B.3})$$

This approximation is more closely related to the full stability matrix in the sense that it respects the fact that the higher couplings in the full system do not coincide with the lower ones. Note that these two different approximations only differ if we choose a non-trivial identification scheme, i.e. if the higher-order couplings are functions of the lower ones.

Identification scheme	$\mu^*$	$\lambda_3^*$	$\lambda_4^*$	$g_3^*$	$g_4^*$	$\bar{\theta}_i$	$\tilde{\theta}_i$		
$g_{n>4} \rightarrow g_3, \lambda_{n>4} \rightarrow \lambda_3$	-0.48	0.092	0.0077	0.62	0.53	5.0	$1.3 \pm 3.4i$	-3.7	-10
						4.2	$-0.62 \pm 1.8i$	-4.7	-9.3
$g_{n>4} \rightarrow g_4, \lambda_{n>4} \rightarrow \lambda_3$	-0.45	0.12	0.028	0.83	0.57	4.7	$2.0 \pm 3.1i$	-2.9	-8.0
						5.0	$0.37 \pm 2.4i$	-5.6	-7.9
$g_{n>4} \rightarrow g_4, \lambda_{n>4} \rightarrow \lambda_4$	physical UV fixed point not found								
$g_{n>4} \rightarrow g_4, \lambda_6 \rightarrow \lambda_4, \lambda_5 \rightarrow \lambda_3$	-0.49	0.086	0.027	0.64	0.56	8.7	$1.4 \pm 3.7i$	-4.3	-11
						5.0	$-0.46 \pm 2.0i$	-5.5	-11

Table B.1.: Properties of the UV fixed point for different identification schemes, i.e. different closures of the flow equations, see App. B.3. The flow equations are computed with momentum dependent anomalous dimensions  $\eta_{\phi_i}$  and bilocally projected Newton's couplings  $g_n(k^2)$ . The critical exponents  $\bar{\theta}_i$  and  $\tilde{\theta}_i$  stem from two approximation of the stability matrix, see App. B.1. An attractive UV fixed point is found in most identification schemes with mildly varying fixed point values. In the first approximation of the stability matrix we always find three attractive directions, while in the second approximation of the stability matrix we find one or three attractive directions, since the real part of one complex pair of eigenvalues is quite close to zero. These results suggest that the present system is rather stable under change of the closure of the flow equations. In the case of the single identification without a physical UV fixed point we found that it had in fact just vanished in the complex plane.

If the expansion scheme is well converged, then the contributions of the higher couplings to the flow of the lower couplings are small, e.g.  $(\partial_{\lambda_{n_{\max}+2}} \lambda_{n_{\max}})|_{\text{FP}} \approx 0$ . In this case, the most relevant eigenvalues of the stability matrices  $\bar{B}$  and  $\tilde{B}$  coincide approximately. The stabilisation of the most relevant eigenvalues was also observed in an expansion in  $R^n$  in [281]. In consequence, a huge deviation in the most relevant eigenvalues of both approximations would clearly indicate a lack of convergence. For this reason, we use the comparison of the different approximations as a first check of convergence.

## B.2. Background couplings

In this Appendix we present the flow equations for the background couplings  $\bar{g}$  and  $\bar{\lambda}$ . They are in particular interesting in the limit  $k \rightarrow 0$  where they become observables. In this limit, the regulator term vanishes by construction and diffeomorphism invariance is restored, which implies that these couplings can be interpreted as physical observables only for vanishing  $k$ .

For notational convenience we reintroduce the coupling  $\lambda_2 = -\mu/2$ . Following [262], we compute the flow of the background couplings with a curvature expansion on an Einstein space. We use a York-decomposition [81, 470] and field redefinitions [247, 413] to cancel the non-trivial Jacobians. The resulting flow equations are given by

$$\partial_t \bar{g} = 2\bar{g} - \bar{g}^2 f_{R^1}(\lambda_2; \eta_\phi), \quad \partial_t \bar{\lambda} = -4\bar{\lambda} + \bar{\lambda} \frac{\partial_t \bar{g}}{\bar{g}} + \bar{g} f_{R^0}(\lambda_2; \eta_\phi), \quad (\text{B.4})$$

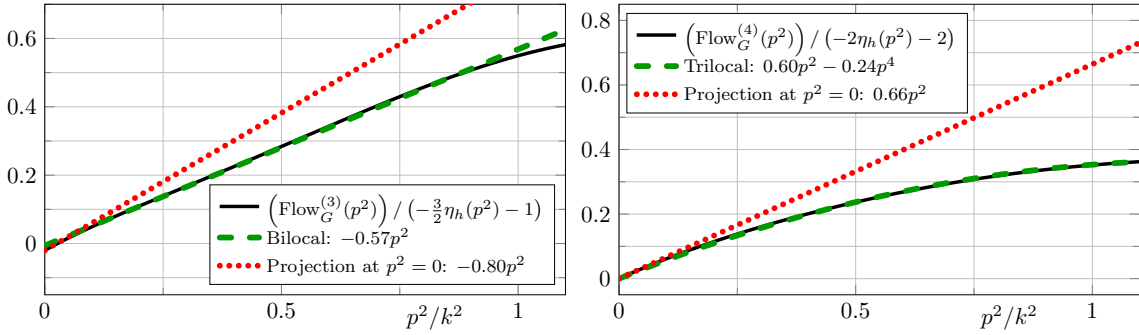


Figure B.1.: Fit of a local momentum projection at  $p^2 = 0$  to the momentum dependence of the flow of the graviton three-point function (left) and the graviton four-point function (right) divided by  $(-\frac{n}{2}\eta_h(p^2) - n + 2)$  as defined in (4.3). The flows are evaluated at  $(\mu, \lambda_3, \lambda_4, g_3, g_4) = (-0.4, 0.1, -0.1, 0.7, 0.5)$  and  $\lambda_6 = \lambda_5 = \lambda_3$  as well as  $g_6 = g_5 = g_4$ , i.e. the same values as in Fig. 4.1 where a non-local momentum projection was used. In comparison to the non-local momentum projection, the local momentum projection does *not* capture the correct momentum dependence in the whole momentum range  $0 \leq p^2 \leq k^2$  since it is sensitive to local momentum fluctuations. Furthermore, it is technically very challenging to project on the  $p^4$ -term due to IR singularities. Note again that the constant parts of the flows are irrelevant for the beta functions since they are extracted from a different tensor projection.

where the functions  $f_{R^0}$  and  $f_{R^1}$  read

$$f_{R^0}(\lambda_2; \eta_\phi) = \frac{1}{24\pi} \left( \frac{(10 - 8\lambda_2)(6 - \eta_h(k^2))}{1 - 2\lambda_2} - 8(6 - \eta_c(k^2)) \right), \quad (B.5)$$

$$f_{R^1}(\lambda_2; \eta_\phi) = \frac{1}{24\pi} \left( \frac{93 + 204\lambda_2 - 300\lambda_2^2 - \eta_h(k^2)(17 + 36\lambda_2 - 60\lambda_2^2)}{3(1 - 2\lambda_2)^2} + 10(5 - \eta_c(k^2)) \right).$$

In consequence the fixed point equations for the background couplings are given by

$$\bar{g}^* = \frac{2}{f_{R^1}(\lambda_2^*, \eta_\phi^*)}, \quad \bar{\lambda}^* = \frac{f_{R^0}(\lambda_2^*, \eta_\phi^*)}{2f_{R^1}(\lambda_2^*, \eta_\phi^*)}. \quad (B.6)$$

Note that the background couplings are non-dynamical, i.e. they do not influence any other coupling. Furthermore, the background couplings only depend on the couplings of the two-point function. Hence only the graviton mass parameter  $\mu$  (or equivalently  $\lambda_2$ ) and the anomalous dimensions  $\eta_h$  and  $\eta_c$  directly affect them.

### B.3. Dependence on the identification scheme

The flow of each  $n$ -point function depends on the couplings of the  $(n + 1)$ -point function and the  $(n + 2)$ -point function, see also Fig. 3.1. For the highest couplings, we consequently do not have a flow equation at hand. In our setup, these are the couplings of the five- and six-point function, i.e.  $\lambda_5$ ,  $\lambda_6$ ,  $g_5$ , and  $g_6$ . In order to close the flow of our system, we need to make an ansatz for these higher order couplings. A natural choice is one that is close to diffeomorphism invariance, i.e. to identify these couplings with a lower order coupling.

In our setup, there are two lower order couplings that correspond to a (partly) diffeomorphism invariant identification scheme, e.g.  $\lambda_5$  can be identified with  $\lambda_3$  or  $\lambda_4$ . In a well converged expansion scheme, the details of the identification should not matter and lead to similar results. In this section, we compare the results for different identification schemes in order to evaluate the stability of our expansion scheme.

The properties of the non-trivial UV fixed point for different identifications schemes are displayed in [Tab. B.1](#). In all identification schemes except for the identification  $g_{n>4} \rightarrow g_4$  and  $\lambda_{n>4} \rightarrow \lambda_4$  we find an attractive UV fixed point. In this case we can see that the fixed point has just vanished in the complex plane. For all other identifications we observe that the fixed point values and the critical exponents vary mildly. Especially the number of attractive directions is consistently three with the first approximation to the stability matrix, c.f. [App. B.1](#). With the second approximation the number of attractive directions varies from one to three since the real part of one complex conjugated pair is close to zero.

In conclusion, this analysis suggests that our system is rather stable with respect to different identification schemes. Only one particular identification scheme has led to the disappearance of the attractive UV fixed point. This constitutes further support for our results in [Sec. 4.3.2](#), where we found that our full system is very stable with respect to the identification of  $g_5$  and  $g_6$ .

## B.4. Possible issues of a local momentum projection

In this section we want to point out some possible issues of a local momentum projection. A local momentum projection is for example a derivative expansion about a certain momentum, usually  $p = 0$ .

The full solution of a flow equation includes a full resolution of the momentum dependence of all vertex flows. For higher  $n$ -point functions this task is computationally extremely challenging due to the high number of momentum variables. We have already argued in [Sec. 3.4.2](#) that this task can be tremendously simplified with a symmetric momentum configuration. We have further shown in [Sec. 4.2.2](#) that the quantity  $\text{Flow}_G^{(n)} / (-\frac{n}{2} \eta_h(p^2) - n + 2)$  is polynomial in  $p^2$ , at least for  $n = 3, 4$ . Thus it is possible to consistently project on each coefficient of this polynomial in the whole momentum range  $0 \leq p^2 \leq k^2$  by employing a non-local momentum projection. In contrast, a local momentum projection scheme does not capture the correct momentum dependence over the whole momentum range  $0 \leq p^2 \leq k^2$  in general since it is sensitive to local momentum fluctuations. Furthermore, it is very challenging to project on the  $p^4$  coefficient or even higher momentum order coefficients due to IR singularities. All these statements are explicitly exemplified in [Fig. B.1](#).

On the other hand, the local momentum projection at  $p = 0$  has the advantage that it allows for analytic flow equations, as discussed in [App. B.6](#). Analytic flow equations are more easily evaluated in the whole theory space, but, as the discussion above suggests, one should be be mindful of the fact that they easily introduce a large error.

We use the analytic flow equations in [Sec. 4.4](#) precisely for the reason that they can easily be evaluated in the whole theory space. Thus we show now that the fixed point properties in this analytic system are qualitatively similar to the full system, despite the error that is introduced by the analytic equations.

The properties of the UV fixed point for different approximations are displayed in [Tab. B.2](#). Truncation 1 corresponds to our full system, i.e. with momentum dependent

Trunc.	$\mu^*$	$\lambda_3^*$	$\lambda_4^*$	$g_3^*$	$g_4^*$		$\bar{\theta}_i$	$\tilde{\theta}_i$
1	−0.45	0.12	0.028	0.83	0.57	4.7	$2.0 \pm 3.1i$	−2.9
						5.0	$0.37 \pm 2.4i$	−5.6
2	−0.41	0.076	0.0055	0.71	0.53	4.0	$1.5 \pm 3.6i$	−3.1
						3.9	$0.38 \pm 4.4i$	−2.3
3	−0.37	0.049	0.0055	1.1	0.83	7.3	$1.7 \pm 2.1i$	−3.0
						7.2	$−0.32 \pm 2.7i$	−4.7
4	−0.23	−0.060	−0.11	0.64	0.55	3.0	$1.9 \pm 1.6i$	−1.7
						2.2	$0.50 \pm 1.7i$	−1.5 ± 0.88i

Table B.2.: Properties of the UV fixed points for different approximations. In the truncations 3 and 4, we set  $\eta_{\phi_i} = 0$ , while in the truncations 1 and 2 we use momentum dependent anomalous dimensions. In truncations 2 and 4, the couplings  $g_{3,4}$  are computed via a derivative expansion at  $p^2 = 0$ , while in the truncations 1 and 3 the couplings  $g_{3,4}(k^2)$  are evaluated with a bilocal projection between  $p^2 = 0$  and  $p^2 = k^2$ . The quality of the truncation decreases from 1 to 4. The fixed point values are obtained with the identification scheme  $\lambda_{n>4} = \lambda_3$  and  $g_{n>4} = g_4$ . The critical exponents  $\bar{\theta}_i$  and  $\tilde{\theta}_i$  stem from two approximation of the stability matrix see App. B.1. The fixed point properties from different approximations are qualitatively very similar. In particular, all fixed points exhibit three relevant directions when the first approximation of the stability matrix is used. Using the second approximation of the stability matrix also results in three relevant directions in three out of four cases.

anomalous dimensions and bilocally evaluated gravitational couplings. Truncation 4 corresponds to the system used in Sec. 4.4, i.e. without anomalous dimensions and with gravitational couplings from a derivative expansion. Truncation 2 and 3 are in between those truncations, i.e. with anomalous dimension but gravitational couplings from a derivative expansion and without anomalous dimensions but with bilocally evaluated gravitational couplings, respectively.

We observe that the UV fixed point exists in all truncations, and that the properties of this fixed point vary mildly. The fixed point values are all located within a small region, with the exception of our simplest truncation. There, the couplings  $\lambda_3$  and  $\lambda_4$  have a different sign compared to the other truncations. Considering the critical exponents we always find three attractive directions with the first approximation of the stability matrix and in three out of four cases with the second approximation of the stability matrix. These results suggest that it is an acceptable approximation to use the analytic flow equations if one is only interested in the qualitative behaviour of the system.

## B.5. Derivation of flow equations

We obtain the flow equations for the individual coupling constants by projecting onto the flow of the graviton  $n$ -point functions, as explained in Sec. 3.4.3.

The equations for the graviton mass parameter  $\mu$  and for the graviton anomalous dimension  $\eta_h$  are extracted from the transverse-traceless part of the flow of the graviton

two-point function. For  $p^2 = 0$ , we obtain the flow of the graviton mass parameter

$$\partial_t \mu = (\eta_h(0) - 2) \mu + \frac{32\pi}{5} \text{Flow}_{tt}^{(hh)}(0). \quad (\text{B.7})$$

We obtain an equation for the graviton anomalous dimension by evaluating the flow of the graviton two-point function bilocally at  $p^2$  and  $-\mu k^2$

$$\eta_h(p^2) = \frac{32\pi}{5(p^2 + \mu k^2)} \left( \text{Flow}_{tt}^{(hh)}(-\mu k^2) - \text{Flow}_{tt}^{(hh)}(p^2) \right). \quad (\text{B.8})$$

The ghost anomalous dimension is obtained from the transverse ghost two-point function

$$\eta_c(p^2) = -\frac{\text{Flow}_T^{(\bar{c}c)}(p^2)}{3p^2}. \quad (\text{B.9})$$

In case of the higher order couplings, we employ the projection operators described in [Sec. 3.4.2](#). For the couplings  $\lambda_n$ , this leads to

$$\partial_t \lambda_n = \left( \frac{n}{2} \eta_h(0) + (n-4) - \frac{n-2}{2} \frac{\partial_t g_n}{g_n} \right) \lambda_n + \frac{g_n^{1-\frac{n}{2}}}{C^{\Lambda_n}} \text{Flow}_{\Lambda_n}^{(n)}(0), \quad (\text{B.10})$$

where the projection dependent constant is defined via  $C^{\Lambda_n} = \Pi_{\Lambda_n} \circ \Pi_{tt}^n \circ \mathcal{T}^{(n)}(0; 1)$ . Here,  $\circ$  denotes the pairwise contraction of indices.

As discussed in [Sec. 3.4.3](#), the gravitational couplings  $g_n(p^2)$  are momentum dependent. In order to simplify the computation we make an approximation of the full momentum dependence. This approximation exploits the fact that the flows are peaked at  $p^2 = k^2$  and consequently we set the feed back on the right-hand side of the flow equation to  $g_n(p^2) \approx g_n(k^2)$ . This closes the flow equation for  $g_n(k^2)$  and thus we only solve this equation. The easiest way to obtain the flow equation for  $g_n(k^2)$  is a bilocal projection at  $p^2 = 0$  and  $p^2 = k^2$ . For  $g_4(k^2)$  we obtain

$$\begin{aligned} \partial_t g_4(k^2) &= 2g_4(k^2) + 2\eta_h(k^2)g_4(k^2) - C_4 g_4(k^2) \lambda_4(\eta_h(k^2) - \eta_h(0)) \\ &\quad + C_{p^2}^{G_4-1} (\text{Flow}_G^{(4)}(k^2) - \text{Flow}_G^{(4)}(0)). \end{aligned} \quad (\text{B.11})$$

The derivation of this equation is based on the assumption that  $\lambda_4$  is small.

In [Sec. 4.2.5](#) we have laid out a strategy to disentangle contributions from different tensor structures, in particular those of  $R$  and  $R^2$ . The flow equations for the  $g_n$  are obtained by a projection onto the  $p^2$  part of  $\text{Flow}_G^{(n)}$  divided by  $(-\frac{n}{2}\eta_h(p^2) - n + 2)$ , see [Sec. 4.2.2](#) and [Sec. 4.2.5](#). The graviton three-point function is at most quadratic in the external momentum, and consequently it is again enough to use a bilocal projection at  $p^2 = 0$  and  $p^2 = k^2$ . Consequently, the flow equation for  $g_3$  is quantitatively equivalent to the previous one if  $\lambda_3$  is small. The graviton four-point function, on the other hand, has  $p^4$  as its highest momentum power, and thus we use a trilocal momentum projection at  $p^2 = 0$ ,  $p^2 = k^2/2$ , and  $p^2 = k^2$ . The flow equations of  $g_3$  and  $g_4$  are then given by

$$\begin{aligned} (1 + \eta_3) \partial_t g_3 &= 2g_3 - 2g_3 C_3 (\partial_t \lambda_3 + 2\lambda_3) \left( \frac{1}{\frac{3}{2}\eta_h(k^2) + 1} - \frac{1}{\frac{3}{2}\eta_h(0) + 1} \right) \\ &\quad + \frac{2}{C_{p^2}^{G_3} \sqrt{g_3}} \left( \frac{\text{Flow}_G^{(3)}(k^2)}{\frac{3}{2}\eta_h(k^2) + 1} - \frac{\text{Flow}_G^{(3)}(0)}{\frac{3}{2}\eta_h(0) + 1} \right), \end{aligned} \quad (\text{B.12})$$

$$\begin{aligned}
(1 + \eta_4) \partial_t g_4 &= 2g_4 - g_4 C_4 (\partial_t \lambda_4 + 2\lambda_4) \left( -\frac{1}{\eta_h(k^2) + 1} + \frac{4}{\eta_h(k^2/2) + 1} - \frac{3}{\eta_h(0) + 1} \right) \\
&\quad + \frac{1}{C_{p^2}^{G_4}} \left( -\frac{\text{Flow}_G^{(4)}(k^2)}{\eta_h(k^2) + 1} + 4 \frac{\text{Flow}_G^{(4)}(k^2/2)}{\eta_h(k^2/2) + 1} - 3 \frac{\text{Flow}_G^{(4)}(0)}{\eta_h(0) + 1} \right), \quad (\text{B.13}) \\
\eta_3 &= \frac{C_3 \lambda_3 - \frac{3}{2} \eta_h(k^2)}{\frac{3}{2} \eta_h(k^2) + 1} - \frac{C_3 \lambda_3}{\frac{3}{2} \eta_h(0) + 1}, \\
\eta_4 &= \frac{-3C_4 \lambda_4}{\eta_h(0) + 1} + 4 \frac{C_4 \lambda_4 - \frac{1}{2} \eta_h(k^2/2)}{\eta_h(k^2/2) + 1} - \frac{C_4 \lambda_4 - \eta_h(k^2)}{\eta_h(k^2) + 1}.
\end{aligned}$$

The constants  $C$  are implicitly defined via  $\Pi_{G_n} \circ \Pi_{tt}^n \circ \mathcal{T}^{(n)}(p^2; \Lambda_n) = C_{\Lambda_n}^{G_n} \Lambda_n + C_{p^2}^{G_n} p^2$ , and we use the abbreviation  $C_n = C_{\Lambda_n}^{G_n} / C_{p^2}^{G_n}$ . Note that the constants  $\eta_n$  are chosen in such a way that  $\eta_n = 0$  for vanishing anomalous dimensions.

Analogously, we can obtain a flow equation for the  $R^2$  coupling of the graviton four-point function  $\omega_4$  by using a trilocal momentum projection, as explained in Sec. 4.2.5. We evaluate the flows at the same momenta as for the trilocal flow equation of  $g_4$ . The equation for  $\omega_4$  then reads

$$\begin{aligned}
(1 + \eta_\omega) \partial_t \omega_4 &= 2\omega_4 - \frac{C_{\Lambda_4}^{G_4}}{C_{\Omega_4}^{G_4}} (\partial_t \lambda_4 + 2\lambda_4) \left( \frac{1}{\eta_h(k^2) + 1} - \frac{2}{\eta_h(k^2/2) + 1} + \frac{1}{\eta_h(0) + 1} \right) \\
&\quad - \frac{\partial_t g_4}{g_4} \left( \frac{C_{\Lambda_4}^{G_4} \lambda_4 + C_{p^2}^{G_4} + C_{\Omega_4}^{G_4} \omega_4}{\eta_h(k^2) + 1} - 2 \frac{C_{\Lambda_4}^{G_4} \lambda_4 + \frac{1}{2} C_{p^2}^{G_4} + \frac{1}{4} C_{\Omega_4}^{G_4} \omega_4}{\eta_h(k^2/2) + 1} + \frac{C_{\Lambda_4}^{G_4} \lambda_4}{\eta_h(0) + 1} \right) \\
&\quad + \frac{1}{C_{\Omega_4}^{G_4} g_4} \left( \frac{\text{Flow}_G^{(4)}(k^2)}{\eta_h(k^2) + 1} - 2 \frac{\text{Flow}_G^{(4)}(k^2/2)}{\eta_h(k^2/2) + 1} + \frac{\text{Flow}_G^{(4)}(0)}{\eta_h(0) + 1} \right), \\
\eta_\omega &= \frac{\eta_h(k^2/2)}{\eta_h(k^2/2) + 1} - \frac{2\eta_h(k^2)}{\eta_h(k^2) + 1}. \quad (\text{B.14})
\end{aligned}$$

The constants  $C$  are again defined via the contraction  $\Pi_{G_n} \circ \Pi_{tt}^n \circ \mathcal{T}^{(n)}(p^2; \Lambda_n) = C_{\Lambda_n}^{G_n} \Lambda_n + C_{p^2}^{G_n} p^2 + C_{\Omega_n}^{G_n} \Omega_4 p^4$ . Again,  $\eta_\omega$  is defined with  $\eta_\omega = 0$  for vanishing anomalous dimensions.

In the previous paragraphs we introduced abbreviations for constants that arise from the projection scheme. The explicit values of these constants are:

$$\begin{aligned}
C^{\Lambda_3} &= \frac{5}{192\pi^2}, & C^{\Lambda_4} &= \frac{371881}{6718464\pi^2}, & C_{\Omega_4}^{G_4} &= -\frac{96203921}{1632586752\pi^2}, \\
C_{\Lambda_4}^{G_4} &= \frac{222485}{60466176\pi^2}, & C_{p^2}^{G_4} &= \frac{6815761}{544195584\pi^2}, & C_4 &= \frac{C_{\Lambda_4}^{G_4}}{C_{p^2}^{G_4}} = \frac{2002365}{6815761}, \\
C_{\Lambda_3}^{G_3} &= -\frac{9}{4096\pi^2}, & C_{p^2}^{G_3} &= \frac{171}{32768\pi^2}, & C_3 &= \frac{C_{\Lambda_3}^{G_3}}{C_{p^2}^{G_3}} = -\frac{8}{19}. \quad (\text{B.15})
\end{aligned}$$

For analytic flow equations for the gravitational couplings  $g_n$ , which are significantly less accurate, see App. B.4, we have to apply a partial derivative with respect to  $p^2$  and

evaluate the result at  $p^2 = 0$ . The resulting equations are given by

$$\partial_t g_n = 2g_n + \frac{ng_n}{n-2} (\eta_h(0) + C_n \lambda_n \eta'_h(0)) + \frac{2}{n-2} \frac{g_n^{2-\frac{n}{2}}}{C_{p^2}^{G_n}} \text{Flow}_G^{(n)'}(0), \quad (\text{B.16})$$

where ' denotes the dimensionless derivative with respect to  $p^2$ . These equations remain completely analytic if we use a Litim-shaped regulator [372] and approximate the anomalous dimensions as constant,  $\eta_\phi(q^2) \approx \text{const.}$

## B.6. Analytic flow equations

All analytic flow equations are derived at  $p^2 = 0$  (see e.g. (B.16)) and with a Litim-shaped regulator [372]. The anomalous dimensions in the momentum integrals are approximated as constant, i.e.  $\eta_{\phi_i}(q^2) \approx \eta_{\phi_i}(k^2)$ . The analytic flow equations are then given by

$$\begin{aligned} \partial_t \mu &= (\eta_h(0) - 2) \mu + \frac{1}{12\pi} \frac{g_4}{(1+\mu)^2} (3(\eta_h - 8) - 8\lambda_4(\eta_h - 6)) \\ &\quad - \frac{1}{180\pi} \frac{g_3}{(1+\mu)^3} (21(\eta_h - 10) - 120\lambda_3(\eta_h - 8) + 320\lambda_3^2(\eta_h - 6)) + \frac{g_3}{5\pi} (\eta_c - 10) \\ \partial_t \lambda_3 &= \left( \frac{3}{2} \eta_h(0) - 1 - \frac{1}{2} \frac{\partial_t g_3}{g_3} \right) \lambda_3 - \frac{1}{8\pi} \frac{g_3^{-\frac{1}{2}} g_5^{\frac{3}{2}}}{(1+\mu)^2} ((\eta_h - 8) - 4\lambda_5(\eta_h - 6)) \\ &\quad - \frac{1}{6\pi} \frac{g_4}{(1+\mu)^3} (3\lambda_4(\eta_h - 8) - 16\lambda_3\lambda_4(\eta_h - 6)) - \frac{g_3}{10\pi} (\eta_c - 12) \\ &\quad + \frac{1}{240\pi} \frac{g_3}{(1+\mu)^4} (11(\eta_h - 12) - 72\lambda_3(\eta_h - 10) + 120\lambda_3^2(\eta_h - 8) - 80\lambda_3^3(\eta_h - 6)) \\ \partial_t \lambda_4 &= \left( 2\eta_h(0) - \frac{\partial_t g_4}{g_4} \right) \lambda_4 + \frac{1}{13387716\pi} \left( \frac{1}{2} \frac{g_6^2 g_4^{-1}}{(1+\mu)^2} (-4472787(\eta_h - 8) + 1639004\lambda_6(\eta_h - 6)) \right. \\ &\quad + \frac{1}{15} \frac{g_4}{(1+\mu)^3} (5066361(\eta_h - 10) - 22517160\lambda_4(\eta_h - 8) + 283174360\lambda_4^2(\eta_h - 6)) \\ &\quad + \frac{2}{15} \frac{g_3^{\frac{1}{2}} g_5^{\frac{3}{2}} g_4^{-1}}{(1+\mu)^3} (3940503(\eta_h - 10) - 60(187643\lambda_3 - 1303286\lambda_5)(\eta_h - 8) \\ &\quad \quad + 417051520\lambda_3\lambda_5(\eta_h - 6)) \\ &\quad + \frac{2}{5} \frac{g_3}{(1+\mu)^4} (-1313501(\eta_h - 12) + 3377574(2\lambda_3 + \lambda_4)(\eta_h - 10) \\ &\quad \quad - 15011440(\lambda_3 + 2\lambda_4)\lambda_3(\eta_h - 8) + 45442920\lambda_3^2\lambda_4(\eta_h - 6)) \\ &\quad + \frac{1}{5} \frac{g_3^2 g_4^{-1}}{(1+\mu)^5} (2874147(\eta_h - 14) - 20879816\lambda_3(\eta_h - 12) + 36027456\lambda_3^2(\eta_h - 10) \\ &\quad \quad + 88161840\lambda_3^3(\eta_h - 8) - 248160672\lambda_3^4(\eta_h - 6)) \\ &\quad \left. - \frac{10426288}{7} \frac{g_3^2}{g_4} (\eta_c - 14) \right) \\ \partial_t g_3 &= \left( 2 + 3\eta_h(0) - \frac{8}{19} \eta'_h(0) \lambda_3 \right) g_3 + \frac{1}{19\pi} \left( \frac{g_3^{\frac{1}{2}} g_5^{\frac{3}{2}}}{(1+\mu)^2} \frac{47}{6} (\eta_h - 6) + \frac{g_3^2}{10} (53(\eta_c - 10) + 480) \right. \end{aligned}$$

$$\begin{aligned}
& + \frac{g_3 g_4}{18(1+\mu)^3} (-45(\eta_h - 8) + 8(30\lambda_3 - 59\lambda_4)(\eta_h - 6) + 360\lambda_3\lambda_4(\eta_h - 4)) \\
& + \frac{g_3 g_4}{(1+\mu)^4} 16(1 - 3\lambda_3)\lambda_4 - \frac{2g_3^2}{15(1+\mu)^5} (229 - 1780\lambda_3 + 3640\lambda_3^2 - 2336\lambda_3^3) \\
& - \frac{g_3^2}{80(1+\mu)^4} (147(\eta_h - 10) - 1860\lambda_3(\eta_h - 8) + 3380\lambda_3^2(\eta_h - 6) + 25920\lambda_3^3(\eta_h - 4)) \\
\partial_t g_4 = & 2 \left( 1 + \eta_h(0) + \frac{2002365}{6815761} \eta'_h(0) \lambda_4 \right) g_4 + \frac{2125764}{6815761\pi} \left( \frac{g_6^2}{(1+\mu)^2} \frac{32830375}{25509168} (\eta_h - 6) \right. \\
& - \frac{g_4^2}{76527504(1+\mu)^3} (11305705(\eta_h - 8) + 61298276\lambda_4(\eta_h - 6) + 308793960\lambda_4^2(\eta_h - 4)) \\
& - \frac{4g_4^2}{3188646(1+\mu)^4} (16061481 + 8(5355213\lambda_4 - 5610604)\lambda_4) \\
& - \frac{g_3^{\frac{1}{2}} g_5^{\frac{3}{2}}}{19131876(1+\mu)^3} \left( -34242339(\eta_h - 8) + (86256922\lambda_3 - 7511302\lambda_5)(\eta_h - 6) \right. \\
& \quad \left. - 4483422\lambda_3\lambda_5(\eta_h - 4) \right) \\
& - \frac{g_3^{\frac{1}{2}} g_5^{\frac{3}{2}}}{(1+\mu)^4} (784609(17 - 32\lambda_3) - 8937232(4 - 9\lambda_3)\lambda_5) \\
& + \frac{g_3 g_4}{90(1+\mu)^4} \left( 323831781(\eta_h - 10) - (894383680\lambda_3 + 203187860\lambda_4)(\eta_h - 8) \right. \\
& \quad \left. - (1296319430\lambda_3 - 1355312560\lambda_4)\lambda_3(\eta_h - 6) - 2929029840\lambda_3^2\lambda_4(\eta_h - 4) \right) \\
& + \frac{g_3 g_4}{15(1+\mu)^5} \left( 26769135(17 + 8\lambda_3(9\lambda_3 - 8)) \right. \\
& \quad \left. - 2(353519805 + 4\lambda_3(742510961\lambda_3 - 514449355))\lambda_4 \right) \\
& + \frac{2g_3 g_4}{9(1+\mu)^4} \left( 6783386859(\eta_h - 10) - (12157310900\lambda_3 + 457106270\lambda_4)(\eta_h - 8) \right. \\
& \quad \left. - (81359010140\lambda_3 + 111943091120\lambda_4)\lambda_3(\eta_h - 6) - 502725688080\lambda_3^2\lambda_4(\eta_h - 4) \right) \\
& + \frac{g_3 g_4}{15(1+\mu)^5} \left( 394709295 - 661068650\lambda_4 + 40(91735671\lambda_4 - 34781816)\lambda_3 \right. \\
& \quad \left. - 8(731880777\lambda_4 - 220800215)\lambda_3^2 \right) \\
& + \frac{g_3^2}{45(1+\mu)^5} \left( -125220803(\eta_h - 12) + 568782360\lambda_3(\eta_h - 10) \right. \\
& \quad \left. + 334912350\lambda_3^2(\eta_h - 8) - 6438366032\lambda_3^3(\eta_h - 6) + 17330657640\lambda_3^4(\eta_h - 4) \right) \\
& - \frac{g_3^2}{3(1+\mu)^6} \left( 112533531 - 855576992\lambda_3 + 3683259968\lambda_3^2 - 7947008128\lambda_3^3 + 6385327072\lambda_3^4 \right) \\
& + 4g_3^2 \left( \frac{23005837}{5}(\eta_c - 12) + 11171540 \right) \tag{B.17}
\end{aligned}$$

# C. Curvature dependence

This Appendix belongs to [Chapter 5](#).

## C.1. Propagator

We use the standard York decomposition to invert the two-point functions. The York-decomposition for the graviton is given by

$$h_{\mu\nu} = h_{\mu\nu}^{\text{tt}} + \frac{1}{d} \bar{g}_{\mu\nu} h^{\text{tr}} + 2\bar{\nabla}_{(\mu} \xi_{\nu)} + \left( \bar{\nabla}_\mu \bar{\nabla}_\nu - \frac{\bar{g}_{\mu\nu}}{d} \bar{\nabla}^2 \right) \sigma. \quad (\text{C.1})$$

and for the ghost by

$$c_\mu = c_\mu^{\text{T}} + \bar{\nabla}_\mu \eta, \quad (\text{C.2})$$

and analogously for the anti ghost. With the field redefinitions according to [\[247, 262, 413\]](#)

$$\xi^\mu \rightarrow \frac{1}{\sqrt{\bar{\Delta} - \frac{\bar{R}}{4}}} \xi^\mu, \quad \sigma \rightarrow \frac{1}{\sqrt{\bar{\Delta}^2 - \bar{\Delta} \frac{\bar{R}}{3}}} \sigma, \quad \eta \rightarrow \frac{1}{\bar{\Delta}} \eta, \quad (\text{C.3})$$

we cancel the non-trivial Jacobians and achieve that all field modes have the same mass dimension. We choose the gauge  $\alpha = \beta = 0$  and choose the regulator proportional to the two-point function

$$R_k = \Gamma^{(2)} \bigg|_{\Lambda \rightarrow 0, R \rightarrow 0} \cdot r_k(p^2). \quad (\text{C.4})$$

Here and in the following in this Appendix,  $p^2$  always refers to the dimensionless spectral values of the scalar Laplacian. For the regulator shape function  $r_k$ , we choose an exponential regulator

$$r_k(x) = \frac{e^{-x^2}}{x}. \quad (\text{C.5})$$

The propagator has the form

$$G = \frac{32\pi}{Z_h} \begin{pmatrix} \frac{1}{p^2(1+r_k(p^2))+\mu+\frac{2}{3}r} & 0 & 0 & 0 \\ 0 & 0 & 0 & 0 \\ 0 & 0 & \frac{-\frac{8}{3}}{p^2(1+r_k(p^2))+\frac{2}{3}\mu} & 0 \\ 0 & 0 & 0 & 0 \end{pmatrix}, \quad (\text{C.6})$$

where the first entry is the transverse traceless mode and the third entry is the trace mode. All other modes vanish due to Landau gauge,  $\alpha = 0$ . Furthermore, we get the

following expressions for the background flow of the different graviton modes, where still the spectral sum/integral or heat-kernel expansion has to be performed,

$$\begin{aligned} \frac{1}{2} \text{Tr}[G\partial_t R]_{h_{tt}} &= \frac{r^2}{768\pi^2} \frac{p^2 (\partial_t r_k(p^2) - \eta_h r_k(p^2))}{p^2 (1 + r_k(p^2)) + \mu + \frac{2}{3}r}, \\ \frac{1}{2} \text{Tr}[G\partial_t R]_{\xi} &= \frac{r^2}{768\pi^2} \frac{p^2 (\partial_t r_k(p^2) - \eta_h r_k(p^2))}{p^2 (1 + r_k(p^2)) - \frac{1}{4}r}, \\ \frac{1}{2} \text{Tr}[G\partial_t R]_{h_{tr}} &= \frac{r^2}{768\pi^2} \frac{p^2 (\partial_t r_k(p^2) - \eta_h r_k(p^2))}{p^2 (1 + r_k(p^2)) + \frac{2}{3}\mu}, \\ \frac{1}{2} \text{Tr}[G\partial_t R]_{\sigma} &= \frac{r^2}{768\pi^2} \frac{p^2 (\partial_t r_k(p^2) - \eta_h r_k(p^2))}{p^2 (1 + r_k(p^2)) - \frac{1}{3}r}. \end{aligned} \quad (\text{C.7})$$

And for the ghosts

$$\begin{aligned} -\text{Tr}[G\partial_t R]_c &= -\frac{r^2}{384\pi^2} \frac{p^2 (\partial_t r_k(p^2) - \eta_c r_k(p^2))}{p^2 (r_k(p^2) + 1) - \frac{r}{4}}, \\ -\text{Tr}[G\partial_t R]_{\eta} &= -\frac{r^2}{384\pi^2} \frac{p^2 (\partial_t r_k(p^2) - \eta_c r_k(p^2))}{p^2 (r_k(p^2) + 1) - \frac{1}{3}r}. \end{aligned} \quad (\text{C.8})$$

## C.2. Flow equations

The flow equation for the transverse traceless part of the graviton two-point function is given by

$$\frac{1}{32\pi} \partial_t \left( Z_h k^2 \left( \mu + p^2 + \frac{2}{3}r \right) \right) = k^2 Z_h \text{Flow}_{tt}^{(2h)}(p^2). \quad (\text{C.9})$$

Here we suppressed the dependences of the couplings on e.g. background curvature  $r$  or spectral values  $p^2$  to improve readability. All dependences are as in Sec. 5.3.2. The expression Flow is used as in (3.23). From (C.9) we obtain the flow equation for the transverse traceless graviton mass parameter

$$\partial_t \mu = (\eta_h - 2)\mu + \frac{2}{3}\eta_h r + 2r\mu' + 32\pi \text{Flow}_{tt}^{(2h)}(p^2 = 0), \quad (\text{C.10})$$

where the ' refers to a derivative with respect to  $r$ . The graviton three-point function is projected in straight analogy to the flat computation [1]. We focus on the transverse traceless part and define the two projection operators  $\Pi_{\Lambda}$  and  $\Pi_G$  as

$$\Pi_{\Lambda} = \Pi_{tt}^3 \circ S_{\text{EH}}^{(3h)}(\Lambda = 1, p^2 = 0, r = 0), \quad \Pi_G = \Pi_{tt}^3 \circ S_{\text{EH}}^{(3h)}(\Lambda = 0, p^2 = 1, r = 0), \quad (\text{C.11})$$

which we use for the projection on  $\lambda_3$  and  $g$ , respectively. The resulting flow equations are

$$\partial_t \left( Z_h^{3/2} k^2 \sqrt{g} \left( \frac{5}{2304} r + \frac{5}{192} \lambda_3 - \frac{9}{4096} p^2 \right) \right) = k^2 Z_h^{3/2} \text{Flow}_{\Lambda}^{(3h)}(p^2),$$

$$\partial_t \left( Z_h^{3/2} k^2 \sqrt{g} \left( -\frac{3}{8192} r - \frac{9}{4096} \lambda_3 + \frac{171}{32768} p^2 \right) \right) = k^2 Z_h^{3/2} \text{Flow}_G^{(3h)}(p^2). \quad (\text{C.12})$$

The flow of  $\lambda_3$  is extracted at vanishing spectral value  $p^2 = 0$ , while the flow of  $g$  is extracted with a derivative with respect to the dimensionless spectral value  $p^2$  at  $p = 0$ . The result is

$$\begin{aligned} \partial_t \lambda_3 = & -2\lambda_3 + 2r\lambda'_3 + \left( \frac{3}{2}\eta_h + \frac{1}{2} \frac{2g - \partial_t g + 2rg'}{g} \right) \left( \lambda_3 + \frac{1}{12}r \right) \\ & + \frac{3}{80} \frac{(32\pi)^2}{\sqrt{g}k} \text{Flow}_\Lambda^{(3h)}(p^2 = 0), \end{aligned} \quad (\text{C.13})$$

$$\begin{aligned} \partial_t g = & 2g + 2rg' + 3\eta_h g - \frac{24}{19} \left( \partial_{p^2} \eta_h \Big|_{p^2=0} \right) \left( \lambda_3 + \frac{1}{6}r \right) g \\ & + \frac{64}{171} (32\pi)^2 \sqrt{g}k \partial_{p^2} \text{Flow}_G^{(3h)} \Big|_{p^2=0}. \end{aligned} \quad (\text{C.14})$$

### C.3. Check of approximations

In Sec. 5.3.1 we have explained that all vertices in a curved background contain uncontracted covariant derivatives. We have circumvented this issue by using the approximation displayed in (5.14). This problem reoccurs during the contraction of the diagrams, since the usual York-decomposition projection operators  $\Pi_i$  are needed, with  $i \in \{\text{tt}, \text{tr}, \dots\}$ . The projection operators are functions of the background Laplacian and the background covariant derivative  $\Pi_i(\bar{\Delta}, \bar{\nabla})$ , where the latter covariant derivatives are again approximated by (5.13) and (5.14). This however causes us to mix up the different spin Laplacians, spin-two  $\Delta_2$  and spin-zero  $\Delta_0$ . Other Laplacians do not occur since the graviton propagator only has a non-vanishing transverse traceless and trace mode. In this dissertation we choose to use the spin-zero Laplacian.

For the background flow this mixing of Laplacians does not occur since the propagator is not a function of the covariant derivative. Hence we use the background flow to estimate the error of our approximation. Here we focus on the transverse traceless and the trace part since these are the relevant modes in the fluctuation computation. The exact result with our regulator is given by

$$\text{Tr} [G\partial_t R]_{\text{tt,tr}} = \sum_{\ell=2}^{\ell_{\max}} m_2(\ell) (G\partial_t R)_{\text{tt}}(\Delta_2(\ell)) + \sum_{\ell=0}^{\ell_{\max}} m_0(\ell) (G\partial_t R)_{\text{tr}}(\Delta_0(\ell)), \quad (\text{C.15})$$

while we compare it to the approximations

$$(\text{C.15}) \approx \sum_{\ell=0}^{\ell_{\max}} m_0(\ell) (5(G\partial_t R)_{\text{tt}} + (G\partial_t R)_{\text{tr}}) (\Delta_0(\ell)) \quad (\text{C.16})$$

$$\approx \sum_{\ell=2}^{\ell_{\max}} m_0(\ell) (5(G\partial_t R)_{\text{tt}} + (G\partial_t R)_{\text{tr}}) (\Delta_0(\ell)) \quad (\text{C.17})$$

$$\approx \sum_{\ell=2}^{\ell_{\max}} m_2(\ell) \left( (G\partial_t R)_{\text{tt}} + \frac{1}{5} (G\partial_t R)_{\text{tr}} \right) (\Delta_2(\ell)). \quad (\text{C.18})$$

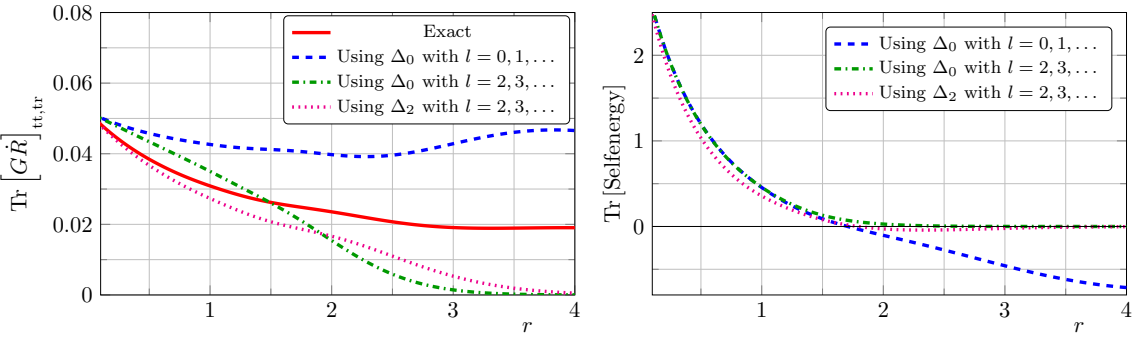


Figure C.1.: Comparison of the trace evaluation using different Laplacians and starting with different eigenvalues. In particular we compare the spin-two Laplacian  $\Delta_2$  and the spin-zero Laplacian  $\Delta_0$  and further we start once from the zero mode and once start from the  $l = 2$  mode. In the left panel we display the background flow  $\text{Tr}[G\partial_t R]$  of the combined transverse traceless and trace mode, where also the exact solution is computed. In the right panel we display the self-energy diagram of the two-point function, which is the second diagram in the graviton two-point flow in Fig. 3.1. From these results we infer that this particular approximation is qualitatively reliable in the range  $r < 2$ .

Here  $\ell_{\max}$  is chosen such that the trace is fully converged in the investigated curvature range and the factors 5 and  $\frac{1}{5}$  appear due to the five transverse traceless modes compared to the one trace mode.

The results are shown in Fig. C.1 in the left panel. For small background curvature  $r$  all results agree qualitatively well. For large background curvature the difference is becoming more significant. This can be easily understood: in the exact result (C.15) only the trace mode is equipped with a zero mode, while in the first approximation (C.16) all modes are equipped with a zero mode. In contrast in the second and third approximation, (C.17) and (C.18), no mode is equipped with a zero mode. The zero modes dominate for large curvature and thus it is clear that the approximation fails in this regime.

In other words, the symmetrised products of covariant derivatives in the projectors are effectively commuting in our approximation. The transverse traceless projection basically traces out the degrees of freedom of the transverse traceless mode and leaves us with a scalar quantity. With this approximation, there is an ambiguity related to the Laplace operator, which can be chosen as the spin-zero or spin-two Laplacian. As already mentioned we choose to use the spin-zero Laplacian without zero modes, i.e. approximation (C.17).

In the right panel of Fig. C.1 we compare these different choices for one particular diagram of the graviton two-point function, where the exact result is not available within our truncation. We observe that the results are almost identical for small curvature, i.e.  $r < 2$ . For  $r > 2$  the results differ qualitatively due to the different treatment of the zero modes. We conclude that the validity of our approximation is bound by  $r < 2$ .

## C.4. Insensitivity on initial conditions

As explained in Sec. 5.3.3 we have to give initial conditions to the beta function since they are the first-order linear differential equations. In principle the initial condition has to be given at vanishing curvature  $r = 0$  since there are the divergences of the differential

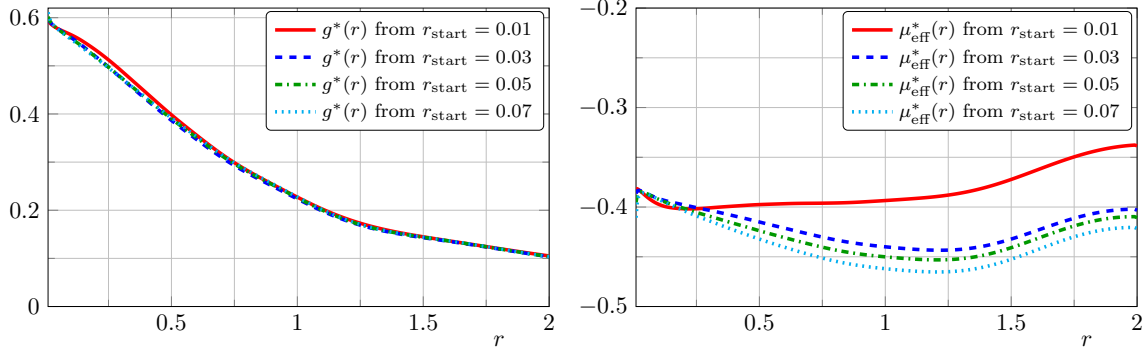


Figure C.2.: Comparison of fixed point functions with initial condition at different curvature values  $r_{\text{start}} \in \{0.01, 0.03, 0.05, 0.07\}$ . In the left panel we compare the fixed point functions of the Newton's coupling  $g(r)$  and in the right panel the effective graviton mass parameter  $\mu_{\text{eff}}(r) = \mu(r) + \frac{2}{3}r$ . Both fixed point functions show only a small dependence on the initial condition. All initial conditions are determined by  $g_i^*(r_{\text{start}}) = g_{i,0}^* + r_{\text{start}} g_{i,1}^*$ , where the zeroth and linear order in  $r$  of the couplings are given by (5.26) and (5.30).

equations. However the spectral sum converges only point wise and the number of modes that have to be included grows exponentially towards  $r \rightarrow 0$ . Consequently we give the initial conditions at some finite  $r_{\text{start}}$  that should be close to  $r = 0$ . The value there is obtained by expanding the heat kernel expansion (5.23). One can then check that the spectral sum and heat kernel agree in the small background curvature regime where both methods converge [410, 411]. In this Appendix we discuss the sensitivity of the fixed point functions to the choice of  $r_{\text{start}}$ .

The initial condition for some coupling  $g_i$  is determined from the zero and first order of the heat-kernel expansion around  $r = 0$ , i.e. by  $g_i^*(r_{\text{start}}) = g_{i,0}^* + r_{\text{start}} g_{i,1}^*$  where  $g_{i,0}^*$  and  $g_{i,1}^*$  are determined by the heat-kernel computation and the solutions are displayed in (5.26) and (5.30). On the one hand the quality of this initial condition gets worse for large  $r_{\text{start}}$  since this is a linear approximation of the curvature dependence of the couplings. On the other hand the quality also gets worse for too small  $r_{\text{start}}$  since we are too close to the singularity at  $r = 0$ . Consequently we have to find a region in between where the fixed point functions for the couplings are stable against small variations of  $r_{\text{start}}$ .

From the chosen  $r_{\text{start}}$  we integrate the differential equations upwards to large  $r$ . Integrating down would quickly run into the singularity at  $r = 0$ . In Fig. C.2 we display the resulting fixed point functions for  $g^*(r)$  and  $\mu_{\text{eff}}^*(r)$  for different choices of  $r_{\text{start}} \in \{0.01, 0.03, 0.05, 0.07\}$ . We observe that the fixed point functions for  $g^*(r)$  (left panel of Fig. C.2) agree almost perfectly for all chosen start values. Only for  $r_{\text{start}} = 0.01$  we observe a tiny deviation. For the fixed point functions of  $\mu_{\text{eff}}^*(r)$  (right panel of Fig. C.2) we observe larger, but still small deviations. Again for  $r_{\text{start}} = 0.01$  the deviations are the largest. We conclude that this start value is too close to the singularity at  $r = 0$ . The results in this dissertation were computed with  $r_{\text{start}} = 0.03$ .

## D. Scalars & fermions with gravity

This Appendix belongs to [Chapter 6](#)

### D.1. Analytic flow equations

Throughout [Chapter 6](#) we have used the full numerical flow equations to compute the UV fixed points. Nevertheless, we derived analytic flow equations, which are, however, less accurate in capturing the momentum dependence of the flow, see App. [B.4](#). The pure gravity contributions are the same as in [\(B.17\)](#) and the matter contributions are given by

$$\begin{aligned} \partial_t g &= \beta_{g,\text{gravity}} + N_f \frac{g^2}{\pi} \left( -\frac{521(6 - \eta_\psi(k^2))}{17100} - \frac{3(5 - \eta_\psi(k^2))}{152} - \frac{13}{380} \right) \\ &\quad + N_s \frac{g^2}{\pi} \left( \frac{10 - \eta_\varphi(k^2)}{1140} - \frac{8}{95} \right), \\ \partial_t \lambda_3 &= \beta_{\lambda_3,\text{gravity}} + N_f \frac{g}{\pi} \left( \frac{8 - \eta_\psi(k^2)}{224} - \frac{7 - \eta_\psi(k^2)}{56} + \frac{17(6 - \eta_\psi(k^2))}{240} \right) \\ &\quad + N_s \frac{g}{\pi} \left( \frac{12 - \eta_\varphi(k^2)}{480} - \frac{10 - \eta_\varphi(k^2)}{80} + \frac{8 - \eta_\varphi(k^2)}{96} \right), \\ \partial_t \mu &= \beta_{\mu,\text{gravity}} + N_f \frac{g}{\pi} \left( \frac{7 - \eta_\psi(k^2)}{63} - \frac{6 - \eta_\psi(k^2)}{6} \right) + N_s \frac{g}{\pi} \left( \frac{10 - \eta_\varphi(k^2)}{120} \right). \end{aligned} \quad (\text{D.1})$$

### D.2. Background quantities

The functions  $f_{R^i}$  in [Sec. 6.5](#) are extracted from [\[424\]](#). In our case they read

$$\begin{aligned} f_{R^0}(\lambda, N_s, N_f) &= \frac{1}{48\pi} \left( \frac{20(6 - \eta_h(k^2))}{1 - 2\lambda} - 16(6 - \eta_c(k^2)) \right. \\ &\quad \left. + 2(6 - \eta_\varphi(k^2))N_s - 8(6 - \eta_\psi(k^2))N_f \right), \\ f_{R^1}(\lambda, N_s, N_f) &= \frac{1}{48\pi} \left( \frac{52(4 - \eta_h(k^2))}{1 - 2\lambda} + 40(4 - \eta_c(k^2)) \right. \\ &\quad \left. - 2(4 - \eta_\varphi(k^2))N_s - 4(4 - \eta_\psi(k^2))N_f \right). \end{aligned} \quad (\text{D.2})$$

In order to obtain the functions in equation [\(D.2\)](#), we reversed the identification of background and dynamical quantities and replaced  $\eta_\phi \rightarrow \eta_\phi(k^2)$  in order to evaluate the anomalous dimension at the values, where the integrals are peaked. Note, that the functions  $f_{R^i}$  depend on the dynamical gravitational coupling  $g$  only via the anomalous dimensions.

# E. UV dominance of gravity

This Appendix belongs to [Chapter 7](#).

## E.1. Regulators

In [Chapter 7](#) we used mostly the optimised or flat regulator [372–375] for all field modes. Specifically, the superfield regulator at  $\bar{g}_{\mu\nu} = \delta_{\mu\nu}$  and  $\bar{A}_\mu = 0$  with flat Euclidean background metric is given by

$$R_k^{ij}(p) = \delta^{ij} \left. \Gamma^{(\phi_i \phi_i^*)}(p) \right|_{\mu=0} r_{\phi_i}(p^2/k^2), \quad r(x) = (x^{-1} - 1) \theta(1-x). \quad (\text{E.1})$$

Here,  $\phi^*$  is the dual superfield with  $\phi^* = (h_{\mu\nu}, -\bar{c}_\mu, c_\mu, A_\mu, -\bar{c}, c)$ . The regulator (E.1) is diagonal in field space keeping in mind the symplectic metric and allows for analytic expressions of the flow [101]. For the general scaling analysis we also discuss more general regulators, in particular we refer to the exponential and sharp regulator with

$$r_{\text{exp}}(x) = \frac{1}{\exp(x) - 1}, \quad r_{\text{sharp}}(x) = \frac{1}{\theta(x-1)} - 1. \quad (\text{E.2})$$

These regulators can be used to scan the space of cutoff functions [477, 478].

## E.2. Regulator dependence of the gluon contribution to the graviton mass parameter

The coefficient  $c_{\mu,a}$ , which parameterises the gluon contribution to the graviton mass parameter, is given by

$$c_{\mu,a} = -\frac{\text{Flow}_a^{(2h)}(p^2=0)}{g(N_c^2-1)} = \frac{1}{3\pi} \int \frac{dx}{(1+r_h(x))^2} \left( \frac{4}{1+r_h(x)} - 3 \right), \quad (\text{E.3})$$

with  $x = \frac{q^2}{k^2}$ ,  $\eta_a = 0$  on the right hand side, and where the angular integration was already performed. We now use that

$$k \partial_k r_h(k, x) = k \frac{\partial x}{\partial k} \partial_x r_h(k, x) = -2x \partial_x r_h(k, x), \quad (\text{E.4})$$

and consequently we get

$$c_{\mu,a} = -\frac{2}{3\pi} \int dx x^2 \left( \partial_x \left( \frac{2}{(1+r_h(x))^2} - 2 \right) - \partial_x \left( \frac{3}{1+r_h(x)} - 3 \right) \right), \quad (\text{E.5})$$

where we added zeros in order to perform the partial integration without boundary terms. The result after partial integration is

$$c_{\mu,a} = \frac{4}{3\pi} \int dx x \frac{r_h(x)(r_h(x)-1)}{(1+r_h(x))^2}. \quad (\text{E.6})$$

Regulator	$c_{\mu,a}$
$r(x) = \frac{1}{\exp(x)-1}$	-0.21
$r(x) = \frac{1}{x} \exp(-x^2)$	-0.027
$r(x) = (\frac{1}{x} - 1)\Theta(1-x)$	0
$r(x) = \frac{1}{x}\Theta(1-x)$	0.034
$r(x) = \frac{10}{x}\Theta(1-x)$	0.17
$r(x) = \frac{1}{\Theta(x-1)} - 1$	$\frac{2}{3\pi} \approx 0.21$

Table E.1.: Gluon contribution to the graviton mass parameter for different regulators. Remarkably the contribution does not only change in size but also its sign.

We have evaluated this integral for different types of regulator shape functions. The results are displayed in Tab. E.1. The flat regulator evaluates this integral to zero, while exponential regulators give a positive sign and step-like or sharp regulators even give a negative sign. The usual expectation is that the regulator changes the size of a contribution but not its sign. In this case, however, two diagrams cancel each other approximately and by changing the regulator we shift the weights between these two diagrams. Thus, any sign of this contribution is possible.

### E.3. Scaling equations

In this Appendix we augment the analysis from Sec. 7.7 by providing scaling equations for all couplings. In particular we are lifting the identification (7.22). Here we extract the fixed point scaling from a flat regulator choice and utilise a reparameterisation of the flow equations that minimises the occurrence of factors of  $1 + \mu$ . Moreover, in the previous chapter we have utilised projections on gravitational couplings  $g_n$  and  $g_{aah}$  within a finite difference construction. In the literature projections with derivatives at vanishing momentum,  $p^2 = 0$ , are often used. It has been argued in App. B.4 that this definition has large ambiguities at  $p^2 = 0$ , which limits its applicability. Still, it has the charm of providing analytic flows and fixed point equations and hence facilitating the access to the current analysis.

The structure of the flow and fixed point equations is more apparent if we absorb  $1/(1 + \mu)$ -factors in the gravitational couplings with

$$\bar{g}_n = g_n \left( \frac{1}{1 + \mu} \right)^{\gamma_n}, \quad \bar{g}_{\bar{c}ch^n} = g_{\bar{c}ch^n} \left( \frac{1}{1 + \mu} \right)^{\gamma_c}, \quad \bar{g}_{a^n h^m} = g_{a^n h^m} \left( \frac{1}{1 + \mu} \right)^{\gamma_a}, \quad (\text{E.7a})$$

with the scaling coefficients

$$\gamma_n = \frac{n}{n-2}, \quad \gamma_a = \gamma_c = 1, \quad (\text{E.7b})$$

and  $\mu, \lambda_n$  are not rescaled. This removes all potentially singular factors  $1/(1 + \mu)$ -factors in the diagrams that stem from the respective powers of the graviton propagators in the

loops. It still leaves us with contributions proportional to  $1/(1 + \mu)$  due to the projection procedure with derivatives at  $p^2 = 0$  and due to regulator insertions. The rescaling power of  $1/(1 + \mu)$  varies between  $1/(1 + \mu)^3$  for the lowest coupling  $g_3$  and  $1/(1 + \mu)$  for  $g_{n \rightarrow \infty}$ .

In the following equations we identify blocks of gravitational couplings: as before all gravitational self-couplings  $\bar{g}_n, \bar{g}_{\bar{c}ch^n}$  are identified with  $\bar{g}_3$  and all  $\lambda_n$  are identified with  $\lambda_3$ . Additionally, we identify all Yang-Mills–gravity interactions  $\bar{g}_{aah^n}$  with  $\bar{g}_{aah}$ . This leads us to

$$\bar{g}_n = \bar{g}_3 = \bar{g}, \quad \lambda_{n>2} = \lambda_3, \quad (\text{E.8a})$$

for the pure gravity couplings and

$$\bar{g}_{\bar{c}ch^n} = \bar{g}_c, \quad \bar{g}_{aah^n} = \bar{g}_a, \quad (\text{E.8b})$$

for the ghost-graviton and gluon-graviton couplings. We emphasise that (E.8) and (E.7a) imply

$$g_n = g_3(1 + \mu)^{\gamma_3 - \gamma_n}, \quad (\text{E.9})$$

with  $\gamma_3 > \gamma_n$ . (E.9) seemingly entails the irrelevance of the lower order couplings  $g_n$  for  $\mu \rightarrow -1$ . However, the lower order couplings contribute to diagrams with more graviton propagators. In combination this leads to a uniform scaling of all diagrams as expected in a scaling limit. Note that the scaling analysis can also be performed if removing the approximation (E.8). It leads to an identical scaling  $\bar{g}_n \sim \bar{g}_3$  and  $\bar{g}_{aah^n} \sim \bar{g}_{aah}$ . The discussion of such a full analysis is deferred to future work.

Here we are only interested in the relative scaling between the pure gravity and Yang-Mills gravity diagrams, and simply discuss the structure of these equations. To that end we use the analytic pure gravity equations expressed with the rescaled couplings (E.7). We also use the identification (E.8), and additionally we suppress the ghost contribution for simplicity. The ghost contribution comes with the same power in  $1 + \mu$  as the gluon contribution. The analysis is facilitated by only using positive coefficients  $c_i, d_i$ , making the relative signs of the different terms apparent. In general the sign of some of these coefficients depends on  $\lambda_3$  and we define them such that they are positive at  $\lambda_3 = 0$ . The explicit values for the coefficients is provided in App. E.5. Within this notation all factors  $1/(1 + \mu)$  in the loops are absorbed in the couplings except the one, which comes from external momentum derivatives of propagators,  $\partial_{p^2}G$ , due to the projection procedure or from regulator insertions. In summary we are led to

$$\begin{aligned} \partial_t \mu &= -(2 - \eta_h) \mu - \bar{g} \left[ c_{\mu,h} + (1 + \mu)(N_c^2 - 1) c_{\mu,a} \frac{\bar{g}_a}{\bar{g}} \right], \\ \partial_t \bar{g} &= (2 + 3\bar{\eta}_h) \bar{g} - \bar{g}^2 \left[ \frac{c_{\bar{g},h}}{1 + \mu} + \frac{d_{\bar{g},h}}{(1 + \mu)^2} + (N_c^2 - 1) c_{\bar{g},a} \left( \frac{\bar{g}_a}{\bar{g}} \right)^{\frac{3}{2}} \right], \\ \partial_t \lambda_3 &= - \left( 1 + \frac{\partial_t \bar{g}}{2\bar{g}} - \frac{3}{2} \bar{\eta}_h \right) \lambda_3 + \bar{g} \left[ \frac{c_{\lambda_3,h}}{1 + \mu} + (N_c^2 - 1) c_{\lambda_3,a} \left( \frac{\bar{g}_a}{\bar{g}} \right)^{\frac{3}{2}} \right], \end{aligned} \quad (\text{E.10a})$$

for the pure gravity couplings. Here the term  $d_{\bar{g},h}/(1 + \mu)^2$  stems from the  $\partial_{p^2}G$  contributions, and all coefficients  $c, d$  from graviton-loops depend on  $\lambda_3$  with  $c(0), d(0) > 0$ . The

ghost-graviton and the gauge-graviton coupling have the flows

$$\begin{aligned}\partial_t \bar{g}_a &= (2 + 2\eta_a + \bar{\eta}_h) \bar{g}_a - \bar{g}_a^2 \left[ -c_{\bar{g}_a,a} + \frac{d_{\bar{g}_a,a}}{1+\mu} + \left( c_{\bar{g}_a,h} - \frac{d_{\bar{g}_a,h}}{1+\mu} \right) \left( \frac{\bar{g}}{\bar{g}_a} \right)^{\frac{1}{2}} \right], \\ \partial_t \bar{g}_c &= (2 + 2\eta_c + \bar{\eta}_h) \bar{g}_c - \bar{g}_c^2 \left[ c_{\bar{g}_c,c} + \frac{d_{\bar{g}_c,c}}{1+\mu} + \left( c_{\bar{g}_c,h} + \frac{d_{\bar{g}_c,h}}{1+\mu} \right) \left( \frac{\bar{g}}{\bar{g}_c} \right)^{\frac{1}{2}} \right].\end{aligned}\quad (\text{E.10b})$$

Here the  $d$ -terms originate from the diagram with a regularised graviton propagator,  $(G\partial_t R_k G)^{(hh)}$ . The coefficients  $c_{i,h}$  and  $d_{i,h}$  are  $\lambda_3$ -dependent as they receive contributions from the diagram with a three-graviton vertex. The signs are chosen such that  $c_{i,h}(0), d_{i,h}(0) > 0$ . The coefficients and the signs in the flow equation for  $\bar{g}_c$  were not derived in this dissertation.

The rescaled graviton anomalous dimension  $\bar{\eta}_h$  reads

$$\bar{\eta}_h = -\frac{\partial_t [Z_h(1+\mu)]}{Z_h(1+\mu)} = \eta_h - \frac{\dot{\mu}}{1+\mu}, \quad (\text{E.11})$$

which includes the scale dependence of the full dressing of the graviton propagator including the mass parameter. The set of anomalous dimensions is given by

$$\begin{aligned}\eta_h &= \bar{g} \left[ c_{\eta_h,h} + \frac{d_{\eta_h,h}}{1+\mu} + (N_c^2 - 1)c_{\eta_h,a} \frac{\bar{g}_a}{\bar{g}} \right], \\ \eta_c &= -\bar{g} \left[ c_{\eta_c,h} + \frac{d_{\eta_c,h}}{1+\mu} \right], \quad \eta_a = -\bar{g}_a \left[ c_{\eta_a,h} - \frac{d_{\eta_a,h}}{1+\mu} \right],\end{aligned}\quad (\text{E.12})$$

and completes the set of flow equations. Again, the graviton contributions to  $\eta_h$  have a  $\lambda_3$ -dependence with  $c_{\eta_h,h}(0), d_{\eta_h,h}(0) > 0$ . All other coefficients do not carry a  $\lambda_3$ -dependence. Note also that the  $\partial_t \mu / (1+\mu)$ -terms in the scaling terms on the right hand side of (E.10) come from the normalisation of the  $\bar{g}$ 's with powers of  $1/(1+\mu)$ . In the  $\bar{g}_n$ -flows this term is  $n/(n-2)\partial_t \mu / (1+\mu)$  derived from the rescaling (E.7a). For the ghost-gravity and gauge gravity couplings it is always the term  $\partial_t \mu / (1+\mu)$  derived from (E.7).

## E.4. Flow equations

Here we recall the results for the pure gravity flow for  $\mu$ ,  $g_3$  and  $\lambda_3$  derived in [1, 3], add the derived gluon contributions, and formulate them in terms of the rescaled couplings

$$\begin{aligned}\bar{g}_n &= g_n \left( \frac{1}{1+\mu} \right)^{\frac{n}{n-2}}, & \bar{g}_c &= g_c \left( \frac{1}{1+\mu} \right), \\ \bar{g}_a &= g_a \left( \frac{1}{1+\mu} \right), & \bar{\eta}_h &= \eta_h - \frac{\dot{\mu}}{1+\mu},\end{aligned}\quad (\text{E.13})$$

see App. E.3 and (E.7) for details. In order to show the interrelation of the different couplings we keep all dependences on the higher couplings  $\bar{g}_n$ . The flow equations are given by

$$\partial_t \mu = - (2 - \eta_h) \mu + \frac{\bar{g}_3}{180\pi} \left[ 21(10 - \eta_h) - 120\lambda_3(8 - \eta_h) + 320\lambda_3^2(6 - \eta_h) \right]$$

$$\begin{aligned}
& -\frac{\bar{g}_4}{12\pi} \left[ 3(8 - \eta_h) - 8\lambda_4(6 - \eta_h) \right] - (1 + \mu) \frac{\bar{g}_c}{5\pi} (10 - \eta_c) + (1 + \mu) (N_c^2 - 1) \frac{\bar{g}_a \eta_a}{60\pi}, \\
\partial_t \lambda_3 = & - \left( 1 + \frac{\partial_t \bar{g}_3}{2\bar{g}_3} - \frac{3}{2} \bar{\eta}_h \right) \lambda_3 + \bar{g}_3 \left\{ + \frac{1}{6\pi} \frac{1}{1 + \mu} \frac{\bar{g}_4}{\bar{g}_3} \left[ 3\lambda_4(8 - \eta_h) - 16\lambda_3\lambda_4(6 - \eta_h) \right] \right. \\
& - \frac{1}{1 + \mu} \frac{1}{240\pi} \left[ 11(12 - \eta_h) - 72\lambda_3(10 - \eta_h) + 120\lambda_3^2(8 - \eta_h) - 80\lambda_3^3(6 - \eta_h) \right] \\
& + \frac{1}{8\pi} \frac{1}{1 + \mu} \left( \frac{\bar{g}_5}{\bar{g}_3} \right)^{\frac{3}{2}} \left[ (8 - \eta_h) - 4\lambda_5(6 - \eta_h) \right] \\
& \left. + \frac{1}{10\pi} \left( \frac{\bar{g}_c}{\bar{g}_3} \right)^{\frac{3}{2}} (12 - \eta_c) + \frac{1}{60\pi} (N_c^2 - 1) \left( \frac{\bar{g}_a}{\bar{g}_3} \right)^{\frac{3}{2}} (3 - \eta_a) \right\}, \\
\partial_t \bar{g}_3 = & (2 + 3\bar{\eta}_h) \bar{g}_3 - \frac{\bar{g}_3^2}{19\pi} \left\{ \frac{1}{(1 + \mu)^2} \frac{2}{15} \left[ 229 - 1780\lambda_3 + 3640\lambda_3^2 - 2336\lambda_3^3 \right] \right. \\
& - \frac{1}{1 + \mu} \frac{1}{80} \left[ 147(10 - \eta_h) - 1860\lambda_3(8 - \eta_h) + 3380\lambda_3^2(6 - \eta_h) + 25920\lambda_3^3(4 - \eta_h) \right] \\
& - \frac{1}{1 + \mu} \frac{\bar{g}_4}{\bar{g}_3} \left[ \frac{1}{18} \left[ 45(8 - \eta_h) - 8(30\lambda_3 - 59\lambda_4)(6 - \eta_h) - 360\lambda_3\lambda_4(4 - \eta_h) \right] \right. \\
& + \frac{16}{1 + \mu} (1 - 3\lambda_3) \lambda_4 \left. \right] + \frac{1}{1 + \mu} \frac{47}{6} \left( \frac{\bar{g}_5}{\bar{g}_3} \right)^{\frac{3}{2}} (6 - \eta_h) \\
& \left. + \left( \frac{\bar{g}_c}{\bar{g}_3} \right)^{\frac{3}{2}} \left[ \frac{50 - 53\eta_c}{10} \right] + (N_c^2 - 1) \left( \frac{\bar{g}_a}{\bar{g}_3} \right)^{\frac{3}{2}} \left[ \frac{133 + \eta_a}{30} \right] \right\}, \\
\partial_t \bar{g}_a = & (2 + 2\eta_a + \bar{\eta}_h) \bar{g}_a - \frac{\bar{g}_a^2}{30\pi} \left\{ - \frac{100 - 13\eta_a}{2} + \frac{13(5 - \eta_h)}{\mu + 1} \right. \\
& \left. + \left( \frac{\bar{g}_3}{\bar{g}_a} \right)^{\frac{1}{2}} \left( \frac{330 - 640\lambda_3 - \eta_a(33 - 80\lambda_3)}{12} + \frac{-15 + 400\lambda_3 - \eta_h(80\lambda_3 - 6)}{3(\mu + 1)} \right) \right\}, \tag{E.14}
\end{aligned}$$

and the anomalous dimension read,

$$\begin{aligned}
\eta_h = & \frac{\bar{g}_3}{4\pi} \left( \frac{\bar{g}_4}{\bar{g}_3} (6 - \eta_h) - \frac{6(8 - \eta_h) + 8(6 - \eta_h)\lambda_3 - 36(4 - \eta_h)\lambda_3^2}{9} + \frac{17 + 8\lambda_3(9\lambda_3 - 8)}{3(1 + \mu)} \right. \\
& \left. - \frac{\bar{g}_c}{\bar{g}_3} \eta_c + (N_c^2 - 1) \frac{\bar{g}_a}{\bar{g}_3} \frac{1 + \eta_a}{3} \right), \\
\eta_c = & - \frac{\bar{g}_c}{9\pi} \left( \frac{8 - \eta_h}{1 + \mu} + 8 - \eta_c \right), \quad \eta_a = - \frac{\bar{g}_a}{8\pi} \left( 8 - \eta_a - \frac{4 - \eta_h}{1 + \mu} \right). \tag{E.15}
\end{aligned}$$

The two terms in the flow equation for  $\bar{g}_3$  proportional to  $1/(1 + \mu)^2$  and the term in  $\eta_h$  proportional to  $1/(1 + \mu)$  signal the derivative expansion at  $p^2 = 0$ . This is the price to

pay for an analytic flow equation. On the other hand the terms proportional to  $1/(1+\mu)$  in  $\bar{g}_a$ ,  $\eta_a$  and  $\eta_c$  come from a regulator insertion in a graviton propagator compared to a ghost or gluon propagator.

## E.5. Coefficients in the scaling equations

The coefficients in the scaling equations in App. E.3 are given here in the approximation (E.8). We assume that the anomalous dimensions satisfy  $|\eta| \leq 2$ : they should not dominate the scaling of the regulator. While the upper bound  $\eta \leq 2$  is a (weak) consistency bound for the regulator, see Sec. 6.3.4, the lower one can be seen as a (weak) consistency bound on the propagators. For  $\eta < -2$  they cease to be well-defined as Fourier transforms of space-time correlations functions (if they scale universally down to vanishing momenta). For simplicity we display the coefficients with  $\lambda_3 = 0$ . Note that all coefficients are defined such that they are always positive. All coefficients can be directly read off from the equations (E.14) and (E.15). The coefficients  $c_{\mu,h}$  and  $c_{\mu,a}$  in the fixed point equation of the mass parameter  $\mu$  are given by

$$c_{\mu,h} = \frac{17}{6\pi} - \frac{2}{15\pi}\eta_h - \frac{1}{5\pi}\eta_c, \quad c_{\mu,a} = -\frac{1}{60\pi}\eta_a. \quad (\text{E.16})$$

Note that the second coefficient is positive since  $\eta_a < 0$ . The coefficients  $c_{\bar{g},h}$  and  $c_{\bar{g},a}$  in the fixed point equation of the pure gravity coupling  $\bar{g}$  read

$$c_{\bar{g},h} = \frac{47}{57\pi} - \frac{53}{190\pi}\eta_h - \frac{37}{190\pi}\eta_c, \quad d_{\bar{g},h} = \frac{598}{285\pi}, \quad c_{\bar{g},a} = \frac{7}{30\pi} + \frac{1}{570\pi}\eta_a, \quad (\text{E.17})$$

while the coefficients  $c_{\lambda_3,h}$  and  $c_{\lambda_3,a}$  in the fixed point equation of  $\lambda_3$  are given by

$$c_{\lambda_3,h} = \frac{33}{20\pi} - \frac{19}{240\pi}\eta_h - \frac{1}{10\pi}\eta_c, \quad c_{\lambda_3,a} = \frac{3}{60\pi} - \frac{1}{60\pi}\eta_a. \quad (\text{E.18})$$

Furthermore the coefficient  $c_{\bar{g}_a}$  in the fixed point equation for the two-gluon–graviton coupling  $\bar{g}_a$  reads

$$\begin{aligned} c_{\bar{g}_a,a} &= \frac{5}{3\pi} - \frac{13}{60\pi}\eta_a, & d_{\bar{g}_a,a} &= \frac{13}{6\pi} - \frac{13}{30\pi}\eta_h, \\ c_{\bar{g}_a,h} &= \frac{11}{12\pi} - \frac{11}{120\pi}\eta_a, & d_{\bar{g}_a,h} &= \frac{1}{6\pi} - \frac{1}{15\pi}\eta_h. \end{aligned} \quad (\text{E.19})$$

We also summarise the coefficients of the anomalous dimensions, to wit

$$\begin{aligned} c_{\eta_h,h} &= \frac{1}{6\pi} - \frac{1}{12\pi}\eta_h - \frac{1}{4\pi}\eta_c, & d_{\eta_h,h} &= \frac{17}{12\pi}, & c_{\eta_h,a} &= \frac{1}{12\pi} + \frac{1}{12\pi}\eta_a, \\ c_{\eta_c} &= \frac{8}{9\pi} - \frac{1}{9\pi}\eta_c, & d_{\eta_c} &= \frac{8}{9\pi} - \frac{1}{9\pi}\eta_h, \\ c_{\eta_a} &= \frac{1}{\pi} - \frac{1}{8\pi}\eta_a, & d_{\eta_a} &= \frac{1}{2\pi} - \frac{1}{8\pi}\eta_h. \end{aligned} \quad (\text{E.20})$$

## F. Effective universality

This Appendix belongs to [Chapter 8](#).

### F.1. Background flow equations

In this Appendix we display the background flow equations. We use a type-I Litim regulator and the gauge  $\alpha = \beta = 0$ . We further employ the York-decomposition [81, 470] with field redefinitions [247, 413]. The result for the gravity part of the background flows agrees with e.g. [262] and App. B.2 while the scalar part agrees with e.g. [424]. The details of the computation are given in App. F.3. The flow of the background couplings are given by

$$\begin{aligned} \partial_t \bar{G} &= (2 + \eta_N) \bar{G}, \\ \partial_t \bar{\Lambda} &= -4\bar{\Lambda} + \frac{\bar{\Lambda}}{\bar{G}} \partial_t \bar{G} + 8\pi \bar{G} \text{Flow}_{\bar{\Gamma}} \Big|_{\sqrt{\bar{g}}\text{-terms}}, \\ \eta_N &= 16\pi \bar{G} \text{Flow}_{\bar{\Gamma}} \Big|_{\sqrt{\bar{g}}\bar{R}\text{-terms}}, \end{aligned} \quad (\text{F.1})$$

where

$$\begin{aligned} \text{Flow}_{\bar{\Gamma}} &= \frac{\sqrt{\bar{g}}}{32\pi^2} \left\{ \left[ \frac{5 - \frac{5}{6}\eta_h}{1 - 2\lambda} + \frac{1 - \frac{1}{6}\eta_h}{1 - \frac{4}{3}\lambda} - 4 - \frac{2}{3}\eta_h + \frac{4}{3}\eta_c + N_s(1 - \frac{1}{6}\eta_\varphi) \right] k^4 \right. \\ &+ \left[ \frac{1}{3} \frac{1 - \frac{1}{4}\eta_h}{1 - \frac{4}{3}\lambda} - \frac{10}{3} \frac{1 - \frac{1}{6}\eta_h}{(1 - 2\lambda)^2} - \frac{5}{3} \frac{1 - \frac{1}{4}\eta_h}{1 - 2\lambda} - \frac{23}{12} - \frac{7}{18}\eta_h + \frac{7}{9}\eta_c + \frac{N_s}{3}(1 - \frac{\eta_\varphi}{4}) \right] k^2 \bar{R} \Big\} \\ &+ \mathcal{O}(\bar{R}^2). \end{aligned} \quad (\text{F.2})$$

Note that the quantities  $\lambda$ ,  $\eta_h$ ,  $\eta_c$ , and  $\eta_\varphi$  can be taken from the respective fluctuation two-point functions. In this case the background couplings are non-dynamical spectators. The usual background field approximation is obtained by setting  $\lambda = \bar{\Lambda}$ ,  $\eta_h = \eta_N$ ,  $\eta_c = 0$ , and  $\eta_\varphi = 0$ .

### F.2. Level-1 flow equations

In this Appendix we display the level-one flow equations that are derived through a Nielsen identity from the background flow equations, see [Sec. 8.6](#). We work with the approximation

$$\frac{\delta}{\delta h_{\mu\nu}} \partial_t \Gamma_k \approx \frac{\delta}{\delta \bar{g}_{\mu\nu}} \partial_t \Gamma_k - \partial_t \left( \frac{1}{2} \text{Tr} \left[ \frac{1}{\sqrt{\bar{g}}} \frac{\delta \sqrt{\bar{g}} R_k}{\delta \bar{g}_{\mu\nu}} G_k \right] \right). \quad (\text{F.3})$$

Consequently we are interested in evaluating

$$\mathcal{I}^{\mu\nu} = I \bar{g}^{\mu\nu} = \frac{1}{2} \text{Tr} \left[ \frac{1}{\sqrt{\bar{g}}} \frac{\delta \sqrt{\bar{g}} R_k}{\delta \bar{g}_{\mu\nu}} G_k \right], \quad (\text{F.4})$$

which gives us, combined with the background flows, the flows for the level-one couplings. The trace appearing in (F.4) can be evaluated using heat kernel techniques. Details of the computation are presented in App. F.3. The result for  $I$  is given by

$$8I = \frac{\sqrt{\bar{g}}}{32\pi^2} \left\{ \left[ \frac{10}{3} \frac{1}{1-2\lambda} + \frac{2}{3} \frac{1}{1-\frac{4}{3}\lambda} - \frac{8}{3} + \frac{2}{3} N_s \right] k^4 \right. \\ \left. + \left[ -\frac{20}{9} \frac{1}{(1-2\lambda)^2} - \frac{5}{2} \frac{1}{1-2\lambda} + \frac{1}{2} \frac{1}{1-\frac{4}{3}\lambda} - \frac{71}{36} + \frac{1}{2} N_s \right] k^2 \bar{R} \right\} + \mathcal{O}(\bar{R}^2). \quad (\text{F.5})$$

We display the result for  $8I$ , since the Nielsen identity enters precisely with this factor in the flow equation for the  $\sqrt{\bar{g}}$ -terms as well as the  $\sqrt{\bar{g}}\bar{R}$ -terms. The reason for this is that  $\mathcal{I}^{\mu\nu}$  enters with a  $\partial_t$  derivative,  $\partial_t \sqrt{\bar{g}}k^4 = 4\sqrt{\bar{g}}k^4$  and  $\partial_t \sqrt{\bar{g}}\bar{R}k^2 = 2\sqrt{\bar{g}}\bar{R}k^2$ , while  $\text{Flow}_{\bar{\Gamma}}$  enters with a  $\delta_{\bar{g}}$  derivative,  $\delta_{\bar{g}}\sqrt{\bar{g}} = \frac{1}{2}\sqrt{\bar{g}}\bar{g}^{\mu\nu}$  and  $\delta_{\bar{g}}\sqrt{\bar{g}}\bar{R} = \frac{1}{4}\sqrt{\bar{g}}\bar{g}^{\mu\nu}\bar{R}$  cf. (F.13). Consequently in both cases they combine to the factor 8 as indicated above. Note that  $\mathcal{I}^{\mu\nu}$  does not contribute to the flow equation for  $\sqrt{\bar{g}}\bar{R}^2$  since  $\partial_t \sqrt{\bar{g}}\bar{R}^2 k^0 = 0$ . This is expected since  $R^2$  and  $R_{\mu\nu}^2$  are marginal couplings and thus their one-loop flow equations are universal. Note furthermore that in the above discussion we have neglected terms like  $\partial_t \lambda$ . Such terms do not change the fixed point values but they can influence the critical exponents.

The flow equations for the level-one couplings can now be expressed by flow of the background couplings plus the improvement from the Nielsen identity, to wit

$$\partial_t \bar{G}_1 = (2 + \eta_{N,1}) \bar{G}_1, \\ \partial_t \bar{\Lambda}_1 = -4\bar{\Lambda}_1 + \frac{\bar{\Lambda}_1}{\bar{G}_1} \partial_t \bar{G}_1 + 8\pi \bar{G}_1 (\text{Flow}_{\bar{\Gamma}} - 8I) \Big|_{\sqrt{\bar{g}}\text{-terms}}, \\ \eta_{N,1} = 16\pi \bar{G}_1 (\text{Flow}_{\bar{\Gamma}} - 8I) \Big|_{\sqrt{\bar{g}}\bar{R}\text{-terms}}. \quad (\text{F.6})$$

Again, the quantities  $\lambda$ ,  $\eta_h$ ,  $\eta_c$ , and  $\eta_\varphi$  can be taken from the respective fluctuation two-point functions. Then the level-one couplings are non-dynamical spectators. Otherwise we can close the equation at the level-one couplings by setting  $\lambda = \bar{\Lambda}_1$ ,  $\eta_h = \eta_{N,1}$  and  $\eta_c = \eta_\varphi = 0$ . The latter is an improved background field approximation.

### F.3. Evaluation of traces

In this Appendix we give a more detailed outline on the computation of the Nielsen identity, see (8.37) and (F.4). We saw in Sec. 8.6.1 that we can write the trace as

$$\mathcal{I}^{\mu\nu} = I \bar{g}^{\mu\nu} = \frac{1}{2} \text{Tr} \left[ \frac{1}{\sqrt{\bar{g}}} \frac{\delta \sqrt{\bar{g}} R_k}{\delta \bar{g}_{\mu\nu}} G_k \right] \\ = \frac{1}{4} \bar{g}^{\mu\nu} \text{Tr} [R_k G_k] + \frac{1}{2} \text{Tr} \left[ \frac{\delta}{\delta \bar{g}_{\mu\nu}} F_{\text{RG}} \right] + \frac{1}{2} \bar{R} \text{Tr} \left[ \frac{\delta}{\delta \bar{g}_{\mu\nu}} F_{\text{RG}}^{(1)} \right] + \mathcal{O}(\bar{R}^2), \quad (\text{F.7})$$

where we have defined

$$F_{\text{RG}}(x) = \int_0^x dx' \frac{\partial R_k(x')}{\partial x'} G_k(x', \bar{R} = 0),$$

$$F_{\text{RG}}^{(1)}(x) = \int_0^x dx' \frac{\partial R_k(x')}{\partial x'} G_k^{(0,1)}(x', \bar{R} = 0). \quad (\text{F.8})$$

In (F.7) we can pull the  $\bar{g}$ -derivative out of the trace. Here we have defined the trace such that we have to there is a factor  $\sqrt{\bar{g}}$  involved. Thus we obtain

$$\begin{aligned} \mathcal{I}^{\mu\nu} &= \frac{1}{4} \bar{g}^{\mu\nu} \text{Tr}[G_k R_k] + \frac{1}{2} \frac{\delta}{\delta \bar{g}_{\mu\nu}} \text{Tr}[F_{\text{RG}}] - \frac{1}{4} \bar{g}^{\mu\nu} \text{Tr}[F_{\text{RG}}] \\ &\quad + \frac{1}{2} \bar{R} \frac{\delta}{\delta \bar{g}_{\mu\nu}} \text{Tr}[F_{\text{RG}}^{(1)}] - \frac{1}{4} \bar{g}^{\mu\nu} \bar{R} \text{Tr}[F_{\text{RG}}^{(1)}] + \mathcal{O}(\bar{R}^2). \end{aligned} \quad (\text{F.9})$$

We now specify these traces to their contributions in order in the background curvature. For this we need to evaluate the background field derivative. Since  $S^4$  is an Einstein manifold, and in particular

$$\bar{R}_{\mu\nu} = \frac{1}{d} \bar{R} \bar{g}_{\mu\nu}. \quad (\text{F.10})$$

Applying a background field derivative, this gives

$$\frac{\delta \bar{R}}{\delta \bar{g}_{\mu\nu}} = -\frac{1}{d} \bar{R} \bar{g}^{\mu\nu} + \bar{g}^{\alpha\beta} \frac{\delta \bar{R}_{\alpha\beta}}{\delta \bar{g}_{\mu\nu}}. \quad (\text{F.11})$$

We further know that

$$\frac{\delta \bar{R}_{\alpha\beta}}{\delta \bar{g}_{\mu\nu}} = \bar{\Delta}_\rho \frac{\delta \Gamma_{\alpha\beta}^\rho}{\delta \bar{g}_{\mu\nu}} - \bar{\Delta}_\alpha \frac{\delta \Gamma_{\rho\beta}^\rho}{\delta \bar{g}_{\mu\nu}}, \quad (\text{F.12})$$

are total derivatives and do not contribute. In summary we have

$$\frac{\delta \sqrt{\bar{g}}}{\delta \bar{g}_{\mu\nu}} = \frac{1}{2} \sqrt{\bar{g}} \bar{g}^{\mu\nu}, \quad \frac{\delta \sqrt{\bar{g}} \bar{R}}{\delta \bar{g}_{\mu\nu}} = \frac{1}{4} \sqrt{\bar{g}} \bar{g}^{\mu\nu} \bar{R}. \quad (\text{F.13})$$

Using this for (F.9) we obtain

$$\begin{aligned} I \Big|_{\sqrt{\bar{g}}\text{-terms}} &= \frac{1}{4} \text{Tr}[G_k R_k] \Big|_{\sqrt{\bar{g}}\text{-terms}}, \\ I \Big|_{\sqrt{\bar{g}}\bar{R}\text{-terms}} &= \frac{1}{4} \left( \text{Tr}[G_k R_k] - \frac{1}{2} \text{Tr}[F_{\text{RG}}] \right) \Big|_{\sqrt{\bar{g}}\bar{R}\text{-terms}}. \end{aligned} \quad (\text{F.14})$$

Remarkably the  $F_{\text{RG}}$ -traces do not contribute to the  $\sqrt{\bar{g}}$ -terms and the  $F_{\text{RG}}^{(1)}$ -traces drop out completely. The latter would contribute to the  $\sqrt{\bar{g}}\bar{R}^2$ -order. In summary we want to compute the traces  $\text{Tr}[G_k R_k]$ ,  $\text{Tr}[F_{\text{RG}}]$  and  $\text{Tr}[G_k \partial_t R_k]$ . The latter we need for the flow of the background couplings, which are also the basis for the level-one flow equations.

With the gauge choice  $\beta = 0$  and  $\alpha \rightarrow 0$ , the product of  $G_k R_k$  is given by the sum of the contributions of the four modes  $h_{\mu\nu}^{\text{tt}}, \xi^\mu, h^{\text{tr}}$ , and  $\sigma$ . They are given by

$$\begin{aligned} (GR)_{h^{\text{tt}}} &= \frac{r_k(x)}{x + r_k(x) - 2\lambda} - \frac{2}{3} \frac{\bar{R}}{k^2} \frac{r_k(x)}{(x + r_k(x) - 2\lambda)^2} + \mathcal{O}(\bar{R}^2), \\ (GR)_\xi &= \frac{r_k(x)}{x + r_k(x)} + \frac{1}{4} \frac{\bar{R}}{k^2} \frac{r_k(x)}{(x + r_k(x))^2} + \mathcal{O}(\bar{R}^2), \end{aligned}$$

	TTT	VT	S
$\text{tr } b_0$	5	3	1
$\text{tr } b_2$	$-\frac{5}{6}R$	$\frac{1}{4}R$	$\frac{1}{6}R$

Table F.1.: Heat kernel coefficients for transverse traceless tensors (TTT), transverse vectors (VT) and scalars (S) on  $S^4$ .

$$(GR)_{h_{\text{tr}}} = \frac{r_k(x)}{x + r_k(x) - \frac{4}{3}\lambda},$$

$$(GR)_\sigma = \frac{r_k(x)}{x + r_k(x)} + \frac{1}{3} \frac{\bar{R}}{k^2} \frac{r_k(x)}{(x + r_k(x))^2} + \mathcal{O}(\bar{R}^2), \quad (\text{F.15})$$

where  $x = \bar{\Delta}/k^2$  is the dimensionless background Laplacian. The vector and scalar ghost modes,  $c$  and  $\eta$ , respectively, are given by

$$(GR)_c = \frac{r_k(x)}{x + r_k(x)} + \frac{1}{4} \frac{\bar{R}}{k^2} \frac{r_k(x)}{(x + r_k(x))^2} + \mathcal{O}(\bar{R}^2),$$

$$(GR)_\eta = \frac{r_k(x)}{x + r_k(x)} + \frac{1}{3} \frac{\bar{R}}{k^2} \frac{r_k(x)}{(x + r_k(x))^2} + \mathcal{O}(\bar{R}^2). \quad (\text{F.16})$$

The generalisations to  $G_k \partial_t R_k$  and  $G_k \partial_{\bar{\Delta}} R_k$  are straightforward. We start with the evaluation of  $\text{Tr} [G_k R_k]$  and write

$$\text{Tr} [G_k R_k] = \frac{1}{16\pi^2} \left[ B_0(\bar{\Delta}) Q_2(R_k G_k) + B_2(\bar{\Delta}) Q_1(R_k G_k) \right] + \mathcal{O}(\bar{R}^2),$$

where

$$Q_n[W] = \frac{1}{\Gamma(n)} \int dx x^{n-1} W(x), \quad B_n = \int d^d x \sqrt{\bar{g}} \text{tr } b_n, \quad (\text{F.17})$$

and  $\text{tr } b_n(\bar{\Delta}_s) \propto \bar{R}^{n/2}$  are the heat kernel coefficients. We can parameterise all graviton and ghost modes from (F.15) and (F.16) with the function

$$W(x) = \frac{r_k(x)}{[x + r_k(x) + a\lambda]^b}, \quad (\text{F.18})$$

with constants  $a$  and  $b$ . This results in

$$Q_2[W] = \frac{1}{6} \frac{k^{6-2b}}{(1+a\lambda)^b}, \quad Q_1[W] = \frac{1}{2} \frac{k^{4-2b}}{(1+a\lambda)^b}. \quad (\text{F.19})$$

Furthermore on the sphere we have

$$B_0(\bar{\Delta}_s) = \sqrt{\bar{g}} \text{tr } b_0, \quad B_2(\bar{\Delta}_s) = \sqrt{\bar{g}} \text{tr } b_2, \quad (\text{F.20})$$

where the trace coefficients are given in Tab. F.1. By specialising the coefficients  $a$  and  $b$  in the general expression above and evaluating the sum over all spin modes, we find

$$\text{Tr} [G_k R_k] = \frac{\sqrt{\bar{g}}}{16\pi^2} \left\{ \left[ \frac{5}{6} \frac{1}{1-2\lambda} + \frac{1}{6} \frac{1}{1-\frac{4}{3}\lambda} - \frac{2}{3} \right] k^4 \bar{R}^0 \right.$$

$$+ \left[ -\frac{5}{9} \frac{1}{(1-2\lambda)^2} - \frac{5}{12} \frac{1}{1-2\lambda} + \frac{1}{12} \frac{1}{1-\frac{4}{3}\lambda} - \frac{7}{18} \right] k^2 \bar{R}^1 \right\} + \mathcal{O}(\bar{R}^2). \quad (\text{F.21})$$

We turn now to the evaluation of  $\text{Tr}[F_{\text{RG}}]$  that can be evaluated in similar fashion, we write

$$\text{Tr}[F_{\text{RG}}] = \frac{1}{16\pi^2} F_{\text{RG}}(-\partial_\tau) \left[ B_0(\bar{\Delta}_s) \tau^{-2} + B_2(\bar{\Delta}_s) \tau^{-1} \right] \Big|_{\tau=0} + \mathcal{O}(\bar{R}^2), \quad (\text{F.22})$$

where we used

$$\text{Tr } f(\bar{\Delta}) = f(-\partial_\tau) \text{Tr } e^{-\tau \bar{\Delta}} \Big|_{\tau=0}. \quad (\text{F.23})$$

In particular, by utilising the identities

$$\frac{1}{\tau^2} = \int_0^\infty dx x e^{-\tau x} \Big|_{\tau=0}, \quad \frac{1}{\tau} = \int_0^\infty dx e^{-\tau x} \Big|_{\tau=0}, \quad (\text{F.24})$$

one can evaluate the action of the differential operators, and we find

$$\begin{aligned} F_{\text{RG}}(-\partial_\tau) \tau^{-2} &= \int_0^\infty dx x F_{\text{RG}}(x) = -\frac{1}{3} \frac{k^{6-2b}}{(1+a\lambda)^b}, \\ F_{\text{RG}}(-\partial_\tau) \tau^{-1} &= \int_0^\infty dx F_{\text{RG}}(x) = -\frac{1}{2} \frac{k^{4-2b}}{(1+a\lambda)^b}, \end{aligned} \quad (\text{F.25})$$

where the last equality in each line holds for the general function

$$F_{\text{RG}}(x) = \int_0^x dy \frac{r'_k(y)}{(y+r_k(y)+a\lambda k^2)^b} = -\frac{x}{(1+a\lambda)^b}, \quad \text{for } x \leq k^2, \quad (\text{F.26})$$

using the flat Litim-type cutoff as before. Specialising the coefficients  $a$  and  $b$  for the various spin modes and summing the contributions we get

$$\begin{aligned} \text{Tr}[F_{\text{RG}}] &= \frac{\sqrt{\bar{g}}}{16\pi^2} \left\{ \left[ -\frac{5}{3} \frac{1}{1-2\lambda} - \frac{1}{3} \frac{1}{1-\frac{4}{3}\lambda} + \frac{4}{3} \right] k^4 \right. \\ &\quad \left. + \left[ \frac{5}{12} \frac{1}{1-2\lambda} - \frac{1}{12} \frac{1}{1-\frac{4}{3}\lambda} + \frac{5}{24} \right] k^2 \bar{R}^1 \right\} + \mathcal{O}(\bar{R}^2). \end{aligned} \quad (\text{F.27})$$

The evaluated traces (F.21) and (F.27) allow us to compute the corrections from the Nielsen identity (F.14). The result is displayed in (F.5) where also the contribution from the minimally coupled scalars is shown. The computation of the latter is the same as the scalar graviton modes.

Last we evaluate  $\text{Tr}[G_k \partial_t R_k]$ , which is done in straight analogy to the previous traces. The heat-kernel functionals are now parameterised with

$$\tilde{W}(x) = \frac{\partial_t k^2 r_k(x)}{[x+r_k(x)+a\lambda]^b}. \quad (\text{F.28})$$

With  $\partial_t k^2 r_k(x) = 2k^2 r_k(x)$  for the flat Litim-type cutoff, we find

$$Q_2[\tilde{W}] = \frac{k^{6-2b}}{(1+a\lambda)^b}, \quad Q_1[\tilde{W}] = \frac{2k^{4-2b}}{(1+a\lambda)^b}. \quad (\text{F.29})$$

where we have suppressed wavefunction renormalisations and anomalous dimensions for readability. The result of summing over all spin modes is displayed in (F.2).

# Acknowledgements

First of all I would like to thank my PhD supervisor Jan Pawłowski. I really enjoyed the endless discussions about physics that taught me a lot of deep understanding in QFT. In particular the policy of the open door, that it is very easy to step by to his office, is worth mentioning and it is one of the cornerstones of the overall pleasant atmosphere within the whole group. I truly appreciated having a lot of freedom to pursue my own research interests and I am grateful that I could suggest new projects, not only for myself but also for new Master students.

I would like to thank Tilman Plehn for being my second PhD advisor, for support to get into the IMPRS graduate school and for being always available for discussions on Higgs physics.

I was very lucky to have during my whole PhD an ongoing collaboration with the Friedrich-Schiller University in Jena. I was always a welcomed guest and enjoyed the luxury of a permanent desk there. For this hospitality I am in debt to Holger Gies. Furthermore I would like to thank the whole theory group there for insightful discussions and the overall open and nice atmosphere that made it very easy for me to step by from time to time.

I would also like to thank Astrid Eichhorn for collaborations on various projects, and for setting up the quantum gravity group, including the many talks and journal clubs. With the format of the quantum gravity group she triggered lots of discussions, which was very beneficial. Furthermore I'm in debt for support with post-doc applications and for pointing out interesting workshops and conferences.

Special thanks also to Michael Scherer, who in particular managed to give me new motivation during some phases of my PhD and also during my post-doc applications.

I am grateful to Joerg Jaeckel for being the second referee to this PhD thesis.

I would like to thank all my collaborators for good teamwork and open fruitful discussions.

I would like to thank the whole quantum gravity group for enjoyable discussions on and off topic. It is very positive that we had a group feeling and also went to play Lasertag or to a bar in the evening. Also the non-gravity group was very important as discussions with them broadened my knowledge into other areas of physics. Also here I want to remark positively that people were active and that we outside of physics played squash, football or we had a beer.

During the course of my PhD I had a sheer endless amount of office mates, with all of them I had only pleasant experiences and always enjoyed the physics discussions and the coffee breaks. The long list comes about due to many different working places: first in Philosophenweg 12, then in the roofchamber of Philosophenweg 16, then 12 again, and not to forget about the office in Jena. It's a pleasure for me to thank them all for the

## ACKNOWLEDGEMENTS

---

encouraging working atmosphere.

I acknowledge funding for my PhD from the International Max Planck Research School for Precision Tests of Fundamental Symmetries. I am grateful that I was through this funding able to participate in many conferences and workshops. The enjoyable IMPRS seminars also gave me the possibility to broaden my physics knowledge to other areas in physics.

I would like to thank the Heidelberg Graduate School for Fundamental Physics for their financial support of some winter and summer schools, that I visited during my PhD, for the bridge funding after my PhD and for the support of the student's seminar, the 'Cold Quantum Coffee'. The latter was a great organisational experience and I'm glad that we have in Heidelberg this unique possibility that allows us to invite people from all over Europe and to put a program together that is broad but still perfectly tailored for the students of the ITP. Here I also would like to thank my co-organisers, Laura Classen, Anton Cyrol, Nicolas Wink and Felix Ziegler, for the efficient and pleasant atmosphere during the organisation.

I am grateful to Anton Cyrol, Stefan Lippoldt and Antonio Pereira for proofreading and for valuable comments on my introduction.

Last but not least I want to thank my parents, Monika and Michael Reichert, and all my friends for endless support outside of physics.

# Bibliography

- [1] N. Christiansen, B. Knorr, J. Meibohm, J. M. Pawłowski, and M. Reichert, “Local Quantum Gravity,” Phys. Rev. D92, 121501 (2015), arXiv:1506.07016 [hep-th].
- [2] J. Meibohm, J. M. Pawłowski, and M. Reichert, “Asymptotic safety of gravity-matter systems,” Phys. Rev. D93, 084035 (2016), arXiv:1510.07018 [hep-th].
- [3] T. Denz, J. M. Pawłowski, and M. Reichert, “Towards apparent convergence in asymptotically safe quantum gravity,” (2016), arXiv:1612.07315 [hep-th].
- [4] N. Christiansen, D. F. Litim, J. M. Pawłowski, and M. Reichert, “One force to rule them all: asymptotic safety of gravity with matter,” (2017), arXiv:1710.04669 [hep-th].
- [5] M. Reichert, A. Eichhorn, H. Gies, J. M. Pawłowski, T. Plehn, and M. M. Scherer, “Probing Baryogenesis through the Higgs Self-Coupling,” (2017), arXiv:1711.00019 [hep-ph].
- [6] N. Christiansen, K. Falls, J. M. Pawłowski, and M. Reichert, “Curvature dependence of quantum gravity,” Phys. Rev. D97, 046007 (2018), arXiv:1711.09259 [hep-th].
- [7] A. Eichhorn, P. Labus, J. M. Pawłowski, and M. Reichert, in preparation .
- [8] W. Pauli, “Relativistic Field Theories of Elementary Particles,” Rev. Mod. Phys. 13, 203 (1941).
- [9] C.-N. Yang and R. L. Mills, “Conservation of Isotopic Spin and Isotopic Gauge Invariance,” Phys. Rev. 96, 191 (1954).
- [10] S. L. Glashow, “Partial Symmetries of Weak Interactions,” Nucl. Phys. 22, 579 (1961).
- [11] S. Weinberg, “A Model of Leptons,” Phys. Rev. Lett. 19, 1264 (1967).
- [12] A. Salam, “Weak and Electromagnetic Interactions,” *8th Nobel Symposium Lerum, Sweden, May 19-25, 1968*, Conf. Proc. C680519, 367 (1968).
- [13] G. ’t Hooft and M. J. G. Veltman, “Regularization and Renormalization of Gauge Fields,” Nucl. Phys. B44, 189 (1972).
- [14] L. Evans and P. Bryant, “LHC Machine,” JINST 3, S08001 (2008).
- [15] F. Englert and R. Brout, “Broken Symmetry and the Mass of Gauge Vector Mesons,” Phys. Rev. Lett. 13, 321 (1964).

- [16] P. W. Higgs, “Broken Symmetries and the Masses of Gauge Bosons,” Phys. Rev. Lett. 13, 508 (1964).
- [17] G. Aad *et al.* (ATLAS), “Observation of a new particle in the search for the Standard Model Higgs boson with the ATLAS detector at the LHC,” Phys. Lett. B716, 1 (2012), arXiv:1207.7214 [hep-ex].
- [18] S. Chatrchyan *et al.* (CMS), “Observation of a new boson at a mass of 125 GeV with the CMS experiment at the LHC,” Phys. Lett. B716, 30 (2012), arXiv:1207.7235 [hep-ex].
- [19] G. Aad *et al.* (ATLAS, CMS), “Measurements of the Higgs boson production and decay rates and constraints on its couplings from a combined ATLAS and CMS analysis of the LHC pp collision data at  $\sqrt{s} = 7$  and 8 TeV,” JHEP 08, 045 (2016), arXiv:1606.02266 [hep-ex].
- [20] L. Landau *et al.*, “Niels Bohr and the development of physics,” Pergamon, London (1955).
- [21] D. Buttazzo, G. Degrassi, P. P. Giardino, G. F. Giudice, F. Sala, A. Salvio, and A. Strumia, “Investigating the near-criticality of the Higgs boson,” JHEP 12, 089 (2013), arXiv:1307.3536 [hep-ph].
- [22] E. Gabrielli, M. Heikinheimo, K. Kannike, A. Racioppi, M. Raidal, and C. Spethmann, “Towards Completing the Standard Model: Vacuum Stability, EWSB and Dark Matter,” Phys. Rev. D89, 015017 (2014), arXiv:1309.6632 [hep-ph].
- [23] G. M. Pelaggi, F. Sannino, A. Strumia, and E. Vigiani, “Naturalness of asymptotically safe Higgs,” Front.in Phys. 5, 49 (2017), arXiv:1701.01453 [hep-ph].
- [24] P. A. R. Ade *et al.* (Planck), “Planck 2015 results. XIII. Cosmological parameters,” Astron. Astrophys. 594, A13 (2016), arXiv:1502.01589 [astro-ph.CO].
- [25] A. D. Sakharov, “Violation of CP Invariance, c Asymmetry, and Baryon Asymmetry of the Universe,” Pisma Zh. Eksp. Teor. Fiz. 5, 32 (1967), [Usp. Fiz. Nauk161,61(1991)].
- [26] N. S. Manton, “Topology in the Weinberg-Salam Theory,” Phys. Rev. D28, 2019 (1983).
- [27] F. R. Klinkhamer and N. S. Manton, “A Saddle Point Solution in the Weinberg-Salam Theory,” Phys. Rev. D30, 2212 (1984).
- [28] P. B. Arnold and L. D. McLerran, “Sphalerons, Small Fluctuations and Baryon Number Violation in Electroweak Theory,” Phys. Rev. D36, 581 (1987).
- [29] P. B. Arnold and L. D. McLerran, “The Sphaleron Strikes Back,” Phys. Rev. D37, 1020 (1988).
- [30] N. Cabibbo, “Unitary Symmetry and Leptonic Decays,” *Meeting of the Italian School of Physics and Weak Interactions Bologna, Italy, April 26-28, 1984*, Phys. Rev. Lett. 10, 531 (1963), [,648(1963)].

- [31] M. Kobayashi and T. Maskawa, “CP Violation in the Renormalizable Theory of Weak Interaction,” *Prog. Theor. Phys.* **49**, 652 (1973).
- [32] M. Trodden, “Electroweak baryogenesis,” *Rev. Mod. Phys.* **71**, 1463 (1999), arXiv:hep-ph/9803479 [hep-ph].
- [33] M. E. Shaposhnikov, “Structure of the High Temperature Gauge Ground State and Electroweak Production of the Baryon Asymmetry,” *Nucl. Phys.* **B299**, 797 (1988).
- [34] M. Dine, P. Huet, J. R. L. Singleton, and L. Susskind, “Creating the baryon asymmetry at the electroweak phase transition,” *Phys. Lett.* **B257**, 351 (1991).
- [35] V. A. Kuzmin, V. A. Rubakov, and M. E. Shaposhnikov, “On the Anomalous Electroweak Baryon Number Nonconservation in the Early Universe,” *Phys. Lett.* **155B**, 36 (1985).
- [36] G. W. Anderson and L. J. Hall, “The Electroweak phase transition and baryogenesis,” *Phys. Rev.* **D45**, 2685 (1992).
- [37] M. Dine, R. G. Leigh, P. Y. Huet, A. D. Linde, and D. A. Linde, “Towards the theory of the electroweak phase transition,” *Phys. Rev.* **D46**, 550 (1992), arXiv:hep-ph/9203203 [hep-ph].
- [38] M. E. Shaposhnikov, “Baryon Asymmetry of the Universe in Standard Electroweak Theory,” *Nucl. Phys.* **B287**, 757 (1987).
- [39] K. Kajantie, M. Laine, K. Rummukainen, and M. E. Shaposhnikov, “Is there a hot electroweak phase transition at  $m(H)$  larger or equal to  $m(W)$ ?” *Phys. Rev. Lett.* **77**, 2887 (1996), arXiv:hep-ph/9605288 [hep-ph].
- [40] K. Rummukainen, M. Tsypin, K. Kajantie, M. Laine, and M. E. Shaposhnikov, “The Universality class of the electroweak theory,” *Nucl. Phys.* **B532**, 283 (1998), arXiv:hep-lat/9805013 [hep-lat].
- [41] F. Csikor, Z. Fodor, and J. Heitger, “Endpoint of the hot electroweak phase transition,” *Phys. Rev. Lett.* **82**, 21 (1999), arXiv:hep-ph/9809291 [hep-ph].
- [42] M. E. Shaposhnikov, “Standard model solution of the baryogenesis problem,” *Phys. Lett.* **B277**, 324 (1992), [Erratum: *Phys. Lett.* **B282**, 483 (1992)].
- [43] M. Fukugita and T. Yanagida, “Baryogenesis Without Grand Unification,” *Phys. Lett.* **B174**, 45 (1986).
- [44] L. Covi, E. Roulet, and F. Vissani, “CP violating decays in leptogenesis scenarios,” *Phys. Lett.* **B384**, 169 (1996), arXiv:hep-ph/9605319 [hep-ph].
- [45] S. Davidson and A. Ibarra, “A Lower bound on the right-handed neutrino mass from leptogenesis,” *Phys. Lett.* **B535**, 25 (2002), arXiv:hep-ph/0202239 [hep-ph].
- [46] G. F. Giudice, A. Notari, M. Raidal, A. Riotto, and A. Strumia, “Towards a complete theory of thermal leptogenesis in the SM and MSSM,” *Nucl. Phys.* **B685**, 89 (2004), arXiv:hep-ph/0310123 [hep-ph].

- [47] W. Buchmuller, P. Di Bari, and M. Plumacher, “Leptogenesis for pedestrians,” *Annals Phys.* 315, 305 (2005), arXiv:hep-ph/0401240 [hep-ph].
- [48] S. Davidson, E. Nardi, and Y. Nir, “Leptogenesis,” *Phys. Rept.* 466, 105 (2008), arXiv:0802.2962 [hep-ph].
- [49] A. I. Bochkarev, S. V. Kuzmin, and M. E. Shaposhnikov, “Electroweak baryogenesis and the Higgs boson mass problem,” *Phys. Lett. B*244, 275 (1990).
- [50] A. G. Cohen, D. B. Kaplan, and A. E. Nelson, “Spontaneous baryogenesis at the weak phase transition,” *Phys. Lett. B*263, 86 (1991).
- [51] A. E. Nelson, D. B. Kaplan, and A. G. Cohen, “Why there is something rather than nothing: Matter from weak interactions,” *Nucl. Phys. B*373, 453 (1992).
- [52] C. Grojean, G. Servant, and J. D. Wells, “First-order electroweak phase transition in the standard model with a low cutoff,” *Phys. Rev. D*71, 036001 (2005), arXiv:hep-ph/0407019 [hep-ph].
- [53] D. Curtin, P. Meade, and C.-T. Yu, “Testing Electroweak Baryogenesis with Future Colliders,” *JHEP* 11, 127 (2014), arXiv:1409.0005 [hep-ph].
- [54] F. P. Huang, P.-H. Gu, P.-F. Yin, Z.-H. Yu, and X. Zhang, “Testing the electroweak phase transition and electroweak baryogenesis at the LHC and a circular electron-positron collider,” *Phys. Rev. D*93, 103515 (2016), arXiv:1511.03969 [hep-ph].
- [55] S. R. Coleman and E. J. Weinberg, “Radiative Corrections as the Origin of Spontaneous Symmetry Breaking,” *Phys. Rev. D*7, 1888 (1973).
- [56] N. Cabibbo, L. Maiani, G. Parisi, and R. Petronzio, “Bounds on the Fermions and Higgs Boson Masses in Grand Unified Theories,” *Nucl. Phys. B*158, 295 (1979).
- [57] P. Q. Hung, “Vacuum Instability and New Constraints on Fermion Masses,” *Phys. Rev. Lett.* 42, 873 (1979).
- [58] M. Lindner, “Implications of Triviality for the Standard Model,” *Z. Phys. C*31, 295 (1986).
- [59] G. Degrassi, S. Di Vita, J. Elias-Miro, J. R. Espinosa, G. F. Giudice, G. Isidori, and A. Strumia, “Higgs mass and vacuum stability in the Standard Model at NNLO,” *JHEP* 08, 098 (2012), arXiv:1205.6497 [hep-ph].
- [60] S. Alekhin, A. Djouadi, and S. Moch, “The top quark and Higgs boson masses and the stability of the electroweak vacuum,” *Phys. Lett. B*716, 214 (2012), arXiv:1207.0980 [hep-ph].
- [61] J. Elias-Miro, J. R. Espinosa, G. F. Giudice, G. Isidori, A. Riotto, and A. Strumia, “Higgs mass implications on the stability of the electroweak vacuum,” *Phys. Lett. B*709, 222 (2012), arXiv:1112.3022 [hep-ph].
- [62] “First combination of Tevatron and LHC measurements of the top-quark mass,” (2014), arXiv:1403.4427 [hep-ex].

[63] A. H. Hoang and T. Teubner, “Top quark pair production close to threshold: Top mass, width and momentum distribution,” Phys. Rev. D60, 114027 (1999), arXiv:hep-ph/9904468 [hep-ph].

[64] A. Juste, S. Mantry, A. Mitov, A. Penin, P. Skands, E. Varnes, M. Vos, and S. Wimpenny, “Determination of the top quark mass circa 2013: methods, subtleties, perspectives,” Eur. Phys. J. C74, 3119 (2014), arXiv:1310.0799 [hep-ph].

[65] A. H. Hoang, “The Top Mass: Interpretation and Theoretical Uncertainties,” in *Proceedings, 7th International Workshop on Top Quark Physics (TOP2014): Cannes, France, September 28-October 3, 2014* (2014) arXiv:1412.3649 [hep-ph].

[66] T. Behnke, J. E. Brau, B. Foster, J. Fuster, M. Harrison, J. M. Paterson, M. Peskin, M. Stanitzki, N. Walker, and H. Yamamoto, “The International Linear Collider Technical Design Report - Volume 1: Executive Summary,” (2013), arXiv:1306.6327 [physics.acc-ph].

[67] V. S. Fadin and V. A. Khoze, “Threshold Behavior of Heavy Top Production in e+ e- Collisions,” JETP Lett. 46, 525 (1987), [Pisma Zh. Eksp. Teor. Fiz. 46, 417 (1987)].

[68] V. S. Fadin and V. A. Khoze, “Production of a pair of heavy quarks in e+ e- annihilation in the threshold region,” Sov. J. Nucl. Phys. 48, 309 (1988), [Yad. Fiz. 48, 487 (1988)].

[69] M. J. Strassler and M. E. Peskin, “The Heavy top quark threshold: QCD and the Higgs,” Phys. Rev. D43, 1500 (1991).

[70] J. R. Espinosa, G. F. Giudice, and A. Riotto, “Cosmological implications of the Higgs mass measurement,” JCAP 0805, 002 (2008), arXiv:0710.2484 [hep-ph].

[71] J. R. Espinosa, G. F. Giudice, E. Morgante, A. Riotto, L. Senatore, A. Strumia, and N. Tetradis, “The cosmological Higgstory of the vacuum instability,” JHEP 09, 174 (2015), arXiv:1505.04825 [hep-ph].

[72] W. E. East, J. Kearney, B. Shakya, H. Yoo, and K. M. Zurek, “Spacetime Dynamics of a Higgs Vacuum Instability During Inflation,” Phys. Rev. D95, 023526 (2017), [Phys. Rev. D95, 023526 (2017)], arXiv:1607.00381 [hep-ph].

[73] A. Joti, A. Katsis, D. Loupas, A. Salvio, A. Strumia, N. Tetradis, and A. Urbano, “(Higgs) vacuum decay during inflation,” JHEP 07, 058 (2017), arXiv:1706.00792 [hep-ph].

[74] A. Eichhorn, H. Gies, J. Jaeckel, T. Plehn, M. M. Scherer, and R. Sondenheimer, “The Higgs Mass and the Scale of New Physics,” JHEP 04, 022 (2015), arXiv:1501.02812 [hep-ph].

[75] R. Sondenheimer, “Nonpolynomial Higgs interactions and vacuum stability,” (2017), arXiv:1711.00065 [hep-ph].

[76] J. R. Espinosa, “Cosmological implications of Higgs near-criticality,” *Proceedings, Higgs cosmology: Newport Pagnell, Buckinghamshire, UK, March 27-28, 2017*, Phil. Trans. Roy. Soc. A376, 20170118 (2018).

[77] G. 't Hooft and M. J. G. Veltman, "One loop divergencies in the theory of gravitation," *Ann. Inst. H. Poincare Phys. Theor. A*20, 69 (1974).

[78] M. H. Goroff and A. Sagnotti, "Quantum Gravity at two Loops," *Phys. Lett.* 160B, 81 (1985).

[79] M. H. Goroff and A. Sagnotti, "The Ultraviolet Behavior of Einstein Gravity," *Nucl. Phys.* B266, 709 (1986).

[80] A. E. M. van de Ven, "Two loop quantum gravity," *Conference on Strings and Symmetries Stony Brook, New York, May 20-25, 1991*, *Nucl. Phys.* B378, 309 (1992).

[81] K. S. Stelle, "Renormalization of Higher Derivative Quantum Gravity," *Phys. Rev.* D16, 953 (1977).

[82] K. S. Stelle, "Classical Gravity with Higher Derivatives," *Gen. Rel. Grav.* 9, 353 (1978).

[83] I. Antoniadis and E. T. Tomboulis, "Gauge Invariance and Unitarity in Higher Derivative Quantum Gravity," *Phys. Rev.* D33, 2756 (1986).

[84] A. M. Polyakov, "Quantum Geometry of Bosonic Strings," *Phys. Lett.* 103B, 207 (1981).

[85] J. H. Schwarz, "Superstring Theory," *Phys. Rept.* 89, 223 (1982).

[86] M. B. Green and J. H. Schwarz, "Anomaly Cancellation in Supersymmetric D=10 Gauge Theory and Superstring Theory," *Phys. Lett.* 149B, 117 (1984).

[87] P. Candelas, G. T. Horowitz, A. Strominger, and E. Witten, "Vacuum Configurations for Superstrings," *Nucl. Phys.* B258, 46 (1985).

[88] E. Witten, "String theory dynamics in various dimensions," *Nucl. Phys.* B443, 85 (1995), arXiv:hep-th/9503124 [hep-th].

[89] N. Seiberg and E. Witten, "String theory and noncommutative geometry," *JHEP* 09, 032 (1999), arXiv:hep-th/9908142 [hep-th].

[90] A. Ashtekar, "New Variables for Classical and Quantum Gravity," *Phys. Rev. Lett.* 57, 2244 (1986).

[91] A. Ashtekar, "New Hamiltonian Formulation of General Relativity," *Phys. Rev.* D36, 1587 (1987).

[92] C. Rovelli and L. Smolin, "Discreteness of area and volume in quantum gravity," *Nucl. Phys.* B442, 593 (1995), [Erratum: *Nucl. Phys.* B456, 753 (1995)], arXiv:gr-qc/9411005 [gr-qc].

[93] C. Rovelli and L. Smolin, "Spin networks and quantum gravity," *Phys. Rev.* D52, 5743 (1995), arXiv:gr-qc/9505006 [gr-qc].

[94] C. Rovelli, "Loop quantum gravity," *Living Rev. Rel.* 1, 1 (1998), arXiv:gr-qc/9710008 [gr-qc].

[95] A. Ashtekar, J. Baez, A. Corichi, and K. Krasnov, “Quantum geometry and black hole entropy,” *Phys. Rev. Lett.* 80, 904 (1998), arXiv:gr-qc/9710007 [gr-qc].

[96] A. Perez, “Spin foam models for quantum gravity,” *Class. Quant. Grav.* 20, R43 (2003), arXiv:gr-qc/0301113 [gr-qc].

[97] A. Ashtekar and J. Lewandowski, “Background independent quantum gravity: A Status report,” *Class. Quant. Grav.* 21, R53 (2004), arXiv:gr-qc/0404018 [gr-qc].

[98] S. Weinberg, “Ultraviolet divergences in quantum theories of gravitation,” *General Relativity: An Einstein centenary survey*, Eds. Hawking, S.W., Israel, W; Cambridge University Press , 790 (1979).

[99] M. Reuter, “Nonperturbative Evolution Equation for Quantum Gravity,” *Phys. Rev. D* 57, 971 (1998), arXiv:hep-th/9605030.

[100] M. Reuter and F. Saueressig, “Renormalization group flow of quantum gravity in the Einstein-Hilbert truncation,” *Phys. Rev. D* 65, 065016 (2002), arXiv:hep-th/0110054 [hep-th].

[101] D. F. Litim, “Fixed points of quantum gravity,” *Phys. Rev. Lett.* 92, 201301 (2004), arXiv:hep-th/0312114 [hep-th].

[102] J. Ambjorn and J. Jurkiewicz, “Four-dimensional simplicial quantum gravity,” *Phys. Lett. B* 278, 42 (1992).

[103] J. Ambjorn and R. Loll, “Nonperturbative Lorentzian quantum gravity, causality and topology change,” *Nucl. Phys. B* 536, 407 (1998), arXiv:hep-th/9805108 [hep-th].

[104] J. Ambjorn, J. Jurkiewicz, and R. Loll, “Emergence of a 4-D world from causal quantum gravity,” *Phys. Rev. Lett.* 93, 131301 (2004), arXiv:hep-th/0404156 [hep-th].

[105] J. Ambjorn, J. Jurkiewicz, and R. Loll, “Reconstructing the universe,” *Phys. Rev. D* 72, 064014 (2005), arXiv:hep-th/0505154 [hep-th].

[106] J. Laiho and D. Coumbe, “Evidence for Asymptotic Safety from Lattice Quantum Gravity,” *Phys. Rev. Lett.* 107, 161301 (2011), arXiv:1104.5505 [hep-lat].

[107] P. Horava, “Quantum Gravity at a Lifshitz Point,” *Phys. Rev. D* 79, 084008 (2009), arXiv:0901.3775 [hep-th].

[108] P. Horava, “Spectral Dimension of the Universe in Quantum Gravity at a Lifshitz Point,” *Phys. Rev. Lett.* 102, 161301 (2009), arXiv:0902.3657 [hep-th].

[109] E. Kiritsis and G. Kofinas, “Horava-Lifshitz Cosmology,” *Nucl. Phys. B* 821, 467 (2009), arXiv:0904.1334 [hep-th].

[110] D. Blas, O. Pujolas, and S. Sibiryakov, “Consistent Extension of Horava Gravity,” *Phys. Rev. Lett.* 104, 181302 (2010), arXiv:0909.3525 [hep-th].

[111] L. Bombelli, J. Lee, D. Meyer, and R. Sorkin, “Space-Time as a Causal Set,” *Phys. Rev. Lett.* 59, 521 (1987).

[112] R. D. Sorkin, “Causal sets: Discrete gravity,” in *Lectures on quantum gravity. Proceedings, School of Quantum Gravity, Valdivia, Chile, January 4-14, 2002* (2003) pp. 305–327, arXiv:gr-qc/0309009 [gr-qc].

[113] J. Henson, “The Causal set approach to quantum gravity,” (2006), arXiv:gr-qc/0601121 [gr-qc].

[114] A. Bonanno and M. Reuter, “Renormalization group improved black hole spacetimes,” Phys. Rev. D62, 043008 (2000), arXiv:hep-th/0002196.

[115] A. Ashtekar, T. Pawłowski, and P. Singh, “Quantum Nature of the Big Bang: Improved dynamics,” Phys. Rev. D74, 084003 (2006), arXiv:gr-qc/0607039 [gr-qc].

[116] S. W. Hawking, “Particle Creation by Black Holes,” In *\*Gibbons, G. W. (ed.), Hawking, S. W. (ed.): Euclidean quantum gravity\** 167-188, Commun. Math. Phys. 43, 199 (1975), [,167(1975)].

[117] S. D. Mathur, “The Information paradox: A Pedagogical introduction,” *Strings, Supergravity and Gauge Theories. Proceedings, CERN Winter School, CERN, Geneva, Switzerland, February 9-13 2009*, Class. Quant. Grav. 26, 224001 (2009), arXiv:0909.1038 [hep-th].

[118] S. Hossenfelder and L. Smolin, “Conservative solutions to the black hole information problem,” Phys. Rev. D81, 064009 (2010), arXiv:0901.3156 [gr-qc].

[119] M. Shaposhnikov and C. Wetterich, “Asymptotic safety of gravity and the Higgs boson mass,” Phys. Lett. B683, 196 (2010), arXiv:0912.0208 [hep-th].

[120] A. Eichhorn and A. Held, “Top mass from asymptotic safety,” Phys. Lett. B777, 217 (2018), arXiv:1707.01107 [hep-th].

[121] A. Eichhorn and H. Gies, “Light fermions in quantum gravity,” New J. Phys. 13, 125012 (2011), arXiv:1104.5366 [hep-th].

[122] J. Meibohm and J. M. Pawłowski, “Chiral fermions in asymptotically safe quantum gravity,” Eur. Phys. J. C76, 285 (2016), arXiv:1601.04597 [hep-th].

[123] S. M. Christensen and M. J. Duff, “Quantum Gravity in two + epsilon Dimension,” Phys. Lett. B79, 213 (1978).

[124] R. Gastmans, R. Kallosh, and C. Truffin, “Quantum Gravity Near Two-Dimensions,” Nucl. Phys. B133, 417 (1978).

[125] L. Smolin, “A Fixed Point for Quantum Gravity,” Nucl. Phys. B208, 439 (1982).

[126] D. J. Gross and F. Wilczek, “Ultraviolet Behavior of Nonabelian Gauge Theories,” Phys. Rev. Lett. 30, 1343 (1973).

[127] H. D. Politzer, “Reliable Perturbative Results for Strong Interactions?” Phys. Rev. Lett. 30, 1346 (1973).

[128] D. J. Gross and F. Wilczek, “Asymptotically Free Gauge Theories. 1,” Phys. Rev. D8, 3633 (1973).

- [129] D. J. Gross and F. Wilczek, “Asymptotically Free Gauge Theories. 2.” *Phys. Rev. D9*, 980 (1974).
- [130] H. D. Politzer, “Asymptotic Freedom: An Approach to Strong Interactions,” *Phys. Rept. 14*, 129 (1974).
- [131] K. G. Wilson, “Renormalization group and critical phenomena. 1. Renormalization group and the Kadanoff scaling picture,” *Phys. Rev. B4*, 3174 (1971).
- [132] K. G. Wilson, “Renormalization group and critical phenomena. 2. Phase space cell analysis of critical behavior,” *Phys. Rev. B4*, 3184 (1971).
- [133] K. G. Wilson and J. B. Kogut, “The Renormalization group and the epsilon expansion,” *Phys. Rept. 12*, 75 (1974).
- [134] K. G. Wilson, “The Renormalization Group: Critical Phenomena and the Kondo Problem,” *Rev. Mod. Phys. 47*, 773 (1975).
- [135] F. J. Dyson, “The S matrix in quantum electrodynamics,” *Phys. Rev. 75*, 1736 (1949).
- [136] J. S. Schwinger, “On the Green’s functions of quantized fields. 1.” *Proc. Nat. Acad. Sci. 37*, 452 (1951).
- [137] J. S. Schwinger, “On the Green’s functions of quantized fields. 2.” *Proc. Nat. Acad. Sci. 37*, 455 (1951).
- [138] F. J. Wegner and A. Houghton, “Renormalization group equation for critical phenomena,” *Phys. Rev. A8*, 401 (1973).
- [139] J. M. Cornwall, R. Jackiw, and E. Tomboulis, “Effective Action for Composite Operators,” *Phys. Rev. D10*, 2428 (1974), cJT.
- [140] J. Polchinski, “Renormalization and Effective Lagrangians,” *Nucl. Phys. B231*, 269 (1984).
- [141] C. Wetterich, “Exact evolution equation for the effective potential,” *Phys. Lett. B301*, 90 (1993), arXiv:1710.05815 [hep-th].
- [142] M. Gockeler, R. Horsley, V. Linke, P. E. L. Rakow, G. Schierholz, and H. Stüber, “Is there a Landau pole problem in QED?” *Phys. Rev. Lett. 80*, 4119 (1998), arXiv:hep-th/9712244 [hep-th].
- [143] S. Kim, J. B. Kogut, and M.-P. Lombardo, “Gauged Nambu-Jona-Lasinio studies of the triviality of quantum electrodynamics,” *Phys. Rev. D65*, 054015 (2002), arXiv:hep-lat/0112009 [hep-lat].
- [144] H. Gies and J. Jaeckel, “Renormalization flow of QED,” *Phys. Rev. Lett. 93*, 110405 (2004), arXiv:hep-ph/0405183 [hep-ph].
- [145] D. J. E. Callaway, “Triviality Pursuit: Can Elementary Scalar Particles Exist?” *Phys. Rept. 167*, 241 (1988).

[146] D. F. Litim and F. Sannino, “Asymptotic safety guaranteed,” JHEP 12, 178 (2014), arXiv:1406.2337 [hep-th].

[147] A. D. Bond, G. Hiller, K. Kowalska, and D. F. Litim, “Directions for model building from asymptotic safety,” JHEP 08, 004 (2017), arXiv:1702.01727 [hep-ph].

[148] R. Mann, J. Meffe, F. Sannino, T. Steele, Z.-W. Wang, and C. Zhang, “Asymptotically Safe Standard Model via Vectorlike Fermions,” Phys. Rev. Lett. 119, 261802 (2017), arXiv:1707.02942 [hep-ph].

[149] G. M. Pelaggi, A. D. Plascencia, A. Salvio, F. Sannino, J. Smirnov, and A. Strumia, “Asymptotically Safe Standard Model Extensions,” (2017), arXiv:1708.00437 [hep-ph].

[150] A. D. Bond and D. F. Litim, “Price of Asymptotic Safety,” (2018), arXiv:1801.08527 [hep-th].

[151] U. Harst and M. Reuter, “QED coupled to QEG,” JHEP 05, 119 (2011), arXiv:1101.6007 [hep-th].

[152] A. Eichhorn and F. Versteegen, “Upper bound on the Abelian gauge coupling from asymptotic safety,” JHEP 01, 030 (2018), arXiv:1709.07252 [hep-th].

[153] A. G. Cohen, D. B. Kaplan, and A. E. Nelson, “Baryogenesis at the weak phase transition,” Nucl. Phys. B349, 727 (1991).

[154] V. A. Rubakov and M. E. Shaposhnikov, “Electroweak baryon number nonconservation in the early universe and in high-energy collisions,” Usp. Fiz. Nauk 166, 493 (1996), [Phys. Usp.39,461(1996)], arXiv:hep-ph/9603208 [hep-ph].

[155] A. Riotto and M. Trodden, “Recent progress in baryogenesis,” Ann. Rev. Nucl. Part. Sci. 49, 35 (1999), arXiv:hep-ph/9901362 [hep-ph].

[156] M. Sher, “Electroweak Higgs Potentials and Vacuum Stability,” Phys. Rept. 179, 273 (1989).

[157] A. G. Cohen, D. B. Kaplan, and A. E. Nelson, “Progress in electroweak baryogenesis,” Ann. Rev. Nucl. Part. Sci. 43, 27 (1993), arXiv:hep-ph/9302210 [hep-ph].

[158] J. M. Cline, “Baryogenesis,” in *Les Houches Summer School - Session 86: Particle Physics and Cosmology: The Fabric of Spacetime Les Houches, France, July 31-August 25, 2006* (2006) arXiv:hep-ph/0609145 [hep-ph].

[159] D. E. Morrissey and M. J. Ramsey-Musolf, “Electroweak baryogenesis,” New J. Phys. 14, 125003 (2012), arXiv:1206.2942 [hep-ph].

[160] T. Konstandin, “Quantum Transport and Electroweak Baryogenesis,” Phys. Usp. 56, 747 (2013), [Usp. Fiz. Nauk183,785(2013)], arXiv:1302.6713 [hep-ph].

[161] Z. Fodor, J. Hein, K. Jansen, A. Jaster, and I. Montvay, “Simulating the electroweak phase transition in the SU(2) Higgs model,” Nucl. Phys. B439, 147 (1995), arXiv:hep-lat/9409017 [hep-lat].

[162] W. Buchmuller, Z. Fodor, and A. Hebecker, “Thermodynamics of the electroweak phase transition,” *Nucl. Phys.* B447, 317 (1995), arXiv:hep-ph/9502321 [hep-ph].

[163] X.-m. Zhang, “Operators analysis for Higgs potential and cosmological bound on Higgs mass,” *Phys. Rev.* D47, 3065 (1993), arXiv:hep-ph/9301277 [hep-ph].

[164] X. Zhang, B. L. Young, and S. K. Lee, “Electroweak sphaleron for effective theory in the limit of large Higgs boson mass,” *Phys. Rev.* D51, 5327 (1995), arXiv:hep-ph/9406322 [hep-ph].

[165] S. Kanemura, Y. Okada, and E. Senaha, “Electroweak baryogenesis and quantum corrections to the triple Higgs boson coupling,” *Phys. Lett.* B606, 361 (2005), arXiv:hep-ph/0411354 [hep-ph].

[166] P. Huang, A. Joglekar, B. Li, and C. E. M. Wagner, “Probing the Electroweak Phase Transition at the LHC,” *Phys. Rev.* D93, 055049 (2016), arXiv:1512.00068 [hep-ph].

[167] A. Kobakhidze, L. Wu, and J. Yue, “Electroweak Baryogenesis with Anomalous Higgs Couplings,” *JHEP* 04, 011 (2016), arXiv:1512.08922 [hep-ph].

[168] Q.-H. Cao, G. Li, B. Yan, D.-M. Zhang, and H. Zhang, “Double Higgs production at the 14 TeV LHC and a 100 TeV  $pp$  collider,” *Phys. Rev.* D96, 095031 (2017), arXiv:1611.09336 [hep-ph].

[169] D. Curtin, P. Meade, and H. Ramani, “Thermal Resummation and Phase Transitions,” (2016), arXiv:1612.00466 [hep-ph].

[170] X. Gan, A. J. Long, and L.-T. Wang, “Electroweak Sphaleron with Dimension-6 Operators,” *Phys. Rev.* D96, 115018 (2017), arXiv:1708.03061 [hep-ph].

[171] Q.-H. Cao, F. P. Huang, K.-P. Xie, and X. Zhang, “Testing the electroweak phase transition in scalar extension models at lepton colliders,” (2017), 10.1088/1674-1137/42/2/023103, arXiv:1708.04737 [hep-ph].

[172] B. Jain, S. J. Lee, and M. Son, “On the Validity of the Effective Potential and the Precision of Higgs Self Couplings,” (2017), arXiv:1709.03232 [hep-ph].

[173] A. Noble and M. Perelstein, “Higgs self-coupling as a probe of electroweak phase transition,” *Phys. Rev.* D78, 063518 (2008), arXiv:0711.3018 [hep-ph].

[174] U. Baur, T. Plehn, and D. L. Rainwater, “Measuring the Higgs boson self coupling at the LHC and finite top mass matrix elements,” *Phys. Rev. Lett.* 89, 151801 (2002), arXiv:hep-ph/0206024 [hep-ph].

[175] U. Baur, T. Plehn, and D. L. Rainwater, “Determining the Higgs boson selfcoupling at hadron colliders,” *Phys. Rev.* D67, 033003 (2003), arXiv:hep-ph/0211224 [hep-ph].

[176] A. Butter, O. J. P. Éboli, J. Gonzalez-Fraile, M. C. Gonzalez-Garcia, T. Plehn, and M. Rauch, “The Gauge-Higgs Legacy of the LHC Run I,” *JHEP* 07, 152 (2016), arXiv:1604.03105 [hep-ph].

[177] K. Holland and J. Kuti, “How light can the Higgs be?” *Lattice hadron physics. Proceedings, 2nd Topical Workshop, LHP 2003, Cairns, Australia, July 22-30, 2003*, Nucl. Phys. Proc. Suppl. 129, 765 (2004), [,765(2003)], arXiv:hep-lat/0308020 [hep-lat].

[178] K. Holland, “Triviality and the Higgs mass lower bound,” *Lattice field theory. Proceedings, 22nd International Symposium, Lattice 2004, Batavia, USA, June 21-26, 2004*, Nucl. Phys. Proc. Suppl. 140, 155 (2005), [,155(2004)], arXiv:hep-lat/0409112 [hep-lat].

[179] J. R. Espinosa, T. Konstandin, and F. Riva, “Strong Electroweak Phase Transitions in the Standard Model with a Singlet,” Nucl. Phys. B854, 592 (2012), arXiv:1107.5441 [hep-ph].

[180] H. Gies, C. Gneiting, and R. Sondenheimer, “Higgs Mass Bounds from Renormalization Flow for a simple Yukawa model,” Phys. Rev. D89, 045012 (2014), arXiv:1308.5075 [hep-ph].

[181] H. Gies and R. Sondenheimer, “Higgs Mass Bounds from Renormalization Flow for a Higgs-top-bottom model,” Eur. Phys. J. C75, 68 (2015), arXiv:1407.8124 [hep-ph].

[182] H. Gies and R. Sondenheimer, “Renormalization Group Flow of the Higgs Potential,” in *Higgs cosmology Newport Pagnell, Buckinghamshire, UK, March 27-28, 2017* (2017) arXiv:1708.04305 [hep-ph].

[183] J. Borchardt, H. Gies, and R. Sondenheimer, “Global flow of the Higgs potential in a Yukawa model,” Eur. Phys. J. C76, 472 (2016), arXiv:1603.05861 [hep-ph].

[184] O. Akerlund and P. de Forcrand, “Higgs-Yukawa model with higher dimension operators via extended mean field theory,” Phys. Rev. D93, 035015 (2016), arXiv:1508.07959 [hep-lat].

[185] D. Y. J. Chu, K. Jansen, B. Knippschild, and C. J. D. Lin, “Higgs-Yukawa model on the lattice,” in *35th International Symposium on Lattice Field Theory (Lattice 2017) Granada, Spain, June 18-24, 2017* (2017) arXiv:1710.09737 [hep-lat].

[186] O. Akerlund, P. de Forcrand, and J. Steinbauer, “Effects of higher dimension operators on the Standard Model Higgs sector,” *Proceedings, 33rd International Symposium on Lattice Field Theory (Lattice 2015): Kobe, Japan, July 14-18, 2015*, PoS Lattice2015, 229 (2016), arXiv:1511.03867 [hep-lat].

[187] J. Berges, N. Tetradis, and C. Wetterich, “Non-perturbative renormalization flow in quantum field theory and statistical physics,” Phys. Rept. 363, 223 (2002), arXiv:hep-ph/0005122.

[188] J. M. Pawłowski, “Aspects of the functional renormalisation group,” Annals Phys. 322, 2831 (2007), arXiv:hep-th/0512261 [hep-th].

[189] H. Gies, “Introduction to the functional RG and applications to gauge theories,” Lect.Notes Phys. 852, 287 (2012), arXiv:hep-ph/0611146 [hep-ph].

[190] J. Braun, “Fermion Interactions and Universal Behavior in Strongly Interacting Theories,” *J.Phys.* G39, 033001 (2012), arXiv:1108.4449 [hep-ph].

[191] I. V. Krive and A. D. Linde, “On the Vacuum Stability Problem in Gauge Theories,” *Nucl. Phys.* B117, 265 (1976).

[192] V. Branchina and H. Faivre, “Effective potential (in)stability and lower bounds on the scalar (Higgs) mass,” *Phys. Rev.* D72, 065017 (2005), arXiv:hep-th/0503188 [hep-th].

[193] V. Branchina, H. Faivre, and V. Pangon, “Effective potential and vacuum stability,” *J. Phys.* G36, 015006 (2009), arXiv:0802.4423 [hep-ph].

[194] A. Eichhorn and M. M. Scherer, “Planck scale, Higgs mass, and scalar dark matter,” *Phys. Rev.* D90, 025023 (2014), arXiv:1404.5962 [hep-ph].

[195] Z. Fodor, K. Holland, J. Kuti, D. Nogradi, and C. Schroeder, “New Higgs physics from the lattice,” *Proceedings, 25th International Symposium on Lattice field theory (Lattice 2007): Regensburg, Germany, July 30-August 4, 2007*, PoS Lattice2007, 056 (2007), arXiv:0710.3151 [hep-lat].

[196] P. Hegde, K. Jansen, C. J. D. Lin, and A. Nagy, “Stabilizing the electroweak vacuum by higher dimensional operators in a Higgs-Yukawa model,” *Proceedings, 31st International Symposium on Lattice Field Theory (Lattice 2013): Mainz, Germany, July 29-August 3, 2013*, PoS Lattice2013, 058 (2014), arXiv:1310.6260 [hep-lat].

[197] D. Y. J. Chu, K. Jansen, B. Knippschild, C. J. D. Lin, K.-I. Nagai, and A. Nagy, “Phase structure and Higgs boson mass in a Higgs-Yukawa model with a dimension-6 operator,” *Proceedings, 32nd International Symposium on Lattice Field Theory (Lattice 2014): Brookhaven, NY, USA, June 23-28, 2014*, PoS LATTICE2014, 278 (2014), arXiv:1501.00306 [hep-lat].

[198] A. Jakovac, I. Kapovari, and A. Patkos, “Scalar mass stability bound in a simple Yukawa-theory from renormalization group equations,” *Mod. Phys. Lett.* A32, 1750011 (2016), arXiv:1508.06774 [hep-th].

[199] A. Jakovac, I. Kapovari, and A. Patkos, “Renormalisation Group determination of scalar mass bounds in a simple Yukawa-model,” *Proceedings, Gribov-85 Memorial Workshop on Theoretical Physics of XXI Century: Chernogolovka, Russia, June 7-20, 2015*, *Int. J. Mod. Phys.* A31, 1645042 (2016), arXiv:1510.05782 [hep-th].

[200] T. Plehn, *Lectures on LHC Physics*, Vol. 886 (2015).

[201] M. A. Shifman, A. I. Vainshtein, M. B. Voloshin, and V. I. Zakharov, “Low-Energy Theorems for Higgs Boson Couplings to Photons,” *Sov. J. Nucl. Phys.* 30, 711 (1979), [Yad. Fiz.30,1368(1979)].

[202] B. A. Kniehl and M. Spira, “Low-energy theorems in Higgs physics,” *Z. Phys.* C69, 77 (1995), arXiv:hep-ph/9505225 [hep-ph].

[203] M. Spira, “Effective Multi-Higgs Couplings to Gluons,” *JHEP* 10, 026 (2016), arXiv:1607.05548 [hep-ph].

[204] O. J. P. Eboli, G. C. Marques, S. F. Novaes, and A. A. Natale, “Twin Higgs Boson Production,” *Phys. Lett.* B197, 269 (1987).

[205] D. A. Dicus, C. Kao, and S. S. D. Willenbrock, “Higgs Boson Pair Production From Gluon Fusion,” *Phys. Lett.* B203, 457 (1988).

[206] E. W. N. Glover and J. J. van der Bij, “Higgs Boson Pair Production via Gluon Fusion,” *Nucl. Phys.* B309, 282 (1988).

[207] T. Plehn, M. Spira, and P. M. Zerwas, “Pair production of neutral Higgs particles in gluon-gluon collisions,” *Nucl. Phys.* B479, 46 (1996), [Erratum: *Nucl. Phys.* B531,655(1998)], arXiv:hep-ph/9603205 [hep-ph].

[208] A. Djouadi, W. Kilian, M. Mühlleitner, and P. M. Zerwas, “Production of neutral Higgs boson pairs at LHC,” *Eur. Phys. J.* C10, 45 (1999), arXiv:hep-ph/9904287 [hep-ph].

[209] X. Li and M. B. Voloshin, “Remarks on double Higgs boson production by gluon fusion at threshold,” *Phys. Rev.* D89, 013012 (2014), arXiv:1311.5156 [hep-ph].

[210] U. Baur, T. Plehn, and D. L. Rainwater, “Examining the Higgs boson potential at lepton and hadron colliders: A Comparative analysis,” *Phys. Rev.* D68, 033001 (2003), arXiv:hep-ph/0304015 [hep-ph].

[211] U. Baur, T. Plehn, and D. L. Rainwater, “Probing the Higgs selfcoupling at hadron colliders using rare decays,” *Phys. Rev.* D69, 053004 (2004), arXiv:hep-ph/0310056 [hep-ph].

[212] J. Baglio, A. Djouadi, R. Gröber, M. M. Mühlleitner, J. Quevillon, and M. Spira, “The measurement of the Higgs self-coupling at the LHC: theoretical status,” *JHEP* 04, 151 (2013), arXiv:1212.5581 [hep-ph].

[213] S. Dawson, S. Dittmaier, and M. Spira, “Neutral Higgs boson pair production at hadron colliders: QCD corrections,” *Phys. Rev.* D58, 115012 (1998), arXiv:hep-ph/9805244 [hep-ph].

[214] J. Grigo, J. Hoff, K. Melnikov, and M. Steinhauser, “On the Higgs boson pair production at the LHC,” *Nucl. Phys.* B875, 1 (2013), arXiv:1305.7340 [hep-ph].

[215] F. Maltoni, E. Vryonidou, and M. Zaro, “Top-quark mass effects in double and triple Higgs production in gluon-gluon fusion at NLO,” *JHEP* 11, 079 (2014), arXiv:1408.6542 [hep-ph].

[216] D. de Florian and J. Mazzitelli, “Higgs pair production at next-to-next-to-leading logarithmic accuracy at the LHC,” *JHEP* 09, 053 (2015), arXiv:1505.07122 [hep-ph].

[217] J. Grigo, J. Hoff, and M. Steinhauser, “Higgs boson pair production: top quark mass effects at NLO and NNLO,” *Nucl. Phys.* B900, 412 (2015), arXiv:1508.00909 [hep-ph].

[218] S. Borowka, N. Greiner, G. Heinrich, S. P. Jones, M. Kerner, J. Schlenk, U. Schubert, and T. Zirke, “Higgs Boson Pair Production in Gluon Fusion at Next-to-Leading Order with Full Top-Quark Mass Dependence,” *Phys. Rev. Lett.* 117, 012001 (2016), [Erratum: *Phys. Rev. Lett.* 117,no.7,079901(2016)], arXiv:1604.06447 [hep-ph].

[219] D. de Florian, M. Grazzini, C. Hanga, S. Kallweit, J. M. Lindert, P. Maierhöfer, J. Mazzitelli, and D. Rathlev, “Differential Higgs Boson Pair Production at Next-to-Next-to-Leading Order in QCD,” *JHEP* 09, 151 (2016), arXiv:1606.09519 [hep-ph].

[220] F. Goertz, A. Papaefstathiou, L. L. Yang, and J. Zurita, “Higgs boson pair production in the D=6 extension of the SM,” *JHEP* 04, 167 (2015), arXiv:1410.3471 [hep-ph].

[221] Q.-H. Cao, B. Yan, D.-M. Zhang, and H. Zhang, “Resolving the Degeneracy in Single Higgs Production with Higgs Pair Production,” *Phys. Lett. B* 752, 285 (2016), arXiv:1508.06512 [hep-ph].

[222] M. Gorbahn and U. Haisch, “Indirect probes of the trilinear Higgs coupling:  $gg \rightarrow h$  and  $h \rightarrow \gamma\gamma$ ,” *JHEP* 10, 094 (2016), arXiv:1607.03773 [hep-ph].

[223] W. Bizon, M. Gorbahn, U. Haisch, and G. Zanderighi, “Constraints on the trilinear Higgs coupling from vector boson fusion and associated Higgs production at the LHC,” *JHEP* 07, 083 (2017), arXiv:1610.05771 [hep-ph].

[224] G. Degrassi, P. P. Giardino, F. Maltoni, and D. Pagani, “Probing the Higgs self coupling via single Higgs production at the LHC,” *JHEP* 12, 080 (2016), arXiv:1607.04251 [hep-ph].

[225] S. Di Vita, C. Grojean, G. Panico, M. Riembau, and T. Vantalon, “A global view on the Higgs self-coupling,” *JHEP* 09, 069 (2017), arXiv:1704.01953 [hep-ph].

[226] M. L. Mangano, T. Plehn, P. Reimitz, T. Schell, and H.-S. Shao, “Measuring the Top Yukawa Coupling at 100 TeV,” *J. Phys. G* 43, 035001 (2016), arXiv:1507.08169 [hep-ph].

[227] R. Contino *et al.*, “Physics at a 100 TeV pp collider: Higgs and EW symmetry breaking studies,” CERN Yellow Report , 255 (2017), arXiv:1606.09408 [hep-ph].

[228] M. J. Dolan, C. Englert, and M. Spannowsky, “Higgs self-coupling measurements at the LHC,” *JHEP* 10, 112 (2012), arXiv:1206.5001 [hep-ph].

[229] A. J. Barr, M. J. Dolan, C. Englert, and M. Spannowsky, “Di-Higgs final states augMT2ed – selecting  $hh$  events at the high luminosity LHC,” *Phys. Lett. B* 728, 308 (2014), arXiv:1309.6318 [hep-ph].

[230] F. Kling, T. Plehn, and P. Schichtel, “Maximizing the significance in Higgs boson pair analyses,” *Phys. Rev. D* 95, 035026 (2017), arXiv:1607.07441 [hep-ph].

[231] V. Barger, L. L. Everett, C. B. Jackson, A. D. Peterson, and G. Shaughnessy, “Measuring the two-Higgs doublet model scalar potential at LHC14,” *Phys. Rev. D* 90, 095006 (2014), arXiv:1408.2525 [hep-ph].

[232] A. Alves, T. Ghosh, and K. Sinha, “Can We Discover Double Higgs Production at the LHC?” *Phys. Rev.* D96, 035022 (2017), arXiv:1704.07395 [hep-ph].

[233] G. Aad *et al.* (ATLAS), “Searches for Higgs boson pair production in the  $hh \rightarrow b\bar{b}\tau\tau, \gamma\gamma WW^*, \gamma\gamma bb, bbbb$  channels with the ATLAS detector,” *Phys. Rev.* D92, 092004 (2015), arXiv:1509.04670 [hep-ex].

[234] V. Khachatryan *et al.* (CMS), “Search for two Higgs bosons in final states containing two photons and two bottom quarks in proton-proton collisions at 8 TeV,” *Phys. Rev.* D94, 052012 (2016), arXiv:1603.06896 [hep-ex].

[235] A. Papaefstathiou, L. L. Yang, and J. Zurita, “Higgs boson pair production at the LHC in the  $b\bar{b}W^+W^-$  channel,” *Phys. Rev.* D87, 011301 (2013), arXiv:1209.1489 [hep-ph].

[236] D. E. Ferreira de Lima, A. Papaefstathiou, and M. Spannowsky, “Standard model Higgs boson pair production in the  $(b\bar{b})(b\bar{b})$  final state,” *JHEP* 08, 030 (2014), arXiv:1404.7139 [hep-ph].

[237] D. Wardrope, E. Jansen, N. Konstantinidis, B. Cooper, R. Falla, and N. Norjoharuddeen, “Non-resonant Higgs-pair production in the  $b\bar{b} b\bar{b}$  final state at the LHC,” *Eur. Phys. J.* C75, 219 (2015), arXiv:1410.2794 [hep-ph].

[238] J. K. Behr, D. Bortoletto, J. A. Frost, N. P. Hartland, C. Issever, and J. Rojo, “Boosting Higgs pair production in the  $b\bar{b}b\bar{b}$  final state with multivariate techniques,” *Eur. Phys. J.* C76, 386 (2016), arXiv:1512.08928 [hep-ph].

[239] Q. Li, Z. Li, Q.-S. Yan, and X. Zhao, “Probe Higgs boson pair production via the  $3l2j + \cancel{E}$  mode,” *Phys. Rev.* D92, 014015 (2015), arXiv:1503.07611 [hep-ph].

[240] J. M. Pawłowski and F. Rennecke, “Higher order quark-mesonic scattering processes and the phase structure of QCD,” *Phys. Rev.* D90, 076002 (2014), arXiv:1403.1179 [hep-ph].

[241] J. de Vries, M. Postma, J. van de Vis, and G. White, “Electroweak Baryogenesis and the Standard Model Effective Field Theory,” *JHEP* 01, 089 (2018), arXiv:1710.04061 [hep-ph].

[242] H. Gies, R. Sondenheimer, and M. Warschinke, “Impact of generalized Yukawa interactions on the lower Higgs mass bound,” *Eur. Phys. J.* C77, 743 (2017), arXiv:1707.04394 [hep-ph].

[243] G. V. Dunne and M. Unsal, “Resurgence and Trans-series in Quantum Field Theory: The  $CP(N-1)$  Model,” *JHEP* 11, 170 (2012), arXiv:1210.2423 [hep-th].

[244] A. J. Helmboldt, J. M. Pawłowski, and N. Strodthoff, “Towards quantitative precision in the chiral crossover: masses and fluctuation scales,” *Phys. Rev.* D91, 054010 (2015), arXiv:1409.8414 [hep-ph].

[245] S. Falkenberg and S. D. Odintsov, “Gauge dependence of the effective average action in Einstein gravity,” *Int.J.Mod.Phys.* A13, 607 (1998), arXiv:hep-th/9612019 [hep-th].

[246] W. Souma, “Nontrivial ultraviolet fixed point in quantum gravity,” *Prog.Theor.Phys.* 102, 181 (1999), arXiv:hep-th/9907027 [hep-th].

[247] O. Lauscher and M. Reuter, “Ultraviolet fixed point and generalized flow equation of quantum gravity,” *Phys. Rev. D*65, 025013 (2002), arXiv:hep-th/0108040.

[248] M. Niedermaier, “The asymptotic safety scenario in quantum gravity: An introduction,” *Class. Quant. Grav.* 24, R171 (2007), arXiv:gr-qc/0610018.

[249] D. F. Litim, “On fixed points of quantum gravity,” *AIP Conf.Proc.* 841, 322 (2006), arXiv:hep-th/0606044 [hep-th].

[250] P. Fischer and D. F. Litim, “Fixed points of quantum gravity in extra dimensions,” *Phys.Lett. B*638, 497 (2006), arXiv:hep-th/0602203 [hep-th].

[251] D. F. Litim, “Fixed Points of Quantum Gravity and the Renormalisation Group,” *Proceedings, Workshop on From quantum to emergent gravity: Theory and phenomenology (QG-Ph): Trieste, Italy, June 11-15, 2007*, (2008), [PoSQG-Ph,024(2007)], arXiv:0810.3675 [hep-th].

[252] A. Eichhorn, H. Gies, and M. M. Scherer, “Asymptotically free scalar curvature-ghost coupling in Quantum Einstein Gravity,” *Phys. Rev. D*80, 104003 (2009), arXiv:0907.1828 [hep-th].

[253] A. Eichhorn and H. Gies, “Ghost anomalous dimension in asymptotically safe quantum gravity,” *Phys. Rev. D*81, 104010 (2010), arXiv:1001.5033 [hep-th].

[254] K. Groh and F. Saueressig, “Ghost wave-function renormalization in Asymptotically Safe Quantum Gravity,” *J. Phys. A*43, 365403 (2010), arXiv:1001.5032 [hep-th].

[255] D. Litim and A. Satz, “Limit cycles and quantum gravity,” (2012), arXiv:1205.4218 [hep-th].

[256] S. Nagy, J. Krizsan, and K. Sailer, “Infrared fixed point in quantum Einstein gravity,” *JHEP* 07, 102 (2012), arXiv:1203.6564 [hep-th].

[257] S. Nagy, B. Fazekas, L. Juhasz, and K. Sailer, “Critical exponents in quantum Einstein gravity,” *Phys. Rev. D*88, 116010 (2013), arXiv:1307.0765 [hep-th].

[258] K. Falls, “Asymptotic safety and the cosmological constant,” *JHEP* 01, 069 (2016), arXiv:1408.0276 [hep-th].

[259] K. Falls, “Renormalization of Newton’s constant,” *Phys. Rev. D*92, 124057 (2015), arXiv:1501.05331 [hep-th].

[260] K. Falls, “Critical scaling in quantum gravity from the renormalisation group,” (2015), arXiv:1503.06233 [hep-th].

[261] D. Benedetti, “Essential nature of Newton’s constant in unimodular gravity,” *Gen. Rel. Grav.* 48, 68 (2016), arXiv:1511.06560 [hep-th].

[262] H. Gies, B. Knorr, and S. Lippoldt, “Generalized Parametrization Dependence in Quantum Gravity,” *Phys. Rev. D*92, 084020 (2015), arXiv:1507.08859 [hep-th].

[263] N. Ohta, R. Percacci, and A. D. Pereira, “Gauges and functional measures in quantum gravity I: Einstein theory,” *JHEP* 06, 115 (2016), arXiv:1605.00454 [hep-th].

[264] K. Falls, “Physical renormalization schemes and asymptotic safety in quantum gravity,” *Phys. Rev. D* 96, 126016 (2017), arXiv:1702.03577 [hep-th].

[265] W. B. Houthoff, A. Kurov, and F. Saueressig, “Impact of topology in foliated Quantum Einstein Gravity,” *Eur. Phys. J. C* 77, 491 (2017), arXiv:1705.01848 [hep-th].

[266] R. de León Ardón, N. Ohta, and R. Percacci, “Path integral of unimodular gravity,” *Phys. Rev. D* 97, 026007 (2018), arXiv:1710.02457 [gr-qc].

[267] A. A. Bytsenko, L. N. Granda, and S. D. Odintsov, “Exact renormalization group and running Newtonian coupling in higher derivative gravity,” *JETP Lett.* 65, 600 (1997), arXiv:hep-th/9705008 [hep-th].

[268] L. N. Granda and S. D. Odintsov, “Effective average action and nonperturbative renormalization group equation in higher derivative quantum gravity,” *Grav. Cosmol.* 4, 85 (1998), arXiv:gr-qc/9801026 [gr-qc].

[269] O. Lauscher and M. Reuter, “Flow equation of quantum Einstein gravity in a higher- derivative truncation,” *Phys. Rev. D* 66, 025026 (2002), arXiv:hep-th/0205062.

[270] A. Codello and R. Percacci, “Fixed Points of Higher Derivative Gravity,” *Phys. Rev. Lett.* 97, 221301 (2006), arXiv:hep-th/0607128.

[271] A. Codello, R. Percacci, and C. Rahmede, “Ultraviolet properties of  $f(R)$ -gravity,” *Int. J. Mod. Phys. A* 23, 143 (2008), arXiv:0705.1769 [hep-th].

[272] P. F. Machado and F. Saueressig, “On the renormalization group flow of  $f(R)$ -gravity,” *Phys. Rev. D* 77, 124045 (2008), arXiv:0712.0445 [hep-th].

[273] E. Manrique and M. Reuter, “Bare Action and Regularized Functional Integral of Asymptotically Safe Quantum Gravity,” *Phys. Rev. D* 79, 025008 (2009), arXiv:0811.3888 [hep-th].

[274] A. Codello, R. Percacci, and C. Rahmede, “Investigating the Ultraviolet Properties of Gravity with a Wilsonian Renormalization Group Equation,” *Annals Phys.* 324, 414 (2009), arXiv:0805.2909 [hep-th].

[275] M. R. Niedermaier, “Gravitational Fixed Points from Perturbation Theory,” *Phys. Rev. Lett.* 103, 101303 (2009).

[276] D. Benedetti, P. F. Machado, and F. Saueressig, “Asymptotic safety in higher-derivative gravity,” *Mod. Phys. Lett. A* 24, 2233 (2009), arXiv:0901.2984 [hep-th].

[277] S. Rechenberger and F. Saueressig, “The  $R^2$  phase-diagram of QEG and its spectral dimension,” *Phys. Rev. D* 86, 024018 (2012), arXiv:1206.0657 [hep-th].

[278] D. Benedetti and F. Caravelli, “The Local potential approximation in quantum gravity,” JHEP 06, 017 (2012), [Erratum: JHEP10,157(2012)], arXiv:1204.3541 [hep-th].

[279] J. A. Dietz and T. R. Morris, “Asymptotic safety in the  $f(R)$  approximation,” JHEP 01, 108 (2013), arXiv:1211.0955 [hep-th].

[280] N. Ohta and R. Percacci, “Higher Derivative Gravity and Asymptotic Safety in Diverse Dimensions,” Class. Quant. Grav. 31, 015024 (2014), arXiv:1308.3398 [hep-th].

[281] K. Falls, D. Litim, K. Nikolakopoulos, and C. Rahmede, “A bootstrap towards asymptotic safety,” (2013), arXiv:1301.4191 [hep-th].

[282] K. Falls, D. F. Litim, K. Nikolakopoulos, and C. Rahmede, “Further evidence for asymptotic safety of quantum gravity,” Phys. Rev. D93, 104022 (2016), arXiv:1410.4815 [hep-th].

[283] J. A. Dietz and T. R. Morris, “Redundant operators in the exact renormalisation group and in the  $f(R)$  approximation to asymptotic safety,” JHEP 07, 064 (2013), arXiv:1306.1223 [hep-th].

[284] M. Demmel, F. Saueressig, and O. Zanusso, “A proper fixed functional for four-dimensional Quantum Einstein Gravity,” JHEP 08, 113 (2015), arXiv:1504.07656 [hep-th].

[285] A. Eichhorn, “The Renormalization Group flow of unimodular  $f(R)$  gravity,” JHEP 04, 096 (2015), arXiv:1501.05848 [gr-qc].

[286] N. Ohta, R. Percacci, and G. P. Vacca, “Flow equation for  $f(R)$  gravity and some of its exact solutions,” Phys. Rev. D92, 061501 (2015), arXiv:1507.00968 [hep-th].

[287] N. Ohta, R. Percacci, and G. P. Vacca, “Renormalization Group Equation and scaling solutions for  $f(R)$  gravity in exponential parametrization,” Eur. Phys. J. C76, 46 (2016), arXiv:1511.09393 [hep-th].

[288] K. Falls, D. F. Litim, K. Nikolakopoulos, and C. Rahmede, “On de Sitter solutions in asymptotically safe  $f(R)$  theories,” (2016), arXiv:1607.04962 [gr-qc].

[289] K. Falls and N. Ohta, “Renormalization Group Equation for  $f(R)$  gravity on hyperbolic spaces,” Phys. Rev. D94, 084005 (2016), arXiv:1607.08460 [hep-th].

[290] N. Ohta, R. Percacci, and A. D. Pereira, “Gauges and functional measures in quantum gravity II: Higher derivative gravity,” Eur. Phys. J. C77, 611 (2017), arXiv:1610.07991 [hep-th].

[291] S. Gonzalez-Martin, T. R. Morris, and Z. H. Slade, “Asymptotic solutions in asymptotic safety,” Phys. Rev. D95, 106010 (2017), arXiv:1704.08873 [hep-th].

[292] K. G. Falls, C. S. King, D. F. Litim, K. Nikolakopoulos, and C. Rahmede, “Asymptotic safety of quantum gravity beyond Ricci scalars,” (2017), arXiv:1801.00162 [hep-th].

[293] D. Benedetti, “On the number of relevant operators in asymptotically safe gravity,” *Europhys. Lett.* 102, 20007 (2013), arXiv:1301.4422 [hep-th].

[294] N. Christiansen, “Four-Derivative Quantum Gravity Beyond Perturbation Theory,” (2016), arXiv:1612.06223 [hep-th].

[295] Y. Hamada and M. Yamada, “Asymptotic safety of higher derivative quantum gravity non-minimally coupled with a matter system,” *JHEP* 08, 070 (2017), arXiv:1703.09033 [hep-th].

[296] H. Gies, B. Knorr, S. Lippoldt, and F. Saueressig, “Gravitational Two-Loop Counterterm Is Asymptotically Safe,” *Phys. Rev. Lett.* 116, 211302 (2016), arXiv:1601.01800 [hep-th].

[297] T. Biswas, E. Gerwick, T. Koivisto, and A. Mazumdar, “Towards singularity and ghost free theories of gravity,” *Phys. Rev. Lett.* 108, 031101 (2012), arXiv:1110.5249 [gr-qc].

[298] L. Modesto, “Super-renormalizable Quantum Gravity,” *Phys. Rev. D* 86, 044005 (2012), arXiv:1107.2403 [hep-th].

[299] A. Bonanno and M. Reuter, “Proper time flow equation for gravity,” *JHEP* 02, 035 (2005), arXiv:hep-th/0410191 [hep-th].

[300] E. Manrique, S. Rechenberger, and F. Saueressig, “Asymptotically Safe Lorentzian Gravity,” *Phys. Rev. Lett.* 106, 251302 (2011), arXiv:1102.5012 [hep-th].

[301] J. Biemans, A. Platania, and F. Saueressig, “Quantum gravity on foliated spacetimes: Asymptotically safe and sound,” *Phys. Rev. D* 95, 086013 (2017), arXiv:1609.04813 [hep-th].

[302] C. Wetterich, “Graviton fluctuations erase the cosmological constant,” *Phys. Lett. B* 773, 6 (2017), arXiv:1704.08040 [gr-qc].

[303] D. Becker, C. Ripken, and F. Saueressig, “On avoiding Ostrogradski instabilities within Asymptotic Safety,” *JHEP* 12, 121 (2017), arXiv:1709.09098 [hep-th].

[304] F. Arici, D. Becker, C. Ripken, F. Saueressig, and W. D. van Suijlekom, “Reflection positivity in higher derivative scalar theories,” (2017), arXiv:1712.04308 [hep-th].

[305] K. Falls, D. F. Litim, and A. Raghuraman, “Black Holes and Asymptotically Safe Gravity,” *Int.J.Mod.Phys. A* 27, 1250019 (2012), arXiv:1002.0260 [hep-th].

[306] K. Falls and D. F. Litim, “Black hole thermodynamics under the microscope,” *Phys. Rev. D* 89, 084002 (2014), arXiv:1212.1821 [gr-qc].

[307] A. Bonanno, B. Koch, and A. Platania, “Cosmic Censorship in Quantum Einstein Gravity,” *Class. Quant. Grav.* 34, 095012 (2017), arXiv:1610.05299 [gr-qc].

[308] A. Bonanno, B. Koch, and A. Platania, “Gravitational collapse in Quantum Einstein Gravity,” (2017), arXiv:1710.10845 [gr-qc].

[309] A. Bonanno, S. J. Gabriele Gionti, and A. Platania, “Bouncing and emergent cosmologies from Arnowitt–Deser–Misner RG flows,” *Class. Quant. Grav.* 35, 065004 (2018), arXiv:1710.06317 [gr-qc].

[310] A. Platania and F. Saueressig, “Functional Renormalization Group flows on Friedman-Lemaître-Robertson-Walker backgrounds,” (2017), arXiv:1710.01972 [hep-th].

[311] N. Alkofer, G. D’Odorico, F. Saueressig, and F. Versteegen, “Quantum Gravity signatures in the Unruh effect,” *Phys. Rev.* D94, 104055 (2016), arXiv:1605.08015 [gr-qc].

[312] C. Pagani and M. Reuter, “Composite Operators in Asymptotic Safety,” *Phys. Rev.* D95, 066002 (2017), arXiv:1611.06522 [gr-qc].

[313] M. Niedermaier and M. Reuter, “The Asymptotic Safety Scenario in Quantum Gravity,” *Living Rev.Rel.* 9, 5 (2006).

[314] R. Percacci, “Asymptotic Safety,” In \*Oriti, D. (ed.): *Approaches to quantum gravity* 111-128 (2007), arXiv:0709.3851 [hep-th].

[315] D. F. Litim, “Renormalisation group and the Planck scale,” *Phil. Trans. Roy. Soc. Lond. A* 369, 2759 (2011), arXiv:1102.4624 [hep-th].

[316] M. Reuter and F. Saueressig, “Quantum Einstein Gravity,” *New J. Phys.* 14, 055022 (2012), arXiv:1202.2274 [hep-th].

[317] R. Percacci, *An Introduction to Covariant Quantum Gravity and Asymptotic Safety*, 100 Years of General Relativity, Vol. 3 (World Scientific, 2017).

[318] A. Bonanno and F. Saueressig, “Asymptotically safe cosmology – A status report,” *Comptes Rendus Physique* 18, 254 (2017), arXiv:1702.04137 [hep-th].

[319] J. C. Ward, “An Identity in Quantum Electrodynamics,” *Phys. Rev.* 78, 182 (1950).

[320] Y. Takahashi, “On the generalized Ward identity,” *Nuovo Cim.* 6, 371 (1957).

[321] N. Nielsen, “On the Gauge Dependence of Spontaneous Symmetry Breaking in Gauge Theories,” *Nucl. Phys.* B101, 173 (1975).

[322] R. Fukuda and T. Kugo, “Gauge Invariance in the Effective Action and Potential,” *Phys. Rev.* D13, 3469 (1976).

[323] J. C. Taylor, “Ward Identities and Charge Renormalization of the Yang-Mills Field,” *Nucl. Phys.* B33, 436 (1971).

[324] A. A. Slavnov, “Ward Identities in Gauge Theories,” *Theor. Math. Phys.* 10, 99 (1972), [Teor. Mat. Fiz. 10, 153 (1972)].

[325] N. Christiansen, D. F. Litim, J. M. Pawłowski, and A. Rodigast, “Fixed points and infrared completion of quantum gravity,” *Phys. Lett.* B728, 114 (2014), arXiv:1209.4038 [hep-th].

[326] A. Codello, G. D’Odorico, and C. Pagani, “Consistent closure of renormalization group flow equations in quantum gravity,” *Phys. Rev.* D89, 081701 (2014), arXiv:1304.4777 [gr-qc].

[327] N. Christiansen, B. Knorr, J. M. Pawłowski, and A. Rodigast, “Global Flows in Quantum Gravity,” *Phys. Rev.* D93, 044036 (2016), arXiv:1403.1232 [hep-th].

[328] B. Knorr and S. Lippoldt, “Correlation functions on a curved background,” *Phys. Rev.* D96, 065020 (2017), arXiv:1707.01397 [hep-th].

[329] B. Knorr, “Infinite order quantum-gravitational correlations,” (2017), arXiv:1710.07055 [hep-th].

[330] E. Manrique and M. Reuter, “Bimetric Truncations for Quantum Einstein Gravity and Asymptotic Safety,” *Annals Phys.* 325, 785 (2010), arXiv:0907.2617 [gr-qc].

[331] E. Manrique, M. Reuter, and F. Saueressig, “Matter Induced Bimetric Actions for Gravity,” *Annals Phys.* 326, 440 (2011), arXiv:1003.5129 [hep-th].

[332] E. Manrique, M. Reuter, and F. Saueressig, “Bimetric Renormalization Group Flows in Quantum Einstein Gravity,” *Annals Phys.* 326, 463 (2011), arXiv:1006.0099 [hep-th].

[333] D. Becker and M. Reuter, “En route to Background Independence: Broken split-symmetry, and how to restore it with bi-metric average actions,” *Annals Phys.* 350, 225 (2014), arXiv:1404.4537 [hep-th].

[334] M. Reuter and H. Weyer, “Background Independence and Asymptotic Safety in Conformally Reduced Gravity,” *Phys. Rev.* D79, 105005 (2009), arXiv:0801.3287 [hep-th].

[335] M. Reuter and H. Weyer, “The Role of Background Independence for Asymptotic Safety in Quantum Einstein Gravity,” *405th WE-Heraeus-Seminar: Quantum Gravity: Challenges and Perspectives Bad Honnef, Germany, April 14-16, 2008*, Gen. Rel. Grav. 41, 983 (2009), arXiv:0903.2971 [hep-th].

[336] I. Donkin and J. M. Pawłowski, “The phase diagram of quantum gravity from diffeomorphism-invariant RG-flows,” (2012), arXiv:1203.4207 [hep-th].

[337] J. A. Dietz and T. R. Morris, “Background independent exact renormalization group for conformally reduced gravity,” *JHEP* 04, 118 (2015), arXiv:1502.07396 [hep-th].

[338] M. Safari, “Splitting Ward identity,” *Eur. Phys. J.* C76, 201 (2016), arXiv:1508.06244 [hep-th].

[339] P. Labus, T. R. Morris, and Z. H. Slade, “Background independence in a background dependent renormalization group,” *Phys. Rev.* D94, 024007 (2016), arXiv:1603.04772 [hep-th].

[340] T. R. Morris, “Large curvature and background scale independence in single-metric approximations to asymptotic safety,” *JHEP* 11, 160 (2016), arXiv:1610.03081 [hep-th].

[341] R. Percacci and G. P. Vacca, “The background scale Ward identity in quantum gravity,” *Eur. Phys. J. C*77, 52 (2017), arXiv:1611.07005 [hep-th].

[342] C. M. Nieto, R. Percacci, and V. Skrinjar, “Split Weyl transformations in quantum gravity,” *Phys. Rev. D*96, 106019 (2017), arXiv:1708.09760 [gr-qc].

[343] N. Ohta, “Background Scale Independence in Quantum Gravity,” *PTEP* 2017, 033E02 (2017), arXiv:1701.01506 [hep-th].

[344] U. Ellwanger, “Flow equations for N point functions and bound states,” *Proceedings, Workshop on Quantum field theoretical aspects of high energy physics: Bad Frankenhausen, Germany, September 20-24, 1993*, *Z. Phys. C*62, 503 (1994), arXiv:hep-ph/9308260 [hep-ph].

[345] T. R. Morris, “The Exact renormalization group and approximate solutions,” *Int. J. Mod. Phys. A*9, 2411 (1994), arXiv:hep-ph/9308265.

[346] V. Branchina, K. A. Meissner, and G. Veneziano, “The Price of an exact, gauge invariant RG flow equation,” *Phys.Lett. B*574, 319 (2003), arXiv:hep-th/0309234 [hep-th].

[347] J. M. Pawłowski, “Geometrical effective action and Wilsonian flows,” (2003), arXiv:hep-th/0310018 [hep-th].

[348] M. Demmel, F. Saueressig, and O. Zanusso, “RG flows of Quantum Einstein Gravity in the linear-geometric approximation,” *Annals Phys.* 359, 141 (2015), arXiv:1412.7207 [hep-th].

[349] H. Kawai, Y. Kitazawa, and M. Ninomiya, “Scaling exponents in quantum gravity near two-dimensions,” *Nucl. Phys. B*393, 280 (1993), arXiv:hep-th/9206081 [hep-th].

[350] A. Nink, “Field Parametrization Dependence in Asymptotically Safe Quantum Gravity,” *Phys. Rev. D*91, 044030 (2015), arXiv:1410.7816 [hep-th].

[351] M. Demmel and A. Nink, “Connections and geodesics in the space of metrics,” *Phys. Rev. D*92, 104013 (2015), arXiv:1506.03809 [gr-qc].

[352] I. H. Bridle, J. A. Dietz, and T. R. Morris, “The local potential approximation in the background field formalism,” *JHEP* 03, 093 (2014), arXiv:1312.2846 [hep-th].

[353] B. S. DeWitt, “Quantum Theory of Gravity. 2. The Manifestly Covariant Theory,” *Phys. Rev.* 162, 1195 (1967).

[354] L. F. Abbott, “Introduction to the Background Field Method,” *Acta Phys. Polon. B*13, 33 (1982).

[355] D. F. Litim and J. M. Pawłowski, “Renormalization group flows for gauge theories in axial gauges,” *JHEP* 0209, 049 (2002), arXiv:hep-th/0203005 [hep-th].

[356] D. F. Litim and J. M. Pawłowski, “Wilsonian flows and background fields,” *Phys.Lett. B*546, 279 (2002), arXiv:hep-th/0208216 [hep-th].

[357] M. Safari and G. P. Vacca, “Covariant and background independent functional RG flow for the effective average action,” JHEP 11, 139 (2016), arXiv:1607.07074 [hep-th].

[358] M. Safari and G. P. Vacca, “Covariant and single-field effective action with the background-field formalism,” Phys. Rev. D96, 085001 (2017), arXiv:1607.03053 [hep-th].

[359] T. R. Morris and A. W. H. Preston, “Manifestly diffeomorphism invariant classical Exact Renormalization Group,” JHEP 06, 012 (2016), arXiv:1602.08993 [hep-th].

[360] C. Wetterich, “Gauge invariant flow equation,” (2016), arXiv:1607.02989 [hep-th].

[361] J. Braun, H. Gies, and J. M. Pawłowski, “Quark Confinement from Color Confinement,” Phys.Lett. B684, 262 (2010), arXiv:0708.2413 [hep-th].

[362] J. Braun, L. M. Haas, F. Marhauser, and J. M. Pawłowski, “Phase Structure of Two-Flavor QCD at Finite Chemical Potential,” Phys.Rev.Lett. 106, 022002 (2011), arXiv:0908.0008 [hep-ph].

[363] J. Braun, A. Eichhorn, H. Gies, and J. M. Pawłowski, “On the Nature of the Phase Transition in  $SU(N)$ ,  $Sp(2)$  and  $E(7)$  Yang-Mills theory,” Eur.Phys.J. C70, 689 (2010), arXiv:1007.2619 [hep-ph].

[364] L. Fister and J. M. Pawłowski, “Confinement from Correlation Functions,” Phys.Rev. D88, 045010 (2013), arXiv:1301.4163 [hep-ph].

[365] U. Reinosa, J. Serreau, M. Tissier, and N. Wschebor, “Deconfinement transition in  $SU(N)$  theories from perturbation theory,” Phys. Lett. B742, 61 (2015), arXiv:1407.6469 [hep-ph].

[366] D. F. Litim and J. M. Pawłowski, “Flow equations for Yang-Mills theories in general axial gauges,” Phys.Lett. B435, 181 (1998), arXiv:hep-th/9802064 [hep-th].

[367] C. S. Fischer, A. Maas, and J. M. Pawłowski, “On the infrared behavior of Landau gauge Yang-Mills theory,” Annals Phys. 324, 2408 (2009), arXiv:0810.1987 [hep-ph].

[368] A. K. Cyrol, L. Fister, M. Mitter, J. M. Pawłowski, and N. Strodthoff, “Landau gauge Yang-Mills correlation functions,” Phys. Rev. D94, 054005 (2016), arXiv:1605.01856 [hep-ph].

[369] C. S. Fischer and J. M. Pawłowski, “Uniqueness of infrared asymptotics in Landau gauge Yang- Mills theory II,” Phys. Rev. D80, 025023 (2009), arXiv:0903.2193 [hep-th].

[370] E. Mottola, “New Horizons in Gravity: The Trace Anomaly, Dark Energy and Condensate Stars,” *Non-perturbative gravity and quantum chromodynamics. Proceedings, 49th Cracow School of Theoretical Physics, Zakopane, Poland, May 31-June 10, 2009*, Acta Phys. Polon. B41, 2031 (2010), arXiv:1008.5006 [gr-qc].

[371] D. Schnoerr, I. Boettcher, J. M. Pawłowski, and C. Wetterich, “Error estimates and specification parameters for functional renormalization,” *Annals Phys.* 334, 83 (2013), arXiv:1301.4169 [cond-mat.quant-gas].

[372] D. F. Litim, “Optimization of the exact renormalization group,” *Phys.Lett.* B486, 92 (2000), arXiv:hep-th/0005245 [hep-th].

[373] D. F. Litim, “Optimized renormalization group flows,” *Phys.Rev.* D64, 105007 (2001), arXiv:hep-th/0103195 [hep-th].

[374] D. F. Litim, “Mind the gap,” *Int.J.Mod.Phys.* A16, 2081 (2001), arXiv:hep-th/0104221 [hep-th].

[375] D. F. Litim and J. M. Pawłowski, “Non-perturbative thermal flows and resummations,” *JHEP* 0611, 026 (2006), arXiv:hep-th/0609122 [hep-th].

[376] S. Folkerts, D. F. Litim, and J. M. Pawłowski, “Asymptotic freedom of Yang-Mills theory with gravity,” *Phys.Lett.* B709, 234 (2012), arXiv:1101.5552 [hep-th].

[377] S. Floerchinger, “Analytic Continuation of Functional Renormalization Group Equations,” *JHEP* 1205, 021 (2012), arXiv:1112.4374 [hep-th].

[378] K. Kamikado, N. Strodthoff, L. von Smekal, and J. Wambach, “Real-Time Correlation Functions in the O(N) Model from the Functional Renormalization Group,” *Eur.Phys.J.* C74, 2806 (2014), arXiv:1302.6199 [hep-ph].

[379] R.-A. Tripolt, N. Strodthoff, L. von Smekal, and J. Wambach, “Spectral Functions for the Quark-Meson Model Phase Diagram from the Functional Renormalization Group,” *Phys.Rev.* D89, 034010 (2014), arXiv:1311.0630 [hep-ph].

[380] J. M. Pawłowski and N. Strodthoff, “Real time correlation functions and the functional renormalization group,” *Phys. Rev.* D92, 094009 (2015), arXiv:1508.01160 [hep-ph].

[381] N. Strodthoff, “Self-consistent spectral functions in the O(N) model from the functional renormalization group,” *Phys. Rev.* D95, 076002 (2017), arXiv:1611.05036 [hep-th].

[382] J. A. M. Verma, “New features of FORM,” (2000), arXiv:math-ph/0010025 [math-ph].

[383] J. Kuipers, T. Ueda, J. A. M. Verma, and J. Vollinga, “FORM version 4.0,” *Comput. Phys. Commun.* 184, 1453 (2013), arXiv:1203.6543 [cs.SC].

[384] D. Brizuela, J. M. Martin-Garcia, and G. A. M. Marugan, “xPert: Computer algebra for metric perturbation theory,” (2008), 10.1007/s10714-009-0773-2, arXiv:0807.0824.

[385] M. Q. Huber and J. Braun, “Algorithmic derivation of functional renormalization group equations and Dyson-Schwinger equations,” *Comput. Phys. Commun.* 183, 1290 (2012), arXiv:1102.5307 [hep-th].

[386] A. K. Cyrol, M. Mitter, and N. Strodthoff, “FormTracer - A Mathematica Tracing Package Using FORM,” *Comput. Phys. Commun.* 219, 346 (2017), arXiv:1610.09331 [hep-ph].

[387] A. Eichhorn, A. Held, and J. M. Pawłowski, “Quantum-gravity effects on a Higgs-Yukawa model,” *Phys. Rev. D* 94, 104027 (2016), arXiv:1604.02041 [hep-th].

[388] A. Bonanno and M. Reuter, “Cosmology of the Planck era from a renormalization group for quantum gravity,” *Phys. Rev. D* 65, 043508 (2002), arXiv:hep-th/0106133.

[389] A. Bonanno and M. Reuter, “Cosmology with self-adjusting vacuum energy density from a renormalization group fixed point,” *Phys. Lett. B* 527, 9 (2002), arXiv:astro-ph/0106468.

[390] E. Bentivegna, A. Bonanno, and M. Reuter, “Confronting the IR Fixed Point Cosmology with High Redshift Supernova Data,” *JCAP* 0401, 001 (2004), arXiv:astro-ph/0303150.

[391] M. Reuter and F. Saueressig, “From big bang to asymptotic de Sitter: Complete cosmologies in a quantum gravity framework,” *JCAP* 0509, 012 (2005), arXiv:hep-th/0507167.

[392] A. Bonanno and M. Reuter, “Entropy signature of the running cosmological constant,” *JCAP* 0708, 024 (2007), arXiv:0706.0174 [hep-th].

[393] S. Weinberg, “Asymptotically Safe Inflation,” *Phys. Rev. D* 81, 083535 (2010), arXiv:0911.3165 [hep-th].

[394] A. Bonanno, “Astrophysical implications of the Asymptotic Safety Scenario in Quantum Gravity,” *PoS CLAQG08*, 008 (2011), arXiv:0911.2727 [hep-th].

[395] A. Bonanno and M. Reuter, “Entropy Production during Asymptotically Safe Inflation,” *Entropy* 13, 274 (2011), arXiv:1011.2794 [hep-th].

[396] B. Koch and I. Ramirez, “Exact renormalization group with optimal scale and its application to cosmology,” *Class. Quant. Grav.* 28, 055008 (2011), arXiv:1010.2799 [gr-qc].

[397] R. Casadio, S. D. H. Hsu, and B. Mirza, “Asymptotic Safety, Singularities, and Gravitational Collapse,” *Phys. Lett. B* 695, 317 (2011), arXiv:1008.2768 [gr-qc].

[398] A. Contillo, “Evolution of cosmological perturbations in an RG-driven inflationary scenario,” *Phys. Rev. D* 83, 085016 (2011), arXiv:1011.4618 [gr-qc].

[399] A. Bonanno, A. Contillo, and R. Percacci, “Inflationary solutions in asymptotically safe  $f(R)$  theories,” *Class. Quant. Grav.* 28, 145026 (2011), arXiv:1006.0192 [gr-qc].

[400] M. Hindmarsh, D. Litim, and C. Rahmede, “Asymptotically Safe Cosmology,” *JCAP* 1107, 019 (2011), arXiv:1101.5401 [gr-qc].

[401] Y.-F. Cai and D. A. Easson, “Asymptotically safe gravity as a scalar-tensor theory and its cosmological implications,” *Phys. Rev. D* 84, 103502 (2011), arXiv:1107.5815 [hep-th].

[402] A. Bonanno, “An effective action for asymptotically safe gravity,” *Phys. Rev.* D85, 081503 (2012), arXiv:1203.1962 [hep-th].

[403] M. Hindmarsh and I. D. Saltas, “ $f(R)$  Gravity from the renormalisation group,” *Phys. Rev.* D86, 064029 (2012), arXiv:1203.3957 [gr-qc].

[404] A. Bonanno and M. Reuter, “Modulated Ground State of Gravity Theories with Stabilized Conformal Factor,” *Phys. Rev.* D87, 084019 (2013), arXiv:1302.2928 [hep-th].

[405] E. J. Copeland, C. Rahmede, and I. D. Saltas, “Asymptotically Safe Starobinsky Inflation,” *Phys. Rev.* D91, 103530 (2015), arXiv:1311.0881 [gr-qc].

[406] D. Becker and M. Reuter, “Propagating gravitons vs. ‘dark matter’ in asymptotically safe quantum gravity,” *JHEP* 12, 025 (2014), arXiv:1407.5848 [hep-th].

[407] I. D. Saltas, “Higgs inflation and quantum gravity: An exact renormalisation group approach,” *JCAP* 1602, 048 (2016), arXiv:1512.06134 [hep-th].

[408] N. G. Nielsen, F. Sannino, and O. Svendsen, “Inflation from Asymptotically Safe Theories,” *Phys. Rev.* D91, 103521 (2015), arXiv:1503.00702 [hep-ph].

[409] A. Bonanno and A. Platania, “Asymptotically safe inflation from quadratic gravity,” *Phys. Lett.* B750, 638 (2015), arXiv:1507.03375 [gr-qc].

[410] R. Cuesta, K. Falls, and D. F. Litim, in preparation .

[411] R. A. Cuesta Ramos, *Quantum gravity and the renormalisation group: from the UV to the IR*, Ph.D. thesis, University of Sussex (2016).

[412] D. Benedetti, “Asymptotic safety goes on shell,” *New J. Phys.* 14, 015005 (2012), arXiv:1107.3110 [hep-th].

[413] D. Dou and R. Percacci, “The running gravitational couplings,” *Class. Quant. Grav.* 15, 3449 (1998), arXiv:hep-th/9707239 [hep-th].

[414] L. N. Granda, “Nonperturbative renormalization group for Einstein gravity with matter,” *Europhys. Lett.* 42, 487 (1998), arXiv:hep-th/0501225 [hep-th].

[415] L. N. Granda, “Nonperturbative Newtonian coupling in Einstein gravity with Dirac fields,” *Nuovo Cim.* B114, 509 (1999), arXiv:hep-th/0501239 [hep-th].

[416] R. Percacci and D. Perini, “Constraints on matter from asymptotic safety,” *Phys. Rev.* D67, 081503 (2003), arXiv:hep-th/0207033.

[417] R. Percacci and D. Perini, “Asymptotic safety of gravity coupled to matter,” *Phys. Rev.* D68, 044018 (2003), arXiv:hep-th/0304222.

[418] G. Narain and R. Percacci, “Renormalization Group Flow in Scalar-Tensor Theories. I,” *Class. Quant. Grav.* 27, 075001 (2010), arXiv:0911.0386 [hep-th].

[419] J. E. Daum, U. Harst, and M. Reuter, “Non-perturbative QEG Corrections to the Yang-Mills Beta Function,” *Gen. Relativ. Gravit.* (2010), 10.1007/s10714-010-1032-2, [*Gen. Rel. Grav.* 43, 2393 (2011)], arXiv:1005.1488 [hep-th].

[420] A. Eichhorn, “Quantum-gravity-induced matter self-interactions in the asymptotic-safety scenario,” *Phys. Rev.* D86, 105021 (2012), arXiv:1204.0965 [gr-qc].

[421] P. Donà and R. Percacci, “Functional renormalization with fermions and tetrads,” *Phys. Rev.* D87, 045002 (2013), arXiv:1209.3649 [hep-th].

[422] A. Eichhorn, “Faddeev-Popov ghosts in quantum gravity beyond perturbation theory,” *Phys. Rev.* D87, 124016 (2013), arXiv:1301.0632 [hep-th].

[423] T. Henz, J. M. Pawłowski, A. Rodigast, and C. Wetterich, “Dilaton Quantum Gravity,” *Phys. Lett.* B727, 298 (2013), arXiv:1304.7743 [hep-th].

[424] P. Donà, A. Eichhorn, and R. Percacci, “Matter matters in asymptotically safe quantum gravity,” *Phys. Rev.* D89, 084035 (2014), arXiv:1311.2898 [hep-th].

[425] P. Donà, A. Eichhorn, and R. Percacci, “Consistency of matter models with asymptotically safe quantum gravity,” *Proceedings, Satellite Conference on Theory Canada 9*, *Can. J. Phys.* 93, 988 (2015), arXiv:1410.4411 [gr-qc].

[426] R. Percacci and G. P. Vacca, “Search of scaling solutions in scalar-tensor gravity,” *Eur. Phys. J.* C75, 188 (2015), arXiv:1501.00888 [hep-th].

[427] P. Labus, R. Percacci, and G. P. Vacca, “Asymptotic safety in O(N) scalar models coupled to gravity,” *Phys. Lett.* B753, 274 (2016), arXiv:1505.05393 [hep-th].

[428] K.-y. Oda and M. Yamada, “Non-minimal coupling in Higgs–Yukawa model with asymptotically safe gravity,” *Class. Quant. Grav.* 33, 125011 (2016), arXiv:1510.03734 [hep-th].

[429] P. Donà, A. Eichhorn, P. Labus, and R. Percacci, “Asymptotic safety in an interacting system of gravity and scalar matter,” *Phys. Rev.* D93, 044049 (2016), [Erratum: *Phys. Rev.* D93,no.12,129904(2016)], arXiv:1512.01589 [gr-qc].

[430] T. Henz, J. M. Pawłowski, and C. Wetterich, “Scaling solutions for Dilaton Quantum Gravity,” *Phys. Lett.* B769, 105 (2017), arXiv:1605.01858 [hep-th].

[431] A. Eichhorn and S. Lippoldt, “Quantum gravity and Standard-Model-like fermions,” *Phys. Lett.* B767, 142 (2017), arXiv:1611.05878 [gr-qc].

[432] N. Christiansen and A. Eichhorn, “An asymptotically safe solution to the U(1) triviality problem,” *Phys. Lett.* B770, 154 (2017), arXiv:1702.07724 [hep-th].

[433] A. Eichhorn and A. Held, “Viability of quantum-gravity induced ultraviolet completions for matter,” *Phys. Rev.* D96, 086025 (2017), arXiv:1705.02342 [gr-qc].

[434] J. Biemans, A. Platania, and F. Saueressig, “Renormalization group fixed points of foliated gravity-matter systems,” *JHEP* 05, 093 (2017), arXiv:1702.06539 [hep-th].

[435] N. Christiansen, A. Eichhorn, and A. Held, “Is scale-invariance in gauge-Yukawa systems compatible with the graviton?” *Phys. Rev.* D96, 084021 (2017), arXiv:1705.01858 [hep-th].

[436] A. Eichhorn, S. Lippoldt, and V. Skrinjar, “Nonminimal hints for asymptotic safety,” *Phys. Rev.* D97, 026002 (2018), arXiv:1710.03005 [hep-th].

[437] A. Eichhorn, A. Held, and C. Wetterich, “Quantum-gravity predictions for the fine-structure constant,” (2017), arXiv:1711.02949 [hep-th].

[438] A. Eichhorn, Y. Hamada, J. Lumma, and M. Yamada, “Quantum gravity fluctuations flatten the Planck-scale Higgs-potential,” (2017), arXiv:1712.00319 [hep-th].

[439] N. Alkofer and F. Saueressig, “Asymptotically safe  $f(R)$ -gravity coupled to matter I: the polynomial case,” (2018), arXiv:1802.00498 [hep-th].

[440] H. Gies and R. Martini, “A curvature bound from gravitational catalysis,” (2018), arXiv:1802.02865 [hep-th].

[441] A. Eichhorn, “Status of the asymptotic safety paradigm for quantum gravity and matter,” in *Black Holes, Gravitational Waves and Spacetime Singularities Rome, Italy, May 9-12, 2017* (2017) arXiv:1709.03696 [gr-qc].

[442] H. A. Weldon, “Fermions without vierbeins in curved space-time,” *Phys. Rev.* D63, 104010 (2001), arXiv:gr-qc/0009086 [gr-qc].

[443] H. Gies and S. Lippoldt, “Fermions in gravity with local spin-base invariance,” *Phys. Rev.* D89, 064040 (2014), arXiv:1310.2509 [hep-th].

[444] S. Lippoldt, “Spin-base invariance of Fermions in arbitrary dimensions,” *Phys. Rev.* D91, 104006 (2015), arXiv:1502.05607 [hep-th].

[445] J. M. Pawłowski, “On Wilsonian flows in gauge theories,” *Int.J.Mod.Phys.* A16, 2105 (2001).

[446] H. Gies, “Running coupling in Yang-Mills theory: A flow equation study,” *Phys. Rev.* D66, 025006 (2002), arXiv:hep-th/0202207 [hep-th].

[447] J. M. Pawłowski, “On Wilsonian flows in gauge theories,” *Acta Phys.Slov.* 52, 475 (2002).

[448] G. Vilkovisky, “The Unique Effective Action in Quantum Field Theory,” *Nucl.Phys.* B234, 125 (1984).

[449] B. S. DeWitt, “The Effective Action,” *Quantum Field Theory and Quantum Statistics*, Vol. 1, Batalin, I.A. (Ed.) et al. , 191 (1988).

[450] S. P. Robinson and F. Wilczek, “Gravitational correction to running of gauge couplings,” *Phys. Rev. Lett.* 96, 231601 (2006), arXiv:hep-th/0509050.

[451] A. R. Pietrykowski, “Gauge dependence of gravitational correction to running of gauge couplings,” *Phys. Rev. Lett.* 98, 061801 (2007), arXiv:hep-th/0606208.

[452] D. J. Toms, “Quantum gravity and charge renormalization,” *Phys. Rev. D*76, 045015 (2007), arXiv:0708.2990 [hep-th].

[453] D. Ebert, J. Plefka, and A. Rodigast, “Absence of gravitational contributions to the running Yang-Mills coupling,” *Phys. Lett. B*660, 579 (2008), arXiv:0710.1002 [hep-th].

[454] Y. Tang and Y.-L. Wu, “Gravitational Contributions to the Running of Gauge Couplings,” *Commun. Theor. Phys.* 54, 1040 (2010), arXiv:0807.0331 [hep-ph].

[455] D. J. Toms, “Quantum gravitational contributions to quantum electrodynamics,” *Nature* 468, 56 (2010), arXiv:1010.0793 [hep-th].

[456] J. F. Donoghue, “Leading quantum correction to the Newtonian potential,” *Phys. Rev. Lett.* 72, 2996 (1994), arXiv:gr-qc/9310024.

[457] S. Folkerts, “Asymptotic Safety for Gravity coupled to Yang-Mills Theory: an RG Study,” Diploma thesis, Heidelberg (2009).

[458] D. F. Litim, M. Mojaza, and F. Sannino, “Vacuum stability of asymptotically safe gauge-Yukawa theories,” *JHEP* 01, 081 (2016), arXiv:1501.03061 [hep-th].

[459] A. D. Bond and D. F. Litim, “Theorems for Asymptotic Safety of Gauge Theories,” *Eur. Phys. J. C*77, 429 (2017), arXiv:1608.00519 [hep-th].

[460] A. D. Bond and D. F. Litim, “More asymptotic safety guaranteed,” (2017), arXiv:1707.04217 [hep-th].

[461] A. D. Bond and D. F. Litim, “Asymptotic safety guaranteed in supersymmetry,” *Phys. Rev. Lett.* 119, 211601 (2017), arXiv:1709.06953 [hep-th].

[462] D. F. Litim and J. M. Pawłowski, “Completeness and consistency of renormalisation group flows,” *Phys. Rev. D*66, 025030 (2002), arXiv:hep-th/0202188 [hep-th].

[463] A. K. Cyrol, M. Mitter, J. M. Pawłowski, and N. Strodthoff, “Non-perturbative quark, gluon and meson correlators of unquenched QCD,” (2017), arXiv:1706.06326 [hep-ph].

[464] A. Eichhorn, H. Gies, and J. M. Pawłowski, “Gluon condensation and scaling exponents for the propagators in Yang-Mills theory,” *Phys. Rev. D*83, 045014 (2011), arXiv:1010.2153 [hep-ph].

[465] S. Diehl, H. C. Krahl, and M. Scherer, “Three-Body Scattering from Nonperturbative Flow Equations,” *Phys. Rev. C*78, 034001 (2008), arXiv:0712.2846 [cond-mat.stat-mech].

[466] J. M. Pawłowski, M. M. Scherer, R. Schmidt, and S. J. Wetzel, “Physics and the choice of regulators in functional renormalisation group flows,” *Annals Phys.* 384, 165 (2017), arXiv:1512.03598 [hep-th].

[467] F. Freire, D. F. Litim, and J. M. Pawłowski, “Gauge invariance and background field formalism in the exact renormalization group,” *Phys. Lett. B*495, 256 (2000), arXiv:hep-th/0009110 [hep-th].

[468] M. M. Anber and J. F. Donoghue, “On the running of the gravitational constant,” Phys. Rev. D85, 104016 (2012), arXiv:1111.2875 [hep-th].

[469] M. Reuter and C. Wetterich, “Effective average action for gauge theories and exact evolution equations,” Nucl. Phys. B417, 181 (1994).

[470] J. J. W. York, “Conformatlly invariant orthogonal decomposition of symmetric tensors on Riemannian manifolds and the initial value problem of general relativity,” J. Math. Phys. 14, 456 (1973).

[471] I. Donkin, “On the geometrical effective action,” Diploma thesis, Heidelberg (2008).

[472] M. Reuter and C. Wetterich, “Gluon condensation in nonperturbative flow equations,” Phys. Rev. D56, 7893 (1997), arXiv:hep-th/9708051 [hep-th].

[473] M. Reuter and H. Weyer, “Conformal sector of Quantum Einstein Gravity in the local potential approximation: non-Gaussian fixed point and a phase of diffeomorphism invariance,” Phys. Rev. D80, 025001 (2009), arXiv:0804.1475 [hep-th].

[474] C. Wetterich, “Quantum correlations for the metric,” Phys. Rev. D95, 123525 (2017), arXiv:1603.06504 [gr-qc].

[475] J. A. Adams, J. Berges, S. Bornholdt, F. Freire, N. Tetradis, and C. Wetterich, “Solving nonperturbative flow equations,” Mod. Phys. Lett. A10, 2367 (1995), arXiv:hep-th/9507093 [hep-th].

[476] J. I. Kapusta and C. Gale, *Finite-temperature field theory: Principles and applications* (Cambridge University Press, 2006).

[477] D. F. Litim, “Critical exponents from optimized renormalization group flows,” Nucl. Phys. B631, 128 (2002), arXiv:hep-th/0203006 [hep-th].

[478] D. F. Litim, “Towards functional flows for hierarchical models,” Phys. Rev. D76, 105001 (2007), arXiv:0704.1514 [hep-th].